MECHANISMS OF ASYNCHRONOUS Ca^{2+} OSCILLATIONS AND THEIR ROLE IN (MAL)FUNCTION OF VASCULAR SMOOTH MUSCLE

by

HARLEY THOMAS TAN SYYONG

B.Sc., University of British Columbia, 2005

A THESIS SUBMITTED IN PARTIAL FULFILMENT OF THE REQUIREMENTS FOR THE DEGREE OF

DOCTOR OF PHILOSOPHY

in

THE FACULTY OF GRADUATE STUDIES

(Pharmacology and Therapeutics)

THE UNIVERSITY OF BRITISH COLUMBIA

(Vancouver)

April 2010

ABSTRACT

Contraction of vascular smooth muscle is regulated by fluctuations in the cytosolic concentration of Ca^{2+}. The spatio-temporal regulation of Ca^{2+} relies on the subcellular architecture of the smooth muscle cell and the juxtaposition of the opposing plasmalemma, sarcoplasmic reticulum, and mitochondria. This thesis addresses two related aspects of Ca^{2+} signaling in vascular smooth muscle: 1) Reversal of the plasma membrane Na^{+}/Ca^{2+} exchanger (NCX) during agonist-mediated stimulation in cultured rat aorta smooth muscle cells, and 2) the primary function of agonist-stimulated asynchronous Ca^{2+} waves and the signaling pathway(s) underlying them in the intact tissue.

Evidence for functional coupling of reverse-mode NCX with canonical transient receptor potential channels (TRPC), specifically TRPC6, was provided in rat aortic smooth muscle cells by demonstrating that NCX reversal was increased following stimulation with ATP and 1-Oleoyl-2-acetyl-sn-glycerol, a diacylglycerol analog. However, this was attenuated by blockade of non-selective cation channels with SKF-96365 and by activation of protein kinase C. These data are consistent with the known properties of TRPC6 and further support that functional coupling of TRPC6 and NCX occurs via a receptor-operated cascade.

A combination of wire myography and confocal microscopy determined that uridine 5'-triphosphate (UTP)-induced tonic contractions in rat basilar artery were associated with sustained repetitive oscillations in cytosolic Ca^{2+} which propagated along the length of the smooth muscle cells as Ca^{2+} waves. Pharmacological characterization of the mechanism of Ca^{2+} waves revealed that they are a result of repetitive cycles of sarcoplasmic reticulum (SR) Ca^{2+} release via inositol 1,4,5-trisphosphate-sensitive channels followed by the refilling of the SR.

Plasmalemmal Ca^{2+} entry via the reverse-mode NCX coupled with the receptor-operated and L-type Ca^{2+} channels is involved in replenishing the SR and supporting the ongoing Ca^{2+} waves.

Finally, phenylephrine-stimulated vascular smooth muscle contraction in mesenteric arteries of a mouse model of Marfan syndrome was significantly inhibited and associated with reduced frequency of Ca^{2+} waves. In addition, endothelium-dependent and endothelium-independent vasodilation was impaired, and vessel stiffness was increased. Together, these vasomotor abnormalities in the resistance vessel may have a negative and detrimental impact on the overall cardiovascular function in Marfan syndrome.

TABLE OF CONTENTS

LIST OF TABLES

LIST OF FIGURES

LIST OF ABBREVIATIONS

2-APB	2-aminoethoxydiphenylborate
$[Ca^{2+}]_i$	intracellular $[Ca^{2+}]$
$[Ca^{2+}]_{MT}$	mitochondrial matrix $[Ca^{2+}]$
$[Ca^{2+}]_o$	extracellular $[Ca^{2+}]$
$[Ca^{2+}]_{subPM}$	subplasmalemmal $[Ca^{2+}]$
$[Na^+]_o$	extracellular $[Na^+]$
$[Na^+]_{subPM}$	subplasmalemmal $[Na^+]$
ACh	acetylcholine
ATP	adenosine triphosphate
BIM	bisindolylmaleimide
BK_{Ca}	Ca^{2+}-sensitive K^+ channels
cADPR	cyclic ADP ribose
cGMP	cyclic guanosine monophosphate
cbEGF	calcium-binding epidermal growth factor-like
COX	cyclooxygenase
CPA	cyclopiazonic acid
DCF	dichlorodihydrofluorescein diacetate
DMSO	dimethyl sulfoxide
E_m	membrane potential
E_{max}	maximal response
E_{NCX}	NCX reversal potential
EC_{50}	half-maximum response
EDHF	endothelium-derived hyperpolarizing factor
EDTA	ethylenediaminetetraacetic acid
EGTA	ethylene glycol tetraacetic acid
ER	endoplasmic reticulum
FBN	fibrillin
GFP	green fluorescent protein
HA1	hemagglutinin
HEPES	4-(2-hydroxyethyl)-1-piperazineethanesulfonic acid
H_2O_2	hydrogen peroxide
I_{CRAC}	Ca^{2+}-release activated Ca^{2+} current
INDO	indomethacin
IP_3	inositol 1,4,5-trisphosphate
IP_3R	inositol-1,4,5-triphosphate receptor
KB-R7943	2-(2-(4-(4-Nitrobenzyloxy)phenyl)ethyl)isothiourea
KCl	potassium chloride
LAP	latency-associated protein
L-NAME	N_ω-Nitro-L-arginine methyl ester
LTBP	latent TGF-β binding protein
MLCK	myosin light chain kinase
MLCP	myosin light chain phosphatase
Na^+/K^+ ATPase	Na^+/K^+ pump
NCX	Na^+/Ca^{2+} exchanger

NMDA	N-methyl-D-aspartic acid
NO	nitric oxide
NSCC	non-selective cation channel
OAG	1-Oleoyl-2-acetyl-sn-glycerol
pD_2	negative logarithm
PE	phenylephrine
PGI_2	prostacyclin
PI	phosphoinositol
PIP_2	phosphatidyl 4,5-bisphosphate
PKC	protein kinase C
PKG	cGMP-dependent protein kinase
PLC	phospholipase C
PM	plasma membrane
PMA	phorbol ester 12-tetradecanoylphorbol-13 acetate
PMCA	plasma membrane Ca^{2+} ATPase
PSS	physiological saline solution
RyR	ryanodine receptor
ROC	receptor operated channel
SEM	mean ± standard error
SERCA	sarco/endoplasmic reticulum Ca^{2+} ATPase
SOC	store-operated channel
SOCE	store-operated Ca^{2+} entry
SOD	superoxide dismutase
SKF-96365	1-[β-(3-(4-Methoxyphenyl)propoxy)-4-methoxyphenethyl]-1H-imidazole hydrochloride, 1-[2-(4-Methoxyphenyl)-2-[3-(4-methoxyphenyl)propoxy]ethyl]imidazole
SNP	sodium nitroprusside
SR	sarcoplasmic reticulum
STIM1	stromal-interacting molecule 1
TGFβ	transforming growth factor beta
TRP	transient receptor potential
TRPC	transient receptor potential canonical
TRPM	transient receptor potential melastatin
TRPV	transient receptor potential vanilloid
TRPP	transient receptor potential polycystic
TRPML	transient receptor potential mucolipin
TRPN	no mechanoreceptor potential C
UTP	uridine 5'-triphosphate
VSMC	vascular smooth muscle cell

ACKNOWLEDGEMENTS

I would like to express my sincere gratitude to my co-supervisors Dr. Cornelis van Breemen and Dr. Kuo-Hsing Kuo, for their excellent scientific guidance, never-ending support, and personal help during my PhD studies. Their scientific knowledge and belief in my abilities have made this thesis possible. I am grateful to my supervisory committee members, Dr. David Fedida and Dr. Ed Moore, for all their insights and suggestions on my projects. I also owe a special thanks to Dr. Ada Chung for sharing her knowledge and experience with me, as well as providing technical and moral support. To all of my labmates at the Child and Family Research Institute, I thank you for all your support and for making my time in the laboratory an enjoyable one. Finally, I would also thank Dr. Chun Seow for giving me with an opportunity work in his laboratory for my directed studies project.

I would like to recognize and thank my parents and my sister for all their love, encouragement, and continual support throughout the years. And to my fiancé Christine Cheung, I thank you for always being so patient and supportive of my work.

Finally, I would like to acknowledge the Natural Sciences and Engineering Research Council of Canada and the Michael Smith Foundation for Health Research for their financial support during my training.

CO-AUTHORSHIP STATEMENT

CHAPTER 2: ATP PROMOTES NCX-REVERSAL IN AORTIC SMOOTH MUSCLE CELLS BY DAG-ACTIVATED NA^+ ENTRY

Damon Poburko, Harley Syyong, and Cornelis van Breemen developed the experimental design and protocols. Harley Syyong and Nicola Fameli performed all the experiments, and Harley Syyong analyzed the data. Harley Syyong and Damon Poburko contributed to the writing of the manuscript, which was revised by Cornelis van Breemen.

CHAPTER 3: MECHANISM OF ASYNCHRONOUS CA^{2+} WAVES UNDERLYING AGONIST-INDUCED CONTRACTION IN THE RAT BASILAR ARTERY

Harley Syyong and Cornelis van Breemen developed the experimental design and protocols. Harley Syyong, Huei-Hsin Clarice Yang, Gina Trinh, and Christine Cheung performed all the animal experiments, and data was analyzed by Harley Syyong. KuoHsing Kuo provided an electron micrograph of the basilar artery smooth muscle cell. Harley Syyong wrote the manuscript which was revised by Cornelis van Breemen.

CHAPTER 4: DYSFUNCTION OF ENDOTHELIUM AND SMOOTH MUSCLE CELLS IN SMALL ARTERIES OF A MOUSE MODEL OF MARFAN SYNDROME

Harley Syyong, Ada Chung, and Cornelis van Breemen developed the experimental design and protocols. Harley Syyong and Huei-Hsin Clarice Yang performed all the animal experiments. The data was analyzed by Harley Syyong, Ada Chung, and Cornelis van Breemen. Harley Syyong wrote the manuscript which was revised by Ada Chung and Cornelis van Breemen.

CHAPTER 1 – INTRODUCTION

1.1 Organization and function of the vasculature

The innermost layer (tunica intima) of the vasculature consists of endothelial cells that provide a continuous lining against the blood. The endothelial cells control the leakage of fluid and proteins from the blood, prevent coagulation, and regulate smooth muscle contraction and differentiation through paracrine signaling (Ross, 1993; Toborek and Kaiser, 1999). The endothelium connects to a thin basal membrane, and in larger arteries there is also a subendothelial layer containing an extracellular mesh and some smooth muscle cells. The next layer is the tunica media, which contains smooth muscle cells enclosed in a basement membrane and suspended in a fibrous extracellular matrix. Elastic laminae are also located between smooth muscle cell layers in larger arteries. The matrix and laminae serve to withstand transmural pressure and to transmit tension to and from the smooth muscle cells. The matrix binds several enzymes and hormones and also influences smooth muscle cell properties by allowing adhesion (Carey, 1991; Ross, 1993). The thickness of the medial layer, the occurrence of elastic laminae, and the orientation of smooth muscle cells all vary between segments of the vasculature. Generally, smooth muscle cells have circular or helical orientation around the vessel lumen, while in some vessels a layer of smooth muscle is also oriented along the longitudinal axis of the cell. The outermost layer of the vascular wall (tunica adventitia) consist of loose connective tissue, longitudinal bundles of smooth muscle cells (primarily in large veins), minute blood vessels (vaso vasorum, in large arteries), and a network of autonomous nerve fibers (Wagenseil and Mecham, 2009).

The main function of vascular smooth muscle is to control the blood flow to tissues and organs, providing the primary route of transportation for nutrients, immune cells, and signaling

molecules in the body. This is achieved by regulating the resistance to flow, which in turn is the basis for a maintained blood pressure. Interactions with other cells (nerve endings, endothelia, and smooth muscle cells), with humoral (circulating hormones and nutrients) and physical factors (blood pressure, blood flow) determine if the vascular smooth muscle will contract, relax, or maintain pressure. In their contractile phenotype, the basic physiological role of vascular smooth muscle is to regulate the diameter of the vessel lumen in order to control perfusion pressure and direct regional blood flow. The control of vascular tone is modulated by numerous factors, such as perfusion pressure, autonomic stimuli, paracrine and autocrine receptor ligands, and oxygen tension (Mchedlishvili, 1980; Zang *et al.,* 2006). However, in damaged vessels, smooth muscle cells can differentiate into a secretory/proliferative phenotype to assist with blood vessel repair (Schwartz *et al.,* 1986). In both phenotypes, changes in the free ionic concentration of Ca^{2+} in the cytosol play a central role in the regulation of multiple functions of smooth muscle. However, with increasing age, poor diet, and lack of exercise, regulation of vascular smooth muscle becomes increasingly prone to failure which can lead to hypertension, vasospasm, and other malfunctions (Ferrari *et al.,* 2003, Proctor and Parker, 2006).

1.1.1 Endothelium

The vascular endothelium consists of a continuous monolayer of cells, lining the luminal surface of the entire vascular system, which provides a structural and metabolic barrier between the blood and the underlying tissues. Endothelial cells are induced to migrate during the process of new capillary blood formation and during repair of the endothelial lining which result from injury of large vessels. The endothelium plays a central role in the regulation of the vascular tone (Furchgott and Zawadzki, 1980), releasing a variety of vasoactive mediators, including

prostaglandins, nitric oxide (NO), and endothelium-derived hyperpolarizing factor (EDHF) to regulate smooth muscle contractility and thus vascular smooth muscle tone (Ramsey *et al.,* 1995; Boutouyrie *et al.,* 1997; Wilkinson *et al.,* 2002; Vanhoutte, 2004).

Within vessels, the endothelial and the smooth muscle cells are separated by connective tissue and the internal elastic membrane. However, these two cell types also establish close contacts with each other, via myo-endothelial bridges that cross fenestration of the internal elastic lamina (Emerson and Segal, 2000; Sandow and Hill, 2000).

1.1.2 Overview of smooth muscle

Smooth muscle comprises the medial layers in the walls of most hollow organs, including the gastrointestinal tract, urogenital tract, and the vasculature, and is a subject of study due to its ability to regulate lumen diameter (Halayko *et al.,* 1997). The term "smooth" refers to the histological appearance of the muscle, which in contrast to skeletal and cardiac muscle does not exhibit striations. The spindle shaped single cells are generally 50-100 μm long and 2-5 μm thick (Bolton *et al.,* 1999). While, t-tubules and elaborate neuromuscular junctions are absent, the sarcoplasmic reticulum (SR) is still well-developed, occupying 1.5–7.5% of the total cell volume (Devine *et al.,* 1972). Neurotransmitters such as acetylcholine or norepinephrine may activate or inhibit smooth muscle cells by diffusing and interacting with specific receptors on the plasma membrane (PM). Smooth muscle is important clinically as it plays a primary role in the pathogenesis of fibroproliferative disorders of the vascular wall associated with diseases such as atherosclerosis (Halayko *et al.,* 1997).

1.1.3 Mechanism of smooth muscle contraction

Each smooth muscle cell contains thick (myosin) and thin (actin) filaments that slide against each other to produce contraction of the cell. The thick and thin filaments are anchored to dense bodies throughout the cytosol and dense bands (or plaques) at the PM (Somlyo, 1985). Smooth muscle contraction is regulated by Ca^{2+}-dependent myosin light chain kinase (MLCK) activation and myosin light chain phosphatase (MLCP) (Kamm and Stull, 1985). Cytosolic free ionic Ca^{2+} is the primary second messenger linking membrane excitation or stimulation to the contraction of smooth muscle cells. During smooth muscle activation, Ca^{2+} levels may increase rapidly to above 10^{-6} M (Sato *et al.,* 1988; Karaki, 1997). This is due to the opening of Ca^{2+} channels in the PM and in intracellular Ca^{2+} stores, where Ca^{2+} is also present at high concentrations. Elevation of Ca^{2+} promotes the binding of 4 Ca^{2+} ions to calmodulin, forming a Ca^{2+}-calmodulin complex which then binds to and activates MLCK. Activated MLCK then phosphorylates the myosin light chain and stimulate the acto-myosin cross-bridge cycling (Rembold and Murphy, 1990; Allen and Walsh, 1994). The activity of MLCK is opposed by MLCP, and the opposing actions of MLCK and MLCP on myosin phosphorylation can also be modulated by Ca^{2+}-independent phosphorylation events, causing an apparent shift in the Ca^{2+} sensitivity of the myofilaments. For example, Rho-kinase can phosphorylate MLCP and impair its dephosphorylation of myosin, thereby favouring contraction (Sward *et al.,* 2003). Phosphorylation of the actin-associated proteins, caldesmon and calponin, also regulate their inhibitory effect on cross-bridge cycling (Allen and Walsh, 1994; El-Mezgueldi, 1996). Relative to cardiac and skeletal muscles, smooth muscle can maintain tension with much less energy expenditure by virtue of a prolonged association of actin and myosin upon myosin dephosphorylation, known as “latch-state” (Hai and Murphy, 1988; Paul, 1990). This model has been expanded into an 8-state model, which

further accounts for the phosphorylation of the thin actin filament (Hai and Kim, 2005), and future iterations may include regulatory influences of proteins such as Rho-kinase.

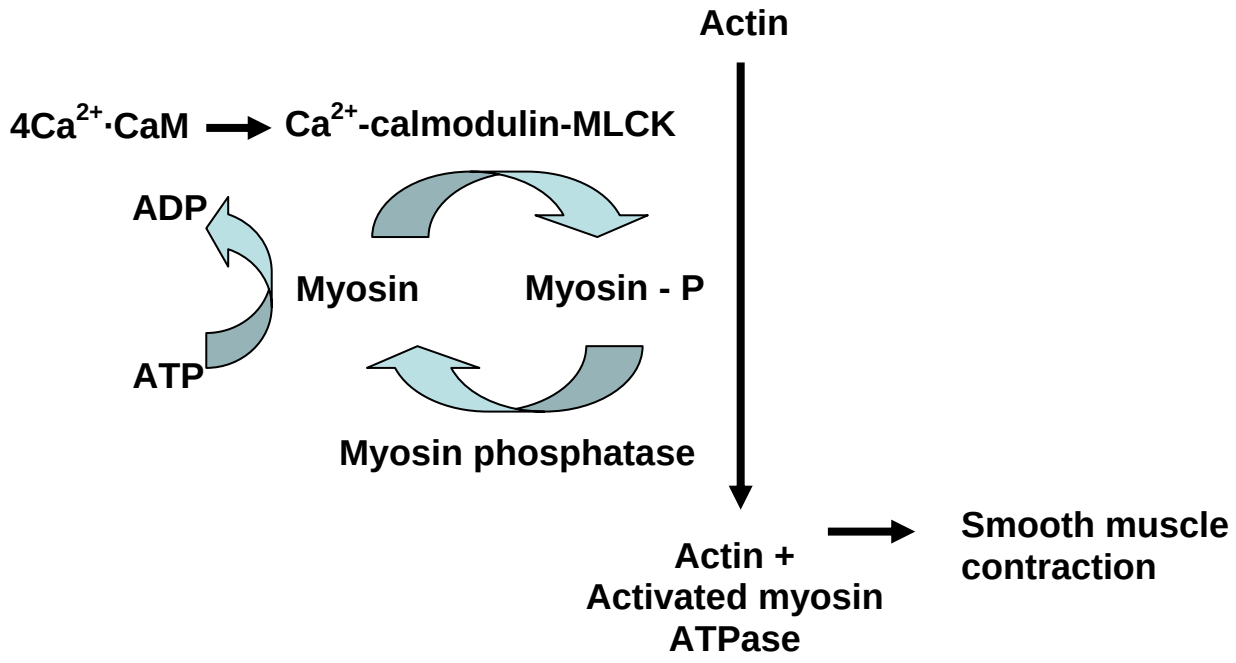

Figure 1.1: Ca^{2+}, calmodulin, MLCK (myosin light-chain kinase), and cross-bridge cycle in smooth muscle. A schematic diagram depicting the activation of the cross-bridge cycle in the smooth muscle cell is shown.

1.2 Mechanisms of Ca^{2+} homeostasis and signaling in vascular smooth muscle

In order for cytosolic Ca^{2+} to increase and stimulate the contractile apparatus or other Ca^{2+} dependent processes, Ca^{2+} must enter the cytosol from the extracellular space or be released into the cytosol from the SR. This section describes the routes by which Ca^{2+} can enter the cytosol.

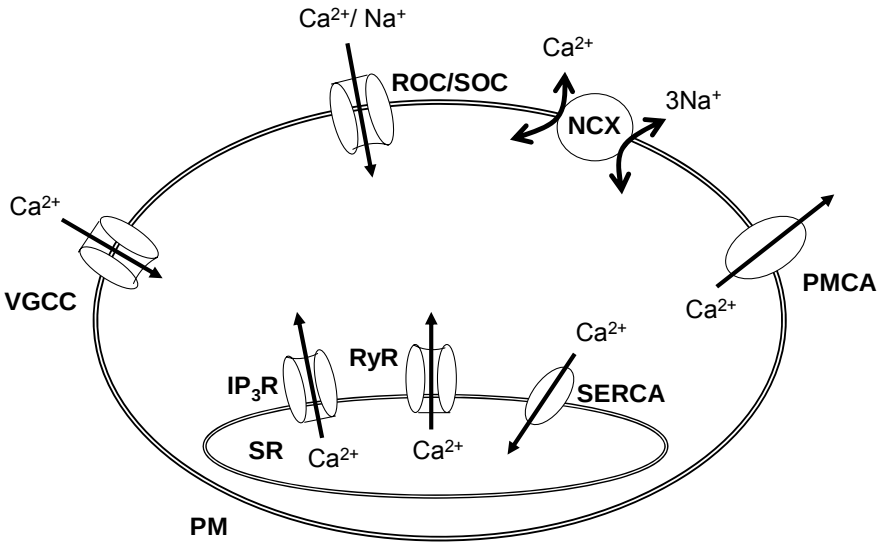

Figure 1.2 Ion channels and receptors involved in regulating intracellular Ca^{2+} concentration in smooth muscle cells. (PM, plasma membrane; SR, sarcoplasmic reticulum; VGCC, voltage-gated Ca^{2+} channel; NCX, Na^{+}/Ca^{2+} exchanger; ROC, receptor-operated channel; SOC, store-operated channel; PMCA, plasma membrane Ca^{2+} ATPase; IP_3R, IP_3 receptor; RyR, ryanodine receptor; SERCA, sarco-endoplasmic reticulum Ca^{2+}-ATPase).

1.2.1 Voltage-gated Ca^{2+} channels

The most important Ca^{2+} channels in vascular smooth muscle are the voltage-operated channels on the PM, of which there are six subtypes. However, only the L-type voltage-gated Ca^{2+} channel is considered to be a major Ca^{2+} influx pathway in smooth muscle (Kuriyama *et al.,* 1995). Due to both voltage-activating and inactivating mechanisms, a window current is defined by the voltages at which L-type Ca^{2+} channels are capable of sustained openings and inward current (Cohen and Lederer, 1987). Although this sustained Ca^{2+} current is smaller than the initial transient currents, it still generates a large Ca^{2+} influx relative to the cell volume (Sanders, 2001). Furthermore, L-type Ca^{2+} channels are modulated by several signaling systems,

particularly activated by vasoconstrictors that activate the protein kinase C (PKC) pathway (Hughes and Bolton, 1995). Additionally, vasodilators that stimulate the production of cyclic-AMP and activate protein kinase A have been reported to both activate and inhibit these channels (Jackson, 2000). These channels are inhibited by increases in $[Ca^{2+}]_i$, dihydropyridines such as nifedipine and other antagonists such as diltiazem (Triggle, 1999; Catterall, 2000).

1.2.2 Receptor-operated and store-operated cation channels

The concept of receptor- and store-operated channels in smooth muscle was introduced over 30 years ago (van Breemen *et al.,* 1978; Bolton, 1979; Casteels and Droogmans, 1981; Bolton and Large, 1986), and it has been known since 1981 that depletion of SR Ca^{2+} stores and activation of G-protein coupled receptors can activate Ca^{2+} influx by mechanisms independent of membrane depolarization through what have been termed store-operated channels (SOC) and receptor operated channels (ROC). ROCs are activated by agonists activating on a range of G-protein coupled receptors, while SOCs are activated following depletion of the Ca^{2+} stores within the SR. It is important to note that receptor-operated currents have shown varying degrees of selectivity for Ca^{2+}, so these channels are sometimes termed non-selective cation channels (NSCCs).

Store-operated Ca^{2+} entry (SOCE) was proposed as a mechanism for receptor-regulated Ca^{2+} influx that allows refilling of the intracellular Ca^{2+} pool once agonist stimulation has finished (Rosado, 2006; Putney, 2007). SOCE involves a number of non-selective Ca^{2+} permeable channels with different biophysical properties. The first identified store-operated channel current, I_{CRAC} (Ca^{2+}-release activated Ca^{2+} current), is mediated through a non-voltage activated, inwardly rectifying channel that is highly selective for Ca^{2+} (Hoth and Penner, 1992; Zweifach and Lewis,

1993; Parekh and Putney, 2005). The nature of the channels that conduct I_{CRAC} has been a matter of investigation and debate. Recently, the protein Orai1 has been proposed to form the pore of the channel mediating I_{CRAC} (Feske *et al.,* 2006; Peinelt *et al.,* 2006; Prakriya *et al.,* 2006; Vig *et al.,* 2006; Zhang *et al.,* 2006). Along with two other subtypes (Orai2 and Orai3), heteromultimetric complexes can be formed that share a high selectivity for Ca^{2+} (Lis *et al.,* 2007). The channel formed by Orai1 has been reported to be regulated by Ca^{2+} store depletion with the participation of an intraluminal Ca^{2+} sensor, stromal-interacting molecule 1 (STIM1), a transmembrane protein located in the SR, which has been identified as the intraluminal Ca^{2+} sensor that communicates the amount of stored Ca^{2+} to the PM SOC channels (Liou *et al.,* 2005; Roos *et al.,* 2005). STIM1 physically moves from locations throughout the membrane of the Ca^{2+} stores to accumulate in regions close to the PM (Wu *et al.,* 2006). The aggregation of STIM1 underneath the PM induces Orai1 clustering at discrete sites in the PM directly opposite to STIM1 clusters, resulting in the activation of SOCE (Xu *et al.,* 2006; Barr *et al.,* 2008).

The transient receptor potential (TRP) proteins have also been suggested as components of SOCs. A number of mammalian homologues of TRP have been found and are classified into three major subfamilies closely related to TRP (transient receptor potential canonical, TRPC; transient receptor potential vanilloid, TRPV; transient receptor potential melastatin, TRPM), two subfamilies that are more distantly related to TRP (transient receptor potential polycystic, TRPP; transient receptor potential mucolipin, TRPML), and a less related no mechanoreceptor potential C (TRPN) group that is expressed in flies and worms (Montell *et al.,* 2002). TRP channels are mostly nonselective for monovalent and divalent cations ($P_{Ca}/P_{Na} \leq 10$), with exceptions including TRPM4 and TRPM5, which shows a great selectivity for monovalent cations, and the

Ca^{2+}-selective TRPV5 and TRPV6. As with Orai proteins, TRP channels lack voltage sensitivity (Venkatachalam and Montell, 2007).

Particular attention has been paid to members of the TRPC subfamily, which has seven related members designated TRPC1-7. These can be divided subgroups: (i) TRPC3, TRPC6 and TRPC7 channels; and (ii) TRPC1, TRPC4 and TRPC5 channels, based on biochemical and functional similarities (Parekh and Putney, 2005), although TRPC2 is a pseudogene in humans and is not functional (Wes *et al.,* 1995). TRPC1 is suggested to be involved in SOCE in both vascular smooth muscle and endothelial cells (Liu *et al.,* 2000; Brough *et al.,* 2001; Xu and Beech, 2001; Rosado *et al.,* 2002). A role for TRPC3 was demonstrated when overexpression enhances SOCE (Zhu *et al.,* 1996; Zhu *et al.,* 1998), while suppression leads to the disappearance of SOCs (Kaznacheyeva *et al.,* 2007). TRPC4 is suggested to be an important component of the channel supporting I_{CRAC}-like currents, which are small currents activated by extracellular Ca^{2+} (Fatherazi *et al.,* 2007). A role for TRPC6 in SOCE has also been proposed in human platelets (Hassock *et al.,* 2002). Thus far, a role for TRPC7 has not been elucidated.

The involvement of TRP proteins as components of SOC has received support from studies reporting that STIM1 directly or indirectly regulates all TRPC proteins, with the exception of TRPC7, in cells with depleted Ca^{2+} stores. For example, STIM1 and TRPC1 have been shown to interact upon Ca^{2+} store depletion (Huang *et al.,* 2006; Lopez *et al.,* 2006). STIM1 has also been reported to interact directly with TRPC2, TRPC4 and TRPC5. Furthermore, STIM1 mediates the interaction of TRPC1 with TRPC3 and of TRPC4 with TRPC6. TRPC hetermultimerization is enhanced by Ca^{2+}-mobilizing agonists, suggesting that store depletion-induced clustering of STIM1 is required for the formation of heteromeric SOCs (Yuan *et al.,* 2007). The number of putative SOCs formed by heteromultimerization of channel subunits has been considerably

enhanced by the demonstration that Orai proteins interact with TRPCs. The interaction of Orai proteins with TRPCs has been reported to confer STIM1-mediated store depletion sensitivity to SOCs (Liao *et al.,* 2007).

Additionally, TRPCs have also been suggested to play a role in receptor-mediated Ca^{2+} entry (Venkatachalam *et al.,* 2002; Clapham, 2003; Freichel *et al.,* 2004; Dietrich *et al.,* 2005a; Dietrich *et al.,* 2005b; Montell, 2005; Parekh and Putney Jr, 2005). Receptor-induced Ca^{2+} signals are crucial to the function of all cells (Berridge *et al.,* 2003) and involve both the release of Ca^{2+} from stores and the entry of Ca^{2+} through channels in the PM (Venkatachalam *et al.,* 2002; Berridge *et al.,* 2003; Parekh and Putney Jr, 2005). ROCs are thought to be activated by diacylglycerol (DAG) that is generated following hydrolysis of phosphatdyl inositol by phospholipase C (Thebault *et al.,* 2005).

The first ROC to be described in vascular smooth muscle was a noradrenaline-evoked cation conductance in rabbit portal vein myocytes (Byrne and Large, 1988). The activation of these channels involves the classical G-protein-coupled phosphoinositol (PI) system, involving stimulation of PI-phospholipase C (PLC) and the production of DAG (Helliwell and Large, 1997). A surprising and novel result from the latter study was that the generation of endogenous DAG, as well as DAG analogs, activated ROCs via a PKC-independent mechanism. Gating by DAG of several NSCCs has been subsequently described, including TRPC3/6/7 channel proteins expressed in cell lines (Hofmann *et al.,* 1999; Inoue *et al.,* 2001; Estacion *et al.,* 2004; Shi *et al.,* 2004) and it has been shown that TRPC6 and TRPC3 proteins are components of native ROCs in portal vein and cerebral artery myocytes (Inoue *et al.,* 2001; Reading *et al.,* 2005).

One functional characteristic distinguishing the two TRPC subgroups is the ability of DAG to activate TRPC3/6/7 channels, but not the TRPC1/4/5 channels (Hoffman *et al.,* 1999;

Venkatachalam *et al.,* 2003; Freichel *et al.,* 2004; Dietrich *et al.,* 2005a; Dietrich *et al.,* 2005b; Parekh and Putney Jr., 2005). DAG appears to have an important dual role in TRPC channels; in addition to rapidly activating TRPC3 channel directly, DAG also mediates a slower PKC-mediated deactivation of the TRPC3 channel (Venkatachalam *et al.,* 2003; Estacion *et al.,* 2006). This bimodal regulation may form the basis of a spectrum of regulatory phenotypes of expressed TRPC channels.

Finally, although the opening of ROCs mediates Ca^{2+} influx, it should be noted that the extracellular concentration of Na^{+} is ~100 fold higher than that of Ca^{2+}. Therefore, the opening of these channels also mediates substantial Na^{+} influx, changing the concentration gradient of Na^{+} to favour reversal of the Na^{+}/Ca^{2+} exchanger and bring Ca^{2+} into the cell (Lee *et al.,* 2001).

1.2.3 Ryanodine and IP_3 receptors

In addition to being an intracellular Ca^{2+} storage site, the SR also releases Ca^{2+} upon activation. Release of Ca^{2+} from the SR is mediated by two types of Ca^{2+} channels: ryanodine-sensitive receptors (RyR) and inositol 1,4,5-trisphosphate (IP_3)-sensitive receptors (IP_3R), each of which is expressed in three isoforms. Both channels are essentially gated by local [Ca^{2+}], such that cyclic ADP-ribose (cADPR) and IP_3 alter the Ca^{2+} affinity of the RyR and IP_3R, respectively. Release of SR Ca^{2+} induced by PLC-linked receptors, such as α-adrenergic receptors, is often associated with the production of IP_3 and subsequent activation of IP_3R (Karaki *et al.,* 1997). In contrast, relatively little is known about linkage between ryanodine receptor activation and the production of cADPR by ADP ribose cyclase (Bai *et al.,* 2005). Rather, the activation of RyR is most often attributed to Ca^{2+}-induced Ca^{2+} release in response to local elevation of Ca^{2+} (Bolton *et al.,* 1999; Gordienko *et al.,* 1998; Putney, Jr., 1993). However,

despite the fact that both receptors release Ca^{2+} into the cytosol, evidence suggests that they may be localized to separate elements of the SR (Golovina and Blaustein, 1997; McGeown, 2004), which may allow each receptor to regulate specific processes in the cell. However, others have suggested that the IP_3R and RyR both access a common SR Ca^{2+} store (Saida and van Breemen, 1984; Lepretre and Mironneau, 1994; McCarron and Olson, 2008).

1.2.3.1 Ryanodine receptors

Named due to their binding to the plant alkaloid ryanodine, the RyRs are endogenously regulated by $[Ca^{2+}]_i$. Three isoforms of RyRs exist, although only RyR2 and RyR3 have been identified in smooth muscle. At low concentrations (<100 μM), ryanodine causes a persistent subconductance state of the channels which may lead to store depletion (Endo, 1977; Rousseau *et al.,* 1987; Hymel *et al.,* 1988; Kanmura *et al.,* 1988; Iino, 1989; Xu *et al.,* 1994), while higher concentrations lock RyRs in a closed state to inhibit Ca^{2+} release (Hayek *et al.,* 2000; Fill and Copello, 2002). This regulation is due to the presence of high- and low- affinity binding sites on the RyR for Ca^{2+} (Marx *et al.,* 2000). In addition, the Ca^{2+}-binding protein calsequestrin located in the SR may be positioned close to and perhaps co-localized together with RyRs (Berchtold *et al.,* 2000; Moore *et al.,* 2004) via junction and triadin proteins (Guo and Campbell, 1995; Zhang *et al.,* 1997) and may enhance opening of the RyRs (Szegedi *et al.,* 1999) when phosphorylated. Xanthines such as caffeine are often used as a tool to empty the SR, as they increase the Ca^{2+} sensitivity of the RyR (Smith *et al.,* 1988; Sitsapesan and Williams, 1990).

The opening of RyRs in smooth muscle are also responsible for the production of Ca^{2+} sparks, localized Ca^{2+} transients which can reach concentrations of 1-10μM, while increasing global intracellular $[Ca^{2+}]$ by <2nM (Jaggar *et al.,* 1998; Nelson *et al.,* 1995; Jaggar *et al.,* 2000).

Ca^{2+} sparks appear to represent the simultaneous activation of a cluster of RyRs, and were proposed to be responsible for the activation of a number of nearby Ca^{2+}-sensitive K^+ channels (BK_{Ca}) on the PM to cause a macroscopic current that was previously described as a spontaneous transient outward current (Benhan and Bolton, 1986; Nelson *et al.,* 1995). BK_{Ca} are uniquely suited to respond to very high local $[Ca^{2+}]$ because they require micromolar $[Ca^{2+}]$ for their activity under physiological conditions (Perez *et al.,* 1999). The opening of BK_{Ca} can hyperpolarize the cell membrane by up to 20mV, providing an important contribution to regulation of vascular tone (Ganitkevich and Isenberg, 1990). Ca^{2+} sparks can also activate spontenaous transient inward currents, which are caused by the opening of Ca^{2+}-sensitive Cl^- channels, resulting in cell membrane depolarization (ZhuGe *et al.,* 1998).

1.2.3.2 IP_3 receptors

Since the demonstration of receptor-mediated PLC activation, Ca^{2+} release in response to IP_3 and the purification and cloning of IP_3Rs, inositol phosphate signaling has been rapidly accepted as an important cellular second messenger system (Berridge, 1993). G protein-linked receptors activate G proteins in the PM which stimulate PLC to split phosphatidyl 4,5-bisphosphate (PIP_2) into DAG and IP_3. DAG activates protein kinase C (PKC), and IP_3 binds to and gates a distinct class of intracellular, endoplasmic reticulum-bound IP_3 receptor channels. The resulting Ca^{2+} release increases $[Ca^{2+}]_i$ within seconds to micromolar concentrations. The Ca^{2+} diffuses to adjacent IP_3Rs (and also RyRs in many cells) channels, initiating the release of more Ca^{2+}.

A biphasic relationship exists between the open probability of IP_3R and Ca^{2+} release (Iino, 1990; Bezprozvanny *et al.,* 1991; Mak *et al.,* 1998), as $[Ca^{2+}]_i$ of ~300 nM provides optimal activation of IP_3R by IP_3, while higher concentrations of $[Ca^{2+}]_i$ decrease the activity of the IP_3R

(Sanders, 2001). However, due to the Ca^{2+} sensitivity of the IP_3R, the RyR may be activated when the IP_3R is no longer active. This has important implications for the participation of the RyR and IP_3R, one being able to activate the other depending on their spatial location on the SR membrane (Iino, 1999).

Heparin is a specific antagonist of IP_3R, but is impermeable to the cell membrane (Ghosh *et al.,* 1988; Kobayashi *et al.,* 1988; Supattapone *et al.,* 1988). Permeable inhibitors such as Xestospongin C (Gafni *et al.,* 1997), and 2-aminophenylborate (2-APB) (Maruyama *et al.,* 1997) are important also pharmacological tools in determining the role of IP_3R in Ca^{2+} signaling, although their selectivity has been questioned (Bilmen and Michelnageli, 2002; Ma *et al.,* 2002).

1.2.4 Ca^{2+} uptake and extrusion mechanisms

Due to the large chemical gradient of extracellular [Ca^{2+}] (2 mM) to cytosolic [Ca^{2+}] (0.1 μM) in smooth muscle, it is critical for the cell to remove Ca^{2+} and prevent accumulation of Ca^{2+}, which may be cytotoxic. Smooth muscle cells have a resting potential between -40 and -60 mV when subjected to normal levels of intravascular pressure (Nelson and Quayle, 1995), meaning that there is also a large inwardly directed electrochemical gradient for Ca^{2+} into the cell. Ca^{2+} also tends to move into resting cells (Poburko *et al.,* 2004c) and must be extruded by energy-dependent mechanisms. Calcium transporters such as the PM Ca^{2+}-ATPase (PMCA) and the sarco/endoplasmic reticulum Ca^{2+}-ATPase (SERCA) play a crucial role in maintaining Ca^{2+} homeostasis by maintaining low resting Ca^{2+} and restoring Ca^{2+} for relaxation of smooth muscle (Floyd and Wray, 2007).

Storage of Ca^{2+} in cellular organelles provides important physiological regulation and the potential for release of Ca^{2+} during physiological signaling. The main Ca^{2+} storage organelle is

the SR, and has a major role in maintaining low $[Ca^{2+}]_i$. The SR is surrounded by a membrane which is not freely permeable to Ca^{2+}, and on which SERCA pumps sit. SERCA actively sequesters cytosolic Ca^{2+} into the SR (Sanders, 2001) and maintains a 10,000-fold concentration gradient between the SR lumen and the cytosol. There are 3 genes encoding for SERCA, and in smooth muscle, the SERCA2b isoform is mainly expressed, with the SERCA2a and SERCA3 isoforms forming the remainder of the SERCA population (Lytton *et al.,* 1989; Wuytack *et al.,* 1989; Eggermont *et al.,* 1990; Amrani *et al.,* 1995; Trepakova *et al.,* 2000; Wu *et al.,* 2001). All SERCAs encode a cytoplasmic region that contains the catalytic site and a transmembrane domain that forms a channel-like structure allowing Ca^{2+} translocation across the membrane (Engelender and De Meis, 1996; Zhang *et al.,* 1998). Phospholamban is a small protein that negatively regulates SERCA; upon phosphorylation via PKC or cGMP-dependent protein kinase (PKG) (Raeymaekers *et al.,* 1990), this inhibition is relieved and SERCA is activated, thereby pumping Ca^{2+} into the SR.

After Ca^{2+} is pumped into the SR, it is buffered and sequestered by proteins such as calreticulin and calsequestrin, which bind large amounts of Ca^{2+} (Milner *et al.,* 1992; Raeymaekers *et al.,* 1993). The total concentration of Ca^{2+} in the SR has been estimated to be as high as 10-15 mM (Nishimura *et al.,* 1989). The specific reversible or irreversible inhibitors of SERCA, cyclopiazonic acid (CPA) and thapsigargin respectively, have been instrumental in understanding the importance of SERCA and the SR in regulating contraction and relaxation of smooth muscle.

Mitochondria also play an important role in Ca^{2+} homeostasis, as they regulate Ca^{2+} release events from both IP_3R and RyR which are important to the propagation of Ca^{2+} waves (Lee *et al.,* 2002; Wellman and Nelson, 2003). Mitochondria can also modulate the activity of PM ion

channels such as SOCs, L-type Ca^{2+} channels, Ca^{2+}-activated K^+ channels, and Ca^{2+}-activated Cl^- channels by buffering local Ca^{2+} gradients (Hoth *et al.,* 1997; Montero *et al.,* 2000; Thyagarajan *et al.,* 2001; Malli *et al.,* 2003a; Malli *et al.,* 2003b). This type of regulation can indirectly affect SR refilling and consequently SR release.

Two other pathways to extrude Ca^{2+} from smooth muscle cells are the PMCA and the Na^+/Ca^{2+} exchanger (NCX), the latter of which is also regulated by the Na^+/K^+ pump (Na^+/K^+-ATPase) (Blaustein and Lederer, 1999). The PMCA uses energy from ATP to pump Ca^{2+} up the electrochemical gradient from the cytosol to the extracellular space. This pump is electron neutral, as the Ca^{2+} pumped to the extracellular space is exchanged for two protons. Therefore, Ca^{2+} extrusion results in the uptake of H^+ and must be compensated by other means, such as Na^+/H^+ exchange (Lucchesi and Berk, 1995).

The NCX can operate in both the forward (Ca^{2+}-efflux) mode and the reverse (Ca^{2+}-influx) mode (Karaki *et al.,* 1997; Laporte and Laher, 1997). Regardless of the mode of operation, the coupling ratio for the NCX is 3 Na^+:1 Ca^{2+} (that is, 1 Ca^{2+} ion is exchanged for every 3 Na^+ ions) (Bolton *et al.,* 1999). Under normal resting conditions, the NCX almost always operates in the forward mode, although depending on the net electrochemical driving force, the NCX can also operate in reverse mode physiologically (Blaustein and Lederer, 1999; Lee *et al.,* 2001). This may happen at restricted subplasmalemmal areas in the cell, such as the close apposition between the PM and superficial SR, where the concentrations of Na^+, Ca^{2+}, and other ions may be different from the cytosol. NCX activity is a function of membrane potential and the local [Ca^{2+}] and [Na^+] on each side of the PM. The reversal potential of the NCX is related by the following equation:

$$E_{NCX} = 3E_{Na} - 2E_{Ca} \qquad (1)$$

In general, $E_{Xz+} = RT/(zF)\ \ln([X^{z+}]_{out}/[X^{z+}]_{in})$, where R is the universal gas constant (8.3 J/mol•K), T the absolute temperature in Kelvin, X^{z+} is a z-valent cation, and F is Faraday's constant (9.65×104 J/V•mol). Under resting conditions, using $V_m = -60$ mV (Haddock and Hill, 2005), $[Na^+]_o = 145$ mM, $[Ca^{2+}]_i = 10^{-4}$ mM, $[Ca^{2+}]_o = 1.5$ mM (Blaustein and Lederer, 1999; Alberts *et al.,* 2002), $E_{Na} = +71.3$mV and $E_{Ca} = +128$mV, which yields $E_{NCX} = -42$ mV. For NCX reversal to occur, E_{NCX} must be more negative than V_m. Therefore, because resting membrane potential is under the stated conditions is −60 mV, the NCX will generally operate in the forward (Ca^{2+}-extrusion) mode.

The NCX can be blocked by 2',4'-dichlorobenzamil (2,4-DCB) in both the forward mode (Blaustein and Lederer, 1999), while KB-R7493 at concentrations of 10 μM or less selectively block the NCX in the reverse (Ca^{2+}-influx) mode (Ladilov *et al.,* 1999). Recently, a more specific and potent NCX inhibitor, SEA0400, has been developed (Tanaka *et al.,* 2002).

1.2.5 Recombinant aequorin as a method of measuring Ca^{2+}

Aequorin is derived from the Pacific jellyfish, *Aequorea victoria*, and is a photoprotein dependent on the presence of Ca^{2+} to emit light based on the reaction shown in Fig. 1.3 (Prendergast, 2000). Aequorin is composed of 189 amino acids and has 3 EF-hand structures which bind Ca^{2+} (Head *et al.,* 2000; Hofer *et al.,* 2000). In addition, a hydrophobic region exists where the protein may interact with its functional chromophore, coelenterazine (Inouye *et al.,* 1985). This protein emits light (466 nm) in the presence of small amounts of Ca^{2+}. However, a functional aequorin molecule is only obtained after the apoaequorin has been incubated with its prosthetic group, coelenterazine and oxygen which form a stable intermediate. When Ca^{2+} binds to the complex, coelenterazine is converted to coelenteramide in an irreversible photochemical

reaction and emits light at 466 nm, which then can be detected and quantified. Aequorin offers many advantages over other standard Ca^{2+} imaging dyes, the most important being the specificity of the probe and direct Ca^{2+} measurement in the area of interest. Additionally, aequorin measurements are virtually free of any background, are extremely sensitive and are not weakened by auto fluorescence (Rizzuto *et al.,* 1994). Some limitations to the use of aequorin include its rapid and irreversible consumption by high Ca^{2+}, which limits experimental duration and design, and relatively low light output which makes it difficult to detect in single cells (Rutter *et al.,* 1996; Hofer *et al.,* 2000).

To transform luminescence values into $[Ca^{2+}]$ values, calibration requires knowledge of the total luminescence contained in the preparation. This relies on the relationship between Ca^{2+} and the ratio (L/L_{max}) between light intensity recorded in physiological conditions, which represents aequorin consumption (L), and that which would have been recorded if all of the aequorin in the cell had been suddenly exposed to a saturating Ca^{2+} (L_{max}). A good estimate of L_{max} can be obtained from the total aequorin light output recorded from the cells after discharging of all the aequorin through the lysing of the cells. As aequorin is being consumed continuously, the value of L_{max} is not constant and decreases steadily during the experiment. The value of L_{max} to be used for Ca^{2+} calculations at every point along the experiment is then calculated as the total light output of the whole experiment minus the light output recorded before that point. Generally, as Ca^{2+} is raised from low levels to high levels, a calibration curve which plots L/L_{max} vs. pCa generally yields a sigmoidal curve with a slope ranging from zero to a maximum of 3 before falling again to zero at saturating $[Ca^{2+}]$ levels. The steep cube-law relationship between aequorin consumption and $[Ca^{2+}]$ is due to the 3 Ca^{2+} binding sites on the aequorin molecule, and

it is between this range that aequorin can give the most accurate measurements (Allen *et al.,* 1977; Cobbold and Rink; 1987; Brini *et al.,* 1995).

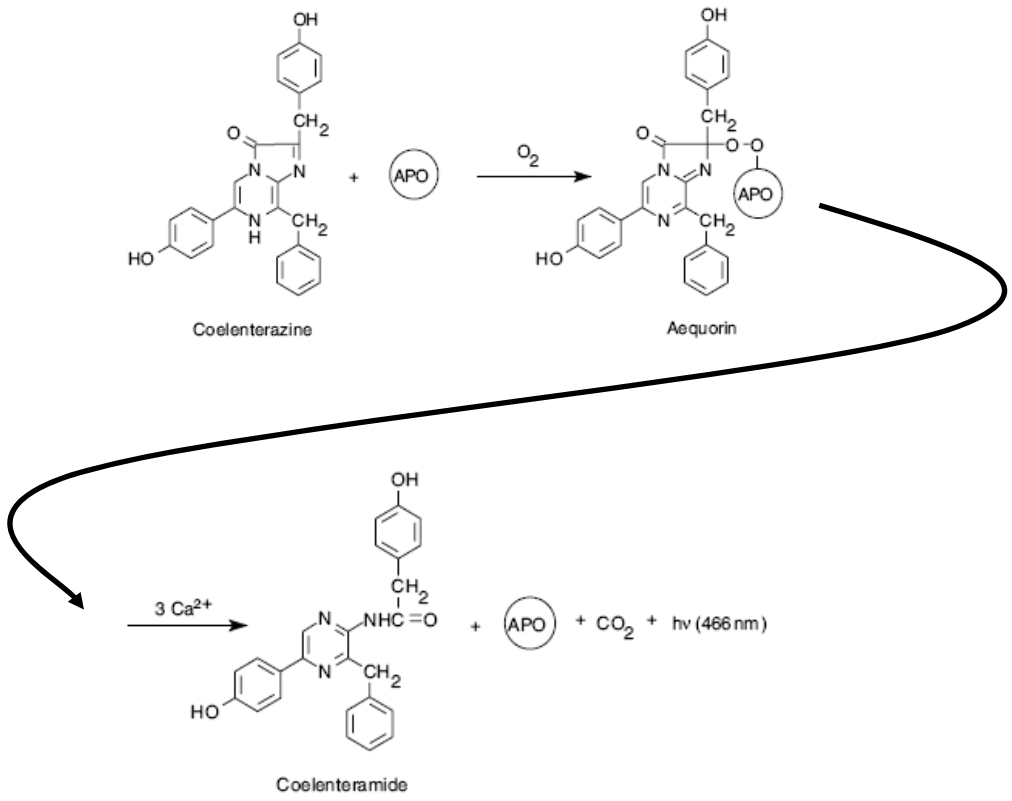

Figure 1.3: Recombination of aequorin. Upon addition of the prosthetic group CoE (coelenterazine), the apoaequorin (APO) will form the function aequorin molecule upon exposure to oxygen. Calcium molecules bind to one of three EF-hand motifs on the aequorin molecule and upon binding produces coelenteramide, the apoaequorin, carbon dioxide, and light at a wavelength of 466 nm (Prendergast, 2000; Chiesa *et al.,* 2001).

Aequorin has been used to specifically measure Ca^{2+} concentrations in various cellular compartments, such as mitochondria and SR, where previously only slightly selective membrane-permeable Ca^{2+} indicators were useful. This is due to aequorin fusing with molecular targeting sequences. Targeted aequorins have been constructed for mitochondria, ER, SR, PM, cytosol and the nucleus (Chiesa *et al.,* 2001). This targeting is achieved by an N-terminal fusion

of the photoprotein with a minimal targeting sequence as C-terminal fusions have been proven unsuccessful. These plasmids are cloned in vectors suitable for transfection, such as pcDNAI or pMT2. Charged liposomes have been used as the method of transfection into smooth muscle cells in this thesis. To ensure correct localization of the plasmids, a hemagglutinin epitope tag (HA1) between the targeting sequence and the aequorin cDNA allows immunolocalization. In addition, a green fluorescent protein (GFP) targeted to the same mitochondrial sequence as used in the aequorin plasmid targeted to the mitochondria has been made to allow for simpler identification of correct localization by imaging with confocal microscopy. Moreover, photoproteins with differing Ca^{2+} sensitivities have been created by mutation of specific amino acids. For example, changing low affinity aequorin by one amino acid (Asp 119 to Ala) modifies it to a high affinity aequorin, which when incubated with a coelenterazine analog, showed rapid millimolar Ca^{2+} transients in a new subpopulation of mitochondria (Montero *et al.,* 2000). Thus, not only can the aequorin be mutated, but coelenterazine analogs can also regulate the Ca^{2+} sensitivity of the functional photoprotein by regulating membrane permeability and regeneration rate (Shimomura *et al.,* 1989; Shimomura *et al.,* 1990; Shimomura *et al.,* 1993). This is especially important in organelles such as the SR or ER where Ca^{2+} content is high and a low affinity aequorin is required.

1.3 Nanodomains and Ca^{2+} signaling in vascular smooth muscle

Ca^{2+} regulates nearly all fast processes in the body, including contraction, chemotaxis, secretion, synaptic transmission, and several slower processes, including fertilization, proliferation, learning, memory, and apoptosis. However, it is unclear how the fluctuations in Ca^{2+} can regulate a multitude of cellular processes. Although cells have developed a variety of

Ca^{2+} sensitive, signal-transducing proteins to tailor their cell-specific regulation of many diverse processes by Ca^{2+} (Berridge *et al.,* 2003), this cannot entirely explain how multiple processes, such as cross-bridge cycling and myosin filamentogenesis in smooth muscle or endothelial nitric oxide and epoxyeicosatrienoic acid production, can be regulated simultaneously. One solution may rely on the physical and temporal separation of numerous targets for Ca^{2+}, combined with the generation of localized cytoplasmic Ca^{2+} gradients (Poburko *et al.,* 2004). For example, mitochondrial dehydrogenases, voltage-gated Ca^{2+} channels, IP_3Rs, and DNAses are located in different subcellular regions and could be selectively activated by focal Ca^{2+} signals. Moreover, activation of certain target proteins by the Ca^{2+}-calmodulin complex could be site-specific, despite the widespread intracellular distribution of calmodulin, since calmodulin can be tethered to effector complexes such as smooth muscle myofilaments (Wilson *et al.,* 2002).

In order to create Ca^{2+} signals with specific temporal and spatial characteristics, it is not sufficient to only have a large variety of ion transport molecules, but also to have these components be strategically clustered around cytoplasmic nanodomains. Analysis of the interaction of Ca^{2+} transport molecules in the PM, the SR, nuclear envelope, and mitochondria suggest that these interactions provide structural basis for the spatially and temporally encoded fluctuations in $[Ca^{2+}]_i$ that are thought to mediate site-specific Ca^{2+} signaling. This interaction takes place in two fundamentally different ways: 1) directed Ca^{2+} supply to or removal from the Ca^{2+}-sensing domains of signal transducing molecules and Ca^{2+} translocators, and 2) Ca^{2+} delivery from a transport site located in one membrane to a second Ca^{2+} transport site located in an apposing membrane. An example of the first type of interaction is the delay of Ca^{2+}-mediated inhibition of L-type Ca^{2+} channels due to nearby mitochondria sequestering Ca^{2+}. The second type of interaction is exemplified by coupling of Ca^{2+} entry through the NCX to SERCA during

store refilling (Lee *et al.,* 2002). The latter process circumvents free diffusion throughout the cytoplasm and typically takes place at organellar junctions where physically restricted diffusion of Ca^{2+} within the narrow cytoplasmic domain is further slowed down by a high density of fixed, negatively charged Ca^{2+} binding sites (Bers, 2001).

This second type of interaction occurs in nanodomains, which are formed at the sites where Ca^{2+} enters the cytoplasm at either the cell surface or at the internal stores, and are defined by the ultrastructural architecture of the cell, such as the close (nanometre-ranged) spatial association of the PM, SR and mitochondria (Poburko *et al.,* 2008; Fameli *et al.,* 2009). The resulting microstructural arrangements of the apposing membranes create diffusional barriers defining different types of junctional spaces within the cytoplasm. The diffusional limitations of these junctional spaces allow for accumulation of ions such as Na^{+} and Ca^{2+} in concentrations greatly exceeding that in the bulk cytoplasm (Rizzuto and Pozzan, 2006; van Breemen *et al.,* 2006). These cytoplasmic nanodomains have important functional implications. For example, Ca^{2+}-sensitive ion channels selective for K^{+}, Cl^{-}, and Ca^{2+} and Ca^{2+}-sensitive enzymes, such as PKC and PLC, which are located in membranes bordering the restricted space between the PM and the superficial SR, can be regulated separately from the myofilaments occupying the bulk of the cytoplasm (Berridge, 2006; Edwards and Pallone, 2007).

1.3.1 Structural and functional considerations of the PM-SR junctional nanodomain

An important physiological nanodomain is the PM-SR junction, formed by the close apposition between the superficial SR and the PM. Much of the SR is associated with the cell membrane (Devine *et al.,* 1972). The SR is composed of an interconnected tubular and sheet-like network with a volume estimated from 1.5-7.5% of the cell depending on the smooth muscle cell

type (Sanders, 2001) and is contiguous with the nuclear envelope (Somlyo, 1985; Nixon *et al.,* 1994). The SR can be classified according to its location as superficial or deep, and electron microscopy shows that the superficial SR forms a flattened pedestal as it approaches the PM, at which point it creates a narrow space which extends on average in two dimensions for about 300-400 nm and has a depth of 15-20 nm (Lee *et al.,* 2002). In vascular smooth muscle cells of the rabbit inferior vena cava, 14.2 ± 0.7% of all the PM (including the necks of caveolae) is closely associated (within 30 nm) with the superficial SR, the junctional width averages 19 ± 1 nm (Lee *et al.,* 2002), and the caveolae protrude through this thin fenestrated junctional SR (Fig 1.4) (Devine *et al.,* 1972; Darby *et al.,* 2000). The narrow cytoplasmic space between the junctional SR and PM is referred to as the PM-SR junctional space and is thought to present an imperfect barrier to diffusion of small molecules and ions, in particular Ca^{2+} and Na^{+}. This is an important physiological mechanism as it allows Na^{+} influx through SOCs/ROCs to build up to a concentration high enough to allow NCX reversal (Lee *et al.,* 2001; Poburko *et al.,* 2006). The resulting Ca^{2+} influx following NCX reversal is essential for refilling of the SR and maintaining the Ca^{2+} waves (Lee *et al.,* 2002).

The structures responsible for the remarkably consistent spacing between the PM-SR junction have not yet been identified, although in some instances "feet" similar to those seen in triadic junctions in skeletal muscle have been reported (Somlyo, 1985), and proteins called junctophilins have been isolated from the diads of cardiac muscle (Takeshima *et al.,* 2000). It is unknown what causes a particular portion of the PM to form a junction, although such junctions are common in caveolae-rich regions of the PM. The junctional PM might have specific chemical characteristics, such as those of cholesterol and sphingolipid-rich lipid rafts, which form platforms for signaling and transport molecules, or plasmalemmal receptors may be

physically linked to SR proteins such as the linkage of metabotropic glutamate receptors to SR release channels via Homer proteins (Feng *et al.,* 2002). Interestingly, the α-1d adrenoceptor contains a consensus sequence for Homer protein binding (Zhong and Minneman, 1999).

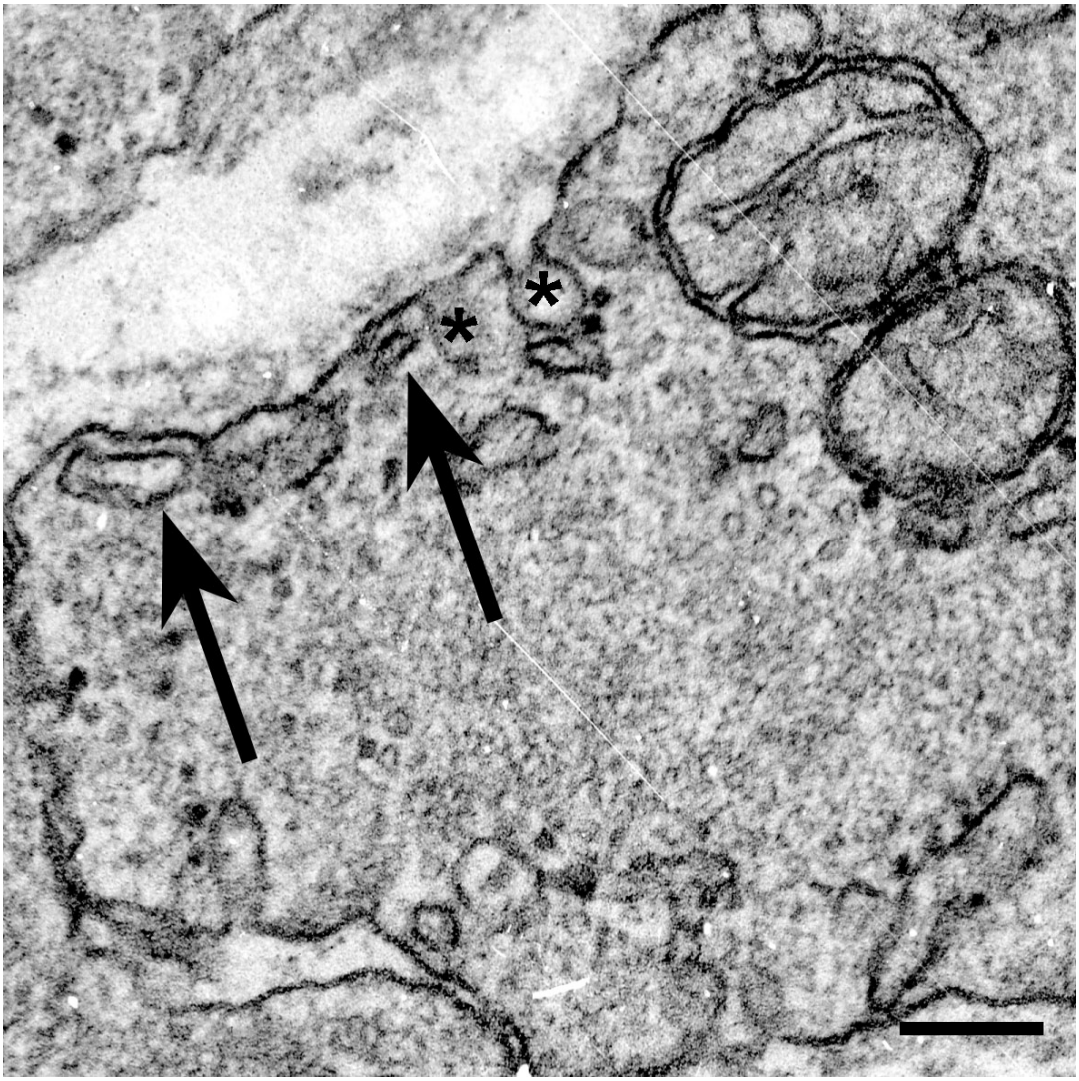

Figure 1.4: Electron microscope cross-sections of smooth muscle cells from rabbit inferior vena cava. The superficial sarcoplasmic reticulum SR (arrows) comes into close contract (~20nm) with the plasma membrane (PM), forming a flattened narrow space termed the PM-SR junction. The PM-SR junctions typically extend to the necks of the caveolae (*) on either side. The black scale bar on the lower right indicates a distance of 200 nm. Image courtesy of Dr. KuoHsing Kuo.

1.3.2 Ca^{2+} oscillations in smooth muscle

It was originally thought that the Ca^{2+} profile following agonist stimulation was a biphasic model, where agonist-mediated receptor activation initially released Ca^{2+} from the SR to initiate contraction and subsequently stimulated Ca^{2+} influx to maintain vascular tone (van Breemen *et al.,* 1978; Bolton, 1979; Streb *et al.,* 1983; Putney, 1986). However, Iino and colleagues (Iino *et al.,* 1994) provided the first description of asynchronous Ca^{2+} oscillations in rat tail artery smooth muscle cells stimulated with norepinephrine, which occurred in the form of repetitive intracellular Ca^{2+} waves that propagated along the longitudinal axis of each smooth muscle cell. The described waves did not spread intercellularly and were not synchronized between neighbouring smooth muscle cells.

Since this initial report, it has become apparent that fluctuations in the average arterial wall $[Ca^{2+}]$ observed previously (Jiang and Morgan, 1989; Meininger *et al.,* 1991) are not representative of Ca^{2+} events within individual smooth muscle cells. Ca^{2+} oscillations have also been described in a variety of other smooth muscle preparations (Boittin *et al.,* 1999; Miriel *et al.,* 1999; Ruehlmann *et al.,* 2000; Jaggar and Nelson, 2000; Bergner and Sanderson, 2002; Perez and Sanderson, 2005; Dai *et al.,* 2007). In large veins and arteries agonist-mediated force development is regulated by recruitment of cells and the frequency of asynchronous, agonist-induced Ca^{2+} oscillations that are primarily generated by the release of Ca^{2+} from the SR (Evans and Sanderson, 1999; Ruehlmann *et al.,* 2000). Agonist-induced contractions are maintained by asynchronous wave-like Ca^{2+} oscillations in single smooth muscle cells, which summate to give a steady-state elevation in Ca^{2+} for the whole tissue (Ruehlmann *et al.,* 2000).

The fact that asynchronous Ca^{2+} oscillations are observed in various smooth muscle cell types across different species has led to speculation of underlying physiological reasons for this

form of signaling. One physiological advantage may be related to the efficacy of Ca^{2+} oscillations in activating contraction. Contractile force is significantly decreased when Ca^{2+} oscillations are abolished by inhibition of SR Ca^{2+} re-uptake, although the average $[Ca^{2+}]_i$ remains elevated (Lee *et al.,* 2001; Sward *et al.,* 2003). This observation indicates a higher force-to-Ca^{2+} ratio when smooth muscle cells are activated with asynchronous Ca^{2+} waves as compared to sustained Ca^{2+} elevation. It has also been proposed that wave-like Ca^{2+} oscillations may be more efficient in activating myofilaments because they utilize the SR network, which penetrates deep into the myoplasm, to deliver Ca^{2+} directly to the myofilaments. This is supported by the fact that myofilaments are not typically observed in the periphery of smooth muscle cells (Lee *et al.,* 2002).

Furthermore, mitochondria contain several Ca^{2+}-sensitive dehydrogenases, and oscillatory Ca^{2+} signaling could serve to modulate frequency-encoded Ca^{2+} sensitive mitochondrial dehydrogenases and gene expression (Poburko *et al.*, 2004a,b). Indeed, it has also been shown in hepatocytes that ER-mediated Ca^{2+} oscillations can efficiently activate certain Ca^{2+}-sensitive dehydrogenases in the mitochondria (Hajnóczky *et al.,* 1995). Finally, since an excessive amount of Ca^{2+} may produce deleterious effects in the cell, an oscillatory rise in Ca^{2+} with efficient delivery of Ca^{2+} to the target myofilaments may minimize the activation of unintended processes such as apoptosis, by avoiding overloading of the cell with an excessive amount of Ca^{2+} over a prolonged period of time.

1.3.3 Mechanism underlying Ca^{2+} oscillations

Although Ca^{2+} oscillations have been observed in vascular smooth muscle for years, their molecular mechanism remains to be fully elucidated. This may be due to the fact that different

blood vessels display different types of rhythmic activity, which impedes consensus between different laboratories. So far, the most detailed description of the ionic mechanism of smooth muscle Ca^{2+} oscillations has been provided for adrenergically stimulated rabbit inferior vena cava (Lee *et al.*, 2002). In this scenario, the initial α_1-receptor stimulation activates PLC which catalyzes the synthesis of IP_3. This leads to SR Ca^{2+} release from IP_3R, which spreads across the cell from Ca^{2+} wave initiation sites. Stimulation of the α_1-receptor or depletion of the SR also leads to opening of receptor-linked NSCCs permeable to Na^+ and Ca^{2+} (Arnon *et al.*, 2000a). The resultant inward current depolarizes the PM, activating L-type Ca^{2+} channels. At the same time, Na^+ is postulated to enter the PM-SR junctional space through the NSCCs to increase the local $[Na^+]$ sufficiently to promote NCX reversal (Lee *et al.*, 2002). Finally, the Ca^{2+} is taken back up into the SR by SERCA.

The PM-SR junction complexes are postulated to be the sites for interactions among the NSCCs, NCX, and SERCA during SR refilling, and are thought to be crucial for the occurrence of the recurring Ca^{2+} waves. This theory is supported by the observation that the low-affinity Na-K-ATPase isoforms $\alpha 2$ and $\alpha 3$ have been localized to the junctional PM (Juhaszova and Blaustein, 1997), which would promote elevated junctional $[Na^+]$ and NCX reversal (Arnon *et al.*, 2000b). Finally, separation of the superficial SR from the PM with calyculin-A results in the abolishment of Ca^{2+} waves (Lee *et al.*, 2005). This may disrupt SR refilling from Ca^{2+} coming from the PM, because as the junction separates the SERCA molecules are not able to capture as many Ca^{2+} molecules (Fameli *et al.*, 2007).

While there is general agreement that the initiation of oscillations and waves is a response to agonists acting on sarcolemmal receptors which releases Ca^{2+} from the SR via IP_3Rs, controversy remains on whether or not Ca^{2+} release from the IP_3Rs then activates RyRs to

generate further release by Ca^{2+}-induced Ca^{2+}-release and to propagate waves, or whether the entire release process arises from IP_3Rs without significant RyR involvement (Mccarron *et al.,* 2003). The former proposal is supported by studies which showed that drugs which block RyRs often abolish Ca^{2+} oscillations initiated by IP_3-generating agonists (Hyvelin *et al.,* 1998; Boittin *et al.,* 1999; Jaggar and Nelson, 2000). This is possibly due to co-localization of RyRs and IP_3Rs, which allows Ca^{2+} released locally by IP_3R to activate adjacent clusters of RyR by Ca^{2+}-induced Ca^{2+} release (Gordienko and Bolton, 2002).

Interestingly, in some small vessels, asynchronous Ca^{2+} waves appear to cause vasodilation. For example, Jaggar (2001) showed in rat cerebral vessels that abolishment of these waves causes vasoconstriction. A proposed mechanism is that the asynchronous Ca^{2+} waves in these vessels may stimulate Ca^{2+}-activated K^+ channels, causing hyperpolarization of the membrane potential, inhibition of L-type Ca^{2+} channels, and muscle relaxation without significant contractile activation (Jaggar, 2001). It is plausible that these Ca^{2+} waves occur around the periphery or the subplasmalemmal region of the smooth muscle cells rather than in the deeper myoplasm, where the myofilaments are located.

1.3.4 Vasomotion

Under certain conditions, such as during application of high concentrations of agonists, Ca^{2+} waves in vascular smooth muscle cells may become synchronized to initiate vasomotion, or spontaneous rhythmical contractions. Although its underlying mechanism and physiological importance is still unclear, these synchronized contractions are spread out over considerable distances and may assist in tissue perfusion, especially during periods of altered metabolism or perfusion pressure (Funk *et al.,* 1983, Meyer *et al.,* 2002). Vasomotion may also provide

oscillation of oxygen tension, which provides better tissue oxygenation (Misrahy *et al.,* 1962). The observation that it is altered under pathophysiological conditions such as hypertension provides evidence of a protective effect (Stansberry *et al.,* 1996).

Vasomotion is associated with oscillations of membrane potential and cytosolic Ca^{2+} concentration (Gustafsson *et al.,* 1993; Peng *et al.,* 1998). The Ca^{2+} oscillations begin as asynchronous oscillations without the generation of tension before being entrained during agonist stimulation into synchronized oscillations which underlie the rhythmical contractions (Miriel *et al.,* 1999; Peng *et al.,* 2001). These oscillations result in the release of Ca^{2+} from IP_3 stores in all forms of rhythmicity studied to date (Mauban *et al.,* 2001; Peng *et al.,* 2001; Haddock and Hill, 2002; Mauban and Wier, 2004). A model has been proposed by Aalkjaer and colleagues where in the presence of the endothelium, which produces a background level of NO to raise the level of cyclic guanosine monophosphate (cGMP), the periodic rise in $[Ca^{2+}]_i$ activates cGMP-dependent, Ca^{2+}-sensitive Cl^- channels. These Cl^- currents cause periodic depolarizations, which rapidly spread between smooth muscle cells (connected through gap junctions) to activate L-type Ca^{2+} channels that play a much more prominent role in small rather than large vessels (Rahman *et al.,* 2005). The synchronization of Ca^{2+} oscillations is made possible as a result of cell-to-cell coupling via gap junctions (Christ *et al.,* 1996; Koenigsberger *et al.,* 2004), which in smooth muscle cells, the predominant connexin subtypes within gap junctions are Cx40 and Cx43 (Li and Simard, 1999). The spreading of electrical ions synchronizes oscillations in membrane potential, thereby oscillating Ca^{2+} influx through L-type Ca^{2+} channels, leading to the synchronized contractions associated with vasomotion (Peng *et al.,* 2001; Aalkjaer and Nilsson, 2005). The resultant periodic Ca^{2+} influx facilitates Ca^{2+}-induced Ca^{2+} release to initiate the next Ca^{2+} wave, which will then occur simultaneously in all the nearby

smooth muscle cells and generate oscillatory vasoconstriction (Peng *et al.,* 2001, Aalkjaer and Nilsson, 2005; Rahman *et al.,* 2005).

The endothelium may also play an important regulatory role in vasomotion, particularly though the myoendothelial gap junctions which connect the endothelial cells to smooth muscle cells (Griffith *et al.,* 2004; Rummery and Hill, 2004). These gap junctions consist of connexin proteins, enabling electrical coupling between the endothelium and smooth muscle cell layer, facilitating the synchronization of vasomotor activity (Haefliger *et al.,* 2004; Haddock *et al.,* 2006). The loss of connexin Cx40 has been associated with irregular vasomotion (de Wit *et al.,* 2003), and myoepithelial gap junction inhibitors can prevent vasomotion in a number of vascular beds (Chaytor *et al.,* 1997; Hill *et al.,* 1999; Bonnet *et al.,* 2001). Finally, myoendothelial gap junctions may also provide the pathway for release factors such as endothelial-dependent hyperpolarizing factor to modulate the contractile activity of the smooth muscle cells (Dora *et al.,* 2003).

1.4 Marfan syndrome

Marfan syndrome is an autosomal dominant disorder caused by mutations in the gene encoding for fibrillin-1, affecting multiple organ systems including cardiovascular, skeletal, ocular, and pulmonary, with a prevalence of around 2-3 in 10,000 individuals (Dietz *et al.,* 1991; Pyeritz, 2000; Judge and Dietz, 2005). The clinical signs of Marfan syndrome were first described in 1875, although the disease was named for pediatrician Antoine-Bernard Marfan, who evaluated a 5-year-old patient in 1896 and described disproportionately long, thin limbs, narrow skull, tall stature, and long, slender digits. Upon reviewing more cases, Marfan also recognized Mendelian inheritance with co-segregating malfunction of mitral valve, congenital

displacement of the lens and excessively long limbs (Pyeritz, 2000; Judge and Dietz, 2005; Chaffins, 2007; Judge and Dietz, 2008). The involvement of the aorta was first described in 1943, and in 1955, the extent of cardiovascular abnormality in aortic dilatation and dissection, as well as aortic valve regurgitation, was documented (Judge and Dietz, 2008).

1.4.1 Clinical manifestations and diagnostic criteria

Marfan syndrome is a pleiotropic disorder, with diverse manifestations in different organ systems resulting from one single mutation. The clinical presentations and severity of the disorder are different depending on the location of the mutation and expressivity in each individual. Due to the lack of genetic heterogeneity, diagnosis of Marfan syndrome is based on clinical features rather than molecular testing (Pyeritz, 2000; Judge and Dietz, 2005; Judge and Dietz, 2008). The first standard (Berlin nosology) for the diagnosis of Marfan syndrome was proposed in 1986, and the criteria focused on the three most prominent organ systems: the skeleton, eyes, and heart and aorta. In 1995, a revision (Ghent nosology) was proposed which recognized family history, included other organ systems, and placed greater emphasis on the skeletal findings. Moreover, the Ghent nosology contained classifications with more stringent and explicit criteria, helping to solve the problem of overdiagnosis or misdiagnosis with the Berlin nosology (Judge and Dietz, 2005; Chaffins, 2007).

The skeletal features, mainly caused by the disproportionate overgrowth of the long bones, are the most striking and immediately evident manifestations of Marfan syndrome. The overgrowth gives rise to abnormally tall stature, arachnodactyly, dolichocephaly, and elongation of limbs which leads to an arm span greater than 1.05 times the height. Another prominent feature is scoliosis or kyphoscoliosis caused by vertebral deformities. Anterior chest deformity

can also result from overgrowth of the ribs (Gray and Davies, 1996; Judge and Dietz, 2005). The main manifestations in the ocular system include severe myopia and lens dislocation, while in the pulmonary system, the most frequently occurring presentation is spontaneous pneumothorax caused by widening of the distal air spaces. Restrictive lung disease is exacerbated in patients with severe chest deformity (Pyeritz, 2000). The skin can also be affected, with the presentation of "stretch marks." Finally, another common manifestation is dural ectasia, an abnormal protrusion of dural membranes (Gray and Davies, 1996; Judge and Dietz, 2005).

Cardiovascular complications are the major cause of morbidity and mortality in patients with Marfan syndrome (Ammash *et al.,* 2008). In the heart, the mitral valves are often affected, which may progress to mitral valve prolapse and in some cases leads to mitral valve regurgitation (Gray and Davies, 1996). However, the most life-threatening manifestations are aortic dilatation and aneurysm, which could result in aortic rupture (Pyeritz, 2000; Judge and Dietz, 2005). Due to their proximity to the heart, aortic root and ascending aorta withstand the highest hemodynamic stress and are the most susceptible to dissection and dilatation (Gray and Davies, 1996). The changes in the walls of the elastic arteries (e.g. fragmentation and disarray of elastic fibers, a paucity of smooth muscle cells, separation of muscle fibers by collagen and mucopolysaccaride) are primarily in the media layer and result in the observed decrease in distensibility and increase in stiffness in the aorta (Pyeritz, 2000). In the clinical setting, pulse wave velocity, which is increased in patients with Marfan syndrome, is a well-established parameter to measure aortic wall stiffness; furthermore, an increase in stiffness is a marker for aortic dilatation and susceptibility to aortic rupture (Hirata *et al.,* 1991; Marque *et al.,* 2001; Vitarelli *et al.,* 2006).

1.4.2 Fibrillin, microfibrils and elastic fibers

Fibrillin assemblies (microfibrils) serve two key physiological functions: the function of a structural support that imparts tissue integrity and the function of a regulator of signaling events that instruct cellular performance (Ramirez *et al.,* 2004; Hubmacher *et al.,* 2006). Microfibrils are the product of the head-to-tail polymerization of fibrillin molecules with the addition of other proteins (Arteaga-Solis *et al.,* 2000; Ramirez and Dietz, 2007). Microfibrils, without association with elastin, form fibrous aggregates to link different constituents of the extracellular matrix and hold tissue components in place (Ramirez *et al.,* 1999). The head-to-tail polymerization gives rise to the bead-to-bead structure with extendibility and flexibility.

Fibrillin, a 350kD connective tissue glycoprotein, is widely distributed in connective tissue matrices of skin, lung, kidney, vasculature, cartilage, tendon, muscle, cornea, and ciliary zonule (Sakai *et al.,* 1986), most of which are later found to be affected in patients with Marfan syndrome. A mutation in the FBN1 gene, which contains 110kb with 56 exons and 10kb of coding sequence (Gray and Davies, 1996) and encodes for the fibrillin-1 protein, was later discovered to be responsible for the classic Marfan syndrome by Dietz and colleagues (Dietz *et al.,* 1991; Pyeritz, 2000; Chaffins, 2007)

Fibrillin proteins are mainly composed of Ca^{2+}-binding epidermal growth factor-like (cbEGF) domains interspersed with domains with homology to transforming growth factor-β (TGF-β) binding proteins or unique cysteine-rich EGF-TGF hybrid domains (Fig 1.5) (Kielty and Shuttleworth, 1995; Arteaga-Solis *et al.,* 2000; Kielty *et al.,* 2002). The cbEGF repeats have six crucial cysteine residues that are vital for disulphide bonding to form stable β-sheets (Gray and Davies, 1996). Ca^{2+} binding sites within the cbEGF domains are also important for stabilizing cbEGFs into a linearly rigid structure, mediating fibrillin monomer interactions and lateral

packing of microfibrils, and organizing the macroaggregates and protecting them against proteolysis (Kielty and Shuttleworth, 1995; Ramirez *et al.,* 1999; Arteaga-Solis *et al.,* 2000). In the most common form (Type I or "Classic") of Marfan syndrome, the mutation occurs in the cbEGF domain and thus reduces the Ca^{2+}-binding affinity of fibrillin-1. The deficiency of Ca^{2+}-binding results in microfibril instability and increased susceptibility to proteolytic degradation by proteases such as matrix metalloproteinases, elastase, and thrombin (Kielty and Shuttleworth, 1995; Ramirez *et al.,* 1999; Williams *et al.*, 2008).

In addition to microfibrillar aggregates, the fibrillin-rich microfibrils also participate in the elastic fibrillogenesis by acting as a template upon which tropoelastin (precursor of mature elastin) is deposited (Kielty *et al.,* 2002). With the elastic and stretchable outer microfibrillar mantle and inner cross-linked elastin core, mature elastic fibers are organized into tissue-specific structures that reflect the mechanical demands of each system (Kielty *et al.,* 2002; Ramirez and Dietz, 2007). For example, the loosely organized network of microfibrils and elastic fibers confers pliability in the skin (Ramirez and Dietz, 2007).

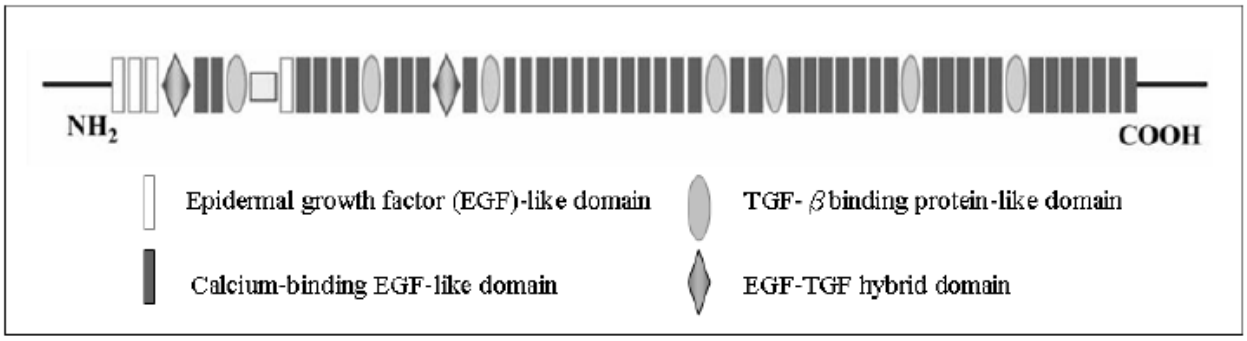

Figure 1.5: Structure of fibrillin-1 protein (Boileau *et al.,* 2005).

1.4.3 Molecular genetics and pathophysiology

Marfan syndrome is an autosomal dominant disorder with high penetrance but variable expressivity (Dietz *et al.,* 1991). For classic Marfan syndrome, linkage analyses have mapped the locus to chromosome 15q21.1, where the gene encoding fibrillin-1 is located (Dietz *et al.,* 1991; Pyeritz, 2000; Boileau *et al.,* 2005; Judge and Dietz, 2005). Approximately 66 to 75% of people with Marfan syndrome inherited the disorder from their parents; however, 25% of the patients have *de novo* mutations (Chaffins, 2007). Currently, over 600 genetic mutations have been identified (Williams *et al.,* 2008), which can be divided into two classes: nonsense and missense. Nonsense mutations account for 38.6% of the mutations and result in premature termination codons and shortened fibrillin-1 molecule; The severity of the disorder is determined by the quantity of mutant mRNA transcripts and the percentage of truncated proteins incorporated into microfibrils. Missense mutations are more common and account for 60% of the mutations. Moreover, 78% of the point mutations locate in the cbEGF modules and affects mostly the cysteine residues or amino acids involved in Ca^{2+} binding. Of the point mutations, 12% are recurrent and affect a region of the DNA where a cytosine nucleotide occurs next to a guanine nucleotide in the linear sequence of bases along its length (CpG) (Gray and Davies, 1996; Boileau *et al.,* 2005). The CpG is a noted mutational hotspot, constituting the single most frequent mutational effect, and may suggest that mutations that cause Marfan syndrome could be truly recurrent (Ollila *et al.,* 1996).

Both haploinsufficiency and dominant negative mechanism, in which abnormal protein interacts and interferes with normal proteins, have been shown to be responsible for disease pathogenesis (Judge *et al.,* 2004; Judge and Dietz, 2008). Haploinsufficiency for the wild-type protein could bring the amount of fibrillin-1 down to the threshold, resulting in phenotypic

consequences (Ramirez and Dietz, 2007). Furthermore, the mutant fibrillin-1 with dominant-negative potential or the recruitment of inflammatory cells by fibrillin-1 degradation products can promote progressive loss of fibrillin-1 with increased proteolytic clearance (Judge *et al.,* 2004; Ramirez and Dietz, 2007). All the above-mentioned processes could lead to the loss of fibrillin-1 in the extracellular matrix and thus a breakdown of tissue integrity. Recently, an upregulation of TGF-β signaling has also been shown to be closely associated with disease progression and responsible for the pathogenesis of Marfan syndrome (Judge and Dietz, 2005; Habashi *et al.,* 2006). Microfibrils containing fibrillin-1 have been shown to not only have structural function but also regulate the signaling pathway of TGF-β, a cytokine that regulates cell proliferation and migration, as well as tissue development (Judge and Dietz, 2005; Lacro *et al.,* 2007). TGFβ is synthesized and secreted as a large latent complex which is composed of three proteins: the latent TGF-β binding protein (LTBP), the active form of TGF-β and the latency-associated protein (LAP) (Matt *et al.,* 2008). The latter two are associated and sequestered by LTBP which provides safe harbour for TGF-β before its release (Byers, 2004). Fibrillin-1 shares a high degree of homology with the LTBP, and indeed, the LTBP of the large latent complex of TGF-β localizes to the microfibrils and interacts directly with fibrillin-1 (Judge and Dietz, 2005; Lacro *et al.,* 2007). Therefore, it has been suggested that some clinical manifestations of Marfan syndrome may result from the failure of latent complex sequestration and subsequent excessive TGF-β release and downstream signaling.

1.4.4 Marfan syndrome and vasomotor function

Marfan syndrome is associated not only with extensive degeneration of elastic fibers, but also with endothelial dysfunction and reduction of smooth muscle contractility in the vasculature

(Chung *et al.,* 2007a,b). The alteration of the structural integrity of elastic fibers leads to reduced distensibility and elasticity (Bunton *et al.,* 2001). Furthermore, alteration of fibrillin-1 may also disrupt the attachment of elastic fibers to the cells in the endothelial layer and impair endothelial permeability (Davis, 1994; Sheremet'eva *et al.,* 2004). Although elastic fiber composition is gradually reduced along the arterial tree, elastin remains an important determinant of passive mechanical properties in mesenteric arteries (Dobrin, 1978; Milnor, 1989; Mulvany and Aalkjaer, 1990; Briones *et al.,* 2003; Gonzalez *et al.,* 2005).

However, little is known about how Marfan syndrome affects vessel elasticity and vasomotor function in the resistance vasculature, although dysfunction of these vessels may have important clinical consequences. For example, aneurysms in peripheral and resistance vessels have been reported in patients with Marfan syndrome (Savolainen *et al.,* 1993; Hatrick *et al.,* 1998; Goffi *et al.,* 2000; Lay *et al.,* 2006), though no clear link has been established between resistance artery dysfunction and aortic dilatation and rupture (Jondeau *et al.,* 1999). Furthermore, maximum forearm blood flow in response to acetylcholine is reduced in patients with Marfan syndrome (Nakamura *et al.,* 2000), and impairment in flow-mediated vasodilation is also observed (Wilson *et al.,* 1999).

Marfan syndrome has been associated with decreased smooth muscle contractility in the aorta (Chung *et al.,* 2007b). No mechanisms have been proposed, although reduced active force may be due to low intrinsic force generation of the contractile filaments or modifications in the coupling between the contractile elements and the cytoskeleton in smooth muscle cells (Rembold and Murphy, 1990). Additionally, decreased association between smooth muscle cells and elastic fibers would reduce the strain on the smooth muscle cells and blunt their response to agonist stimulation (Bunton *et al.,* 2001). Furthermore, upregulation of matrixmetalloproteinase-2 and

matrixmetalloproteinase-9 in Marfan syndrome may inhibit Ca^{2+} entry from the extracellular space and reduce vessel contraction (Chew *et al.,* 2004; Chung *et al.,* 2007b; Chung *et al.,* 2008), although further investigation is required to elucidate possible involvement of Ca^{2+} signaling and myofilament contractile mechanisms.

1.4.5 Mouse models of marfan syndrome

Several mouse models with different mutations in the Fbn1 gene have been developed, and many of these mouse lines display typical manifestations of Marfan syndrome, including aortic root aneurysm, mitral valve thickening, lung emphysema, and long-bone overgrowth (Dietz and Mecham, 2000; Ramirez *et al.,* 2004). A common mouse model of Marfan syndrome used experimentally is heterozygous for a cysteine substitution (C1039G) in the cbEGF-like domain in *Fbn1* (*Fbn1*$^{C1039G/+}$), the most common class of mutation observed in classic Marfan syndrome (Habashi *et al.,* 2006; Judge *et al.,* 2004; Ng *et al.,* 2004). This mutant transgene harbors a naturally occurring human mutation (C1663R). In a patient with the missense mutation, normal synthesis of fibrillin-1 was observed; however, fibrillin-1 deposition was impaired (Judge *et al.,* 2004). Similarly, in murine cells heterozygous for the mutation (C1039G), histological examination consistently demonstrated a reduction in the deposition of microfibrils (Judge *et al.,* 2004). In addition to histological similarities, the *Fbn1*$^{C1039G/+}$ mouse model also demonstrates similar clinical manifestations which are common to Marfan patients. For example, there is progressive deterioration of the aortic wall with elastic fiber fragmentation and disarray of vascular smooth muscle cells which eventually led to aortic dilatation (Judge *et al.,* 2004). Furthermore, skeletal deformities common in Marfan syndrome, including kyphosis and overgrowth of the ribs, are also observed in this model.

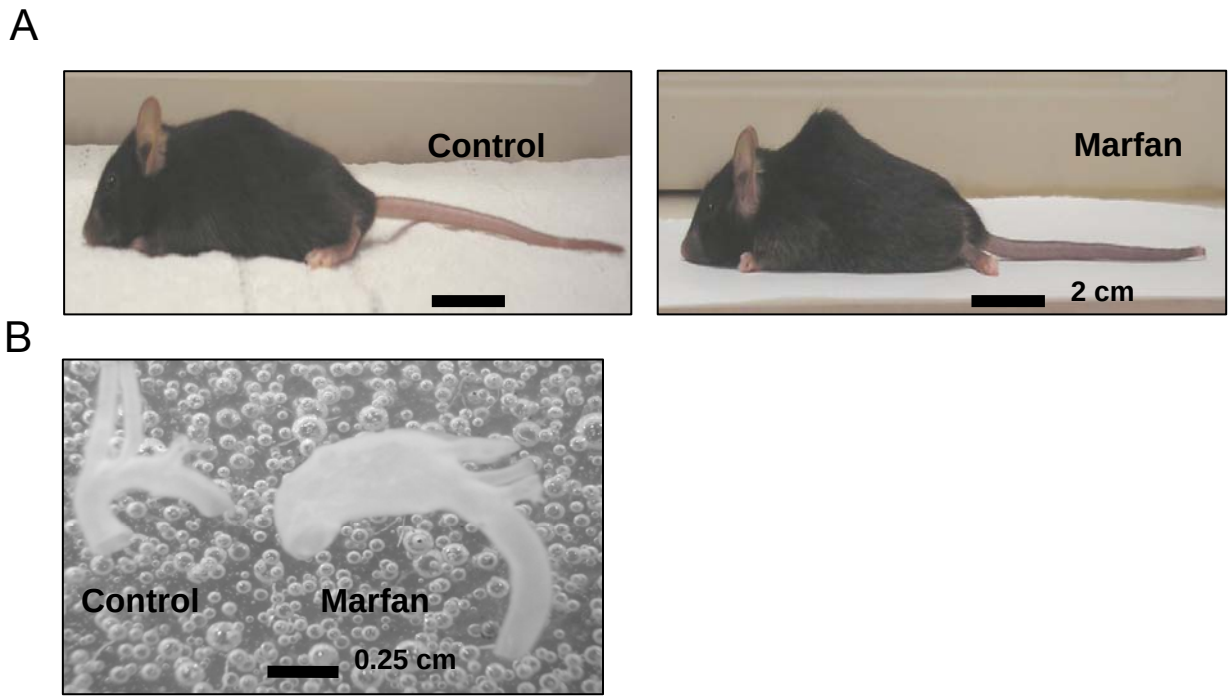

Figure 1.6: Mouse model of Marfan syndrome. A. The heterozygous (*Fbn1*$^{C1039G/+}$) mouse, the mouse model used in this study, has phenotypes (e.g. kyphoscoliosis) similar to those of the patients with Marfan syndrome. **B.** The mouse carrying the Fbn1$^{C1039G/+}$ mutation (Marfan mouse) developed an aneurysm in the aortic arch which was absent in the control.

1.5 Summary of proposed research objectives

My projects have sought to better understand Ca^{2+} homeostasis and signaling using both cultured vascular smooth muscle cells and intact tissue. I had 3 specific aims:

- To provide evidence for functional coupling of receptor-operated non-selective cation channels and the Na^{+}/Ca^{2+} exchanger (NCX) in rat aortic smooth muscle cells, I:
  - transfected cells with aequorin targeted to mitochondrial matrix to directly measure mitochondrial Ca^{2+} levels upon NCX reversal, with our lab having previously demonstrated that mitochondria buffer NCX-mediated Ca^{2+} entry.

- determined whether Ca^{2+} entry through NCX reversal, stimulated by removal of extracellular Na^{+}, was increased following stimulation with ATP and the diacylglycerol analog 1-Oleoyl-2-acetyl-*sn*-glycerol, both activators of receptor-operated channels.

- To investigate the mechanism of agonist-stimulated Ca^{2+} waves and determine their relationship with tonic contraction in rat basilar artery smooth muscle, I:
  - measured intracellular Ca^{2+} levels loaded smooth muscle cells with the Ca^{2+}-sensitive dye Fluo-4AM and measured tonic contraction using a small vessel myograph.
  - characterized the properties of uridine-5'-triphosphate (UTP)-stimulated Ca^{2+} waves and contraction and measured the effect of various pharmacological inhibitors (nifedipine, SKF-96365, KBR-7943, cyclopiazonic acid, 2-APB, ryanodine, tetracaine).

- To determine whether stiffness, vasomotor function, and Ca^{2+} signaling were affected in mesenteric resistance vessels in a mouse model of Marfan syndrome, I:
  - used an accepted mouse model ($Fbn1^{C1039G/+}$) of Marfan syndrome, with their littermates as controls, at 3, 6, and 10 months of age.
  - characterized vessel elasticity, smooth muscle cell contraction, calcium signaling, and endothelium-dependent and endothelium-independent relaxation using various pharmacological agents.

My work related to these aims resulted in three articles which form the basis of the next three chapters. In addition, I have also co-authored another article on related aspects of vascular signaling.

1.6 References

Aalkaer C, Nilsson H (2005). Vasomotion: cellular background for the oscillator and for the synchronization of smooth muscle cells. *Br J Pharmacol* **144:** 605-16.

Alberts B, Johnson A, Lewis J *et al.* (2002). In: Alberts B, Johnson A, Lewis J, Raff M, Roberts K, Walter P (eds). *Molecular Biology of the Cell.* Garland Science: New York, pp 616-657.

Allen DG, Blinks JR, Prendergast FG (1977). Aequorin luminescence: relation of light emission to calcium concentration--a calcium-independent component. *Science* **195:** 996-8.

Allen BG, Walsh MP (1994). The biochemical basis of the regulation of smooth-muscle contraction. *Trends Biochem Sci* **19:** 362-8.

Ammash NM, Sundt TM, Connolly HM (2008). Marfan syndrome-diagnosis and management. *Curr Probl Cardiol* **33:** 7-39.

Amrani Y, Magnier C, Enouf J, Wuytack F, and Bronner C (1995) Ca2+ increase and Ca(2+)-influx in human tracheal smooth muscle cells: role of Ca2+ pools controlled by sarco-endoplasmic reticulum Ca(2+)-ATPase 2 isoform. *Br J Pharmacol* **115:** 1204-1210

Arnon A, Hamlyn JM, Blaustein MP (2000a). Na(+) entry via store-operated channels modulates Ca(2+) signaling in arterial myocytes. *Am J Physiol Cell Physiol* **278:** C163-73.

Arnon A, Hamlyn JM, Blaustein MP (2000b). Ouabain augments Ca2+ transients in arterial smooth muscle without raising cytosolic Na+. *Am J Physiol Heart Circ Physiol* **279:** H679-H691.

Arteaga-Solis E, Gayraud B, Ramirez F (2000). Elastic and collagenous networks in vascular diseases. *Cell Struct Funct* **25:** 69-72.

Bai N, Lee HC, Laher I (2005). Emerging role of cyclic ADP-ribose (cADPR) in smooth muscle. *Pharmacol Ther* **105:** 189-207.

Barr VA, Bernot KM, Srikanth S, Gwack Y, Balagopalan L, Regan CK, *et al.* (2008). Dynamic movement of the calcium sensor STIM1 and the calcium channel Orai1 in activated T-cells: puncta and distal caps. *Mol Biol Cell* **19:** 2802-17.

Benham CD, Bolton TB (1986). Spontaneous transient outward currents in single visceral and vascular smooth muscle cells of the rabbit. *J Physiol* **381:** 385–406.

Berchtold MW, Brinkmeier H, Müntener M (2000). Calcium ion in skeletal muscle: its crucial role for muscle function, plasticity, and disease. *Physiol Rev* **80:** 1215-65.

Bergner A, Sanderson MJ (2002). Acetylcholine-induced calcium signaling and contraction of airway smooth muscle cells in lung slices. *J Gen Physiol* **119:** 187-98.

Bers DM (2001). Sources and sinks of activator calcium. In: *Excitation-contraction coupling and cardiac contractile force.* Kluwer Academic Publishers: Dordrecht, pp 39-56.

Berridge MJ (1993). Cell signalling. A tale of two messengers. *Nature* **365:** 388-9.

Berridge, MJ (2006). Calcium microdomains: Organization and function. *Cell Calcium* **40:** 405-412.

Berridge MJ, Bootman MD, Roderick HL (2003). Calcium signalling: dynamics, homeostasis and remodelling. *Nat Rev Mol Cell Biol* **4:** 517–29.

Bezprozvanny I, Watras J, Ehrlich BE (1991). Bell-shaped calcium-response curves of Ins(1,4,5)P3- and calcium-gated channels from endoplasmic reticulum of cerebellum. *Nature* **351:** 751-4.

Bilmen JG, Michelangeli F (2002). Inhibition of the type 1 inositol 1,4,5-trisphosphate receptor by 2-aminoethoxydiphenylborate. *Cell Signal* **14:** 955-60.

Blaustein MP, Lederer WJ (1999). Sodium/calcium exchange: its physiological implications. *Physiol Rev* **79:** 763-854.

Boileau C, Jondeau G, Mizuguchi T, Matsumoto N (2005). Molecular genetics of marfan syndrome. *Curr Opin Cardiol* **20:** 194-200.

Boittin FX, Macrez N, Halet G, Mironneau J (1999). Norepinephrine-induced Ca(2+) waves depend on InsP(3) and ryanodine receptor activation in vascular myocytes. *Am J Physiol* **277:** C139-51.

Bolton TB (1979). Mechanisms of action of transmitters and other substances on smooth muscle. *Physiol Rev* **59:** 606-718.

Bolton TB, Large WA (1986). Are junction potentials essential? Dual mechanism of smooth muscle cell activation by transmitter released from autonomic nerves. *Q J Exp Physiol* **71:** 1-28.

Bolton TB, Prestwich SA, Zholos AV, Gordienko DV (1999). Excitation-contraction coupling in gastrointestinal and other smooth muscles. *Annu Rev Physiol* **61:** 85-115.

Bonnet S, Hyvelin JM, Bonnet P, Marthan R, Savineau JP (2001). Chronic hypoxia-induced spontaneous and rhythmic contractions in the rat main pulmonary artery. *Am J Physiol Lung Cell Mol Physiol* **281:** L183–L192.

Boutouyrie P, Bézie Y, Lacolley P, Challande P, Chamiot-Clerc P, Benetos A *et al.* (1997). In vivo/in vitro comparison of rat abdominal aorta wall viscosity. Influence of endothelial function. *Arterioscler Thromb Vasc Biol* **17**: 1346-55.

Brini M, Marsault R, Bastianutto C, Alvarez J, Pozzan T, Rizzuto R (1995). Transfected aequorin in the measurement of cytosolic Ca2+ concentration ([Ca2+]c). A critical evaluation. *J Biol Chem* **270:** 9896-903.

Briones AM, González JM, Somoza B, Giraldo J, Daly CJ, Vila E, *et al.* (2003). Role of elastin in spontaneously hypertensive rat small mesenteric artery remodelling. *J Physiol* **552**: 185-95.

Brough GH, Wu S, Cioffi D, Moore TM, Li M, Dean N, et al. (2001). Contribution of endogenously expressed Trp1 to a Ca2+-selective, store-operated Ca2+ entry pathway. FASEB J 15: 1727-38.

Bunton TE, Biery NJ, Myers L, Gayraud B, Ramirez F, Dietz HC (2001). Phenotypic alteration of vascular smooth muscle cells precedes elastolysis in a mouse model of Marfan syndrome. *Circ Res* **88**: 37-43.

Byers PH (2004). Determination of the molecular basis of marfan syndrome: A growth industry. *J Clin Invest* **114:** 161-3.

Byrne NG, Large WA (1988). Membrane ionic mechanisms activated by noradrenaline in cells isolated from the rabbit portal vein. *J Physiol* **404:** 557-73.

Carey DJ (1991). Control of growth and differentiation of vascular cells by extracellular matrix proteins. *Annu Rev Physiol* **53:** 161-177.

Casteels R, Droogmans G (1981). Exchange characteristics of the noradrenaline-sensitive calcium store in vascular smooth muscle cells or rabbit ear artery. *J Physiol* **317:** 263-79.

Catterall WA (2000). Structure and regulation of voltage-gated Ca2+ channels. *Annu Rev Cell Dev Biol* **16:** 521-55.

Chaffins JA (2007). Marfan syndrome. *Radiol Technol* **78:** 222,36; quiz 237-9.

Chaytor AT, Evans WH, Griffith TM (1997). Peptides homologous to extracellular loop motifs of connexin 43 reversibly abolish contractile activity in rabbit arteries. *J Physiol* **503:** 99–110.

Chew DK, Conte MS, Khalil RA (2004). Matrix metalloproteinase-specific inhibition of Ca2+ entry mechanisms of vascular contraction. *J Vasc Surg* **40**: 1001-10.

Chiesa A, Rapizzi E, Tosello V, Pinton P, de Virgilio M, Fogarty KE, *et al.* (2001). Recombinant aequorin and green fluorescent protein as valuable tools in the study of cell signalling. *Biochem J* **355:** 1-12.

Christ GJ, Spray DC, el-Sabban M, Moore LK, Brink PR (1996). Gap junctions in vascular tissues. Evaluating the role of intercellular communication in the modulation of vasomotor tone. *Circ Res* **79:** 631-46.

Chung AW, Au Yeung K, Cortes SF, Sandor GG, Judge DP, Dietz HC *et al*. (2007a). Endothelial dysfunction and compromised eNOS/Akt signaling in the thoracic aorta during the progression of Marfan syndrome. *Br J Pharmacol* **150**:1075-83.

Chung AW, Au Yeung K, Sandor GG, Judge DP, Dietz HC, van Breemen C (2007b). Loss of elastic fiber integrity and reduction of vascular smooth muscle contraction resulting from the upregulated activities of matrix metalloproteinase-2 and -9 in the thoracic aortic aneurysm in Marfan syndrome. *Circ Res* **101**: 512-22.

Chung AW, Yang HH, Radomski MW, van Breemen C (2008). Long-term doxycycline is more effective than atenolol to prevent thoracic aortic aneurysm in marfan syndrome through the inhibition of matrix metalloproteinase-2 and -9. *Circ Res* **102**: e73-85.

Clapham DE (2003). TRP channels as cellular sensors. *Nature* **426:** 517–24.

Cobbold PH, Rink TJ (1987). Fluorescence and bioluminescence measurement of cytoplasmic free calcium. Biochem J **248:** 313-28.

Cohen NM, Lederer WJ (1987). Calcium current in isolated neonatal rat ventricular myocytes. *J Physiol* **391:** 169-191.

Dai J, Lee CH, Poburko D, Szado T, Kuo KH, van Breemen C (2007). Endothelin-1-mediated wave-like [Ca2+]i oscillations in intact rabbit inferior vena cava. *J Vasc Res* **44:** 495-503.

Darby PJ, Kwan CY, Daniel EE (2000). Caveolae from canine airway smooth muscle contain the necessary components for a role in Ca(2+) handling. *Am J Physiol Lung Cell Mol Physiol* **279:** L1226-1235.

Davis EC (1994). Immunolocalization of microfibril and microfibril-associated proteins in the subendothelial matrix of the developing mouse aorta. *J Cell Sci* **107**: 727-36.

Devine CE, Somlyo AV, Somlyo AP (1972). Sarcoplasmic reticulum and excitation-contraction coupling in mammalian smooth muscles. *J Cell Biol* **52:** 690-718.

de Wit C, Roos F, Bolz SS, Pohl U (2003). Lack of vascular connexin 40 is associated with hypertension and irregular arteriolar vasomotion. *Physiol Genomics* **13:** 169-77.

Dietrich A, Mederos YS, Schnitzler M, Gollasch M, Gross V, Storch U, *et al.* (2005a) Increased vascular smooth muscle contractility in TRPC6–/– mice. *Mol Cell Biol* **25:** 6980–9.

Dietrich A, Schnitzler M, Kalwa H, Storch U, Gudermann T (2005b). Functional characterization and physiological relevance of the TRPC3/6/7 subfamily of cation channels. *Naunyn Schmiedebergs Arch Pharmacol* **371:** 257–65.

Dietz HC, Cutting GR, Pyeritz RE, Maslen CL, Sakai LY, Corson GM, *et al.* (1991). Marfan syndrome caused by a recurrent de novo missense mutation in the fibrillin gene. *Nature* **352:** 337-9.

Dietz HC, Mecham RP (2000). Mouse models of genetic diseases resulting from mutations in elastic fiber proteins. *Matrix Biol* **19:** 481-8.

Dobrin, PB (1978). Mechanical properties of arteries. *Physiol Rev* **58**: 397-460.

Dora KA, Sandow SL, Gallagher NT, Takano H, Rummery NM, Hill CE, *et al.* (2003). Myoendothelial gap junctions may provide the pathway for EDHF in mouse mesenteric artery. *J Vasc Res* **40:** 480-90.

Edwards A, Pallone, TL (2007). Modification of cytosolic calcium signaling by subplasmalemmal microdomains. *Am J Physiol Renal Physiol* **292:** F1827-1845.

Eggermont JA, Wuytack F, Verbist J, and Casteels R (1990) Expression of endoplasmic-reticulum Ca2(+)-pump isoforms and of phospholamban in pig smooth-muscle tissues. *Biochem J* **271:** 649-653.

El-Mezgueldi M (1996). Calponin. *Int J Biochem Cell Biol* **28:** 1185-1189.

Emerson GG, Segal SS (2000). Electrical coupling between endothelial cells and smooth muscle cells in hamster feed arteries: role in vasomotor control. *Circ Res* **87:** 474–479.

Endo M (1977). Calcium release from the sarcoplasmic reticulum. *Physiol Rev* **57:** 71-108.

Engelender S, De Meis L (1996). Pharmacological differentiation between intracellular calcium pump isoforms. *Mol Pharmacol* **50:** 1243-52.

Estacion M, Li S, Sinkins WG, Gosling M, Bahra P, Poll C, *et al.* (2004). Activation of human TRPC6 channels by receptor stimulation. *J Biol Chem* **279:** 22047-56.

Estacion M, Sinkins WG, Jones SW, Applegate MA, Schilling WP (2006). Human TRPC6 expressed in HEK 293 cells forms non-selective cation channels with limited Ca2+ permeability. *J Physiol* **572:** 359-77.

Evans JH, Sanderson MJ (1999). Intracellular calcium oscillations induced by ATP in airway epithelial cells. *Am J Physiol* **277:** L30-L41.

Fameli N, van Breemen C, Kuo KH (2007). A quantitative model for linking Na+/Ca2+ exchanger to SERCA during refilling of the sarcoplasmic reticulum to sustain [Ca2+] oscillations in vascular smooth muscle. *Cell Calcium* **42:** 565-575.

Fameli N, Kuo KH, van Breemen C (2009). A model for the generation of localized transient [Na+] elevations in vascular smooth muscle. *Biochem Biophys Res Commun* **389:** 461-5.

Fatherazi S, Presland RB, Belton CM, Goodwin P, Al-Qutub M, Trbic Z, *et al.* (2007). Evidence that TRPC4 supports the calcium selective I(CRAC)-like current in human gingival keratinocytes. *Pflugers Arch* **453:** 879-89.

Feng W, Tu J, Yang T, Vernon PS, Allen PD, Worley PF, *et al.* (2002). Homer regulates gain of ryanodine receptor type 1 channel complex. *J Biol Chem* **277:** 44722-44730.

Ferrari AU, Radaelli A, Centola M (2003). Invited review: aging and the cardiovascular system. *J Appl Physiol* **95:** 2591-7.

Feske S, Gwack Y, Prakriya M, Srikanth S, Puppel SH, Tanasa B, *et al.* (2006). A mutation in Orai1 causes immune deficiency by abrogating CRAC channel function. *Nature* **441:** 179-85.

Fill M, Copello JA (2002). Ryanodine receptor calcium release channels. *Physiol Rev* **82:** 893-922.

Floyd R, Wray S (2007). Calcium transporters and signalling in smooth muscles. *Cell Calcium* **42:** 467-76.

Freichel M, Vennekens R, Olausson J, Hoffmann M, Müller C, Stolz S, *et al.* (2004). Functional role of TRPC proteins in vivo: Lessons from TRPC-deficient mouse models. *Biochem Biophys Res Commun* **322:** 1352–8.

Funk W, Endrich B, Messmer K, Intaglietta M (1983). Spontaneous arteriolar vasomotion as a determinant of peripheral vascular resistance. *Int J Microcirc Clin Exp* **2:** 11–25.

Furchgott RF, Zawadzki JV (1980). The obligatory role of endothelial cells in the relaxation of arterial smooth muscle by acetylcholine. *Nature* **288:** 373–376.

Gafni J, Munsch JA, Lam TH, Catlin MC, Costa LG, Molinski TF, *et al.* (1997). Xestospongins: potent membrane permeable blockers of the inositol 1,4,5-trisphosphate receptor. *Neuron* **19:** 723-33.

Ganitkevich V, Isenberg, G (1990). Isolated guinea pig coronary smooth muscle cells. Acetylcholine induces hyperpolarization due to sarcoplasmic reticulum calcium release activating potassium channels. *Circ Res* **67:** 525–528.

Ghosh TK, Eis PS, Mullaney JM, Ebert CL, Gill DL (1988). Competitive, reversible, and potent antagonism of inositol 1,4,5-trisphosphate-activated calcium release by heparin. *J Biol Chem* **263:** 11075-9.

Go M, Sekiguchi K, Nomura H, Kikkawa U, Nishizuka Y (1987). Further studies on the specificity of diacylglycerol for protein kinase C activation. *Biochem Biophys Res Commun* **144:** 598-605.

Goffi L, Chan R, Boccoli G, Ghiselli R, Saba V (2000). Aneurysm of a jejunal branch of the superior mesenteric artery in a patient with Marfan's syndrome. *J Cardiovasc Surg* **41**: 321-3.

Golovina VA, Blaustein MP (1997). Spatially and functionally distinct Ca2+ stores in sarcoplasmic and endoplasmic reticulum. *Science* **275:** 1643-1648.

González JM, Briones AM, Starcher B, Conde MV, Somoza B, Daly C *et al.* (2005). Influence of elastin on rat small artery mechanical properties. *Exp Physiol* **90**: 463-8.

Gordienko DV, Bolton TB (2002). Crosstalk between ryanodine receptors and IP(3) receptors as a factor shaping spontaneous Ca(2+)-release events in rabbit portal vein myocytes. J *Physiol* **542:** 743-62.

Gordienko DV, Bolton TB, Cannell MB (1998). Variability in spontaneous subcellular calcium release in guinea-pig ileum smooth muscle cells. *J Physiol* **507**: 707-20.

Gray JR, Davies SJ (1996). Marfan syndrome. *J Med Genet* **33:** 403-8.

Griffith TM, Chaytor AT, Edwards DH (2004). The obligatory link: role of gap junctional communication in endothelium-dependent smooth muscle hyperpolarization. *Pharmacol Res* **49:** 551-64.

Guo W, Campbell KP (1995). Association of triadin with the ryanodine receptor and calsequestrin in the lumen of the sarcoplasmic reticulum. *J Biol Chem* **270:** 9027-30.

Gustafsson H, Mulvany MJ, Nilsson H (1993). Rhythmic contractions of isolated small arteries from rat: influence of the endothelium. *Acta Physiol Scand* **148:** 153–163.

Habashi JP, Judge DP, Holm TM, Cohn RD, Loeys BL, Cooper TK, *et al.* (2006). Losartan, an AT1 antagonist, prevents aortic aneurysm in a mouse model of marfan syndrome. *Science* **312:** 117-21.

Haddock RE, Hill CE (2002). Differential activation of ion channels by inositol 1,4,5-trisphosphate (IP3)- and ryanodine-sensitive calcium stores in rat basilar artery vasomotion. *J Physiol* **545:** 615-27.

Haddock RE, Hill CE (2005). Rhythmicity in arterial smooth muscle. *J Physiol* **566:** 645-56.

Haddock RE, Grayson TH, Brackenbury TD, Meaney KR, Neylon CB, Sandow SL, *et al.* (2006). Endothelial coordination of cerebral vasomotion via myoendothelial gap junctions containing connexins 37 and 40. *Am J Physiol Heart Circ Physiol* **291:** H2047-56.

Haefliger JA, Nicod P, Meda P (2004). Contribution of connexins to the function of the vascular wall. *Cardiovasc Res* **62:** 345-56.

Hai CM, Kim HR (2005). An expanded latch-bridge model of protein kinase C-mediated smooth muscle contraction. *J Appl Physiol* **98:** 1356-1365.

Hai CM, Murphy RA (1988). Cross-bridge phosphorylation and regulation of latch state in smooth muscle. *Am J Physiol* **254:** C99-106.

Hajnóczky G, Robb-Gaspers LD, Seitz MB, Thomas AP (1995). Decoding of cytosolic calcium oscillations in the mitochondria. *Cell* **82:** 415-24.

Halayko AJ, Rector E, Stephens NL (1997). Characterization of molecular determinants of smooth muscle cell heterogeneity. *Can J Physiol Pharmacol* **75:** 917-929.

Hassock SR, Zhu MX, Trost C, Flockerzi V, Authi KS (2002). Expression and role of TRPC proteins in human platelets: evidence that TRPC6 forms the store-independent calcium entry channel. *Blood* **100:** 2801-11.

Hatrick AG, Malcolm PN, Burnand KG, Irvine AT (1998). A superficial femoral artery aneurysm in a patient with Marfan's syndrome. *Eur J Vasc Endovasc Surg* **15**: 459-60.

Hayek SM, Zhu X, Bhat MB, Zhao J, Takeshima H, Valdivia HH *et al.* (2000). Characterization of a calcium-regulation domain of the skeletal-muscle ryanodine receptor. *Biochem J* **351:** 57-65.

Head JF, Inouye S, Teranishi K, Shimomura O (2000). The crystal structure of the photoprotein aequorin at 2.3 A resolution. *Nature* **405:** 372-6.

Helliwell RM, Large WA (1997). Alpha 1-adrenoceptor activation of a non-selective cation current in rabbit portal vein by 1,2-diacyl-sn-glycerol. *J Physiol* **499:** 417-28.

Hill CE, Eade J, Sandow SL (1999). Mechanisms underlying spontaneous rhythmical contractions in irideal arterioles of the rat. *J Physiol* **521:** 507–16.

Hirata K, Triposkiadis F, Sparks E, Bowen J, Wooley CF, Boudoulas H (1991). The marfan syndrome: Abnormal aortic elastic properties. *J Am Coll Cardiol* **18:** 57-63.

Hofer AM, Curci S, Doble MA, Brown EM, Soybel DI (2000). Intercellular communication mediated by the extracellular calcium-sensing receptor. *Nat Cell Biol* **2:** 392-8.

Hofmann T, Obukhov AG, Schaefer M, Harteneck C, Gudermann T, Schultz G (1999). Direct activation of human TRPC6 and TRPC3 channels by diacylglycerol. *Nature* **397:** 259-63.

Hoth M, Fanger CM, Lewis RS (1997). Mitochondrial regulation of store-operated calcium signaling in T lymphocytes. *J Cell Biol* **137:** 633–648.

Hoth M, Penner R (1992). Depletion of intracellular calcium stores activates a calcium current in mast cells. *Nature* **355:** 353-6.

Huang GN, Zeng W, Kim JY, Yuan JP, Han L, Muallem S, *et al.* (2006). STIM1 carboxyl-terminus activates native SOC, I(crac) and TRPC1 channels. *Nat Cell Biol* **8:** 1003-10.

Hubmacher D, Tiedemann K, Reinhardt DP (2006). Fibrillins: from biogenesis of microfibrils to signaling functions. *Curr Top Dev Biol* **75:** 93–122

Hughes AD, Bolton TB (1995). Action of angiotensin II, 5-hydroxytryptamine and adenosine triphosphate on ionic currents in single ear artery cells of the rabbit. *Br J Pharmacol* **116:** 2148-2154.

Hymel L, Inui M, Fleischer S, Schindler H (1988). Purified ryanodine receptor of skeletal muscle sarcoplasmic reticulum forms Ca2+-activated oligomeric Ca2+ channels in planar bilayers. *Proc Natl Acad Sci U S A* **85:** 441-5.

Hyvelin JM, Guibert C, Marthan R, Savineau JP (1998). Cellular mechanisms and role of endothelin-1-induced calcium oscillations in pulmonary arterial myocytes. *Am J Physiol* **275:** L269-82.

Iino M (1989). Calcium-induced calcium release mechanism in guinea pig taenia caeci. *J Gen Physiol* **94:** 363-83.

Iino M (1990). Biphasic Ca2+ dependence of inositol 1,4,5-trisphosphate-induced Ca release in smooth muscle cells of the guinea pig taenia caeci. *J Gen Physiol* **95:** 1103-22.

Iino M (1999). Dynamic regulation of intracellular calcium signals through calcium release channels. *Mol Cell Biochem* **190:** 185-90.

Iino M, Kasai H, Yamazawa T (1994). Visualization of neural control of intracellular Ca2+ concentration in single vascular smooth muscle cells in situ. *EMBO J* **13:** 5026-5031.

Inoue R, Okada T, Onoue H, Hara Y, Shimizu S, Naitoh S, *et al.* (2001). The transient receptor potential protein homologue TRP6 is the essential component of vascular alpha(1)-adrenoceptor-activated Ca(2+)-permeable cation channel. *Circ Res* **88:** 325-32.

Inouye S, Noguchi M, Sakaki Y, Takagi Y, Miyata T, Iwanaga S *et al.* (1985). Cloning and sequence analysis of cDNA for the luminescent protein aequorin. *Proc Natl Acad Sci U S A* **82:** 3154-8.

Jackson WF (2000). Ion channels and vascular tone. *Hypertension* **35:** 173-178.

Jaggar JH (2001). Intravascular pressure regulates local and global Ca(2+) signaling in cerebral artery smooth muscle cells. *Am J Physiol Cell Physiol* **281:** C439-48.

Jaggar JH, Porter VA, Lederer WJ, Nelson MT (2000). Calcium sparks in smooth muscle. *Am J Physiol Cell Physiol* **278:** C235-56.

Jaggar JH, Nelson MT (2000). Differential regulation of Ca(2+) sparks and Ca(2+) waves by UTP in rat cerebral artery smooth muscle cells. *Am J Physiol Cell Physiol* **279:** C1528-39.

Jaggar JH, Stevenson AS, Nelson MT (1998). Voltage dependence of Ca2**+** sparks in intact cerebral arteries. *Am J Physiol Cell Physiol* **274:** C1755–C1761.

Jiang MJ and Morgan KG (1989). Agonist-specific myosin phosphorylation and intracellular calcium during isometric contractions of arterial smooth muscle. *Pflugers Arch* **413:** 637-643.

Jondeau G, Boutouyrie P, Lacolley P, Laloux B, Dubourg O, Bourdarias JP *et al.* (1999). Central pulse pressure is a major determinant of ascending aorta dilation in Marfan syndrome. *Circulation* **99**: 2677-81.

Judge DP, Dietz HC (2005). Marfan's syndrome. *Lancet* **366**: 1965-76.

Judge DP, Dietz HC (2008). Therapy of marfan syndrome. *Annu Rev Med* **59:** 43-59.

Juhaszova M, Blaustein MP (1997). Na+ pump low and high ouabain affinity alpha subunit isoforms are differently distributed in cells. *Proc Natl Acad Sci U S A.* **94:** 1800-5.

Kamm KE, Stull JT (1985). The function of myosin and myosin light chain kinase phosphorylation in smooth muscle. *Ann Rev Pharmacol Toxicol* **25:** 592-620.

Kanmura Y, Missiaen L, Raeymaekers L, Casteels R (1988). Ryanodine reduces the amount of calcium in intracellular stores of smooth-muscle cells of the rabbit ear artery. *Pflugers Arch* **413:** 153-9.

Karaki H, Ozaki H, Hori M, Mitsui-Saito M, Amano K, Harada K *et al.* (1997). Calcium movements, distribution, and functions in smooth muscle. *Pharmacol Rev* **49:** 157-230.

Kaznacheyeva E, Glushankova L, Bugaj V, Zimina O, Skopin A, Alexeenko V, *et al.* (2007). Suppression of TRPC3 leads to disappearance of store-operated channels and formation of a new type of store-independent channels in A431 cells. *J Biol Chem* **282:** 23655-62.

Kielty CM, Shuttleworth CA (1995). Fibrillin-containing microfibrils: Structure and function in health and disease. *Int J Biochem Cell Biol* **27:** 747-60.

Kielty CM, Wess TJ, Haston L, Ashworth JL, Sherratt MJ, Shuttleworth CA (2002). Fibrillin-rich microfibrils: elastic biopolymers of the extracellular matrix. *J Muscle Res Cell Motil*

23: 581-96.

Kobayashi S, Somlyo AV, Somlyo AP (1988). Heparin inhibits the inositol 1,4,5-trisphosphate-dependent, but not the independent, calcium release induced by guanine nucleotide in vascular smooth muscle. *Biochem Biophys Res Commun* **153:** 625-31.

Koenigsberger M, Sauser R, Lamboley M, Beny JL, Meister JJ (2004). Ca2+ dynamics in a population of smooth muscle cells: modeling the recruitment and synchronization. *Biophys J* **87**: 92–104.

Kuriyama H, Kitamura K, Nabata H (1995). Pharmacological and physiological significance of ion channels and factors that modulate them in vascular tissues. *Pharmacol Rev* **47:** 387-573.

Lacro RV, Dietz HC, Wruck LM, Bradley TJ, Colan SD, Devereux RB, *et al.* (2007). Rationale and design of a randomized clinical trial of beta-blocker therapy (atenolol) versus angiotensin II receptor blocker therapy (losartan) in individuals with marfan syndrome. *Am Heart J* **154:** 624-31.

Ladilov Y, Haffner S, Balser-Schäfer C, Maxeiner H, Piper HM (1999). Cardioprotective effects of KB-R7943: a novel inhibitor of the reverse mode of Na+/Ca2+ exchanger. *Am J Physiol* **276:** H1868-76.

Laporte R, Laher I (1997). Sarcoplasmic reticulum-sarcolemma interactions and vascular smooth muscle tone. *J Vasc Res* **34:** 325-43.

Lay CS, Yu CJ, Tyan YS (2006). Abdominal aortic dissection with acute mesenteric ischemia in a patient with Marfan syndrome. *J Chin Med Assoc* **69**: 326-9.

Lee CH, Kuo KH, Dai J, Leo JM, Seow CY, van Breemen C (2005). Calyculin-A disrupts subplasmalemmal junction and recurring Ca2+ waves in vacular smooth muscle. *Cell Calcium* **37:** 9-16.

Lee CH, Poburko D, Kuo KH, Seow CY, van Breemen C (2002). Ca(2+) oscillations, gradients, and homeostasis in vascular smooth muscle. *Am J Physiol Heart Circ Physiol* **282:** H1571-83.

Lee CH, Poburko D, Sahota P, Sandhu J, Ruehlmann DO, van Breemen C (2001). The mechanism of phenylephrine-mediated [Ca(2+)](i) oscillations underlying tonic contraction in the rabbit inferior vena cava. *J Physiol* **534:** 641-650.

Lepretre N, Mironneau J (1994). Alpha 2-adrenoceptors activate dihydropyridine-sensitive calcium channels via Gi-proteins and protein kinase C in rat portal vein myocytes. *Pflugers Arch* **429:** 253-261.

Li X, Simard JM (1999). Multiple connexins form gap junction channels in rat basilar artery smooth muscle cells. *Circ Res* **84:** 1277-84.

Liao Y, Erxleben C, Yildirim E, Abramowitz J, Armstrong DL, Birnbaumer L (2007). Orai proteins interact with TRPC channels and confer responsiveness to store depletion. *Proc Natl Acad Sci U S A* **104:** 4682-7.

Liou J, Kim ML, Heo WD, Jones JT, Myers JW, Ferrell JE Jr, *et al.* (2005). STIM is a Ca2+ sensor essential for Ca2+-store-depletion-triggered Ca2+ influx. *Curr Biol* **15:** 1235-41.

Lis A, Peinelt C, Beck A, Parvez S, Monteilh-Zoller M, Fleig A, *et al.* (2007). CRACM1, CRACM2, and CRACM3 are store-operated Ca2+ channels with distinct functional properties. *Curr Biol* **17:** 794-800.

Liu X, Wang W, Singh BB, Lockwich T, Jadlowiec J, O'Connell B, *et al.* (2000). Trp1, a candidate protein for the store-operated Ca(2+) influx mechanism in salivary gland cells. *J Biol Chem* **275:** 3403-11.

López JJ, Salido GM, Pariente JA, Rosado JA (2006). Interaction of STIM1 with endogenously expressed human canonical TRP1 upon depletion of intracellular Ca2+ stores. *J Biol Chem* **281:** 28254-64.

Lucchesi PA, Berk BC (1995). Regulation of sodium-hydrogen exchange in vascular smooth muscle. *Cardiovasc Res* **29:** 172-7.

Lytton J, Westlin M, and Hanley MR (1991). Thapsigargin inhibits the sarcoplasmic or endoplasmic reticulum Ca-ATPase family of calcium pumps. *J Biol Chem* **266:** 17067-17071

Ma HT, Venkatachalam K, Li HS, Montell C, Kurosaki T, Patterson RL, *et al*. (2001). Assessment of the role of the inositol 1,4,5-trisphosphate receptor in the activation of transient receptor potential channels and store-operated Ca2+ entry channels. *J Biol Chem* **276:** 18888-96.

Mak DO, McBride S, Foskett JK (1998). Inositol 1,4,5-trisphosphate [correction of tris-phosphate] activation of inositol trisphosphate [correction of tris-phosphate] receptor Ca2+ channel by ligand tuning of Ca2+ inhibition. *Proc Natl Acad Sci U S A* **95:** 15821-5.

Malli R, Frieden M, Osibow K, Graier WF (2003a). Mitochondria efficiently buffer subplasmalemmal Ca2+ elevation during agonist stimulation. *J Biol Chem* **278:** 10807–10815.

Malli R, Frieden M, Osibow K, Zoratti C, Mayer M, Demaurex N *et al.* (2003b). Sustained Ca2+ transfer across mitochondria is essential for mitochondrial Ca2+ buffering, store-operated Ca2+ entry, and Ca2+ store refilling, *J Biol Chem* **278:** 44769–44779.

Marque V, Kieffer P, Gayraud B, Lartaud-Idjouadiene I, Ramirez F, Atkinson J (2001). Aortic wall mechanics and composition in a transgenic mouse model of marfan syndrome. *Arterioscler Thromb Vasc Biol* **21:** 1184-9.

Mauban JR, Lamont C, Balke CW, Wier WG (2001). Adrenergic stimulation of rat resistance arteries affects Ca(2+) sparks, Ca(2+) waves, and Ca(2+) oscillations. *Am J Physiol Heart Circ Physiol* **280:** H2399-405.

Mauban JR, Wier WG (2004). Essential role of EDHF in the initiation and maintenance of adrenergic vasomotion in rat mesenteric arteries. *Am J Physiol Heart Circ Physiol* **287:** H608-16.

Maruyama T, Kanaji T, Nakade S, Kanno T, Mikoshiba K (1997). 2APB, 2-aminoethoxydiphenyl borate, a membrane-penetrable modulator of Ins(1,4,5)P3-induced Ca2+ release. *J Biochem* **122:** 498-505.

Marx SO, Reiken S, Hisamatsu Y, Jayaraman T, Burkoff D, Rosemblit N *et al.* (2000). PKA phosphorylation dissociates FKBP12.6 from the calcium release channel (ryanodine receptor): defective regulation in failing hearts. *Cell* **101:** 365-376.

Matt P, Habashi J, Carrel T, Cameron DE, Van Eyk JE, Dietz HC (2008). Recent advances in understanding marfan syndrome: Should we now treat surgical patients with losartan? *J Thorac Cardiovasc Surg* **135:** 389-94.

McCarron JG, Bradley KN, MacMillan D, Muir TC (2003). Sarcolemma agonist-induced interactions between InsP3 and ryanodine receptors in Ca2+ oscillations and waves in smooth muscle. *Biochem Soc Trans* **31:** 920-4.

McCarron JG, Olson ML (2008). A single luminally continuous sarcoplasmic reticulum with apparently separate Ca2+ stores in smooth muscle. *J Biol Chem* **283:** 7206-18.

McGeown JG (2004). Interactions between inositol 1,4,5-triphosphate receptors and ryanodine receptors in smooth muscle: one store or two? *Cell Calcium* **35:** 613-619.

Mchedlishvili G (1980). Physiological mechanisms controlling cerebral blood flow. *Stroke* **11:** 240-8.

Meininger GA, Zawieja DC, Falcone JC, Hill MA, Davey JP (1991). Calcium measurement in isolated arterioles during myogenic and agonist stimulation. *Am J Physiol Heart Circ Physiol* **26:** H950-H959.

Meyer C, De Vries G, Davidge ST, Mayes DC (2002). Reassessing the mathematical modeling of the contribution of vasomotion to vascular resistance. *J Appl Physiol* **92:** 888–889.

Milner RE, Famulski KS, Michalak M (1992). Calcium binding proteins in the sarcoplasmic/endoplasmic reticulum of muscle and nonmuscle cells. *Mol Cell Biochem* **112:** 1-13.

Milnor WR (1989). In: Collins N (ed). *Hemodynamics*. Williams & Wilkins: Baltimore, pp. 84-90.

Miriel VA, Mauban JR, Blaustein MP, Wier WG (1999). Local and cellular Ca2+ transients in smooth muscle of pressurized rat resistance arteries during myogenic and agonist stimulation. *J Physiol* **518:** 815-824.

Misrahy GA, Hardwick DF, Brooks CJ, Garwood VP, Hall WP (1962). Bone, bone marrow, and brain oxygen. *Am J Physiol* **202:** 225–231.

Montell C, Birnbaumer L, Flockerzi V, Bindels RJ, Bruford EA, Caterina MJ *et al.* (2002). A unified nomenclature for the superfamily of TRP cation channels. *Mol Cell* **9:** 229-31

Montell C (2005). The TRP superfamily of cation channels. *Sci STKE* **272:** Re3.

Montero M, Alonso MT, Camicero E, Cuchillo-Ibáñez I, Albillos A, García AG *et al.* (2000). Chromaffin-cell stimulation triggers fast millimolar mitochondrial Ca2+ transients that modulate secretion. *Nat Cell Biol*. **2:** 57–61.

Moore ED, Voigt T, Kobayashi YM, Isenberg G, Fay FS, Gallitelli MF, *et al.* (2004). Organization of Ca2+ release units in excitable smooth muscle of the guinea-pig urinary bladder. *Biophys J* **87:** 1836-47.

Mulvany MJ, Aalkjaer C (1990). Structure and function of small arteries. *Physiol Rev* **70**: 921-61.

Nakamura M, Itoh S, Makita S, Ohira A, Arakawa N, Hiramori K (2000). Peripheral resistance vessel dysfunction in Marfan syndrome. *Am Heart J* **139**: 661-6.

Nelson MT, Cheng H, Rubart M, Santana LF, Bonev AD, Knot HJ *et al.* (1995) Relaxation of arterial smooth muscle by calcium sparks. *Science* **270:** 633–637.

Nelson MT, Quayle JM (1995). Physiological roles and properties of potassium channels in arterial smooth muscle. *Am J Physiol* **268:** C799-822.

Ng CM, Cheng A, Myers LA, Martinez-Murillo F, Jie C, Bedja D *et al.* (2004). TGF-beta-dependent pathogenesis of mitral valve prolapse in a mouse model of Marfan syndrome. *J Clin Invest* **114**: 1586–1592.

Nishimura J, Khalil RA, van Breemen C (1989). Agonist-induced vascular tone. *Hypertension* **13:** 835-844.

Nixon GF, Mignery GA, Somlyo AV (1994). Immunogold localization of inositol 1,4,5-triphosphate receptors and characterization of ultrastructural features of the sarcoplasmic reticulum in phasic and tonic smooth muscle. *J Muscle Res Cell Motil* **15:** 682-700.

Ollila J, Lappalainen I, Vihinen M (1996). Sequence specificity in CpG mutation hotspots. *FEBS Lett* **396:** 119-22.

Parekh AB, Putney JW Jr (2005). Store-operated calcium channels. *Physiol Rev* **85:** 757-810.

Paul RJ (1990). Smooth muscle energetics and theories of cross-bridge regulation. *Am J Physiol* **258:** C369-375.

Peinelt C, Vig M, Koomoa DL, Beck A, Nadler MJ, Koblan-Huberson M, *et al.* (2006). Amplification of CRAC current by STIM1 and CRACM1 (Orai1). *Nat Cell Biol* **8:** 771-3.

Peng HL, Ivarsen A, Nilsson H, Aalkjær C (1998). On the cellular mechanism for the effect of acidosis on vascular tone. *Acta Physiol Scand* **164:** 517–525.

Peng H, Matchkov V, Ivarsen A, Aalkjaer C, Nilsson H (2001). Hypothesis for the initiation of vasomotion. *Circ Res* **88:** 810-815.

Perez GJ, Bonev AD, Patlak JB, Nelson MT (1999). Functional coupling of ryanodine receptors to KCa channels in smooth muscle cells from rat cerebral arteries. *J Gen Physiol* **113:** 229–238.

Perez JF, Sanderson MJ (2005). The contraction of smooth muscle cells of intrapulmonary arterioles is determined by the frequency of Ca2+ oscillations induced by 5-HT and KCl. *J Gen Physiol* **125:** 555-67.

Poburko D, Kuo KH, Dai J, Lee CH, van Breemen C (2004a). Organellar junctions promote targeted Ca2+ signaling in smooth muscle: why two membranes are better than one. *Trends Pharmacol Sci* **25:** 8-15.

Poburko D, Lee CH, and van Breemen C. (2004b). Vascular smooth muscle mitochondria at the cross roads of Ca2+ regulation. *Cell Calcium* **35:** 509–521.

Poburko D, Lhote P, Szado T, Behra T, Rahimian R, McManus B *et al.* (2004c). Basal calcium entry in vascular smooth muscle. *Eur J Pharmacol* **505:** 19-29.

Poburko D, Potter K, van Breemen E, Fameli N, Liao CH, Basset O, *et al.* (2006). Mitochondria buffer NCX-mediated Ca2+-entry and limit its diffusion into vascular smooth muscle cells. *Cell Calcium* **40:** 359-71.

Poburko D, Fameli N, Kuo KH, van Breemen C (2008). Ca2+ signaling in smooth muscle: TRPC6, NCX and LNats in nanodomains. *Channels (Austin)* **2:** 10-2.

Prakriya M, Feske S, Gwack Y, Srikanth S, Rao A, Hogan PG (2006). Orai1 is an essential pore subunit of the CRAC channel. *Nature* **443:** 230-3.

Prendergast FG (2000). Bioluminescence illuminated. *Nature* **405:** 291-3.

Proctor DN, Parker BA (2006). Vasodilation and vascular control in contracting muscle of the aging human. *Microcirculation* **13:** 315-27.

Putney JW Jr (1986). A model for receptor-regulated calcium entry. *Cell Calcium* **7:** 1-12.

Putney JW Jr (1993). Excitement about calcium signaling in inexcitable cells. *Science* **262:** 676-8.

Putney JW Jr (2007). New molecular players in capacitative Ca2+ entry. *J Cell Sci* **120:** 1959-65.

Pyeritz RE (2000). The Marfan syndrome. *Annu Rev Med* **51**:481-510.

Raeymaekers L, Eggermont JA, Wuytack F, Casteels R (1990). Effects of cyclic nucleotide dependent protein kinases on the endoplasmic reticulum Ca2+ pump of bovine pulmonary artery. *Cell Calcium* **11:** 261-8.

Raeymaekers L, Verbist J, Wuytack F, Plessers L, Casteels R (1993). Expression of Ca2+ binding proteins of the sarcoplasmic reticulum of striated muscle in the endoplasmic reticulum of pig smooth muscles. *Cell Calcium* **14:** 581-9.

Rahman A, Matchkov V, Nilsson H, Aalkjaer C (2005). Effects of cGMP on coordination of vascular smooth muscle cells of rat mesenteric small arteries. *J Vasc Res* **42:** 301-11.

Ramirez F, Dietz HC (2007). Fibrillin-rich microfibrils: Structural determinants of morphogenetic and homeostatic events. *J Cell Physiol* **213:** 326-30.

Ramirez F, Gayraud B, Pereira L (1999). Marfan syndrome: New clues to genotype-phenotype correlations. *Ann Med* **31:** 202-7.

Ramirez F, Sakai L, Dietz HC, Rifkin DB (2004). Fibrillin microfibrils: multipurpose extracellular networks in organismal physiology. *Physiol Genomics* **19:** 151-4.

Ramsey MW, Goodfellow J, Jones CJ, Luddington LA, Lewis MJ, Henderson AH (1995). Endothelial control of arterial distensibility is impaired in chronic heart failure. *Circulation* **92**: 3212-9.

Reading SA, Earley S, Waldron BJ, Welsh DG, Brayden JE (2005). TRPC3 mediates pyrimidine receptor-induced depolarization of cerebral arteries. *Am J Physiol Heart Circ Physiol* **288:** H2055-61.

Rembold CM, Murphy RA (1990). Muscle length, shortening, myoplasmic [Ca2+], and activation of arterial smooth muscle. *Circ Res* **66:** 1354-61.

Rizzuto R, Bastianutto C, Brini M, Murgia M, Pozzan T (1994). Mitochondrial Ca2+ homeostasis in intact cells. *J Cell Biol* **126:** 1183-94.

Rizzuto R, Pozzan T (2006). Microdomains of intracellular Ca2+: molecular determinants and functional consequents. *Physiol Rev* **86:** 369-408.

Ruehlmann DO, Lee CH, Poburko D, van Breemen C (2000). Asynchronous Ca(2+) waves in intact venous smooth muscle. *Circ Res* **86:** E72-9.

Roos J, DiGregorio PJ, Yeromin AV, Ohlsen K, Lioudyno M, Zhang S, *et al.* (2005). STIM1, an essential and conserved component of store-operated Ca2+ channel function. *J Cell Biol* **169:** 435-45.

Rosado JA (2006). Discovering the mechanism of capacitative calcium entry. *Am J Physiol Cell Physiol* **291:** C1104-6.

Rosado JA, Brownlow SL, Sage SO (2002). Endogenously expressed Trp1 is involved in store-mediated Ca2+ entry by conformational coupling in human platelets. *J Biol Chem* **277:** 42157-63.

Ross, R (1993). The pathogenesis of atherosclerosis: a perspective for the 1990s. *Nature* **362:** 801-809.

Rousseau E, Smith JS, Meissner G (1987). Ryanodine modifies conductance and gating behavior of single Ca2+ release channel. *Am J Physiol* **253:** C364-8.

Rummery NM, Hill CE (2004). Vascular gap junctions and implications for hypertension. *Clin Exp Pharmacol Physiol* **31:** 659-67.

Rutter GA, Burnett P, Rizzuto R, Brini M, Murgia M, Pozzan T, *et al.* (1996). Subcellular imaging of intramitochondrial Ca2+ with recombinant targeted aequorin: significance for the regulation of pyruvate dehydrogenase activity. *Proc Natl Acad Sci U S A* **93:** 5489-94.

Saida K, van Breemen C (1984). Characteristics of the norepinephrine-sensitive Ca2+ store in vascular smooth muscle. *Blood Vessels* **21:** 43-52.

Sakai LY, Keene DR, Engvall E (1986). Fibrillin, a new 350-kD glycoprotein, is a component of extracellular microfibrils. *J Cell Biol* **103:** 2499-509.

Sanders KM (2001). Mechanisms of calcium handling in smooth muscles. *J Appl Physiol* **91:** 1438-1449.

Sandow SL, Hill CE (2000). Incidence of myoendothelial gap junctions in the proximal and distal mesenteric arteries of the rat is suggestive of a role in endothelium-derived hyperpolarizing factor-mediated responses. *Circ Res* **86:** 341–346.

Sato K, Ozaki H, Karaki H (1988). Changes in cytosolic calcium level in vascular smooth muscle strip measured simultaneously with contraction using fluorescent calcium indicator fura 2. *J Pharmacol Exp Ther* **246:** 294-300.

Savolainen H, Savola J, Savolainen A (1993). Aneurysm of the iliac artery in Marfan's syndrome. *Ann Chir Gynaecol.* **82**: 203-5.

Schwartz SM, Campbell GR, Campbell JH (1986). Replication of smooth muscle cells in vascular disease. *Circ Res* **58:** 427-44.

Sheremet'eva GF, Ivanova AG, Belov IuV, Gens AP, Kocharian EZ (2004). A comparative study of the aortic wall in patients with Marfan's syndrome and Erdheim's disease. *Angiol Sosud Khir* **10**: 22-9.

Shi J, Mori E, Mori Y, Mori M, Li J, Ito Y, *et al.* (2004). Multiple regulation by calcium of murine homologues of transient receptor potential proteins TRPC6 and TRPC7 expressed in HEK293 cells. *J Physiol* **561:** 415-32.

Shimomura O, Inouye S, Musicki B, Kishi Y (1990). Recombinant aequorin and recombinant semi-synthetic aequorins. Cellular Ca2+ ion indicators. *Biochem J* **270:** 309-12.

Shimomura O, Kishi Y, Inouye S (1993). The relative rate of aequorin regeneration from apoaequorin and coelenterazine analogues. *Biochem J* **296:** 549-51.

Shimomura O, Musicki B, Kishi Y (1989). Semi-synthetic aequorins with improved sensitivity to Ca2+ ions. *Biochem J* **261:** 913-20.

Sitsapesan R, Williams AJ (1990). Mechanisms of caffeine activation of single calcium-release channels of sheep cardiac sarcoplasmic reticulum. *J Physiol* **423:** 425-39.

Smith JS, Imagawa T, Ma J, Fill M, Campbell KP, Coronado R (1988). Purified ryanodine receptor from rabbit skeletal muscle is the calcium-release channel of sarcoplasmic reticulum. *J Gen Physiol* **92:** 1-26.

Somlyo AP (1985). Excitation-contraction coupling and the ultrastructure of smooth muscle. *Circ Res* **57:** 497-507.

Stansberry KB, Shapiro SA, Hill MA, McNitt PM, Meyer MD, Vinik AI (1996). Impaired peripheral vasomotion in diabetes. *Diabetes Care* **19:** 715–721.

Streb H, Irvine RF, Berridge MJ, Schulz I (1983). Release of Ca2+ from a nonmitochondrial intracellular store in pancreatic acinar cells by inositol-1,4,5-trisphosphate. *Nature* **306:** 67-69.

Supattapone S, Worley PF, Baraban JM, Snyder SH (1988). Solubilization, purification, and characterization of an inositol trisphosphate receptor. *J Biol Chem* **263:** 1530-4.

Sward K, Mita M, Wilson DP, Deng JT, Susnjar M, Walsh MP (2003). The role of RhoA and Rho-associated kinase in vascular smooth muscle contraction. *Curr Hypertens Rep* **5:** 66-72.

Szegedi C, Sárközi S, Herzog A, Jóna I, Varsányi M (1999). Calsequestrin: more than 'only' a luminal Ca2+ buffer inside the sarcoplasmic reticulum. *Biochem J* **337:** 19-22.

Takeshima H, Komozaki S, Nishi M, Iino M, Kangawa K (2000). Junctophilins: a novel family of junctional membrane complex proteins. *Mol Cell* **6:** 11-22.

Tanaka H, Nishimaru K, Aikawa T, Hirayama W, Tanaka Y, Shigenobu K (2002). Effect of SEA0400, a novel inhibitor of sodium-calcium exchanger, on myocardial ionic currents. *Br J Pharmacol* **135:** 1096-100.

Thebault S, Zholos A, Enfissi A, Slomianny C, Dewailly E, Roudbaraki M, *et al.* (2005). Receptor-operated Ca(2+) entry mediated by TRPC3/TRPC6 proteins in rat prostate smooth muscle (PS1) cell line. *J Cell Physiol* **204:** 320-328.

Thyagarajan B, Poteser M, Romanin C, Kahr H, Zhu MX, Groschner K (2001). Expression of Trp3 determines sensitivity of capacitative Ca2+ entry to nitric oxide and mitochondrial Ca2+ handling. Evidence for a role of Trp3 as a subunit of capacitative Ca2+ entry channels. *J Biol Chem* **276:** 48149–48158.

Toborek M and Kaiser S (1999). Endothelial cell functions: relationship to atherogenesis. *Basic Res Cardiol* **94:** 295-314.

Trepakova ES, Csutora P, Hunton DL, Marchase RB, Cohen RA, and Bolotina VM (2000) Calcium influx factor directly activates store-operated cation channels in vascular smooth muscle cells. *J Biol Chem* **275:** 26158-26163.

Triggle, DJ (1999). The pharmacology of ion channels: with particular reference to voltage-gated Ca2+ channels. *Eur J Pharmacol* **375:** 311-25.

van Breemen C, Aaronson P, Loutzenhiser R (1978). Sodium-calcium interactions in mammalian smooth muscle. *Pharmacol Rev* **30:** 167-208.

van Breemen C, Poburko D, Okon EB (2006). TRP proteins: a new dimension in the treatment of occlusive vascular disease. *Circ Res* **98:** 446-447.

Venkatachalam K, Montell C (2007). TRP channels. *Annu Rev Biochem* **76:** 387-417.

Vanhoutte PM (2004). Endothelium-dependent hyperpolarizations: the history. *Pharmacol Res* **49**: 503-8.

Venkatachalam K, van Rossum DB, Patterson RL, Ma HT, Gill DL (2002). The cellular and molecular basis of store-operated calcium entry. *Nat Cell Biol* **4:** E263–72.

Vig M, Peinelt C, Beck A, Koomoa DL, Rabah D, Koblan-Huberson M, *et al.* (2006). CRACM1 is a plasma membrane protein essential for store-operated Ca2+ entry. *Science* **312:** 1220-3.

Vitarelli A, Conde Y, Cimino E, D'Angeli I, D'Orazio S, Stellato S, *et al.* (2006). Aortic wall mechanics in the marfan syndrome assessed by transesophageal tissue doppler echocardiography. *Am J Cardiol* **97:** 571-7.

Wagenseil JE, Mecham RP (2009). Vascular extracellular matrix and arterial mechanics. *Physiol Rev* **89:** 957-89.

Wellman GC, Nelson MT (2003). Signaling between SR and plasmalemma in smooth muscle: sparks and the activation of Ca(2+)-sensitive ion channels. *Cell Calcium* **34:** 211–229.

Wes PD, Chevesich J, Jeromin A, Rosenberg C, Stetten G, Montell C (1995). TRPC1, a human homolog of a Drosophila store-operated channel. *Proc Natl Acad Sci U S A* **92:** 9652-6.

Wilkinson IB, Qasem A, McEniery CM, Webb DJ, Avolio AP, Cockcroft JR (2002). Nitric oxide regulates local arterial distensibility in vivo. *Circulation* **105**: 213-7.

Williams A, Davies S, Stuart AG, Wilson DG, Fraser AG (2008). Medical treatment of marfan syndrome: a time for change. *Heart* **94:** 414-21.

Wilson DG, Bellamy MF, Ramsey MW, Goodfellow J, Brownlee M, Davies S, *et al.* (1999). Endothelial function in Marfan syndrome: selective impairment of flow-mediated vasodilation. *Circulation* **99**: 909-15.

Wilson DP, Sutherland C, Walsh MP (2002). Ca2+ activation of smooth muscle contraction: evidence for the involvement of calmodulin that is bound to the triton insoluble fraction even in the absence of Ca2+. *J Biol Chem* **277:** 2186-2192.

Wu KD, Bungard D, and Lytton J (2001). Regulation of SERCA Ca2+ pump expression by cytoplasmic [Ca2+] in vascular smooth muscle cells. *Am J Physiol* **280:** C843-C851.

Wu MM, Buchanan J, Luik RM, Lewis RS (2006). Ca2+ store depletion causes STIM1 to accumulate in ER regions closely associated with the plasma membrane. *J Cell Biol* **174:** 803-13.

Wuytack F, Eggermont JA, Raeymaekers L, Plessers L, and Casteels R (1989). Antibodies against the non-muscle isoform of the endoplasmic reticulum Ca2(+)-transport ATPase. *Biochem J* **264:** 765-769.

Xu L, Lai FA, Cohn A, Etter E, Guerrero A, Fay FS *et al.* (1994). Evidence for a Ca(2+)-gated ryanodine-sensitive Ca2+ release channel in visceral smooth muscle. *Proc Natl Acad Sci U S A* **91:** 3294-8.

Xu P, Lu J, Li Z, Yu X, Chen L, Xu T (2006). Aggregation of STIM1 underneath the plasma membrane induces clustering of Orai1. *Biochem Biophys Res Commun* **350:** 969-76.

Xu SZ, Beech DJ (2001). TrpC1 is a membrane-spanning subunit of store-operated Ca(2+) channels in native vascular smooth muscle cells. *Circ Res* **88:** 84-7.

Yuan JP, Zeng W, Huang GN, Worley PF, Muallem S (2007). STIM1 heteromultimerizes TRPC channels to determine their function as store-operated channels. *Nat Cell Biol* **9:** 636-45.

Zang WJ, Zacharia J, Lamont C, Wier WG (2006). Sympathetically evoked Ca2+ signaling in arterial smooth muscle. *Acta Pharmacol Sin* **27:** 1515-25.

Zhang KM, Hu P, Wang SW, Wright LD, Wechsler AS, Spratt JA, *et al.* (1998). The beta2-agonist salbutamol affects the expression of phospholamban and both isoforms of SERCA in canine skeletal muscle and blocks changes in these induced by neuromuscular stimulation. *Pflugers Arch* **435:** 511-7.

Zhang SL, Yeromin AV, Zhang XH, Yu Y, Safrina O, Penna A, *et al.* (2006). Genome-wide RNAi screen of Ca(2+) influx identifies genes that regulate Ca(2+) release-activated Ca(2+) channel activity. *Proc Natl Acad Sci U S A* **103:** 9357-62.

Zhang Y, Shao Z, Somlyo AP, Somlyo AV (1997). Cryo-atomic force microscopy of smooth muscle myosin. *Biophys J* **72:** 1308-18.

Zhong H, Minneman KP (1999). Alpha1-adrenoceptor subtypes *Eur J Pharmacol* **375:** 261-276.

ZhuGe R, Sims SM, Tuft RA, Fogarty KE, Walsh JV (1998). Ca2**+** sparks activate K**+** and Cl- channels, resulting in spontaneous transient currents in guinea-pig tracheal myocytes. *J Physiol* **513:** 711–718.

Zhu X, Jiang M, Birnbaumer L (1998). Receptor-activated Ca2+ influx via human Trp3 stably expressed in human embryonic kidney (HEK)293 cells. Evidence for a non-capacitative Ca2+ entry. *J Biol Chem* **273:** 133-42.

Zhu X, Jiang M, Peyton M, Boulay G, Hurst R, Stefani E, Birnbaumer L (1996). trp, a novel mammalian gene family essential for agonist-activated capacitative Ca2+ entry. *Cell* **85:** 661-71.

Zweifach A, Lewis RS (1993). Mitogen-regulated Ca2+ current of T lymphocytes is activated by depletion of intracellular Ca2+ stores. *Proc Natl Acad Sci U S A* **90:** 6295-9.

CHAPTER 2 - ATP PROMOTES NCX-REVERSAL IN AORTIC SMOOTH MUSCLE CELLS BY DAG-ACTIVATED NA^+ ENTRY[1]

2.1 Introduction

The Na^+/Ca^{2+} exchanger (NCX) is important in maintaining Ca^{2+} homeostasis in vascular smooth muscle, operating both in the forward (Ca^{2+}-efflux) and reverse (Ca^{2+}-influx) modes (Blaustein and Lederer, 1999; Brini *et al.,* 2002). NCX reversal has been shown by our laboratory and others to be responsible for Ca^{2+} entry following agonist stimulation in different cell types (Lee *et al.,* 2001; Takai *et al.,* 2004; Zhang *et al.,* 2005; Poburko *et al.,* 2006). Furthermore, reverse-mode NCX contributes to increased vascular tone and may be important in salt-sensitive hypertension (Iwamoto *et al.,* 2005).

Smooth muscle cell contraction depends on the regulation of cytosolic Ca^{2+}. Following stimulation of phospholipase C (PLC)-linked receptors, the Ca^{2+} profile in the cytosol is characterized by a transient increase due to release of sarcoplasmic reticulum (SR) Ca^{2+} stores, followed by a sustained plateau due to Ca^{2+} influx across the plasma membrane (PM). The transient phase is due to the production of inositol-1,4,5-triphosphate (IP_3) and the resulting opening of IP_3-sensitive channels (IP_3R) on the SR, while the sustained phase is due to the opening of receptor-operated channels (ROCs) and L-type voltage-gated Ca^{2+} channels. While the identity and mechanism of activation of ROCs remains to be fully elucidated, members of the transient receptor potential channel (TRP) family, especially from the ‘‘canonical’’ subfamily (TRPC), form non-selective cation channels (NSCCs) with many of the same properties as ROCs (Gudermann *et al.,* 2004).

[1] A version of this chapter has been published. Syyong HT, Poburko D, Fameli N, van Breemen C (2007). ATP promotes NCX-reversal in aortic smooth muscle cells by DAG-mediated Na+ entry. *Biochem Biophys Res Commun.* **357:** 1177-1182.

Agonist-induced NCX reversal has been suggested to be due in part to localized elevation of Na^+ at the subplasmalemmal junctions where both the NSCC and NCX are thought to co-localize (Arnon *et al.,* 2000). Previous studies support both physical and functional coupling of TRPC3 with NCX in HEK-293 cells (Rosker *et al.,* 2004). TRPC6 is closely related to TRPC3, and in rat aortic smooth muscle cells TRPC6 is expressed to greater levels than TRPC3 (Soboloff *et al.,* 2005; Maruyama *et al.,* 2006). TRPC6 is activated by diacylglycerol (DAG) and forms a NSCC with a Na^+:Ca^{2+} permeability ratio of ~1:5 (Inoue *et al.,* 2001; Estacion *et al.,* 2006). Our laboratory has recently provided the first evidence of functional coupling between TRPC6 and reverse-mode NCX in rat aortic smooth muscle cells (Lemos *et al.,* 2007). Following up on these findings, we now provide further evidence for functional coupling of TRPC6 and reverse-mode NCX by demonstrating that NCX reversal is potentiated following stimulation of rat aortic smooth muscle cells with ATP, which we know to elevate intracellular [Na^+] (Poburko *et al.,* 2006).

We used mitochondria-targeted aequorin to monitor mitochondrial Ca^{2+} as an indirect, but localized, measure of NCX reversal in cultured rat aortic smooth muscle cells. Aequorin is a powerful tool used to measure rapid changes in cellular [Ca^{2+}] and can be targeted to organelles such as the mitochondria to measure [Ca^{2+}] (Rizzuto *et al.,* 1992). Due to the close spatial association with the PM and superficial SR, a sub-population of mitochondria play an important role in Ca^{2+} homeostasis and can be stimulated to take up Ca^{2+} entry mediated by reverse-mode NCX following purinergic receptor stimulation; thereby buffering Ca^{2+} influx and preventing rapid diffusion throughout the cytosol (Szado *et al.,* 2003; Dai *et al.,* 2005; Poburko *et al.,* 2006).

2.2 Methods

2.2.1 Smooth muscle cell culture

Rat aortic smooth muscle cells were cultured as described previously (Szado *et al.,* 2003; Poburko *et al.,* 2006). Briefly, cells were stored in 90% DMEM / 10% DMSO in liquid nitrogen and used between passages 8 and 12. Cells were incubated at 37°C in a humidified atmosphere of 5% CO_2. For experiments, cells were plated on 13 mm Thermanox coverslips (Nunc, Life Technologies).

2.2.2 Expression of aequorin

Rat aortic smooth muscle cells were transiently transfected with a pcDNAI expression vector encoding apo-aequorin containing the amino terminal targeting sequence for human cytochrome oxidase VIII (mitoaequorin). Cells were allowed to grow on cover slips for 1 day before being washed with Ca^{2+}/Mg^{2+} free phosphate-buffered saline (PBS) that was replaced with 500 μL of DMEM (Dulbecco's modified Eagle's media (Sigma, D1152), 10% FCS, 100 U/mL penicillin G, 100 μg/mL streptomycin, MEM vitamin solution, and MEM essential and non-essential amino acid solution) before transfection. Cells were transfected using TransFectin (Bio-Rad) as per manufacturer's instructions (1 μg DNA per coverslip and a lipid:DNA ratio of 1:1) and were used for experiments the next day.

2.2.3 Measurement of mitochondrial [Ca^{2+}]

Mito-aequorin was reconstituted in coelenterazine (5 μM) in serum-free DMEM for 2–4 h before experiments. The coverslip was held in a 0.5-ml chamber heated constantly at 37 °C and was placed 5 mm from the photon detector. Cells were superfused at 1 mL/min with physiological

salt solution (PSS, in mM: NaCl 145, KCl 5, $MgCl_2$ 1, 4-(2-hydroxyethyl)-1-piperazineethanesulfonic acid (HEPES) 5, glucose 10, and $CaCl_2$ 1.2, pH 7.6). For $0Na^+$–PSS, Na^+ was replaced with 145 mM N-methyl-D-glucamine. Luminescence was detected by photomultiplier tubes (EMI 9789 and P25232, Electron Tubes Inc., USA) and photon emission was recorded at 1 Hz with EM6 photon-counting software (Electron Tubes Inc., USA). The EMI 9789 was coupled to an AD6 analog-digital converter and a CT-2 counting module (Electron Tubes Inc., USA), while the P25232 is a self-contained photon counting system. The offline-calibration of the photon emission to $[Ca^{2+}]$ was performed as previously described using the method of Allen and Blinks (Allen *et al.,* 1977; Allen and Blinks, 1978; Brini *et al.,* 1995; Szado *et al.,* 2003).

2.2.4 Experimental protocol

Rat aortic smooth muscle cells were initially superfused with PSS for 2 min, followed by $0Na^+$–PSS for 3 min, 9 min with PSS (recovery period), $0Na^+$–PSS for 3 min, and finally, PSS for 3 min. At the end of the protocol, cells were permeabilized with digitonin (100 μM) and then exposed to 10 mM $CaCl_2$ to determine total aequorin expression. The degree of recovery of NCX reversal was measured by taking the ratio of the two $0Na^+$–PSS mediated $[Ca^{2+}]_{MT}$ peaks ($0Na_2/0Na_1$ ratio). To determine the effects of ATP (1 mM) or the diacylglycerol analog 1-Oleoyl-2-acetyl-sn-glycerol (OAG, 100 μM) on the degree of recovery of NCX reversal, agonists were superfused (for 3 min) 3 min after the first $0Na^+$–PSS stimulation. To examine the effects of SKF-96365 (50 μM), a receptor-operated channel (ROC) antagonist, phorbol ester 12-tetradecanoylphorbol- 13 acetate (PMA, 1 μM), a direct activator of protein kinase C (PKC), or bisindolylmaleimide I (BIM, 500 nM), an inhibitor of PKC, these drugs were added for 2 min (1

min after the first $0Na^+$–PSS stimulation) prior to the application of ATP or OAG and continuation of the regular protocol.

2.2.5 Chemicals

All drugs were dissolved in DMSO to make stock solutions, except for ATP (distilled water). Drugs were then diluted to the appropriate concentration in PSS. 1-Oleoyl-2-acetyl-sn-glycerol (OAG) and bisindolylmaleimide I (BIM) were obtained from Calbiochem (San Diego, CA, USA). ATP, SKF-96365, and PMA were obtained from Sigma (St. Louis, MO, USA).

2.2.6 Statistical analysis

Values are expressed as means ± standard error (SEM). Means were compared using the most robust test appropriate to each experimental design. Groups of three or more means were compared by ANOVA with pair-wise comparisons made by Bonferroni post hoc tests. Traces are representative of at least six independent experiments performed in duplicate. Data were compiled and analyzed using GraphPad Prism 4.0, in coordination with Microsoft Excel. NCSS was used to perform statistical tests.

2.3 Results

2.3.1 Mitochondrial Ca^{2+} uptake following $0Na^+$–PSS stimulation is due to NCX reversal

NCX reversal induced by $0Na^+$–PSS results in an initial rapid increase in mitochondrial Ca^{2+} ($[Ca^{2+}]_{MT}$), which diminishes and is followed by a plateau phase (Fig. 2.1A). The transient increase is due to Ca^{2+}-influx following reversal of the NCX, while the plateau is due to

inhibition of Ca^{2+} extrusion by blockade of forward-mode NCX (Poburko *et al.*, 2006). The $0Na_2/0Na_1$ ratio is dependent on both the recovery period (time between $0Na^+$ and PSS stimulations) as well as the duration of the $0Na^+$–PSS stimulation. During 3 or 5 min $0Na^+$–PSS stimulation, the $0Na_2/0Na_1$ ratio is significantly smaller after 1 min of recovery compared to the $0Na_2/0Na_1$ ratios after 3 or 9 min recovery, which does not significantly differ from each other (Fig. 2.2B). However, if $0Na^+$–PSS stimulation is limited to 30 s, which is still sufficient to reach peak $[Ca^{2+}]_{MT}$, then the $0Na_2/0Na_1$ ratio is equivalently recovered after 1 or 3 min between stimulations (Fig. 2.1B).

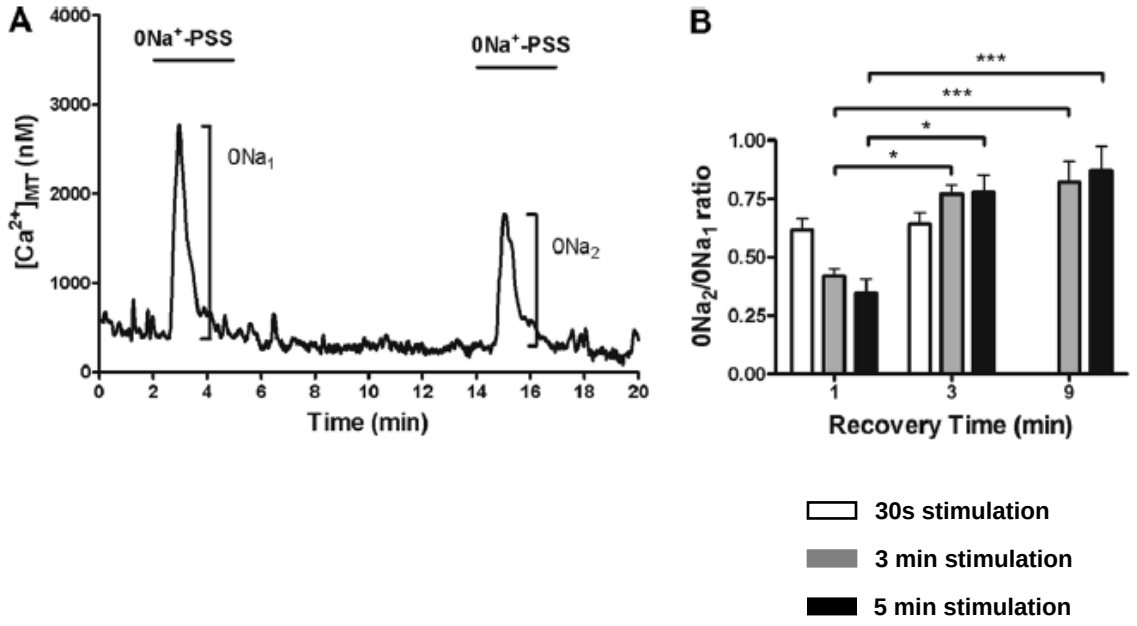

Figure 2.1: Recovery kinetics of $0Na^+$-PSS stimulation in mitochondria-targeted aequorin. A. The amplitude of the second $0Na^+$-mediated $[Ca^{2+}]_{MT}$ peak ($0Na_2$) was typically smaller than the first $[Ca^{2+}]_{MT}$ peak ($0Na_1$). **B.** The $0Na_2/0Na_1$ ratio, indicating the degree of NCX reversal recovery, is dependent on the time of stimulation with $0Na^+$-PSS. The $0Na_2/0Na_1$ ratio is not significantly different after 1 or 3 min of recovery (time between consecutive 30 s $0Na^+$ stimulations). However, the $0Na_2/0Na_1$ ratio is significantly lower after 1 min recovery (time between consecutive 3 or 5 min $0Na^+$ stimulations) compared to 3 and 9 min recovery time. Data were compared by one-way ANOVA, Bonferroni pairwise post-test. * $P < 0.05$, *** $P < 0.001$.

2.3.2 NCX reversal is increased upon purinergic receptor stimulation but inhibited by antagonists of NSCCs

Stimulation of rat aortic smooth muscle cells with ATP (1 mM) between consecutive $0Na^+$–PSS stimulations always increased the second $[Ca^{2+}]_{MT}$ peak compared to the first $[Ca^{2+}]_{MT}$ peak (Fig. 2.2A). This is reflected in the increased $0Na_2/0Na_1$ ratio compared to control (Fig. 2.2C). Furthermore, the DAG analog, 1-Oleoyl-2-acetyl-sn-glycerol (100 μM, OAG), similarly increased the $0Na_2/0Na_1$ ratio (Fig. 2.2C).

Based on reports that DAG can activate members of the TRPC family (Venkatachalam *et al.*, 2003), we hypothesized that PLC-mediated DAG generation increases Na^+ entry into the cells by opening NSCCs and thereby enhances NCX reversal upon removal of extracellular Na^+. To test this hypothesis by inhibiting NSCCs, we applied SKF-96365 (50 μM) to the rat aortic smooth muscle cells prior to stimulation with ATP or OAG. SKF-96365 inhibited the ATP and OAG-mediated increases in NCX reversal, but did not directly affect the $0Na_2/0Na_1$ ratio (Fig. 2.2B,D).

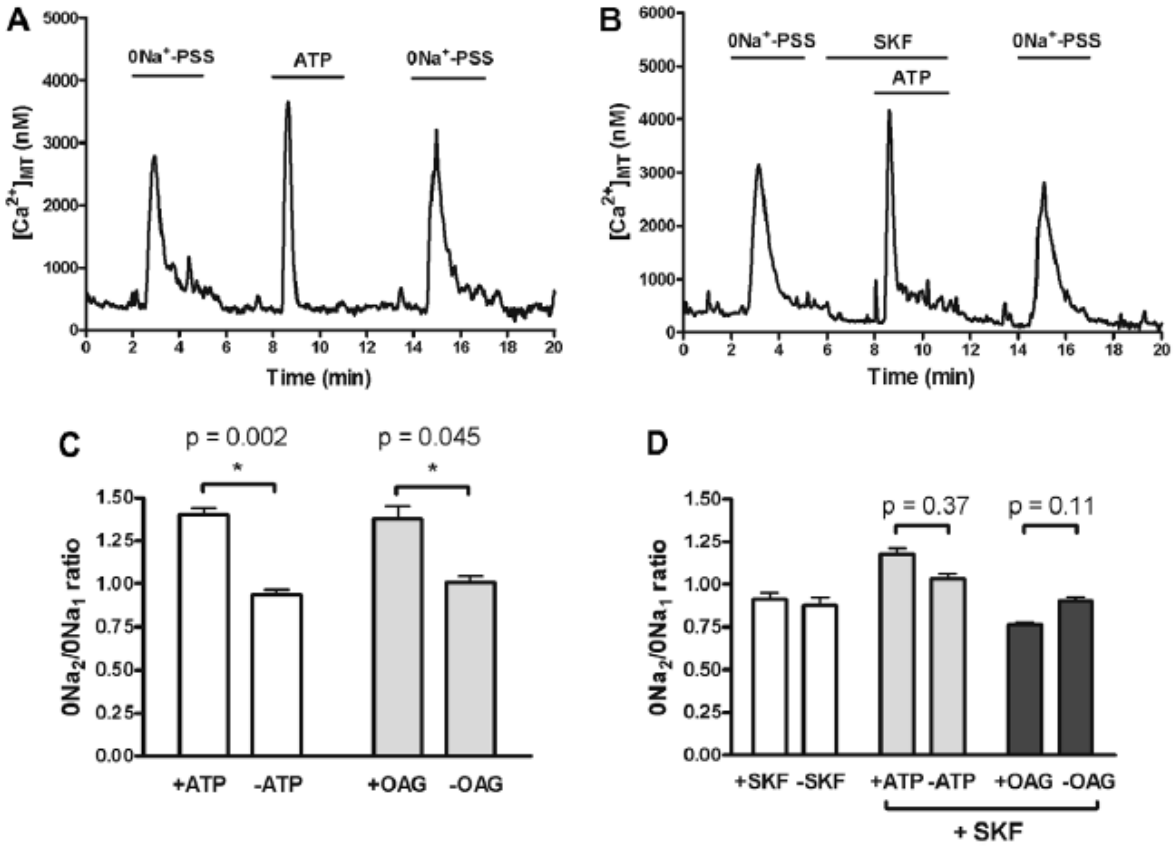

Figure 2.2 SKF-96365 (SKF) attenuates ATP- and 1-Oleoyl-2-acetyl-sn-glycerol (OAG)-induced increase in NCX reversal. A. Representative trace when cells are stimulated with ATP (1 mM) between consecutive $0Na^+$ stimulations, showing a greater amplitude of the second $0Na^+$–PSS mediated $[Ca^{2+}]_{MT}$ peak compared to the first. **B.** Representative trace when cells are incubated with SKF (50 μM) for 2 min prior to stimulation with ATP between consecutive $0Na^+$ stimulations, showing a reduced amplitude of the second $0Na^+$–PSS mediated $[Ca^{2+}]_{MT}$ peak compared to A. **C.** Stimulation with ATP or OAG (100 μM) between consecutive $0Na^+$ stimulations significantly increases the $0Na_2/0Na_1$ ratio. **D.** The increase in the $0Na_2/0Na_1$ ratio due to ATP and OAG is attenuated in the presence of SKF (50 μM). Data were analyzed using paired t-tests. *P*-values are shown for specific comparisons. * $P < 0.05$.

2.3.3 Protein kinase C has an inhibitory effect on NCX reversal

To determine the possible involvement of PKC in the purinergically activated cascade, rat aortic smooth muscle cells were pre-treated with the PKC inhibitor bisindolylmaleimide I (BIM, 500 nM, Fig. 2.3A,C). Pre-treatment of the rat aortic smooth muscle cells with BIM prior to ATP stimulation had no significant effect on the $0Na_2/0Na_1$ ratio. When rat aortic smooth muscle cells

were pre-treated with PMA (1 μM) to activate PKC prior to ATP stimulation, the $0Na_2/0Na_1$ ratio was significantly decreased (Fig. 2.3B,D).

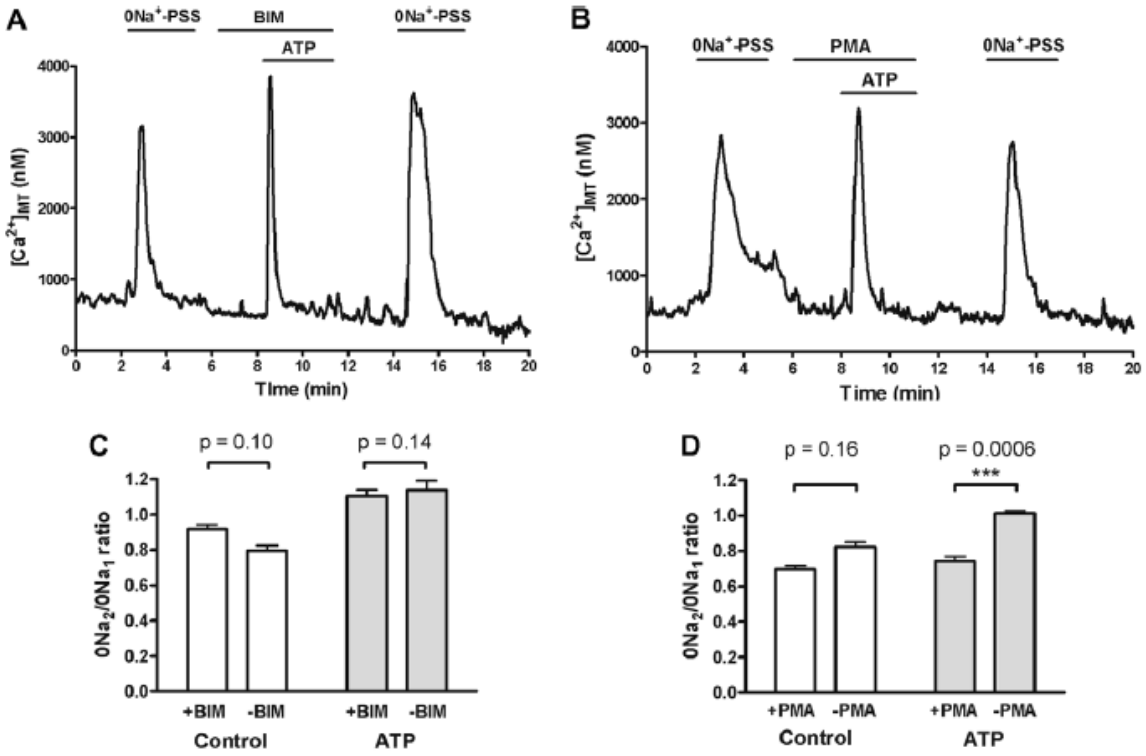

Figure 2.3 Role of protein kinase C (PKC) in ATP-stimulated NCX reversal. A. Representative trace when cells are pre-incubated with bisindolylmaleimide I (BIM, 500 nM) for 2 min prior to stimulation with ATP (1 mM) between consecutive $0Na^+$ stimulations. **B.** Representative trace when cells preincubated with 12-tetradecanoylphorbol-13 acetate (PMA, 1 μM) for 2 min prior to stimulation with ATP (1 mM) between consecutive $0Na^+$ and PSS stimulations. **C.** Inhibition of PKC with BIM (500 nM) alone or during stimulation with ATP (1 mM) does not change the $0Na_2/0Na_1$ ratio. **D.** Direct activation of PKC by PMA (1 μM) alone does not change the $0Na_2/0Na_1$ ratio, although PMA application prior to ATP stimulation (1 mM) significantly decreases the $0Na_2/0Na_1$ ratio. Data were analyzed using paired t-tests. *P*-values are shown for specific comparisons. *** $P < 0.001$.

2.4 Discussion

Acute removal of extracellular Na^+ causes transient reversal of the NCX, resulting in Ca^{2+} entry, by reversing the plasmalemmal Na^+-gradient (Poburko *et al.*, 2006). The Ca^{2+} entry by

reverse-mode NCX eventually declines as the intracellular [Na^+] decreases, explaining the transient nature of the mitochondrial Ca^{2+} response to $0Na^+$–PSS. Based on the observation that recovery of the $0Na^+$–PSS response is stabilized after 1 min following a 30 s stimulation, while requiring 3 min following 3 or 5 min stimulation, we concluded that the reduced response to a second $0Na^+$ stimulation was due to depletion of intracellular Na^+, rather than the NCX being directly inhibited by Ca^{2+}, as has been suggested (Opuni and Reeves, 2000).

Diacylglycerol (DAG) has been shown to activate TRPC6 channels following agonist stimulation of G-protein coupled receptors (Estacion *et al.,* 2006). In these smooth muscle cells, ATP activates metabotropic P_2Y, G-protein coupled receptors resulting in the production of IP_3 and DAG (Szado *et al.,* 2003). Furthermore, ATP stimulation has also been demonstrated to increase cytosolic [Na^+], which promotes NCX reversal (Poburko *et al.,* 2006). Having previously shown that TRPC6 is expressed in these cells (Poburko *et al.,* 2004) and that its activation is essential to agonist-induced Ca^{2+} entry via reverse-mode NCX (Lemos *et al.,* 2007), our current findings suggest that DAG provides the stimulatory link between purinergic receptor activation and the opening of TRPC6-containing ROCs. Although DAG is an activator of TRPC6, DAG and its analogs are also well-known activators of protein kinase C (PKC) (Go *et al.,* 1987, Lee and Severson, 1994; Albert and Large, 2004). PKC in turn has been reported to inhibit TRPC6 (Venkatachalam *et al.,* 2003; Estacion *et al.,* 2006).

The IC_{50} of BIM for PKC subtypes a, b, and c (the most common Ca^{2+}-dependent PKC subtypes) is reported to range from 16 to 20 nM, so 500 nM should completely inhibit PKC activity (Toullec *et al.,* 1991; Albert *et al.,* 2003). This suggests that PKC does not directly regulate the activation of NSCCs by ATP in these cells and is consistent with previous findings showing that PKC does not activate these channels (Venkatachalam *et al.,* 2003). While PKC has

been reported to directly activate Ca^{2+} influx via reverse-mode NCX (Aiello *et al.,* 2005), such an effect is unlikely under these conditions given the PMA-mediated decrease in the $0Na_2/0Na_1$ ratio. Rather, our present results are consistent with recent observations demonstrating that OAG-induced cation entry mediated by TRPC6 channels is not activated by PKC, but rather can be inhibited by PKC if it is activated prior to stimulation with OAG or ATP (Venkatachalam *et al.,* 2003). Our current results raise the question of why ATP stimulation results in a net increase in NCX reversal in response to $0Na^+$–PSS if DAG activates both TRPC6 and PKC. One simple explanation is that PKC activation during ATP stimulation is not sufficient to inhibit TRPC6, which is consistent with the lack of observable effects of BIM. On the other hand, two different PLC pathways might be activated upon ATP stimulation: one of which directly activates TRPC6, while the other activates PKC, as has been suggested in previous studies of TRPC6-like channels (Toullec *et al.,* 1991; Lee and Severson, 1994; Albert *et al.,* 2003; Albert and Large, 2004). In our system, ATP stimulation may not recruit the appropriate PKC isoforms to the cell membrane, while the application of the high concentration of PMA likely activates all PKC isoforms. However, further experiments are required to clarify whether and/or where PKC is activated during ATP stimulation in these cells.

In conclusion, this study adds to our recently published work by providing further mechanistic insight into the functional linkage between reverse-mode NCX and TRPC6. We show that agonist-stimulated production of DAG is important to the increased Na^+ entry that facilitates the reversal of NCX, which is an essential component of the agonist-mediated Ca^{2+} entry in rat aortic smooth muscle cells. We also show that Na^+ entry can be inhibited by PKC activation, but that this effect is not sufficiently prominent during purinergic stimulation to abolish the stimulatory effect of DAG.

2.5 References

Aiello EA, Villa-Abrille MC, Dulce RA, Cingolani HE, Pérez NG (2005). Endothelin-1 stimulates the Na+/Ca2+ exchanger reverse mode through intracellular Na+ (Na+i)-dependent and Na+i-independent pathways. *Hypertension* **45:** 288-93.

Albert AP, Piper AS, Large WA (2003). Properties of a constitutively active Ca2+-permeable non-selective cation channel in rabbit ear artery myocytes. *J Physiol* **549:** 143-56.

Albert AP, Large WA (2004). Inhibitory regulation of constitutive transient receptor potential-like cation channels in rabbit ear artery myocytes. *J Physiol* **560:** 169-80.

Allen DG, Blinks JR, Prendergast FG (1977). Aequorin luminescence: relation of light emission to calcium concentration--a calcium-independent component. *Science* **195:** 996-8.

Allen DG, Blinks JR (1978). Calcium transients in aequorin-injected frog cardiac muscle. *Nature* **273:** 509-13.

Arnon A, Hamlyn JM, Blaustein MP (2000). Na(+) entry via store-operated channels modulates Ca(2+) signaling in arterial myocytes. *Am J Physiol Cell Physiol* **278:** C163-73.

Blaustein MP and Lederer WJ (1999). Sodium/calcium exchange: its physiological implications. *Physiol Rev* **79:** 763–854.

Brini M, Marsault R, Bastianutto C, Alvarez J, Pozzan T, Rizzuto R (1995). Transfected aequorin in the measurement of cytosolic Ca2+ concentration ([Ca2+]c): a critical evaluation. *J Biol Chem* **270:** 9896-903.

Brini M, Manni S, Carafoli E (2002). Recombinant expression of the plasma membrane Na(+)/Ca(2+) exchanger affects local and global ca(2+) homeostasis in chinese hamster ovary cells. *J Biol Chem* **277:** 38693–38699.

Dai J, Kuo KH, Leo JM, van Breemen C, Lee CH (2005). Rearrangement of the close contact between the mitochondria and the sarcoplasmic reticulum in airway smooth muscle. *Cell Calcium* **37:** 333–340.

Estacion M, Sinkins WG, Jones SW, Applegate MA, Schilling WP (2006). Human TRPC6 expressed in HEK 293 cells forms non-selective cation channels with limited Ca2+ permeability. *J Physiol* **572:** 359-77.

Go M, Sekiguchi K, Nomura H, Kikkawa U, Nishizuka Y (1987). Further studies on the specificity of diacylglycerol for protein kinase C activation. *Biochem Biophys Res Commun* **144:** 598-605.

Gudermann T, Mederos y Schnitzler M, Dietrich A (2004). Receptor-operated cation entry--more than esoteric terminology? *Sci STKE* **243**: pe35

Inoue R, Okada T, Onoue H, Hara Y, Shimizu S, Naitoh S, *et al.* (2001). The transient receptor potential protein homologue TRP6 is the essential component of vascular alpha(1)-adrenoceptoractivated Ca(2+)-permeable cation channel. *Circ Res* **88:** 325–332.

Iwamoto T, Kita S, Katsuragi T (2005). Salt-sensitive hypertension, Na+/Ca2+ exchanger, and vascular smooth muscle. *Trends Cardiovasc Med* **15:** 273-7.

Lee CH, Poburko D, Sahota P, Sandhu J, Ruehlmann DO, van Breemen C (2001). The mechanism of phenylephrine-mediated [Ca(2+)](i) oscillations underlying tonic contraction in the rabbit inferior vena cava. *J Physiol* **534:** 641-650.

Lee MW, Severson DL (1994). Signal transduction in vascular smooth muscle: diacylglycerol second messengers and PKC action. *Am J Physiol* **267:** C659-78.

Lemos VS, Poburko D, Liao CH, Cole WC, van Breemen C (2007). Na+ entry via TRPC6 causes Ca2+ entry via NCX reversal in ATP stimulated smooth muscle cells. *Biochem Biophys Res Commun* **352:** 130-4.

Maruyama Y, Nakanishi Y, Walsh EJ, Wilson DP, Welsh DG, Cole WC (2006). Heteromultimeric TRPC6-TRPC7 channels contribute to arginine vasopressin-induced cation current of A7r5 vascular smooth muscle cells. *Circ Res* **98:** 1520-7.

Opuni K, Reeves JP (2000). Feedback inhibition of sodium/calcium exchange by mitochondrial calcium accumulation. *J Biol Chem* **275:** 21549-54.

Poburko D, Lhote P, Szado T, Behra T, Rahimian R, McManus B, *et al.* (2004). Basal calcium entry in vascular smooth muscle. *Eur J Pharmacol* **505:** 19-29.

Poburko D, Potter K, van Breemen E, Fameli N, Liao CH, Basset O, *et al.* (2006). Mitochondria buffer NCX-mediated Ca2+-entry and limit its diffusion into vascular smooth muscle cells. *Cell Calcium* **40:** 359-71.

Rizzuto R, Simpson AW, Brini M, Pozzan T (1992). Rapid changes of mitochondrial Ca2+ revealed by specifically targeted recombinant aequorin. *Nature* **358:** 325–327.

Rosker C, Graziani A, Lukas M, Eder P, Zhu MX, Romanin C, *et al.* (2004). Ca(2+) signaling by TRPC3 involves Na(+) entry and local coupling to the Na(+)/Ca(2+) exchanger. *J Biol Chem* **279:** 13696-704.

Soboloff J, Spassova M, Xu W, He LP, Cuesta N, Gill DL (2005). Role of endogenous TRPC6 channels in Ca2+ signal generation in A7r5 smooth muscle cells. *J Biol Chem* **280:** 39786-94.

Szado T, Kuo KH, Bernard-Helary K, Poburko D, Lee CH, Seow C, *et al.* (2003). Agonist-induced mitochondrial Ca2+ transients in smooth muscle. *FASEB J* **17:** 28-37.

Takai N, Yamada A, Muraki K, Watanabe M, Imaizumi Y (2004). KB-R7943 reveals possible involvement of Na(+)-Ca2+ exchanger in elevation of intracellular Ca2+ in rat carotid arterial myocytes. *J Smooth Muscle Res* **40:** 35-42.

Toullec D, Pianetti P, Coste H, Bellevergue P, Grand-Perret T, Ajakane M, *et al.* (1991). The bisindolylmaleimide GF 109203X is a potent and selective inhibitor of protein kinase C. *J Biol Chem* **266:** 15771-81.

Venkatachalam K, Zheng F, Gill DL (2003). Regulation of canonical transient receptor potential (TRPC) channel function by diacylglycerol and protein kinase C. *J Biol Chem* **278:** 29031-40.

Zhang S, Yuan JX, Barrett KE, Dong H (2005). Role of Na+/Ca2+ exchange in regulating cytosolic Ca2+ in cultured human pulmonary artery smooth muscle cells. *Am J Physiol Cell Physiol* **288:** C245-52.

CHAPTER 3 - MECHANISM OF ASYNCHRONOUS CA^{2+} WAVES UNDERLYING AGONIST-INDUCED CONTRACTION IN THE RAT BASILAR ARTERY[2]

3.1 Introduction

Uridine 5'-triphosphate (UTP) is a potent constrictor of cerebral arteries which exerts its effects through purinergic P2Y receptors and the phospholipase C pathway (Urquilla, 1978; Strobaek *et al.*, 1996; Horiuchi *et al.*, 2001). Brain tissue is especially rich in UTP and cerebral vessels have greater reactivity to UTP compared with other vessels (Shirasawa *et al.*, 1983; Hardebo *et al.*, 1987). UTP may be involved in the regulation of cerebrovascular tone under both physiological conditions and pathophysiological reactions in disease states such as subarachnoid haemorrhage or migraine (Debdi *et al.*, 1992; Boarder and Hourani, 1998; Burnstock, 1998).

Smooth muscle contraction is initiated by an increase of intracellular Ca^{2+} ($[Ca^{2+}]_i$) from resting levels of ~100 nM to values up to 1 mM. In general, the $[Ca^{2+}]_i$ profile following stimulation is biphasic, consisting of a rapid transient rise in $[Ca^{2+}]_i$ from sarcoplasmic reticulum (SR) Ca^{2+} release followed by a plateau phase, which is mediated by Ca^{2+} entry from voltage-gated Ca^{2+} channels and store/receptor-operated channels (van Breemen *et al.*, 1978; Bolton, 1979; Streb *et al.*, 1983; Putney, 1986). The advent of confocal microscopy has allowed the employment of physiological preparations to examine the Ca^{2+} signals in individual *in situ* vascular smooth muscle cells (VSMCs) of intact blood vessels. It has since become apparent that the average arterial wall $[Ca^{2+}]_i$ observed previously is not representative of the Ca^{2+} signaling events within individual VSMCs, which are capable of generating Ca^{2+} signals with varying spatial and temporal patterns (Lee *et al.*, 2002). Among these signals are Ca^{2+} waves, which are

[2] A version of this chapter has been published. Syyong HT, Yang HH, Trinh G, Cheung C, Kuo KH, van Breemen C (2009). Mechanism of asynchronous Ca(2+) waves underlying agonist-induced contraction in the rat basilar artery. *Br J Pharmacol* **156:** 587-600.

manifested as changes in $[Ca^{2+}]_i$ which travel the length of VSMCs, and constitute a specialized form of agonist-induced Ca^{2+} signalling which appears to be involved in contractile regulation. Since 1994 when they were first described, Ca^{2+} waves have been observed in the smooth muscle fibres of a variety of intact blood vessels, including cerebral vessels (Iino *et al.*, 1994; Asada *et al.*, 1999; Miriel *et al.*, 1999; Jaggar, 2001; Lee *et al.*, 2001; Peng *et al.*, 2001). Although there are likely to be underlying physiological reasons for signalling with Ca^{2+} waves (as opposed to steady state $[Ca^{2+}]_i$ elevations), the mechanisms behind how Ca^{2+} waves within individual VSMCs signal for contraction remain poorly understood.

Ca^{2+} waves in cerebral arteries can be induced by a variety of stimuli, including vasoconstrictor agonists such as UTP, pressure and alkaline pH (Jaggar and Nelson, 2000; Jaggar, 2001; Heppner *et al.*, 2002). In cerebral arteries, UTP stimulation shifts Ca^{2+} sparks to Ca^{2+} waves through the differential regulation of inositol-1,4,5-triphosphate receptors (IP_3Rs) and ryanodine receptors (RyRs) (Jaggar and Nelson, 2000). From studies in cultured basilar artery smooth muscle cells, it is generally accepted that UTP induces vasoconstriction by a combination of stimulated plasma membrane Ca^{2+} entry and SR Ca^{2+} release (Sima *et al.*, 1997). However, little is known about the mechanism underlying between agonist-induced Ca^{2+} waves and their relationship to vasoconstriction in the cerebral vasculature.

In our present study, we investigated the mechanism of UTP-induced Ca^{2+} waves in the rat basilar artery, focusing on the mode(s) of Ca^{2+} entry involved in sustaining the UTP-induced cyclical release of Ca^{2+} by identifying the Ca^{2+} transport molecules involved in the generation and maintenance of UTP-induced Ca^{2+} waves.

3.2 Methods

3.2.1 Tissue preparation

Male Sprague-Dawley rats (250-350g) were obtained from Charles River and housed in the institutional animal facility (University of British Columbia, Child and Family Research Institute) under standard animal room conditions (12h light-12h dark, at 25ºC, 2 animals in a cage). All the experiments and procedures were carried out in accordance with the guidelines of the University of British Columbia. Rats were anesthetized with a mixture of ketamine hydrochloride (70 mg•kg^{-1}) and xylazine hydrochloride (5 mg•kg^{-1}) given intraperitoneally. The brain was quickly removed and placed in ice-cold, oxygenated (95% O_2-5% CO_2) Krebs solution. The basilar artery (180-280 μm in diameter) was removed, carefully cleaned, and cut into 2 mm segments. Endothelial denudation was achieved by gently rubbing the inside of the vessel with a 40μm tungsten wire.

3.2.2 Measurement of intracellular Ca^{2+}

The arterial rings were loaded with Fluo-4AM (5 μM with 5 μM Pluronic F-127, 1 hr at 37ºC) and isometrically mounted, followed by a 30 min washout time in 4-(2-hydroxyethyl)-1-piperazineethanesulfonic acid (HEPES)-buffered physiological saline solution (PSS). Sustained Ca^{2+} waves were induced by 100 μM UTP, and all mechanistic studies were done at this concentration. Images were acquired on an upright Olympus BX50WI microscope with a 60x water-dipping objective (NA 0.9) and equipped with an Ultraview confocal imaging system (Perkin-Elmer). The rate of image acquisition was 3 frames/s. The tissue was illuminated using the 488nm line of an Argon-Krypton laser and a high-gain photomultiplier tube collected the emission at wavelengths between 505 and 550 nm. The scanned regions correspond to a 91.685 x

66.68 μm area (or 248 x 328 pixels). The representative fluorescence traces shown reflect the averaged fluorescence signals from a region of 3 x 3 pixels (1.69 μm^2) of the smooth muscle cell. The frequency of Ca^{2+} waves was determined by counting the number of waves occurring within a period of 50s. The measured changes in Fluo-4 fluorescence level are proportional to the relative changes in $[Ca^{2+}]_i$. All parameters (laser intensity, gain, etc) were maintained constant during the experiment. The confocal images were analyzed off-line with the Ultraview 4.0 Software (Perkin-Elmer). Fluorescence traces were extracted from the movies to exclude nuclear regions and traces were normalized to initial fluorescence values.

3.2.3 Measurement of isometric force

Basilar artery segments were mounted isometrically in a small vessel wire myograph (A/S Danish Myotechnology, Aarhus N, Denmark), using two 40 μm tungsten wires, for measuring generated force. The chambers were kept at 37ºC and bubbled continuously with 95% O_2-5% CO_2 in Krebs solution. Optimal tension was determined in preliminary experiments by subjecting arterial segments to different resting tensions and stimulating with 60 mM KCl. The vessels were stretched to the optimal tension (obtained from preliminary experiments, the maximal force generation given in response to 60 mM KCl; 3mN) for 60 min. The vessels were challenged twice with 60 mM KCl before experiments were continued. The percent of contraction compared to the second 60 mM KCl-induced contraction was recorded at different concentrations of UTP and concentration-response curves were constructed. Tonic contraction was induced by 100 μM UTP and all mechanistic studies done at this concentration. The negative logarithm (pD_2) of the concentration of UTP giving half-maximum response (EC_{50}) was

assessed by linear interpolation on the semilogarithm concentration-response curve [$pD_2 = -\log(EC_{50})$].

3.2.4 Statistics

Values are expressed as mean ± standard error (SEM) from at least six independent experiments. Statistical analysis and construction of concentration-response curves were performed using GraphPad Prism 4.0 software (San Diego, CA, USA). Differences between groups were analyzed by Student's two-tailed *t*-test. Statistical significance was defined as P-values <0.05.

3.2.5 Drugs, solutions, and chemicals

HEPES-PSS containing (in mM) NaCl 140, glucose 10, KCl 5, HEPES 5, $CaCl_2$ 1.5, and $MgCl_2$ 1 (pH 7.4) was used for all confocal studies. Hi-K^+ (60 mM extracellular K^+) PSS was identical in composition to normal PSS with the exception of (in mM) NaCl 85 and KCl 60. Zero-Ca^{2+} PSS was prepared in the same way as normal PSS, but $CaCl_2$ was replaced with 1 mM ethylene glycol tetraacetic acid (EGTA). Krebs solution containing (in mM) NaCl 119, glucose 11.1, KCl 4.7, $CaCl_2$ 1.6, KH_2PO_4 1.18, $MgSO_4$ 1.17, and ethylenediaminetetraacetic acid (EDTA) 0.023 (pH 7.4) were used for all isometric contraction studies. UTP, CPA, 2-APB, nifedipine, SKF-96365, tetracaine, and pluronic F-127 were obtained from Sigma-Aldrich (Oakville, Ontario, Canada). Ryanodine and KB-R7943 were obtained from Calbiochem (Gibbstown, NJ, USA). Fluo-4AM was purchased from Molecular Probes (Eugene, OR).

3.3 Results

3.3.1 Relation between UTP-induced tonic contraction and UTP-induced Ca^{2+}-waves

UTP produced tonic contraction in a concentration-dependent manner, with a pEC_{50} of 4.34 ± 0.13 and maximal response (E_{max}) of 105.5 ± 7.3% (normalized to contraction at 60 mM KCl, n = 9 animals, Fig. 3.1A,B). At 100 μM UTP, the average contraction was 70.3 ± 4.5% (n = 12 animals, normalized to contraction at 60 mM KCl). In parallel experiments, confocal microscopy was used to observe changes in $[Ca^{2+}]_i$ within the smooth muscle cells following UTP stimulation. In the absence of UTP, asynchronous Ca^{2+} waves of low amplitude were observed in a small percentage (< 10%) of the cells, similar to the "Ca^{2+} ripples" described previously in rat tail artery (Asada *et al.,* 1999). Application of UTP induced a large transient Ca^{2+} response which was followed by sustained repetitive oscillations in intracellular $[Ca^{2+}]_i$ which propagated along the length of the smooth muscle cell as Ca^{2+} waves (Fig. 3.1C and 3.2). The frequency of Ca^{2+} waves increased in a concentration-dependent manner, closely paralleling the development of force (Fig. 3.1D, pEC_{50} = 4.74 ± 0.14, maximum frequency = 0.089 ± 0.007Hz, 109 cells from 12 animals). At 100 μM UTP, the average frequency of the Ca^{2+} waves was 0.082 ± 0.005 Hz (n = 48 cells from 8 animals). The number of cells displaying Ca^{2+} waves were also concentration-dependent; at 100 μM UTP, 91.34 ± 2.45 % of cells displayed at least one Ca^{2+} wave (n = 48 cells from 8 animals, Fig. 3.1E). The velocity of wave propagation, illustrated in Fig. 3.1F, also shows a strong correlation with UTP concentration; At the highest concentrations, wave propagation speeds reached 67.51 ± 3.62 μm/s (n = 10 cells from 4 animals). The Ca^{2+} waves originated from distinct intracellular foci and propagated down the longitudinal axis of the individual smooth muscle cells (Fig. 3.2). They did not appear to propagate intercellularly, and were sustained during the entire experimental period.

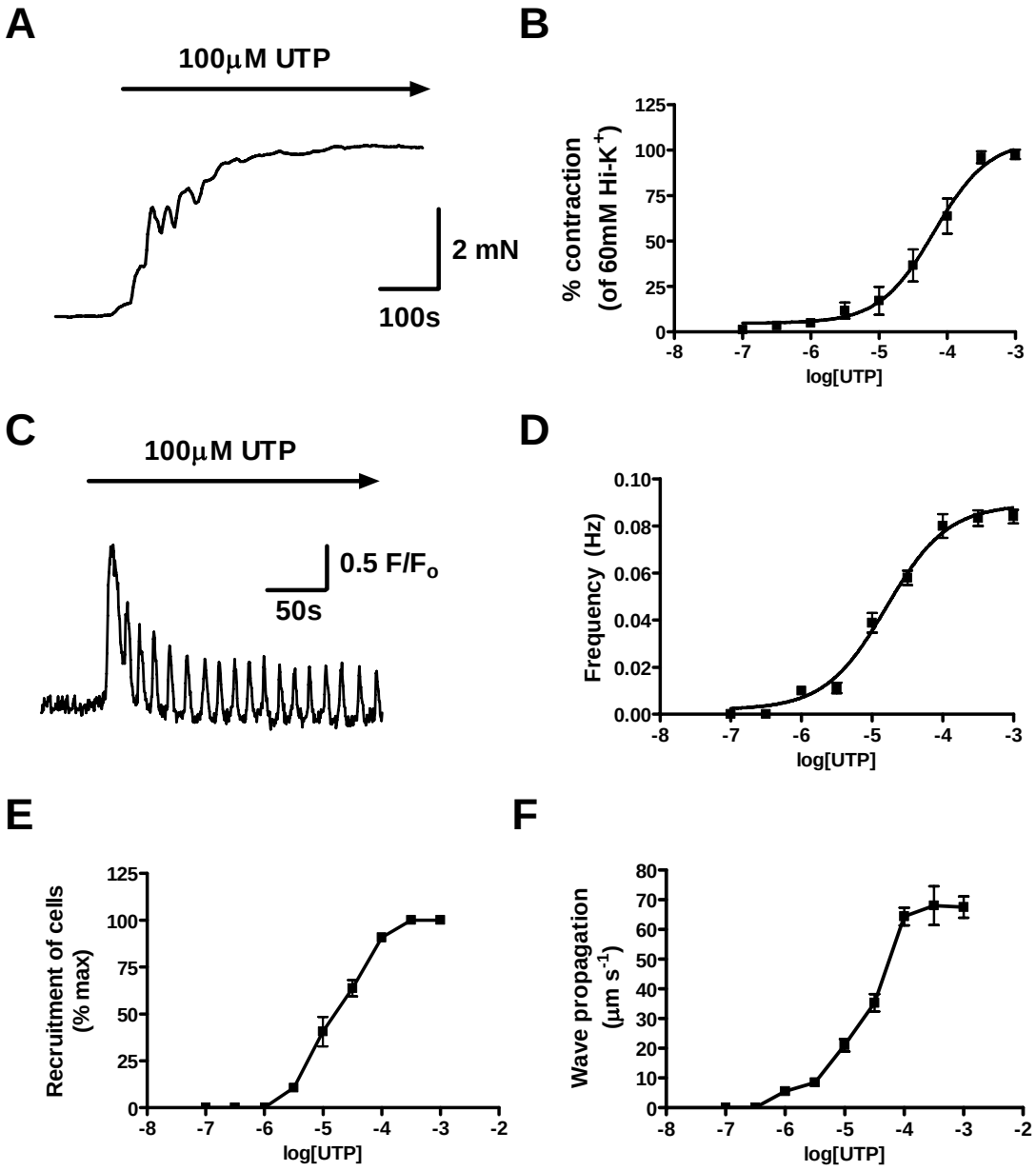

Figure 3.1: Properties of uridine 5'-triphosphate (UTP, 100 μM)-induced Ca^{2+} waves underlying tonic contraction in rat basilar artery. A. UTP-induced tonic contraction. Traces are representative of results from 6 animals. **B.** Concentration-response curve for UTP-induced tonic contraction. pEC_{50} = 4.24 ± 0.13 (n = 9 animals) **C.** In parallel experiments, application of UTP produced sustained Ca^{2+} oscillations which propagated along the cell as waves. Experimental Ca^{2+} traces are representative of results from 58 cells from 6 animals. **D.** Concentration-response curve for frequency of UTP-induced Ca^{2+} waves pEC_{50} = 4.74 ± 0.14 (n = 109 cells from 12 animals). **E.** A greater percentage of smooth muscle cells generated Ca^{2+} signals as UTP concentration increased. This recruitment occurred between 3 and 1000 μM, with maximal recruitment

achieved at 300 μM UTP (n = 90 cells from 10 animals). The number of cells firing is expressed as a percentage of cells responding to maximal concentration. **F.** The apparent propagation speed of the Ca^{2+} waves was correlated to increasing UTP concentration (n = 87 cells from 11 animals).

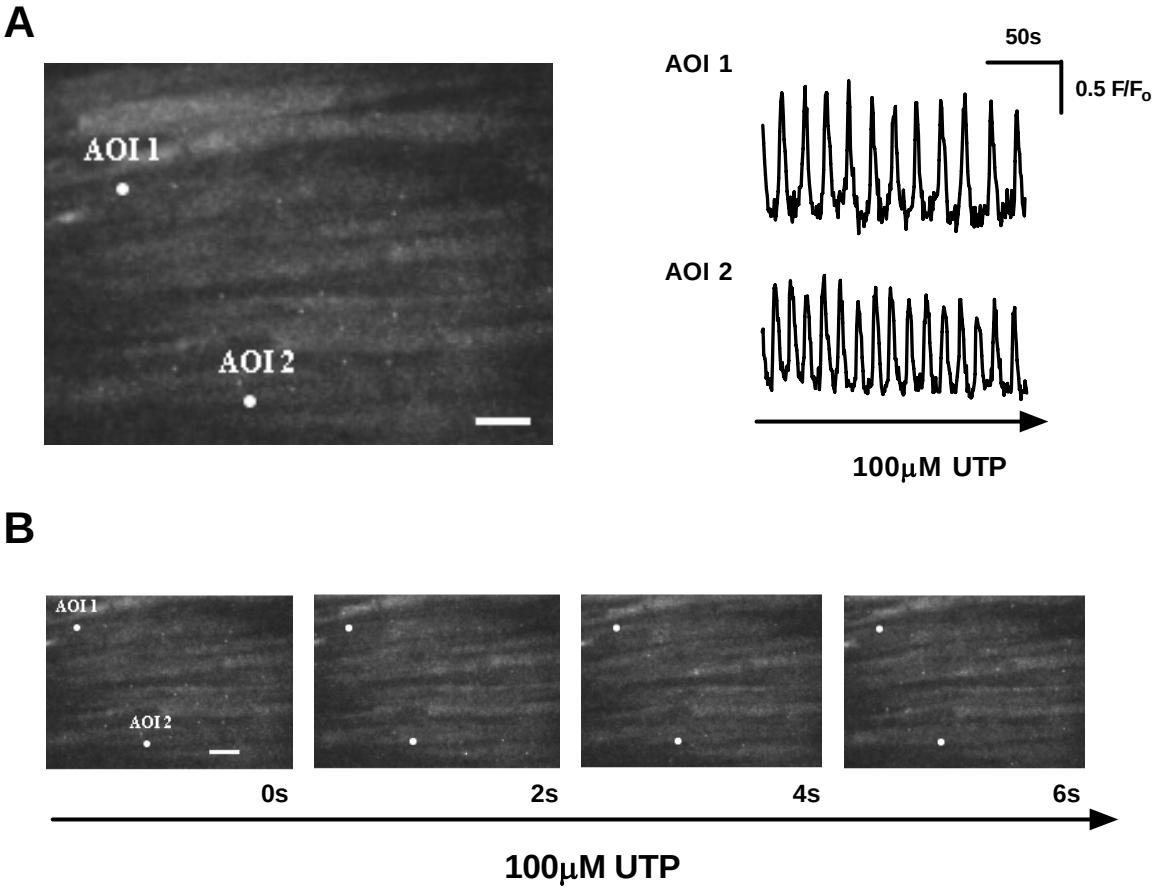

Figure 3.2: Uridine 5'-triphosphate (UTP, 100 μM)-induced Ca^{2+} waves in rat basilar artery. A. $[Ca^{2+}]_i$ changes in 2 intracellular regions from 2 different smooth muscle cells upon UTP stimulation are depicted in the Ca^{2+} traces taken from the steady state of UTP-induced Ca^{2+} waves. It should be noted that the Ca^{2+} waves occurred at different frequencies. Experimental Ca^{2+} traces are representative of results from 58 cells in 6 animals. **B.** Intact rat basilar artery smooth muscle cells challenged with UTP displayed Ca^{2+} waves which originated from distinct intracellular foci and propagated along the longitudinal axis of the smooth muscle cells (indicated by AOI1 and AOI2). The area of AOI is 3x3 pixels (1.69 μm^2). Scale bar = 10 μm.

3.3.2 Dependence of UTP-induced Ca^{2+}-waves on extracellular Ca^{2+} influx

There are two potential sources of Ca^{2+} that can contribute to the generation of UTP-induced Ca^{2+} waves: Ca^{2+} release from the intracellular stores and Ca^{2+} influx from the extracellular space. To determine the contribution of extracellular Ca^{2+} to the initiation and maintenance of UTP-induced Ca^{2+} waves, extracellular Ca^{2+} was removed prior to and during UTP stimulation, respectively. Removal of extracellular Ca^{2+} immediately prior to UTP stimulation reduced the Ca^{2+} signal to only a few transient Ca^{2+} waves (n = 39 cells from 6 animals, Fig. 3.3A), while UTP-induced Ca^{2+} waves were completely abolished in the absence of extracellular Ca^{2+} within 1 minute of treatment (n = 34 cells from 5 animals) (Fig. 3.3B), showing that extracellular Ca^{2+} influx was necessary for maintenance of Ca^{2+} waves.

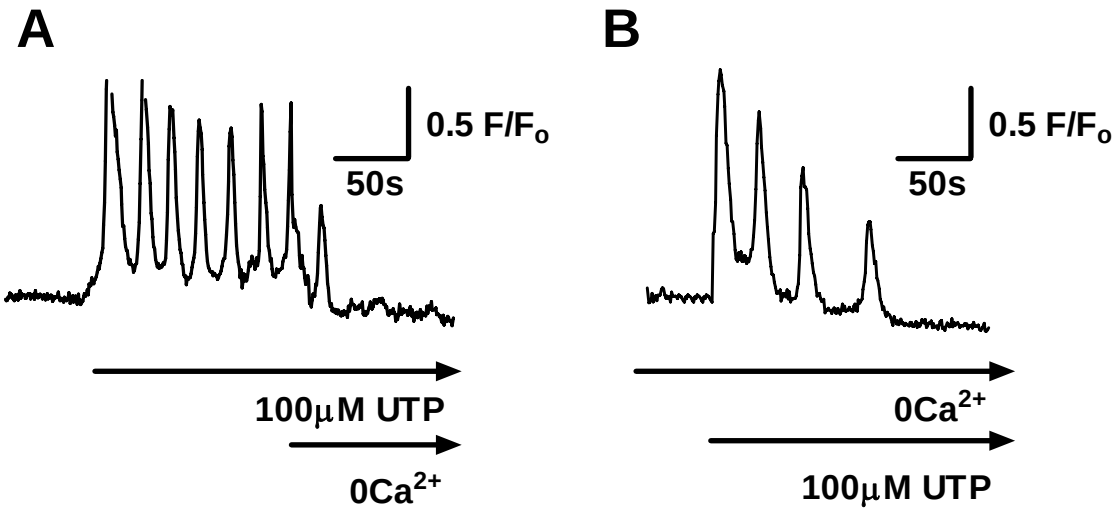

Figure 3.3: Extracellular Ca^{2+} influx is required for maintenance of uridine 5'-triphosphate (UTP, 100 μM)-induced Ca^{2+} waves. A. Removal of extracellular Ca^{2+} during ongoing UTP-induced Ca^{2+} waves results in their abolishment within 1 minute. Traces shown are representative of 39 cells from 6 animals. **B.** Removal of extracellular Ca^{2+} immediately prior to UTP stimulation limits Ca^{2+} signaling to transient Ca^{2+} waves. Traces shown are representative of 34 cells from 5 animals.

To further define the Ca^{2+} entry pathways involved in maintaining UTP-induced Ca^{2+} waves, nifedipine, a selective inhibitor of L-type Ca^{2+} channels, and SKF-96365, an inhibitor of receptor-operated and store-operated channels, were used. Nifedipine (10 μM) reduced the frequency of 100 μM UTP-induced Ca^{2+} waves to 59.25 ± 3.86 % of control, while the combined application of nifedipine and SKF-96365 (50 μM) completely abolished the Ca^{2+} waves ($P <$ 0.001, n = 42 cells from 8 animals). In parallel, application of nifedipine (10 μM) significantly reduced tonic contraction to 52.14 ± 3.46 % of control ($P < 0.001$, n = 6 animals), while the combined application of nifedipine and SKF-96365 (50 μM) decreased tonic contraction to 2.17 ± 1.10 % of control ($P < 0.001$, n = 5 animals) (Fig. 3.4A,B). It should also be noted that nifedipine (10 μM) completely abolished the contraction induced by 60 mM KCl (data not shown).

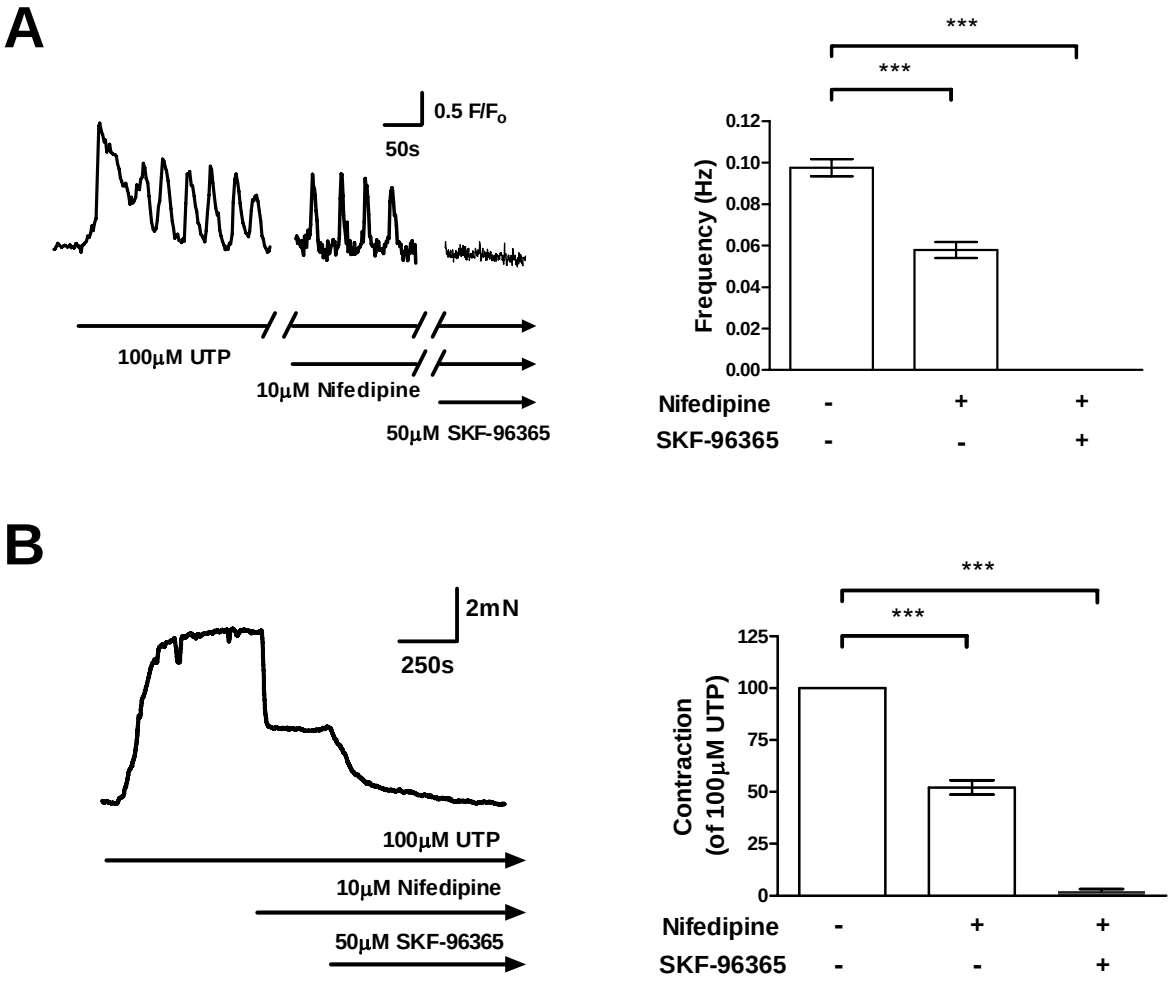

Figure 3.4: Effect of nifedipine and SKF-96365 on uridine 5'-triphosphate (UTP, 100 μM)-induced Ca^{2+} waves and tonic contraction. A. The frequency of Ca^{2+} waves is significantly reduced (59.25 ± 3.86% of control) following nifedipine (10 μM) application, but not abolished. The nifedipine-insensitive component is completely abolished following addition of SKF-96365 (50 μM). **B.** UTP-induced tonic contraction is significantly reduced to 52.14 ± 3.46 % of control by nifedipine (10 μM) and almost completely abolished (2.17 ± 1.10% of control) after SKF-96365 (50 μM). *** - $P <$ 0.001. Dashed lines indicate a 2 minute interval.

In addition to the conventional plasmalemmal Ca^{2+} permeable channels, the Na^+/Ca^{2+} exchanger operating in the reverse-mode is also an important pathway for Ca^{2+} entry in smooth

muscle cells (Lee *et al.*, 2002; Poburko *et al.*, 2006; Fameli *et al.*, 2007). KB-R7943, an inhibitor of reverse-mode NCX at low (≤ 10 μM) concentrations, was used to examine whether reverse-mode Na^+/Ca^{2+} exchange is involved in supporting nifedipine-insensitive Ca^{2+} waves (Iwamoto *et al.*, 1996; Ladilov *et al.*, 1999). The application of KB-R7943 (10 μM) abolished nifedipine-insensitive Ca^{2+} waves ($P < 0.001$, n = 34 cells from 6 animals) and inhibited tonic contraction to 3.56 ± 1.00 % of control ($P < 0.001$, n = 7 animals) (Fig. 3.5A,B). Application of KB-R7943 (10 μM) by itself also abolished UTP-induced Ca^{2+} waves ($P < 0.001$, n = 29 cells from 4 animals) and tonic contraction ($P < 0.001$, n = 4 animals), suggesting that Ca^{2+} entry through reverse-mode Na^+/Ca^{2+} exchange plays an important role in maintenance of Ca^{2+} waves even when L-type Ca^{2+} channels are operative (Fig. 3.5C,D). Although KB-R7943 (10 μM) reduced 60 mM KCl induced tonic contraction by 10.6% ± 3.0%, this effect was not significant ($P = 0.08$, n = 5 animals) (Fig. 3.6A). KB-R7943 may also inhibit store-operated channels (Arakawa *et al.*, 2000). To test for possible effects on store-operated channels, we used UTP (100 μM) to stimulate sustained Ca^{2+} waves and then applied cyclopiazonic acid (10 μM, CPA), an inhibitor of the sarco(endo)plasmic reticulum Ca^{2+}-ATPase, to inhibit SR Ca^{2+} reuptake. This resulted in an elevation of cytosolic Ca^{2+} levels, on which KB-R7943 had no effect, but the addition of SKF-96365 brought Ca^{2+} levels to baseline (Fig. 3.6B). This suggests that KB-R7943 did not abolish the Ca^{2+} waves through blockade of store/receptor-operated channels. It is also important to note that extracellular Na^+-depletion with the use of zero-Na^+ PSS also abolished the Ca^{2+} waves, which further supports the role of reverse-mode Na^+/Ca^{2+} exchange (data not shown).

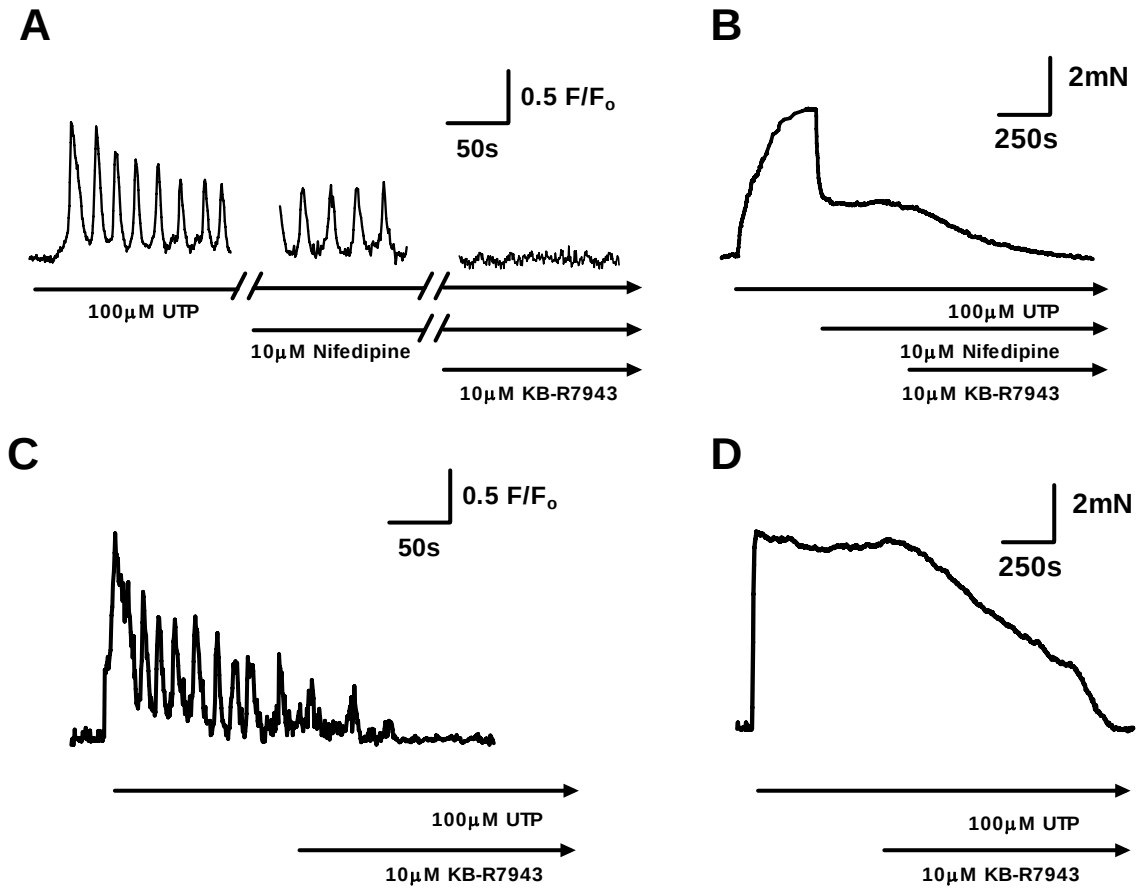

Figure 3.5: Effect of the reverse-mode Na^+/Ca^{2+} exchanger inhibitor KB-R7943 on uridine 5'-triphosphate (UTP, 100 μM)-induced Ca^{2+} waves and tonic contraction. **A.** Blockade of reverse (Ca^{2+}-entry) mode Na^+/Ca^{2+} exchange using KB-R7943 (10 μM) abolished the nifedipine-resistant UTP-induced Ca^{2+} waves ($P < 0.001$, n = 34 cells from 6 animals) **B.** Similarly, KB-R7943 (10 μM) also inhibited the nifedipine-insensitive tonic contraction to 3.56 ± 1.00 % of control ($P < 0.001$ n = 6 animals) **C.** Application of KB-R7943 (10 μM) alone reduced the frequency of UTP-induced Ca^{2+} waves, followed by complete abolishment ($P < 0.001$, n = 29 cells from 4 animals) **D.** KB-R7943 (10 μM) alone also abolished UTP-induced tonic contraction ($P < 0.001$, n = 5 animals).

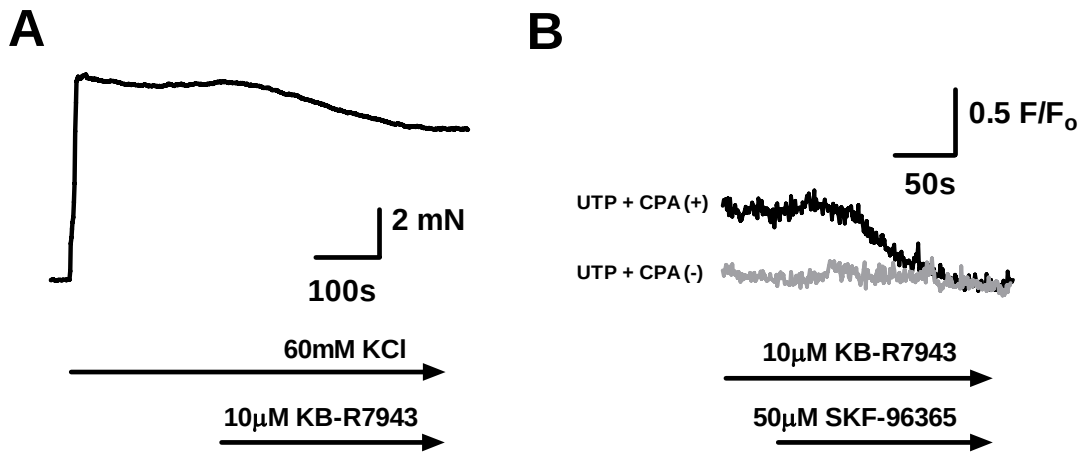

Figure 3.6: Effects of KB-R7943 on L-type Ca^{2+} channels and store/receptor-operated channels in rat basilar artery. A. Application of KB-R7943 reduced tonic contraction induced by 60 mM KCl by 10.6% ± 3.0% (P = 0.08, n = 5 animals). **B.** Application of UTP (100 μM) followed by CPA (10 μM) resulted in a maintained elevation in Ca^{2+} (solid black line). Application of KB-R7943 (10 μM) did not affect this plateau response, whereas the addition of SKF-96365 (50 μM) abolished the maintained Ca^{2+} elevation and returned to pre-stimulation baseline level (solid gray line). Representative trace shown is typical of the responses obtained in 36 cells from 4 rats.

3.3.3 Dependence of UTP-induced Ca^{2+}-waves on SR Ca^{2+} release

The all-or-none wave-like nature of Ca^{2+} signal in the rat basilar artery suggests regenerative Ca^{2+} release from the SR. If this is the case, blockade of SR Ca^{2+} uptake should completely inhibit the Ca^{2+} waves. The application of CPA (10 μM) to ongoing UTP-induced Ca^{2+} waves resulted in a broadening of the Ca^{2+} waves followed by their complete abolishment, leaving a significant elevation in baseline $[Ca^{2+}]_i$ corresponding to 35 ± 4 % of the peak $[Ca^{2+}]$ of the Ca^{2+} waves ($P < 0.001$, n = 38 cells from 6 animals) (Fig. 3.7A). In parallel, CPA (10 μM) also produced a 79.3 ± 1.7 % inhibition of the UTP-induced tonic contraction (Fig. 3.7B, $P < 0.001$, n = 5 animals).

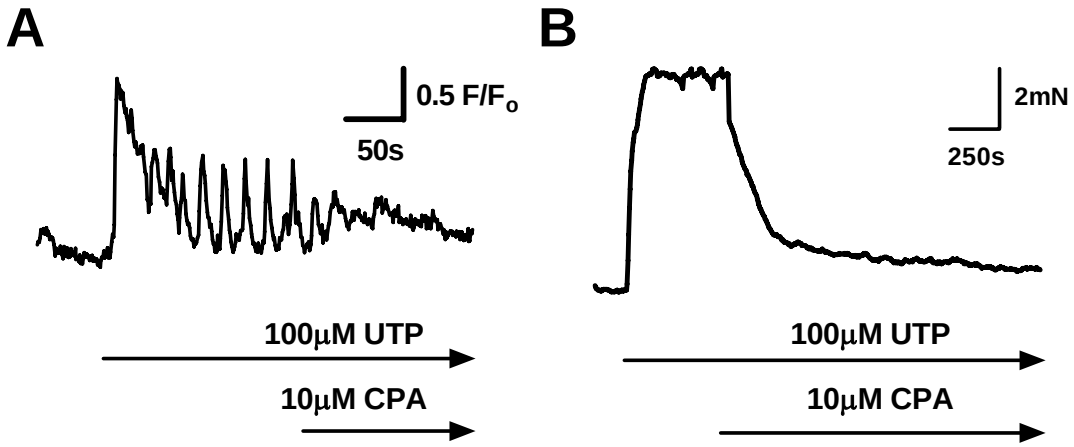

Figure 3.7: Effect of blockade of the sarco(endo)plasmic reticulum Ca^{2+} ATPase by cyclopiazonic acid (CPA) on uridine 5'-triphosphate (UTP, 100 μM)-induced Ca^{2+} waves. A. Addition of CPA (10 μM) to ongoing UTP-induced Ca^{2+} waves completely abolished the oscillations, leaving a small but significant elevation in baseline Ca^{2+} which corresponds to 35 ± 4 % of the peak [Ca^{2+}] of the asynchronous Ca^{2+} oscillations ($P <$ 0.001, n = 28 cells from 5 animals) **B.** Application of CPA (10 μM) produced a 79.3 ± 1.7 % inhibition of the UTP-induced tonic contraction ($P < 0.001$, n = 5 animals).

Ca^{2+} release from the SR can be mediated through either the inositol-1,4,5-triphosphate receptor (IP_3R) and/or the ryanodine receptor (RyR). 2-aminoethoxydiphenylborate (2-APB, 100 μM), an inhibitor of IP_3Rs in smooth muscle cells (Missiaen *et al.,* 2001), was used to examine the role of IP_3Rs in UTP-induced Ca^{2+} waves. Addition of 2-APB (100 μM) to ongoing Ca^{2+} waves immediately abolished them (n = 31 cells from 5 animals), and inhibited tonic contraction to 3.4 ± 0.7% of the control level ($P < 0.001$, n = 6 animals) (Fig. 3.8A,B). Furthermore, UTP (100 μM) failed to elicit a Ca^{2+} transient or contraction in basilar arteries pre-incubated for 30 minutes with 2-APB (Fig. 3.8C,D).

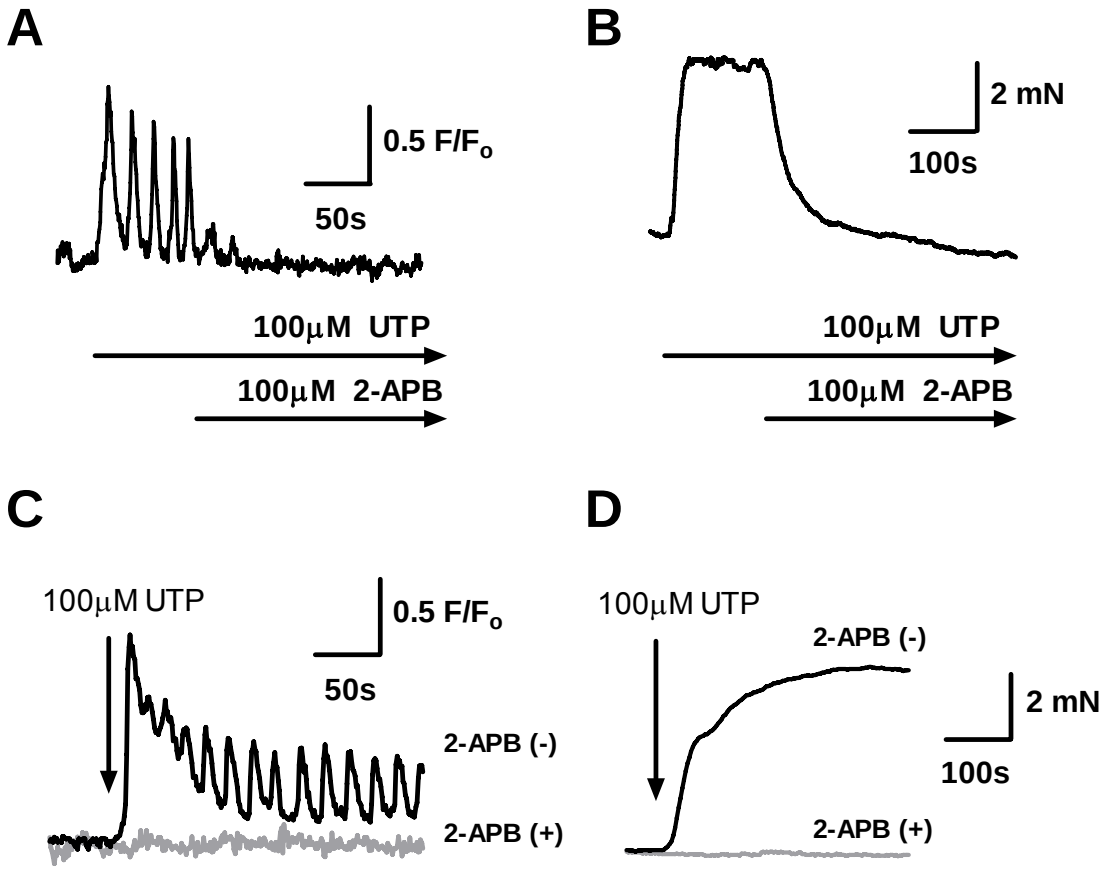

Figure 3.8: Effect of 2-aminoethoxydiphenylborate (2-APB) on uridine 5'-triphosphate (UTP, 100 μM)-induced Ca^{2+} waves and tonic contraction. A. The application of 2-APB (100 μM) immediately abolished UTP-induced Ca^{2+} waves (n = 31 cells from 5 animals) **B.** 2-APB (100 μM) decreased UTP-induced tonic contraction to 3.4 ± 0.7% of the control level ($P < 0.001$, n = 6 animals). **C.** UTP stimulation after pretreatment of vessels with 2-APB (100 μM) for 30 minutes failed to elicit a Ca^{2+} response (solid gray line, $P < 0.0001$, n= 24 cells from 3 animals). In contrast, control vessels without 2-APB (100 μM) preincubation (solid black line) displayed Ca^{2+} waves after UTP stimulation. **D.** UTP stimulation after pretreatment of vessels with 2-APB (100 μM) for 30 minutes failed to induce contraction (solid gray line, $P < 0.0001$, n = 5 animals) compared to control vessels without 2-APB preincubation (solid black line).

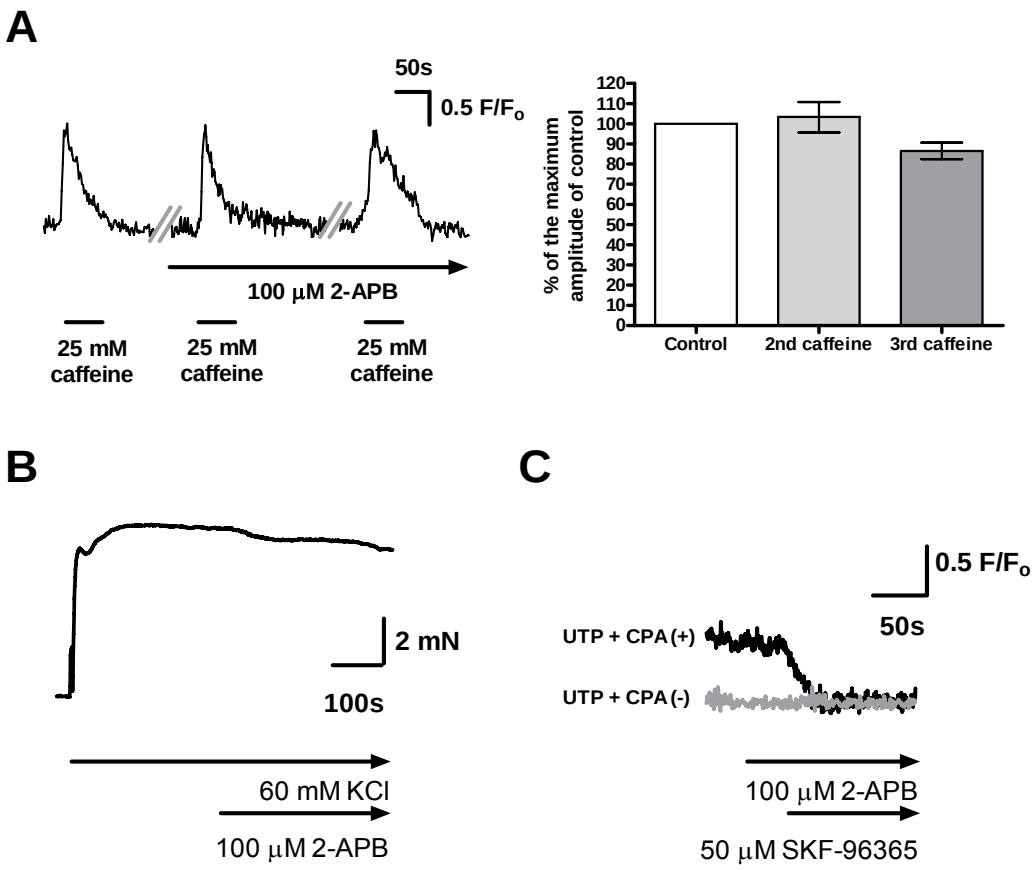

Figure 3.9: Effects of 2-aminoethoxydiphenylborate (2-APB) on the ryanodine-sensitive SR Ca^{2+} release channels, sarco(endo)plasmic reticulum Ca^{2+} ATPase, L-type Ca^{2+} channels, and store-operated channels in rat basilar artery. A. *Left:* Three pulses of caffeine (25 mM) were applied with a 5-min interval between each pulse (dashed lines). Maximum amplitude of the caffeine-induced Ca^{2+} transient from the first pulse reflects control SR Ca^{2+} level as Ca^{2+} from the SR is released through the opened RyR channels. After the addition of 2-APB (100 μM), the second pulse of caffeine resulted in a single Ca^{2+} transient whose maximum amplitude is similar to the first pulse (103.3 ± 7.6% of control, $P = 0.66$, n = 6 animals). The third pulse of caffeine resulted in a Ca^{2+} transient whose maximum amplitude was slightly, but not significantly, diminished by 13.4 ± 4.1% compared with the first pulse ($P = 0.11$, n = 6 animals). *Right:* Bar graph comparing the average maximum amplitude of the second and third caffeine pulses to the third pulse (n = 6 animals). **B.** Application of 2-APB (100 μM) reduced tonic contraction induced by 60 mM KCl by 14.8 ± 4.3% ($P = 0.041$, n = 6 animals). **(c)** Application of UTP (100 μM) followed by CPA (10 μM) resulted in a maintained elevation in Ca^{2+} (black solid line). Application of 2-APB (100 μM) did not affect this plateau response, whereas the addition of SKF-96365 (50 μM) abolished the maintained Ca^{2+} elevation and returned to pre-stimulation baseline level (gray solid line). Representative trace shown is typical of the responses obtained in 30 cells from 4 rats.

It therefore appears that the opening of the IP_3Rs is required for UTP-mediated vasoconstriction and Ca^{2+} waves. However, as the specificity of 2-APB has been questioned, it was important to examine the selectivity of 2-APB in our preparation, especially with regard to Ca^{2+} translocators such as RyRs, sarco(endo)plasmic reticulum Ca^{2+} ATPase, the store-operated channels, and the L-type Ca^{2+} channels. As shown in Fig. 3.9A, pre-treatment with 2-APB (100 μM) did not significantly affect the peak amplitude of caffeine (25 mM)-induced Ca^{2+} release (103.3 ± 7.6% of the control, $P = 0.66$, n = 5 animals), and therefore appears to be inactive against RyRs. Furthermore, 2-APB marginally affected SR refilling, as the peak amplitude of the third caffeine-induced Ca^{2+} transient was decreased slightly, but not significantly by 13.4 ± 4.1% ($P = 0.11$, n = 6 animals).

To test for direct effects on Ca^{2+} entry pathways, the effects of 2-APB on L-type Ca^{2+} channels and store-operated channels, two plasmalemmal channels important to UTP-mediated Ca^{2+} waves, were examined. 2-APB (100 μM) reduced 60 mM KCl-induced tonic contraction by 14.8 ± 4.3% (Fig. 3.9B, $P = 0.041$, n = 6 animals). However, this slight inhibition of L-type Ca^{2+} channels cannot account for the complete inhibition of UTP-induced tonic contraction by 2-APB, as blockade of L-type Ca^{2+} channels with nifedipine only reduced force by 52%.

In addition to L-type Ca^{2+} channels, store-operated channels are also important for maintaining the Ca^{2+} waves. 2-APB has been reported to have non-selective effects on store-operated channels (Bootman *et al.,* 2002). We stimulated the vessel with UTP (100 μM) to generate sustained Ca^{2+} waves and then applied CPA (10 μM) to inhibit SR Ca^{2+} reuptake, resulting in a maintained elevation of $[Ca^{2+}]$ and depletion of the SR (Fig. 3.9C). The application of 2-APB (100 μM) did not affect the $[Ca^{2+}]_i$ plateau, although Ca^{2+} returned to baseline upon

the subsequent addition of the store-operated channel blocker SKF-96365 (50 μM), indicating that in this preparation 2-APB does not inhibit the store-operated channels directly.

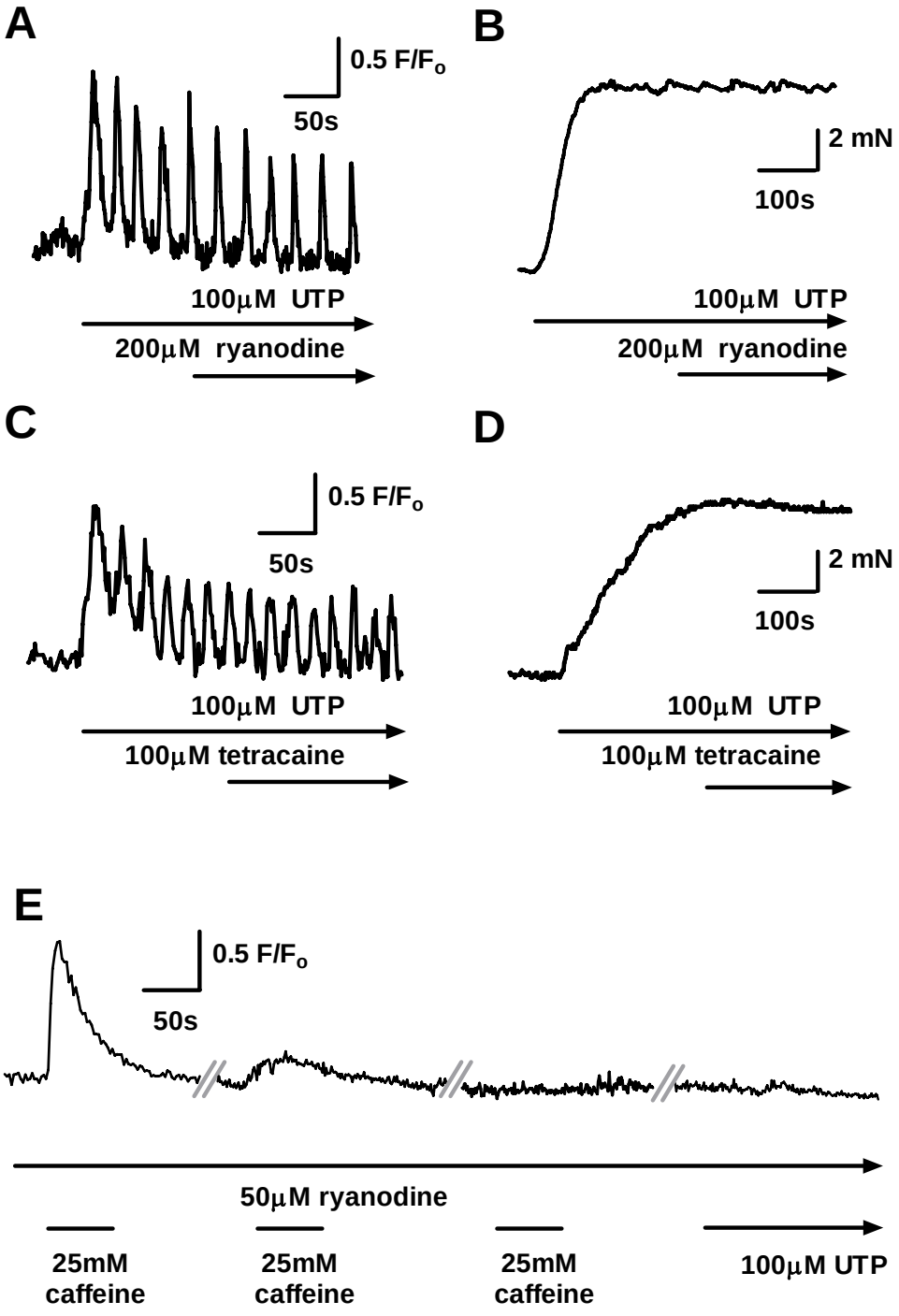

Figure 3.10: Effect of ryanodine, tetracaine, and caffeine-induced depletion of SR Ca^{2+} stores on uridine 5'-triphosphate (UTP, 100 μM)-induced Ca^{2+} waves and tonic contraction in rat basilar artery. A. Application of a high concentration (200 μM) of ryanodine did not affect ongoing UTP-induced Ca^{2+} waves ($P = 0.67$, n = 33 cells from 5 animals) **B.** Ryanodine (200 μM) also did not affect UTP-induced tonic contraction ($P = 0.71$, n = 5 animals). **C.** High-concentration (100 μM) tetracaine also did not affect ongoing UTP-induced Ca^{2+} waves ($P = 0.71$, n = 29 cells from 4 animals) **D.** Tetracaine (100 μM) had no significant effect on UTP-induced tonic contraction ($P = 0.64$, n = 5 animals). **E.** To determine effects of depletion of RyR-sensitive SR Ca^{2+} stores, the artery was exposed to three 1-minute treatments of caffeine (25 mM) in the continuous presence of ryanodine (50 μM) resulted in depletion of SR Ca^{2+} stores. The second stimulation of caffeine produced a much reduced Ca^{2+} transient, while the third stimulation produced no Ca^{2+} response. After depletion of SR Ca^{2+} stores, stimulation with UTP (100 μM) in the presence of ryanodine failed to elicit a Ca^{2+} response. Dashed lines indicate a 5 minute interval.

Although the opening of IP_3Rs are required for UTP-mediated Ca^{2+} waves and contraction, it does not rule out Ca^{2+} release through the RyR, another type of SR Ca^{2+} release channel which is functionally important in smooth muscle cells. To assess the involvement of RyRs, high-concentrations of ryanodine (200 μM) and tetracaine (100 μM) were used to lock RyRs in their closed configuration. Neither ryanodine nor tetracaine had any effect on the frequency of the ongoing UTP-induced Ca^{2+} waves ($P = 0.67$, n = 33 cells from 5 animals; $P = 0.71$, n = 29 cells from 4 animals, respectively) or tonic contraction ($P = 0.64$, n = 5 animals; $P = 0.64$, n = 6 animals) (Fig. 3.10A,B,C,D). This supported the notion that Ca^{2+} release from the RyR-dependent SR store is not responsible for the generation of Ca^{2+} waves. To explore this issue further, RyRs were locked in the subconductance state by preincubation with ryanodine (50 μM) followed by a brief (1 min) exposure to caffeine (25 mM). The first caffeine exposure caused a transient Ca^{2+} response, whereas a second exposure elicited a much-reduced Ca^{2+} transient, and the third failed to elicit any Ca^{2+} transient at all (Fig. 3.10E). We interpreted the final lack of Ca^{2+} transient in response to caffeine to indicate that release of Ca^{2+} through RyRs on the SR was no longer possible due to depletion of SR Ca^{2+} content and/or the locking of RyRs in an open

state. UTP (100 μM) stimulation immediately after depletion of the RyR-sensitive store no longer elicited a Ca^{2+} response. These results suggest that IP_3Rs and RyRs have access to a common SR Ca^{2+} store, but that opening of RyRs do not appear to be critical for the maintenance of UTP-induced Ca^{2+} waves.

3.4 Discussion

The presence of agonist-induced Ca^{2+} waves in cerebral arteries has been documented by various groups (Jaggar and Nelson 2000; Jaggar, 2001; Heppner *et al.*, 2002), but a detailed investigation of their underlying mechanisms has not yet been conducted. We have investigated the link between agonist-induced Ca^{2+} waves and tonic contraction using an *in situ* preparation of the rat basilar artery and have systematically studied the ionic mechanisms underlying these Ca^{2+} waves, which appear to be similar to those described in vascular smooth muscle from larger conduit blood vessels (Lee *et al.*, 2002). Our studies of UTP-induced Ca^{2+} waves were performed in isometrically stretched arteries, which are similar to the conditions in which UTP-induced Ca^{2+} waves were first described (Jaggar and Nelson, 2000), and may shed new light on how wall tension may be regulated in the basilar artery.

The response to UTP is typified by repetitive transient elevations in Ca^{2+} which originate in distinct intracellular foci and then spread out as waves over the length of the smooth muscle cell. The cells respond independently of each other in that the Ca^{2+} waves are asynchronous and that the cells vary in their sensitivity to UTP, such that recruitment of responding cells increases with increasing UTP concentration. Furthermore, the propagation velocity and frequency also increases with increasing UTP concentration and have similar dose-response relationships (Fig. 3.1C,D). Functionally, it appears that Ca^{2+} waves underlie tonic contraction, as their inhibition

with nifedipine, SKF-96365, KB-R7943, or 2-APB is association with complete inhibition of force (Fig. 3.4, 3.5, 3.8). Finally, the lack of synchronicity between neighbouring smooth muscle cells explains how summation of individual-cell Ca^{2+} waves can lead to tonic contraction, as the summation of Ca^{2+} signals in all the cells averages out to be a steady state Ca^{2+} increase in whole vessels (Ruehlmann *et al.,* 2000; Mauban *et al.,* 2001). The apparent importance of Ca^{2+} waves for tonic contraction is further demonstrated when their abolishment by CPA markedly reduces force by 80%, although the average $[Ca^{2+}]_i$ remains significantly elevated above baseline (Fig. 3.7). This indicates a higher force-to-$[Ca^{2+}]_i$ ratio when smooth muscle cells are activated with Ca^{2+} waves as compared with sustained $[Ca^{2+}]_i$, suggesting that Ca^{2+} waves represent a more efficient method to deliver Ca^{2+} to activate myosin light-chain kinase, which is tethered to the contractile filaments (Lee *et al.,* 2001; Wilson *et al.,* 2002). However, contraction is ultimately determined by the level of phosphorylation of myosin light chain, which is both Ca^{2+} dependent and Ca^{2+}-independent (Weber *et al.,* 1999). Currently, the way in which Ca^{2+} waves might be related to this level of phosphorylation is unknown.

The UTP-induced Ca^{2+} waves appear to be propagated by regenerative Ca^{2+} release from the SR network, as depletion of SR Ca^{2+} stores with CPA abolishes the oscillations (Fig. 3.7). Extracellular Ca^{2+} influx appears to be critical for the maintenance of Ca^{2+} waves, although the ability of Ca^{2+} waves to persist for a time in the absence of Ca^{2+} is likely due to several Ca^{2+} transport mechanisms. In smooth muscle, a proportion of the Ca^{2+} released by the SR is inevitably extruded to the extracellular space by the actions of the plasma membrane Ca^{2+}-ATPase (PMCA), and in a Ca^{2+}-free medium all Ca^{2+} release from the SR is irreversibly lost to the extracellular space (Leijten and van Breemen, 1986). However, removal of Ca^{2+} towards the extracellular space is in competition with SR Ca^{2+} reuptake through the sarco(endo)plasmic

reticulum Ca^{2+} ATPase, which allows the SR to continue releasing decreasing amounts of Ca^{2+} to sustain the Ca^{2+} waves. Finally, a third mechanism of Ca^{2+} unloading of the SR during Ca^{2+}-free conditions is the transfer of Ca^{2+} release by the peripheral ryanodine receptors (RyRs) towards the forward-mode (Ca^{2+}-extrusion) Na^{+}/Ca^{2+} exchange, a mechanism which as been described in both smooth muscle cells and endothelial cells (Nazer and van Breemen, 1998; Liang *et al.,* 2004). Therefore, without refilling of the SR, all of the Ca^{2+} is eventually extruded resulting in the disappearance of the Ca^{2+} waves.

Influx of extracellular Ca^{2+} through L-type Ca^{2+} channels is central in the control of cerebrovascular arterial diameter (Nelson *et al.,* 1990). However, it is interesting that the UTP-induced Ca^{2+} waves were not abolished by nifedipine, but only reduced in frequency. One mechanism through which frequency could be decreased is that the absence of stimulated Ca^{2+} influx through L-type Ca^{2+} channels may reduce the rate of refilling of the SR Ca^{2+} store. As SR luminal Ca^{2+} can regulate IP_3R channel opening probability, a reduced rate of SR Ca^{2+} refilling can result in a decreased frequency of SR Ca^{2+} release at the wave initiation site (Meldolesi and Pozzan, 1998). Similarly, blockade of L-type Ca^{2+} channels in pressurized mouse mesenteric arteries, which abolished myogenic tone, also reduced the frequency of phenylephrine-induced Ca^{2+} oscillations (Zacharia *et al.,* 2007). However, pressure-induced Ca^{2+} waves in small rat cerebral arteries were completely abolished by diltiazem (Jaggar, 2001). Although the larger cerebral vessels, such as the basilar artery, share some properties of resistance vessels (Toyoda *et al.,* 1996), these differing observations may be the result of tissue differences, with respect to relative involvement of the various Ca^{2+} entry mechanisms. Furthermore, these apparent mechanistic differences may also be attributed to different physiological conditions, for example pressurization versus tension. For example, the development of myogenic tone may influence the

Ca^{2+} signal elicited by agonists (Zacharia *et al.,* 2007). Consequently, comparisons between the mechanisms of Ca^{2+} waves must take differences in vascular beds and experimental preparations into consideration.

Another major finding in this study is that UTP-induced Ca^{2+} waves are abolished by KB-R7943, an inhibitor of reverse-mode Na^+/Ca^{2+} exchanger-mediated Ca^{2+} entry across the plasma membrane (Iwamoto *et al.,* 1996; Ladilov *et al.,* 1999). The plasma membrane Na^+/Ca^{2+} exchanger is a transmembrane protein that normally couples the influx of Na^+ ions to the efflux of Ca^{2+} ions in a 3:1 ratio (Philipson and Nicoll, 2000). However, Na^+ entry through receptor- and store-operated channels which are functionally coupled to the Na^+/Ca^{2+} exchanger may influence the dynamics Na^+/Ca^{2+} exchange, as Na^+ accumulates regionally in a restricted subplasmalemmal space between the superficial SR and the plasma membrane (Arnon *et al.,* 2000; Poburko *et al.,* 2004; Lemos *et al.,* 2007). This build-up in subcellular Na^+ was hypothesized to change the electrochemical gradient to favour Ca^{2+} influx through NCX reversal, which in turn refills the SR Ca^{2+} stores (Lee *et al.,* 2001). This would explain our findings that the nifedipine-resistant Ca^{2+} waves and tonic contraction are similarly sensitive to both SKF-96365, an inhibitor of store- and receptor operated channels, and KB-R7943.

However, to achieve NCX reversal, the subplasmalemmal Na^+ ($[Na^+]_{subPM}$) must reach at least the level of K_m. Although the concentration of $[Na^+]_{subPM}$ has not been measured in this preparation, we have predicted from our studies with rat aortic smooth muscle cells that reverse-mode Na^+/Ca^{2+} exchange should occur when $[Na^+]_{subPM}$ exceeds 23-25mM, assuming E_m = -60mV, $E_{NCX} = 3E_{Na} - 2E_{Ca}$, $[Ca^{2+}]_o$ = 1.2mM, $[Ca^{2+}]_{subPM}$ = 500nM, and $[Na^+]_o$ = 145mM (where $[Ca^{2+}]_o$ = extracellular $[Ca^{2+}]$, $[Ca^{2+}]_{subPM}$ = subplasmalemmal $[Ca^{2+}]$, and $[Na^+]_o$ = extracellular $[Na^+]$) (Poburko *et al.,* 2006). Recently, Poburko and colleagues provided the first direct

demonstration of localized subcellular increases in Na^+ through receptor-operated/store-operated channels to ≥ 30 mM (Poburko *et al.,* 2007), which is consistent with estimates of Na^+ ranging from 24 to 40mM in ventricular myocytes (Wendt-Gallitelli *et al.,* 1993; Isenberg *et al.,* 2003). In addition, the space constant for the subplasmalemmal Na^+ gradient in ventricular myocytes is 28nm, which is highly consistent with the intermembrane separation (~20nm) in PM-SR junctions in the rat basilar artery preparation (unpublished observations). Furthermore, given that the resting membrane potential in rat basilar artery is approximately -43mV (Haddock and Hill, 2002), and that a more depolarized membrane decreases $[Na^+]_{subPM}$ required for NCX reversal, it seems plausible that reverse-mode Na^+/Ca^{2+} exchange is a physiological route of Ca^{2+} entry in cerebral arteries. This is especially relevant as our finding that KB-R7943 abolishes Ca^{2+} waves suggests that SR refilling is critically dependent on reverse-mode Na^+/Ca^{2+} exchange during UTP stimulation (Fig. 3.5C). Although it remains to be investigated, this may serve as an example of privileged delivery of Ca^{2+} from a transport site located in one membrane to a second Ca^{2+} transport site in an apposing membrane, a process which serves to circumvent free diffusion throughout the cytoplasm (Poburko *et al.,* 2004; Fameli *et al.,* 2007). In addition to its inhibition of reverse-mode Na^+/Ca^{2+} exchange, KB-R7943 has been also been reported to have effects on L-type Ca^{2+} and store-operated channels, neuronal nicotinic acetylcholine receptors, the N-methyl-D-aspartic acid (NMDA) receptor, and norepinephrine transporter (Watano *et al.,* 1996; Sobolevsky and Khodorov, 1999; Arakawa *et al.,* 2000; Iwamoto, 2004). However, in our preparation, KB-R7943 does not significantly inhibit L-type Ca^{2+} channels or store-operated channels, which supported the notion that it is the reverse-mode Na^+/Ca^{2+} exchange, which is important refilling the SR to maintain Ca^{2+} waves.

UTP exerts its effects on metabotropic purinergic P_2Y receptors, and has been shown to augment Ca^{2+} release via an increase in cytoplasmic IP_3 (Strobaek, 1996; Sima *et al.,* 1997). To investigate the role of IP_3Rs, we used 2-APB, a small molecular weight membrane permeable modulator of the IP_3R (Missiaen *et al.,* 2001). However, its use to block IP_3Rs has been criticized for its nonspecific effects on other ion transport mechanisms, notably its inhibition of store-operated channels (Broad *et al.,* 2001; Ma *et al.,* 2001; Ratz and Berg, 2006). Importantly in our preparation, 2-APB immediately abolished ongoing Ca^{2+} waves and tonic contraction, and did not affect caffeine-releasable Ca^{2+} stores, which is consistent with an action of 2-APB to block IP_3Rs (Fig. 3.9A). Furthermore, preincubation with 2-APB did not elicit a Ca^{2+} response or contraction. It also had only a minor insignificant effect on SR Ca^{2+} reuptake. 2-APB had no significant inhibition on store-operated channels, and although it does affect L-type Ca^{2+} channels, the slight inhibition observed could not have accounted for the abolishment of Ca^{2+} waves (Fig. 3.9B,C). Therefore, our findings support the notion that opening of IP_3R channels is not only responsible for the initial Ca^{2+} release, but is also required for subsequent regenerative release of Ca^{2+} underlying the propagation of the Ca^{2+} waves. Acetylcholine-induced Ca^{2+} waves in rat portal vein myocytes are also dependent on activation of IP_3Rs, although interestingly the IP_3R_2 subtype, which is most sensitive to Ca^{2+}, appears to be most important for the propagation of Ca^{2+} waves (Morel *et al.,* 2003; Fritz *et al.,* 2008). It should also be noted that the Ca^{2+} waves are maintained by the intrinsic sensitivity of the IP_3R_2 subtype to cytosolic $[Ca^{2+}]_i$, and not due to oscillation of IP_3 levels (Fritz *et al.,* 2008). A possible scenario in the rat basilar artery is that UTP-induced Ca^{2+} wave begins with elevation of IP_3. The IP_3 sensitizes the IP_3R to Ca^{2+}, and when Ca^{2+} reaches a threshold concentration the release channels open (Streb *et al.,* 1983; Ferris *et al.*, 1992). As the concentration of UTP is raised, the concentrations of IP_3 and basal $[Ca^{2+}]_i$

are also raised, which shortens the time required for Ca^{2+} to reach threshold value for the initiation of the next wave. The regenerative nature depends on the positive feedback of increasing Ca^{2+} on the IP_3 sensitivity of IP_3R. This mechanism, combined with the fact that IP_3 sensitizes the IP_3R to Ca^{2+}, ensures that both the frequency and velocity increase with increasing UTP concentration. However, knowledge of the IP_3 dynamics in our preparation is required before this conclusion can be established.

The observed effect of 2-APB indicates an essential role of IP_3Rs in the initiation and maintenance of UTP-induced Ca^{2+} waves, but does not exclude involvement of RyRs. Although there is general agreement that the initiation of oscillations and waves is a response to agonists acting on sarcolemmal receptors which releases Ca^{2+} from the SR via IP_3Rs, controversy remains whether or not Ca^{2+} release from the IP_3Rs then activates RyRs to generate further release by Ca^{2+}-induced Ca^{2+}-release and to propagate waves, or whether the entire release process arises from IP_3Rs without significant RyR involvement (Mccarron *et al.,* 2003). The former proposal is supported by studies which showed that drugs which block RyRs often abolish Ca^{2+} oscillations initiated by IP_3-generating agonists (Hyvelin *et al.,* 1998; Boittin *et al.,* 1999; Jaggar and Nelson, 2000). This is possibly due to co-localization of RyRs and IP_3Rs, which allows Ca^{2+} released locally by IP_3R activates adjacent clusters of RyR by Ca^{2+}-induced Ca^{2+} release (Gordienko and Bolton, 2002). On the other hand, some preparations which lack a Ca^{2+}-induced Ca^{2+} release mechanism still exhibit Ca^{2+} waves (DeLisle and Welsh, 1992; Lechleiter and Clapham, 1992). Furthermore, in pressurized rat mesenteric artery, RyRs do not appear to play a role in agonist-stimulated Ca^{2+} waves (Lamont and Wier, 2004). It is important to note here that many studies which utilize pharmacological tools to inhibit RyRs, such as the plant alkaloid ryanodine, are complicated by the concentration-dependent effects in different tissues. For example, low

concentrations (< 100 μM) of ryanodine cause persistent opening of the channels which may lead to store depletion (Rousseau *et al.,* 1987, Kanmura *et al.,* 1988, Xu *et al.,* 1994), while higher concentrations are reported to lock RyRs in a closed state to inhibit Ca^{2+} release (Fill and Copello, 2002). Furthermore, the drugs may also block IP_3-mediated Ca^{2+} signals themselves (either directly or indirectly) without RyR involvement in Ca^{2+} increase.

In our preparation, depletion of the RyR-sensitive Ca^{2+} stores using a combination of caffeine and low concentration of ryanodine to lock the RyRs in a subconductance state eliminated the ability of UTP to induce Ca^{2+} oscillations (Fig. 3.10). The concentration of ryanodine (50 μM) we used which is greater than the concentration which is known to lock RyRs in an open state in smooth muscle (Iino *et al.,* 1988; Kanmura *et al.,* 1988). This suggests that the IP_3R and RyR both access a common SR Ca^{2+} store such that the depletion of RyR stores prevents Ca^{2+} oscillations, as has been demonstrated (Lepretre and Mironneau, 1994; McCarron and Olson, 2008), but does not prove that RyRs participate in the propagation of Ca^{2+} waves. Therefore, we used a high concentration of ryanodine (200 μM) to lock the RyRs in the closed-configuration and found that UTP-induced Ca^{2+} waves were not affected (Fig. 3.10). Additionally, we used tetracaine (100 μM), which is not dependent on the opening of RyRs to exert their effects, and also found that the Ca^{2+} waves were not affected (Györke *et al.,* 1997). This is in contrast to the rat cerebral arteries, where ryanodine (10 μM) inhibited UTP-induced Ca^{2+} waves (Jaggar and Nelson, 2000). However, it should be noted that in the same preparation, ryanodine also inhibited Ca^{2+} sparks, likely as a result of SR Ca^{2+} store depletion. Additionally, another possibility is that in our preparation and in others, the RyRs do not play a role because they are not localized near the IP_3Rs. However, well-controlled double-labeling of the IP_3Rs and RyRs at electron microscopic resolutions is required before such a conclusion can be made.

It is interesting to note that the mechanism of UTP-induced asynchronous Ca^{2+} waves elicited in this study shares some similarities to the mechanism of Ca^{2+} oscillations underlying spontaneous vasomotion, as they were not abolished by nifedipine, dependent on a functional SR, and were abolished by antagonists of IP_3 (Haddock and Hill, 2002; 2005). This is more significant in light of the fact that asynchronous Ca^{2+} waves often precede the rhythmic contraction of blood vessels, or vasomotion, which has been observed to occur spontaneously or in response to high concentrations of agonist stimulation, and may have physiological and pathophysiological importance (Gratton *et al.,* 1998; Hudetz *et al.,* 1998, Shimamura *et al.,* 1999; Rücker *et al.,* 2000). In agonist-stimulated vasomotion, asynchronous Ca^{2+} waves are first initiated without the generation of tension. In the presence of the endothelium, the periodic increases in $[Ca^{2+}]_i$ activate cGMP-dependent, Ca^{2+}-sensitive Cl^- channels, which cause Cl^- currents which depolarize the membrane periodically. The depolarization spreads rapidly through neighbouring cells and activates L-type Ca^{2+} channels, facilitating Ca^{2+} influx which facilitates Ca^{2+}-induced Ca^{2+}-release to initiate the next Ca^{2+} wave, which will then occur simultaneously in all the nearby smooth muscle cells and generate oscillatory vasomotion (Peng *et al.,* 2001; Rahman *et al.,* 2005).

Similarly, with spontaneous vasomotion, the trigger for synchronicity of Ca^{2+} waves is thought to be due to the activation of a chloride-dependent Ca^{2+} channel (Haddock and Hill, 2002). The resulting depolarization then spreads quickly to neighbouring cells, such that L-type Ca^{2+} channels are simultaneously activated. The resulting Ca^{2+} influx then facilitates Ca^{2+}-induced Ca^{2+} release to initiate a synchronous Ca^{2+} release and contraction. In the study by Haddock and Hill (2002), synchronized Ca^{2+} waves were abolished upon blockade of L-type Ca^{2+} channels with nifedipine, but asynchronous Ca^{2+} oscillations persisted in individual

cells, which supports the hypothesis that the entrainment of L-type Ca^{2+} channels are important in synchronized Ca^{2+} oscillations. Synchronization of Ca^{2+} oscillations between VSMCs underlying vasomotion is critically dependent on the coordination of Ca^{2+} signals within individual VSMCs leading to synchronized Ca^{2+} responses and the development of simultaneous contractions along the vessel length (Christ *et al.,* 1996). In small vessels, this coordination may be dependent on an intact endothelium, which may be one reason why we did not observe synchronized Ca^{2+} waves upon UTP stimulation in our preparation (Haddock and Hill, 2005).

In summary, the data presented in this article show that multiple Ca^{2+} translocating proteins are involved in the generation of Ca^{2+} waves in UTP-stimulated smooth muscle cells of the rat basilar artery. These Ca^{2+} waves appear to be produced by repetitive cycles of SR Ca^{2+} release which are mediated by IP_3Rs, followed by SERCA-mediated SR Ca^{2+} re-uptake of Ca^{2+} entry involving L-type Ca^{2+} channels, ROCs/SOCs, and reverse-mode NCX. In general, the mechanisms of the Ca^{2+} waves in the basilar artery are similar to those in the large conduit vessels, which may indicate a common Ca^{2+} signaling mechanism which initiates and sustains Ca^{2+} waves in the vasculature.

3.5 References

Arakawa N, Sakaue M, Yokoyama I, Hashimoto H, Koyama Y, Baba A, *et al.* (2000). KB-R7943 inhibits store-operated Ca(2+) entry in cultured neurons and astrocytes. *Biochem Biophys Res Commun* **279:** 354-7.

Arnon A, Hamlyn JM, Blaustein MP (2000). Na(+) entry via store-operated channels modulates Ca(2+) signaling in arterial myocytes. *Am J Physiol Cell Physiol* **278:** C163-73.

Asada Y, Yamazawa T, Hirose K, Takasaka T, Iino M (1999). Dynamic Ca2+ signalling in rat arterial smooth muscle cells under the control of local renin-angiotensin system. *J Physiol* **521:** 497-505.

Boarder MR, Hourani SM (1998). The regulation of vascular function by P2 receptors: multiple sites and multiple receptors. *Trends Pharmacol Sci* **19:** 99-107.

Bootman MD, Collins TJ, Mackenzie L, Roderick HL, Berridge MJ, Peppiatt CM (2002). 2-aminoethoxydiphenyl borate (2-APB) is a reliable blocker of store-operated Ca2+ entry but an inconsistent inhibitor of InsP3-induced Ca2+ release. *FASEB J* **16:** 1145-50.

Boittin FX, Macrez N, Halet G, Mironneau J (1999). Norepinephrine-induced Ca(2+) waves depend on InsP(3) and ryanodine receptor activation in vascular myocytes. *Am J Physiol* **277:** C139-51.

Bolton TB (1979). Mechanisms of action of transmitters and other substances on smooth muscle. *Physiol Rev* **59:** 606-718.

Broad LM, Braun FJ, Lievremont JP, Bird GS, Kurosaki T, Putney JW Jr (2001). Role of the phospholipase C-inositol 1,4,5-trisphosphate pathway in calcium release-activated calcium current and capacitative calcium entry. *J Biol Chem*. **276:** 15945-52.

Burnstock G (1998). History of extracellular nucleotides and their receptors. In: Turner JT, Weisman GA, Fedan JS (eds). *The P2 nucleotide receptors.* Humana Press: New Jersey, pp 3-40.

Christ GJ, Spray DC, el-Sabban M, Moore LK, Brink PR (1996). Gap junctions in vascular tissues. Evaluating the role of intercellular communication in the modulation of vasomotor tone. *Circ Res* **79**: 631-46.

Debdi M, Seylaz J, Sercombe R (1992). Early changes in rabbit cerebral artery reactivity after subarachnoid hemorrhage. *Stroke* **23:** 1154-1162.

DeLisle S, Welsh MJ (1992). Inositol trisphosphate is required for the propagation of calcium waves in Xenopus oocytes. *J Biol Chem* **267:** 7963-6.

Fameli N, van Breemen C, Kuo KH (2007). A quantitative model for linking Na+/Ca2+ exchanger to SERCA during refilling of the sarcoplasmic reticulum to sustain [Ca2+] oscillations in vascular smooth muscle. *Cell Calcium* **42:** 565-575.

Ferris CD, Cameron AM, Huganir RL, Snyder SH (1992). Quantal calcium release by purified reconstituted inositol 1,4,5-trisphosphate receptors. *Nature* **356:** 350-2.

Fill M, Copello JA (2002). Ryanodine receptor calcium release channels. *Physiol Rev* **82:** 893-922.

Fritz N, Mironneau J, Macrez N, Morel JL (2008). Acetylcholine-induced Ca(2+) oscillations are modulated by a Ca(2+) regulation of InsP (3)R2 in rat portal vein myocytes. *Pflugers Arch* **456:** 277-83.

Gordienko DV, Bolton TB (2002). Crosstalk between ryanodine receptors and IP(3) receptors as a factor shaping spontaneous Ca(2+)-release events in rabbit portal vein myocytes. J *Physiol* **542:** 743-62.

Gratton RJ, Gandley RE, McCarthy JF, Michaluk WK, Slinker BK, McLaughlin MK (1998). Contribution of vasomotion to vascular resistance: a comparison of arteries from virgin and pregnant rats. *J Appl Physiol* **85:** 2255-60.

Györke S, Lukyanenko V, Györke I (1997). Dual effects of tetracaine on spontaneous calcium release in rat ventricular myocytes. *J Physiol* **500:** 297-309

Haddock RE, Hill CE (2002). Differential activation of ion channels by inositol 1,4,5-trisphosphate (IP3)- and ryanodine-sensitive calcium stores in rat basilar artery vasomotion. *J Physiol* **545:** 615-27.

Haddock RE, Hill CE (2005). Rhythmicity in arterial smooth muscle. *J Physiol* **566:** 645-56.

Hardebo JE, Kahrstrom J, Owman C (1987). P1- and P2-purine receptors in brain circulation. *Eur J Pharmacol* **144:** 343-352.

Heppner TJ, Bonev AD, Santana LF, Nelson MT (2002). Alkaline pH shifts Ca2+ sparks to Ca2+ waves in smooth muscle cells of pressurized cerebral arteries. *Am J Physiol Heart Circ Physiol* **283:** H2169-76.

Horiuchi T, Dietrich HH, Tsugane S, Dacey Jr RG (2001). Analysis of purine- and pyrimidine-induced vascular responses in the isolated rat cerebral arteriole. *Am J Physiol Heart Circ Physiol* **280:** H767-76.

Hudetz AG, Biswal BB, Shen H, Lauer KK, Kampine JP (1998). Spontaneous fluctuations in cerebral oxygen supply An introduction. *Adv Exp Med Biol*.**454:** 551-9.

Hyvelin JM, Guibert C, Marthan R, Savineau JP (1998). Cellular mechanisms and role of endothelin-1-induced calcium oscillations in pulmonary arterial myocytes. *Am J Physiol* **275:** L269-82.

Iino M, Kasai H, Yamazawa T (1994). Visualization of neural control of intracellular Ca2+ concentration in single vascular smooth muscle cells in situ. *EMBO J* **13:** 5026-5031.

Iino M, Kobayashi T, Endo M (1988). Use of ryanodine for functional removal of the calcium store in smooth muscle cells of the guinea-pig. *Biochem Biophys Res Commun* **152:** 417-22.

Isenberg G, Kazanski V, Kondratev D, Gallitelli MF, Kiseleva I, Kamkin A (2003). Differential effects of stretch and compression on membrane currents and [Na+]c in ventricular myocytes. *Prog Biophys Mol Biol* **82:** 43–56.

Iwamoto T, Watano T, Shigekawa M (1996). A novel isothiourea derivative selectively inhibits the reverse mode of Na+/Ca2+ exchange in cells expressing NCX1. *J Biol Chem* **271:** 22391-22397.

Iwamoto T (2004). Forefront of Na+/Ca2+ exchanger studies: molecular pharmacology of Na+/Ca2+ exchange inhibitors. *J Pharmacol Sci.* **96:** 27-32.

Jaggar JH (2001). Intravascular pressure regulates local and global Ca(2+) signaling in cerebral artery smooth muscle cells. *Am J Physiol Cell Physiol* **281:** C439-48.

Jaggar JH, Nelson MT (2000). Differential regulation of Ca(2+) sparks and Ca(2+) waves by UTP in rat cerebral artery smooth muscle cells. *Am J Physiol Cell Physiol* **279:** C1528-39.

Kanmura Y, Missiaen L, Raeymaekers L, Casteels R (1988). Ryanodine reduces the amount of calcium in intracellular stores of smooth-muscle cells of the rabbit ear artery. *Pflugers Arch*. **413:** 153-9.

Ladilov Y, Haffner S, Balser-Schäfer C, Maxeiner H, Piper HM (1999). Cardioprotective effects of KB-R7943: a novel inhibitor of the reverse mode of Na+/Ca2+ exchanger. *Am J Physiol* **276**: H1868-76.

Lamont C, Wier WG (2004). Different roles of ryanodine receptors and inositol (1,4,5)-trisphosphate receptors in adrenergically stimulated contractions of small arteries. *Am J Physiol Heart Circ Physiol* **287:** H617-25.

Lechleiter JD, Clapham DE (1992). Molecular mechanisms of intracellular calcium excitability in X. laevis oocytes. *Cell* **69:** 283-94.

Lee CH, Poburko D, Kuo KH, Seow CY, van Breemen C (2002). Ca(2+) oscillations, gradients, and homeostasis in vascular smooth muscle. *Am J Physiol Heart Circ Physiol* **282:** H1571-83.

Lee CH, Poburko D, Sahota P, Sandhu J, Ruehlmann DO, van Breemen C (2001). The mechanism of phenylephrine-mediated [Ca(2+)](i) oscillations underlying tonic contraction in the rabbit inferior vena cava. *J Physiol* **534:** 641-650.

Lemos VS, Poburko D, Liao CH, Cole WC, van Breemen C (2007). Na+ entry via TRPC6 causes Ca2+ entry via NCX reversal in ATP stimulated smooth muscle cells. *Biochem Biophys Res Commun* **352**: 130-4.

Leijten PA, van Breemen C (1986). The relationship between noradrenaline-induced contraction and 45Ca efflux stimulation in rabbit mesenteric artery. *Br J Pharmacol* **89:** 739-747.

Lepretre N, Mironneau J (1994). Alpha 2-adrenoceptors activate dihydropyridine-sensitive calcium channels via Gi-proteins and protein kinase C in rat portal vein myocytes. *Pflugers Arch* **429:** 253-261.

Liang W, Buluc M, van Breemen C, Wang X (2004). Vectorial Ca2+ release via ryanodine receptors contributes to Ca2+ extrusion from freshly isolated rabbit aortic endothelial cells. *Cell Calcium* **36:** 431-43.

Ma HT, Venkatachalam K, Li HS, Montell C, Kurosaki T, Patterson RL *et al*. (2001). Assessment of the role of the inositol 1,4,5-trisphosphate receptor in the activation of transient receptor potential channels and store-operated Ca2+ entry channels. *J Biol Chem* **276:** 18888-96.

Mauban JR, Lamont C, Balke CW, Wier WG. (2001). Adrenergic stimulation of rat resistance arteries affects Ca(2+) sparks, Ca(2+) waves, and Ca(2+) oscillations. *Am J Physiol Heart Circ Physiol* **280:** H2399-405.

McCarron JG, Bradley KN, MacMillan D, Muir TC (2003). Sarcolemma agonist-induced interactions between InsP3 and ryanodine receptors in Ca2+ oscillations and waves in smooth muscle. *Biochem Soc Trans* **31:** 920-4.

McCarron JG, Olson ML (2008). A single luminally continuous sarcoplasmic reticulum with apparently separate Ca2+ stores in smooth muscle. *J Biol Chem* **283:** 7206-18.

Meldolesi J, Pozzan T (1998). The endoplasmic reticulum Ca2+ store: a view from the lumen. *Trends Biochem Sci* **23:** 10-4.

Miriel VA, Mauban JR, Blaustein MP, Wier WG (1999). Local and cellular Ca2+ transients in smooth muscle of pressurized rat resistance arteries during myogenic and agonist stimulation. *J Physiol* **518:** 815-824.

Missiaen L, Callewaert G, De Smedt H, Parys JB (2001). 2-Aminoethoxydiphenyl borate affects the inositol 1,4,5-trisphosphate receptor, the intracellular Ca2+ pump and the non-specific Ca2+ leak from the non-mitochondrial Ca2+ stores in permeabilized A7r5 cells. *Cell Calcium* **29:** 111-116.

Morel JL, Fritz N, Lavie JL, Mironneau J (2003). Crucial role of type 2 inositol 1,4,5-trisphosphate receptors for acetylcholine-induced Ca2+ oscillations in vascular myocytes. *Arterioscler Thromb Vasc Biol* **23:** 1567-75.

Nazer MA, van Breemen C (1998). Functional linkage of Na(+)-Ca2+ exchange and sarcoplasmic reticulum Ca2+ release mediates Ca2+ cycling in vascular smooth muscle. *Cell Calcium* **24:** 275-83.

Nelson MT, Patlak JB, Worley JF, Standen NB (1990). Calcium channels, potassium channels, and voltage dependence of arterial smooth muscle tone. *Am J Physiol* **259:** C3-18.

Peng H, Matchkov V, Ivarsen A, Aalkjaer C, Nilsson H (2001). Hypothesis for the initiation of vasomotion. *Circ Res* **88:** 810-815.

Philipson KD, Nicoll DA (2000). Sodium-calcium exchange: a molecular perspective. *Annu Rev Physiol* **62:** 111-133.

Poburko D, Kuo KH, Dai J, Lee CH, van Breemen C (2004). Organellar junctions promote targeted Ca2+ signaling in smooth muscle: why two membranes are better than one. *Trends Pharmacol Sci* **25:** 8-15.

Poburko D, Liao CH, Lemos VS, Lin E, Maruyama Y, Cole WC, *et al.* (2007). Transient receptor potential channel 6-mediated, localized cytosolic [Na+] transients drive Na+/Ca2+ exchanger-mediated Ca2+ entry in purinergically stimulated aorta smooth muscle cells. *Circ Res* **101:** 1030-1038.

Poburko D, Potter K, van Breemen E, *et al* (2006). Mitochondria buffer NCX-mediated Ca2+-entry and limit its diffusion into vascular smooth muscle cells. *Cell Calcium* **40**: 359-71.

Putney JW, Jr (1986). A model for receptor-regulated calcium entry. *Cell Calcium* **7:** 1-12.

Rahman A, Matchkov V, Nilsson H, Aalkjaer C (2005). Effects of cGMP on coordination of vascular smooth muscle cells of rat mesenteric small arteries. *J Vasc Res* **42:** 301-11.

Ratz PH, Berg KM (2006). 2-Aminoethoxydiphenyl borate inhibits KCl-induced vascular smooth muscle contraction. *Eur J Pharmacol* **541:** 177-83.

Rousseau E, Smith JS, Meissner G (1987). Ryanodine modifies conductance and gating behavior of single Ca2+ release channel. *Am J Physiol* **253:** C364-8.

Rücker M, Strobel O, Vollmar B, Roesken F, Menger MD (2000). Vasomotion in critically perfused muscle protects adjacent tissues from capillary perfusion failure. *Am J Physiol Heart Circ Physiol* **279:** H550-8.

Ruehlmann DO, Lee CH, Poburko D, van Breemen C (2000). Asynchronous Ca(2+) waves in intact venous smooth muscle. *Circ Res.* **86:** E72-9.

Shimamura K, Sekiguchi F, Sunano S (1999). Tension oscillation in arteries and its abnormality in hypertensive animals. *Clin Exp Pharmacol Physiol* **26:** 275-84.

Shirasawa Y, White RP, Robertson JT (1983). Mechanisms of the contractile effect induced by uridine 5-triphosphate in canine cerebral arteries. *Stroke* **14:** 347-355.

Sima B, Weir BK, Macdonald RL, Zhang H (1997). Extracellular nucleotide-induced [Ca2+]i elevation in rat basilar smooth muscle cells. *Stroke* **28:** 2053-9.

Sobolevsky AI, Khodorov BI (1999). Blockade of NMDA channels in acutely isolated rat hippocampal neurons by the Na^+/Ca^{2+} exchange inhibitor KB-R7943. *Neuropharmacology* **38:** 1235–1242

Streb H, Irvine RF, Berridge MJ, Schulz I (1983). Release of Ca2+ from a nonmitochondrial intracellular store in pancreatic acinar cells by inositol-1,4,5-trisphosphate. *Nature* **306:** 67-69.

Strobaek D, Olesen SP, Christophersen P, Dissing S (1996). P2-purinoceptor-mediated formation of inositol phosphates and intracellular Ca2+ transients in human coronary artery smooth muscle cells. *Br J Pharmacol* **118:** 1645-1652.

Toyoda K, Fujii K, Ibayashi S, Sadoshima S, Fujishima M (1996). Changes in arterioles, arteries, and local perfusion of the brain stem during hemorrhagic hypertension. *Am J Physiol* **270:** H1350-4.

Urquilla PR (1978). Prolonged contraction of isolated human and canine cerebral arteries induced by uridine 5'-triphosphate. *Stroke* **9:** 133-136.

van Breemen C, Aaronson P, Loutzenhiser R (1978). Sodium-calcium interactions in mammalian smooth muscle. *Pharmacol Rev* **30:** 167-208.

Watano T, Kimura J, Morita T, Nakanishi H. (1996) A novel antagonist, No. 7943, of the Na^+/Ca^{2+} exchange current in guinea-pig cardiac ventricular cells. *Br J Pharmacol* **119**: 555−563.

Weber LP, Van Lierop JE, Walsh MP (1999). Ca2+-independent phosphorylation of myosin in rat caudal artery and chicken gizzard myofilaments. *J Physiol* **516:** 805-24.

Wendt-Gallitelli MF, Voigt T, Isenberg G (1993). Microheterogeneity of subsarcolemmal sodium gradients. Electron probe microanalysis in guinea-pig ventricular myocytes. *J Physiol* **472:** 33– 44.

Wilson DP, Sutherland C, Walsh MP (2002). Ca2+ activation of smooth muscle contraction: evidence for the involvement of calmodulin that is bound to the triton insoluble fraction even in the absence of Ca2+. *J Biol Chem* **277:** 2186-2192.

Xu L, Lai FA, Cohn A, Etter E, Guerrero A, Fay FS, Meissner G (1994). Evidence for a Ca(2+)-gated ryanodine-sensitive Ca2+ release channel in visceral smooth muscle. *Proc Natl Acad Sci U S A* **91:** 3294-8.

Zacharia J, Zhang J, Wier WG (2007). Ca2+ signaling in mouse mesenteric small arteries: myogenic tone and adrenergic vasoconstriction. *Am J Physiol Heart Circ Physiol* **292:** H1523-32.

CHAPTER 4 – DYSFUNCTION OF ENDOTHELIUM AND SMOOTH MUSCLE CELLS IN SMALL ARTERIES OF A MOUSE MODEL OF MARFAN SYNDROME[3]

4.1 Introduction

Marfan syndrome is an autosomal dominant disorder caused by mutations in the gene encoding for fibrillin-1 and affects many tissues, including those of the cardiovascular, skeletal, ocular and pulmonary systems (Dietz *et al.*, 1991; Pyeritz, 2000; Judge and Dietz, 2005). Fibrillin-1 is the structural glycoprotein for microfibrils, which act as scaffolding proteins for elastin deposition and formation of elastic fibres (Reinhardt *et al.*, 1995). Abnormalities in the formation and integrity of elastic fibres in Marfan syndrome cause weakening of the blood vessel walls and are especially pronounced in the aorta due to its high (~50%) elastin content, which normally allows it to buffer pressure variations during the cardiac cycle and permit constant blood flow and organ perfusion (Rosenbloom, 1993; Safar and London, 1994). Weakening of the aortic wall leads to root dilatation, dissection and eventual rupture, the major cause of death in patients with Marfan syndrome (Murdoch *et al.*, 1972).

Marfan syndrome is associated not only with extensive degeneration of elastic fibres, but also with endothelial dysfunction and reduction of smooth muscle contractility in the vasculature (Chung *et al.*, 2007a,b). The alteration of the structural integrity of elastic fibres leads to reduced distensibility and elasticity (Bunton *et al.*, 2001). Furthermore, alteration of fibrillin-1 may also disrupt the attachment of elastic fibres to the cells in the endothelial layer and impair endothelial permeability (Davis, 1994; Sheremet'eva *et al.*, 2004). Although elastic fibre composition is gradually reduced along the arterial tree, elastin remains an important determinant of passive mechanical properties in mesenteric arteries (Dobrin, 1978; Milnor, 1989; Mulvany and

[3] A version of this chapter has been published. Syyong HT, Chung AW, Yang HH, van Breemen C (2009). Dysfunction of endothelial and smooth muscle cells in small arteries of a mouse mdoel of Marfan syndrome. *Br. J Pharmacol.* **158:** 1597-1608.

Aalkjaer, 1990; Briones *et al.*, 2003; González *et al.*, 2005). However, little is known about how Marfan syndrome affects vessel elasticity and vasomotor function in the resistance vasculature, although dysfunction of these vessels may have important clinical consequences. For example, aneurysms in peripheral and resistance vessels have been reported in patients with Marfan syndrome (Savolainen *et al.*, 1993; Hatrick *et al.*, 1998; Goffi *et al.*, 2000; Lay *et al.*, 2006), although no clear link has been established between resistance artery dysfunction and aortic dilatation and rupture (Jondeau *et al.*, 1999). Furthermore, maximum forearm blood flow in response to acetylcholine (ACh) is reduced in patients with Marfan syndrome (Nakamura *et al.*, 2000), and impairment in flow-mediated vasodilation is also observed (Wilson *et al.*, 1999).

In the present study, we compared the stiffness and vascular function of resistance-sized mesenteric arteries from a mouse model of Marfan syndrome with those from their wild-type littermates. We conclude that during the progression of Marfan syndrome, mesenteric arteries show signs of increased stiffness. Furthermore, the contractile function of smooth muscle cells and endothelium-dependent and endothelium-independent vasorelaxation are all markedly impaired. Therefore, we suggest that Marfan syndrome should be considered as a disorder not only in the aorta, but also in the peripheral resistance vasculature.

4.2 METHODS

4.2.1 Experimental animals and tissue preparation

Heterozygous ($Fbn1^{C1039G/+}$) mice were mated to C57BL/6 mice to produce equal numbers of $Fbn1^{C1039G/+}$ Marfan subjects and wild-type controls as described previously (Judge *et al.,* 2004; Ng *et al.,* 2004; Habashi *et al.,* 2006; Chung *et al.,* 2007a,b). Both strains were housed in the institutional animal facility (Child and Family Research Institute, University of British

Columbia) under standard animal room conditions (12h light-12h dark, at 25ºC, 2-5 animals in a cage), and all animal procedures were approved by the institutional Animal Ethics Board. Mice at ages 3 (n = 30), 6 (n = 30), and 10 (n = 30) months were anesthetized with a mixture of ketamine hydrochloride (80 $mg \cdot kg^{-1}$) and xylazine hydrochloride (12 $mg \cdot kg^{-1}$) intraperitoneally for experimentation. The mesenteric arcade was excised and placed in ice-cold oxygenated (95% O_2-5% CO_2) 4-(2-hydroxyethyl)-1-piperazineethanesulfonic acid (HEPES)-buffered physiological saline salt (HEPES-PSS) solution. Second-order branches of the mesenteric artery with diameters of 130-150 μm were dissected and cut into 2 mm segments.

4.2.2 Mechanical properties

"Vessel elasticity" was deduced from the stress–strain curves. In a small vessel myograph (A/S Danish Myotechnology, Aarhus, Denmark), a 2 mm mesenteric artery segment was stretched by increasing the distance between the 2 stainless wires (= increase in length of vascular smooth muscle cell) and held at each length for 1 min. The chambers were kept at 37ºC and bubbled continuously with 95% O_2-5% CO_2 in HEPES-PSS solution. Initially, 2 wires were adjusted to L_o, at which the vessel was not stretched. The inside circumference of the mesenteric segment was measured as twice the distance between 2 wires, plus the wire circumference, plus 2 wire radii (2x40 μm). The distance between the 2 wires was then increased by 25 μm, and the new length was denoted as "L." The developed force (mN) was divided by the surface area (= inside circumference of the segment x length of the segment) of the blood vessel segment (mm^2) to calculate the wall stress (mN/mm^2). The procedure was repeated until the vessel was unable to maintain its tone. The $\Delta L/L_o$ and the wall stress were fitted on an exponential curve. "Passive force" was measured by repeating the above procedures in a Ca^{2+}-free HEPES-PSS solution

prepared by replacing $CaCl_2$ with 320 μM ethylene glycol tetraacetic acid (EGTA) to eliminate smooth muscle cell contractility. "Total force" was determined by assessing the active contractility at each level of stretch in response to depolarization (60 mM KCl).

To study the "reversibility of vessel contractility" after stretching, the mesenteric segment was stimulated with 60 mM KCl at the optimal tension ($\Delta L/L_0$ is approximately equal to 2.0, a value that gives the maximal force generation in response to KCl), then stretched to either $\Delta L/L_0$ = 2.5, 3.0, 3.5 or 4.0 for 3 min, and restored to optimal tension. Contraction was induced after 3 min, and the percentage of developed force change compared to the optimal tension was calculated.

4.2.3 Measurement of isometric force

Mesenteric artery segments were isometrically mounted in a small vessel wire myograph (A/S Danish Myotechnology, Aarhus N, Denmark) using two 40 μm tungsten wires for measuring generated force. The chambers were kept at 37ºC and bubbled continuously with 95% O_2-5% CO_2 in HEPES-PSS. Optimal tension (4 mN) was determined in preliminary experiments by subjecting arterial segments to different resting tensions and stimulating with 60 mM KCl. The vessels were stretched to the optimal tension (the maximal force generation given in response to 60 mM KCl, which were the same for control and Marfan mouse mesenteric arteries; 4 mN) for 60 min. The vessels were challenged twice with 60 mM KCl before experiments were continued. Tonic contraction was induced by 3 μM phenylephrine (PE) and all mechanistic studies were performed at this concentration. Concentration-response curves of PE-induced contraction were constructed, and the negative logarithm (pD_2) of the concentration of PE giving

half-maximum response (EC_{50}) was assessed by linear interpolation on the semilogarithm concentration-response curve [$pD_2 = -\log(EC_{50})$].

To determine endothelium-dependent and endothelium-independent relaxations, vessels were pre-contracted with 3 μM PE before making cumulative applications of acetylcholine (ACh) or sodium nitroprusside (SNP) (1 nM – 10 μM), respectively. Control concentration response curves to ACh were produced and compared to those in vessels pre-treated with N_{ω}-Nitro-L-arginine methyl ester (L-NAME, 200 μM), indomethacin (10 μM), or catalase (1000 $U \cdot mL^{-1}$) for 30 min. Other vessels were pre-treated with L-NAME (200 μM) and indomethacin (10 μM) for 30 min and concentration-response curves to ACh were produced. These responses were then repeated in the presence of catalase (1000 $U \cdot mL^{-1}$) or carbenoxolone (100 μM). Percent relaxation was calculated as the percent decrease in force with respect to the initial PE (3 μM)-induced precontraction, and the percent relaxation was used to construct the concentration-response curves of ACh-induced relaxation.

4.2.4 Measurement of intracellular Ca^{2+}

The arterial rings were loaded with Fluo-4AM (5 μM with 5 μM Pluronic F-127, 1 hr at 37ºC) and isometrically mounted, followed by a 30 min washout time in HEPES-PSS. Sustained Ca^{2+} waves were induced by 3 μM PE, and all mechanistic studies were done at this concentration. Images were acquired on an upright Olympus BX50WI microscope with a 40x water-dipping objective (NA 0.9) and equipped with an Ultraview confocal imaging system (Perkin-Elmer). The rate of image acquisition was 3 frames/s. The tissue was illuminated using the 488nm line of an Argon-Krypton laser and a high-gain photomultiplier tube collected the emission at wavelengths between 505 and 550 nm. The scanned regions correspond to a 91.69 x

66.68 μm area (or 248 x 328 pixels). The representative fluorescence traces shown reflect the averaged fluorescence signals from a region of 3 x 3 pixels (1.69 μm^2) of the smooth muscle cell. The frequency of Ca^{2+} waves was determined by counting the number of waves occurring within 50s. The measured changes in Fluo-4 fluorescence level are proportional to the relative changes in $[Ca^{2+}]_i$. All parameters (laser intensity, gain, etc) were maintained constant during the experiment. The confocal images were analyzed off-line with the Ultraview 5.5 Software (Perkin-Elmer). Fluorescence traces were extracted from the movies to exclude nuclear regions and traces were normalized to initial fluorescence values.

4.2.5 Detection of H_2O_2 production from endothelial cells

Mesenteric artery segments of control and Marfan mice were cut into rings and then opened longitudinally. The vascular strip was loaded with dichlorodihydrofluorescein diacetate (DCF, 5 μM), a peroxide-sensitive fluorescence dye (Ohba *et al.,* 1994), for 10 min at 25°C. Images were acquired on an upright Olympus BX50WI microscope with a 60x water-dipping objective (NA 0.9) equipped with an Ultraview confocal imaging system (Perkin-Elmer, USA). The tissue was illuminated using the 488nm line of an argon-krypton laser and a high-gain photomultiplier tube collected the emission at wavelengths between 505 and 550 nm. The tissue was preincubated with indomethacin (10 μM) and L-NAME (200 μM) for 30 min, and then stimulated with ACh (10 μM). Additionally, the effect of catalase (1000 $U \cdot mL^{-1}$) on the ACh-induced increase in fluorescence intensities was also determined.

4.2.6 Statistics

Values are expressed as mean ± standard error (SEM) from at least six independent experiments. Statistical analysis and construction of concentration-response curves were performed using GraphPad Prism 4.0 software (San Diego, CA, USA). Differences between control and Marfan groups were analyzed by Student's two-tailed *t*-test. Statistical significance was defined as *P*-values <0.05.

4.2.7 Drugs, solutions, and chemicals

HEPES-PSS containing (in mM) NaCl 130, HEPES 10, glucose 6, KCl 4, $NaHCO_3$ 4, $CaCl_2$ 1.8, $MgSO_4$ 1.2, KH_2PO_4 1.18, and ethylenediaminetetraacetic acid (EDTA) 0.03 (pH 7.4) was used for all studies. Hi-K^+ (60 mM extracellular K^+) HEPES-PSS was identical in composition to normal HEPES-PSS with the exception of (in mM) NaCl 74 and KCl 60. PE, SNP, L-NAME, catalase, carbenoxolone, indomethacin, and pluronic F-127 were obtained from Sigma-Aldrich (Oakville, Ontario, Canada). Fluo-4AM and dichlorodihydrofluorescein diacetate (DCF) were purchased from Molecular Probes (Eugene, OR). Superoxide dismutase was obtained from Calbiochem (San Diego, CA, USA)

4.3 RESULTS

4.3.1 Vessel stiffening and weakness in marfan mesenteric artery

In the measurement of stiffness, stress increases exponentially as a function of vessel diameter. At 3 months of age, the fitted curves for the stress-strain relationship from control and Marfan vessels were not significantly different (Fig. 4.1A). However, at 6 and 10 months of age,

the slope of the stress-strain curves from the Marfan vessels was increased compared with that of the control vessels, which indicates increased stiffness (Fig. 4.1B,C).

However, true elasticity also implies the capability to return to the original conformation or length, a situation which is analogous to an elastic band. To test this elasticity, we measured the "reversibility of mesenteric artery elasticity" by comparing 2 stress-strain curves from control and Marfan vessels at 6 and 10 months of age. Since we did not observe any increase in stiffness in the Marfan vessels at 3 months of age, these measurements were not done in this group. We found that the apparent vessel elasticity in the second measurement remained for the most part unchanged in the control vessels, but was highly increased in the Marfan vessels (Fig. 4.2). This may suggest a weakening of the vessel wall at 10 months of age, and a similar observation was also found at 6 months of age (data not shown). We also measured the effects of stretch on contractility in 6 and 10 month old mice. After distending to $\Delta L/L_o = 2.5$, the 60mM KCl-induced contraction in the Marfan vessels at both 6 and 10 months of age (normalized to the optimal contraction recorded at $\Delta L/L_o = 2.0$) was not significantly decreased. However, distending to $\Delta L/L_o = 3.0$ reduced the Marfan vessel contraction to 74.0 ± 5.9% and 42.0 ± 15.8%, while contraction in the control vessels were reduced to 93.2 ± 1.5% and 69.1 ± 3.0% at 6 and 10 months of age, respectively (Fig. 4.3). Further distension to $\Delta L/L_o = 3.5$ reduced contractility in Marfan vessels to 43.5 ± 8.7% and 24.6 ± 9.6%, while in control contraction was reduced to 76.8 ± 0.3% and 51.7 ± 3.1%. Distention to $\Delta L/L_o = 4.0$ reduced contractility in Marfan vessels to 22.2 ± 5.0% and 5.3 ± 3.2%, while in controls it was 58.4 ± 3.1% and 29.0 ± 3.3%. Thus impairment due to stretch was significantly greater in the Marfan than the control mice.

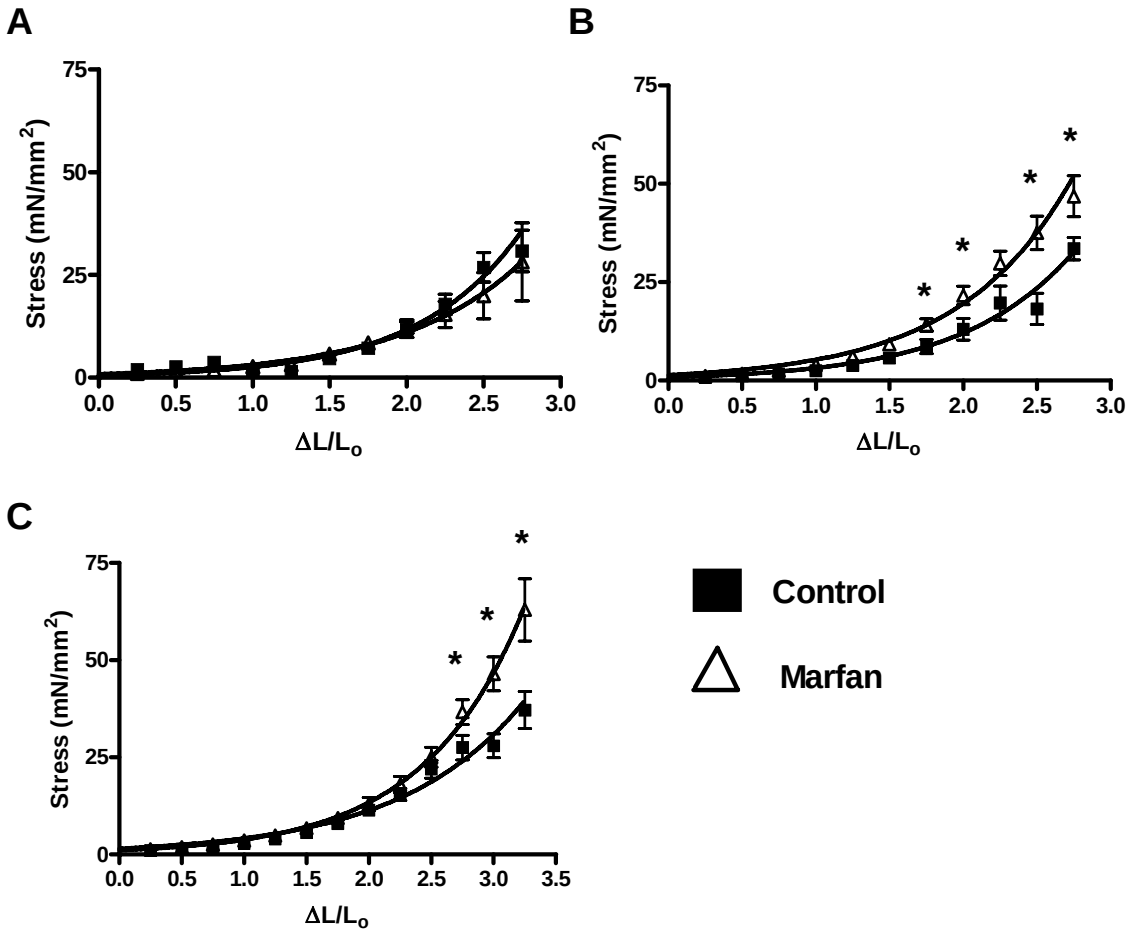

Figure 4.1 Vessel elasticity during aging in mesenteric arteries. Elasticity was tested in Marfan (triangle) and control (filled square) mice from **(A)** 3, **(B)** 6, and **(C)** 10 months of age (* $P < 0.05$ vs. control, n = 8-12).

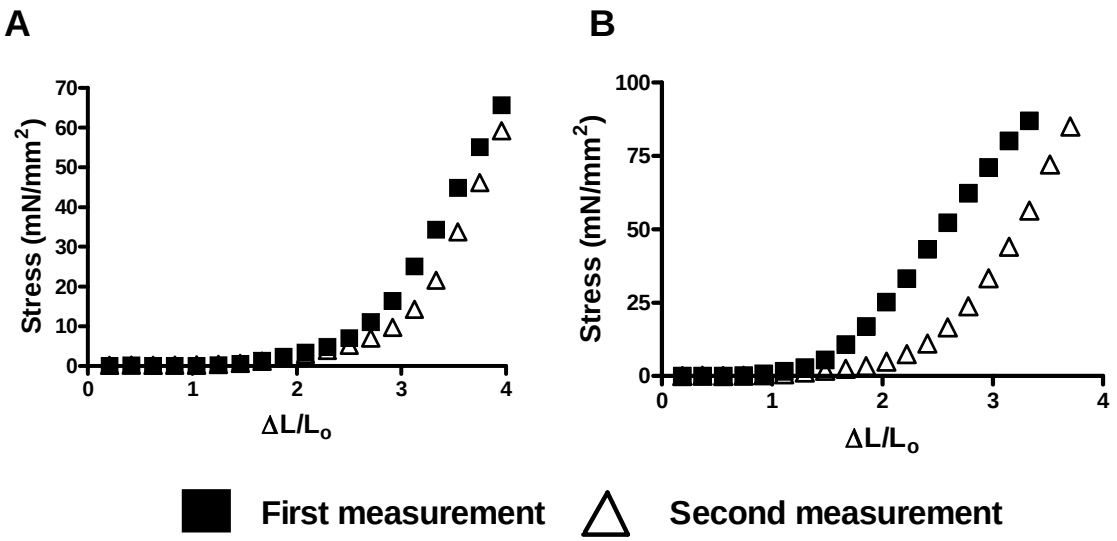

Figure 4.2 Reversibility of mesenteric artery elasticity. In **(A)** control and **(B)** Marfan mice at 10 months of age, reversibility of elasticity was tested by performing two consecutive stress-strain measurements. Vessel elasticity from the first (square) and second (triangle) measurement was compared in each group. Representative results are shown from 3 independent experiments.

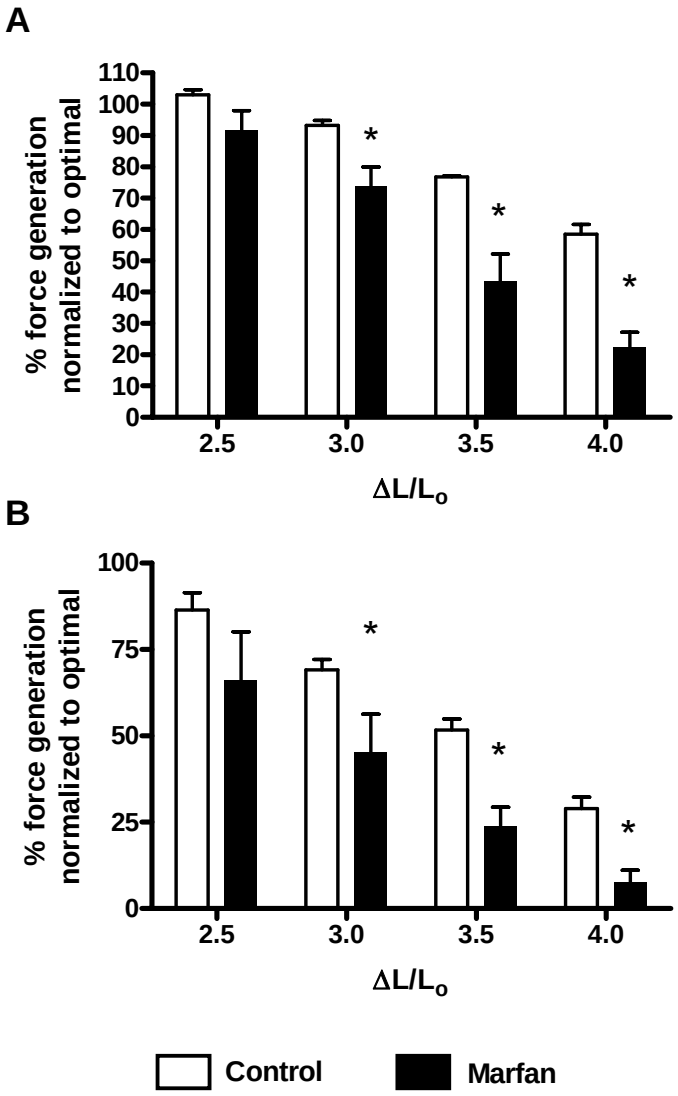

Figure 4.3 Reversibility of contractile function of mesenteric arteries from control and marfan mice. Contractile function was determined from both control and Marfan mice **(A)** 6 and **(B)** 10 months of age after stretching at $\Delta L/L_o$ = 2.5, 3.0, 3.5, and 4.0. After being stretched for 3 minutes and restored to optimal tension, vessels were stimulated with 60 mM KCl (* - $P < 0.05$ vs. control, n = 6-8). Values (%) are changes of force generation normalized to that at the optimal tension.

4.3.2 Reduced contractile function of smooth muscle cells in marfan mesenteric artery

To determine if smooth muscle contractile function is affected in Marfan mesenteric arteries, we stimulated the vessels with both KCl (60mM) depolarization and PE. From 3 months of age

onward, vasoconstriction in response to KCl-induced depolarization in Marfan vessels was significantly less (2.41 ± 0.21 mN) compared to that in age-matched controls (3.31 ± 0.23 mN), a 28% reduction (Fig. 4.4A). At 6 and 10 months of age, contractility of the Marfan vessels was reduced to only 3.15 ± 0.39 mN (30% reduction) and 2.51 ± 0.32 mN (52% reduction), respectively, compared to 4.43 ± 0.38 mN and 5.15 ± 1.06 mN in the age-matched control vessels.

Application of PE produced tonic contraction in a concentration-dependent manner at all ages in both control and Marfan mice (Fig. 4.4B). Although there was no significant difference at 3 months of age, maximal contraction was significantly reduced at 6 and 10 months of age in the Marfan vessels, 3.29 ± 0.60 mN and 2.60 ± 3.1 mN, respectively, compared to 5.49 ± 0.62 mN and 4.20 ± 0.70 mN in age-matched controls (Fig. 4.4B). However, there were no significant differences in pEC_{50} values at all ages (3 months: Control 6.37 ± 0.17, Marfan 6.02 ± 0.25; 6 months Control 5.83 ± 0.21, Marfan 5.72 ± 0.21; 10 months Control 5.95 ± 0.23, Marfan 5.66 ± 0.42).

To further examine smooth muscle contractile function, we measured the active force in response to KCl-depolarization. Control arteries at 3 months of age generated active force over a range of strain $\Delta L/L_{o,}$ 0.2 to 1.7, while control arteries at 6 and 10 months of age generated active force over a range of strain $\Delta L/L_{o,}$ 0.2 to 2.0 (Fig. 4.5). However, this range was markedly reduced in the Marfan vessels at all age groups. Furthermore, the maximum active force generated in the Marfan mesenteric vessels was also markedly reduced at all age groups by 52% (3 months), 56% (6 months), and 66% (10 months) compared with the age-matched controls, respectively.

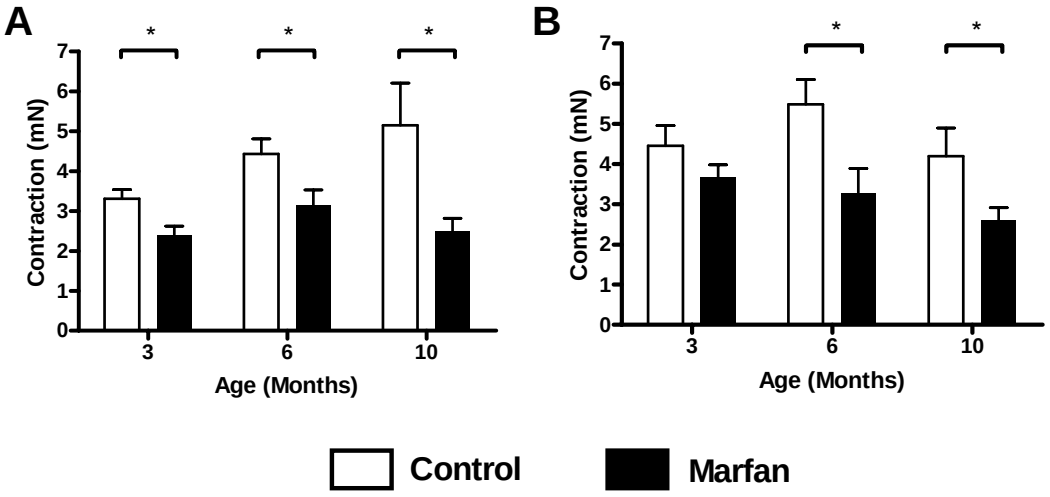

Figure 4.4: Isometric force measurement in response to KCl and PE in control and marfan mice. Maximal force generated in response to **(A)** 60 mM KCl and **(B)** PE (3 μM) was compared between control and Marfan vessels (* - $P < 0.05$ vs. control, n = 8-12).

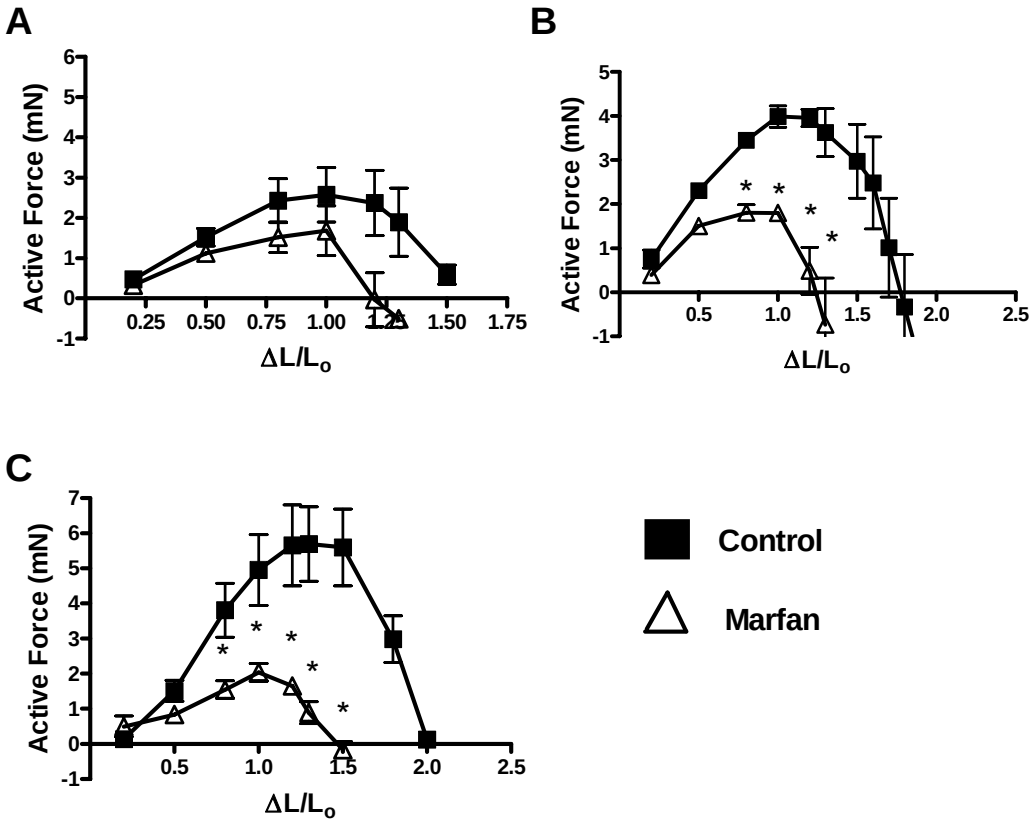

Figure 4.5: Active force in control and marfan mice. Active force, the difference between total and passive force, was compared between control (filled square) and Marfan (triangle) vessels from **(A)** 3, **(B)** 6, and **(C)** 10 months of age (* - $P < 0.05$ vs. control, n = 8-12).

4.3.3 Frequency of PE-induced Ca^{2+} waves is reduced in marfan syndrome

In both control and Marfan vessels, stimulation with PE (3 μM) induced a large transient Ca^{2+} response in both control and Marfan vessels at all ages, which was followed by repetitive transient elevations in Ca^{2+} which originate in distinct intracellular foci and then spread out as waves over the length of the smooth muscle cell (Appendix A). The Ca^{2+} waves were asynchronous and did not propagate intercellularly. The frequency of PE-stimulated Ca^{2+} waves increased in a concentration-dependent manner at all ages and closely paralleled the development of force in both control and Marfan mice (pEC_{50}; 3 months: Control 6.49 ± 0.26, Marfan 6.28 ± 0.30 ; 6 months Control 6.01 ± 0.19, Marfan 5.79 ± 0.21; 10 months Control 6.03 ± 0.12, Marfan 6.01 ± 0.21). However, the average frequency of the PE-stimulated Ca^{2+} waves was significantly reduced in Marfan vessels compared to control vessels at 6 (Control 0.075 ± 0.005 Hz, Marfan 0.033 ± 0.004 Hz; $P < 0.05$) and 10 months (Control 0.052 ± 0.007 Hz, Marfan 0.031 ± 0.003 Hz; $P < 0.05$), but not at 3 months (Control: 0.068 ± 0.006 Hz, Marfan: 0.056 ± 0.005 Hz) of age (Appendix B). The average frequency of PE-stimulated Ca^{2+} waves was also reduced in control mice at 10 months compared to 6 months of age (0.052 ± 0.006 Hz vs. 0.075 ± 0.005 Hz; $P < 0.05$) (Appendix B). The number of cells displaying at least one Ca^{2+} wave was also significantly reduced in Marfan mice at 6 (Control: 74.51 ± 5.45%, Marfan: 49.71 ± 6.72%; $P < 0.05$) and 10 months (Control: 52.67 ± 5.93%, Marfan: 37.84 ± 5.52%; $P < 0.05$) of age, but not at 3 months (Control: 82.70 ± 3.68 %, Marfan 71.97 ± 5.42%) of age. At 6 months of age, more cells display

Ca^{2+} waves in response to PE-stimulation compared to at 10 months of age (71.68 ± 5.20% vs. 48.38 ± 6.65%) (Appendix B).

4.3.4 Reduced endothelium-dependent and independent relaxation in marfan mesenteric artery

In PE (3 μM)-precontracted vessels from control and Marfan mice, addition of ACh resulted in a concentration-dependent relaxation at all age groups (Fig. 4.6). There was no difference in the maximal response (E_{max}) to ACh (10 μM)-induced relaxation between Marfan and control vessels in mice at 3 months of age, although E_{max} in Marfan vessels at 6 and 10 months of age were 69.7% and 44.9% of the controls, respectively. It should be noted that the maximal relaxation values did not tend to change with increasing age in the control animals. Values for pEC_{50} for ACh indicated that at 6 months of age, the Marfan vessels were less sensitive to ACh than the controls (6.49 ± 0.21 vs. 7.17 ± 0.30, respectively). This difference was not seen at 3 (7.17 ± 0.12 vs. 7.23 ± 0.11 in control and Marfan, respectively) and 10 months of age (6.03 ± 0.30 vs. 6.23 ± 0.16, Marfan and control, respectively).

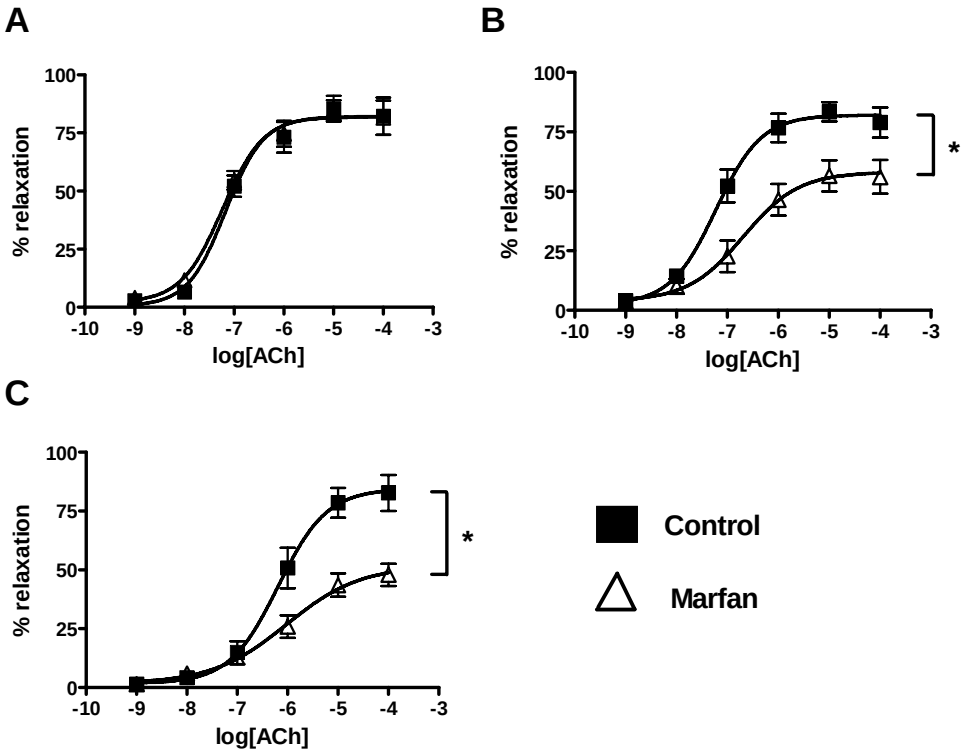

Figure 4.6 Endothelium-dependent relaxation in mesenteric arteries from control and marfan mice. Concentration-response curve of acetylcholine (ACh)-induced relaxation in phenylephrine (3 μM)-precontracted mesenteric arteries from control and Marfan mice at **(A)** 3, **(B)** 6, and **(C)** 10 months of age (* - $P < 0.05$ vs. control, n = 8-12).

Endothelium-independent vasodilatation was studied by the addition of sodium nitroprusside (SNP), a nitric oxide (NO) donor which bypasses endogenous NO production by endothelial cells, and resulted in complete dilatation in PE-precontracted control and Marfan mesenteric vessels at 6 and 10 months of age (Fig. 4.7). Although there was no difference in E_{max} of SNP-relaxation between control and Marfan vessels, there was a significant increase in the pEC_{50} in Marfan vessels at 6 months ($pEC_{50} = 5.64 \pm 0.11$, control $pEC_{50} = 7.34 \pm 0.04$) and 10 months ($pEC_{50} = 5.99 \pm 0.07$, control $pEC_{50} = 6.99 \pm 0.14$), indicating that the Marfan vessels are less sensitive to NO at these ages. However there was no significant difference in pEC_{50} at 3 months of age (data not shown).

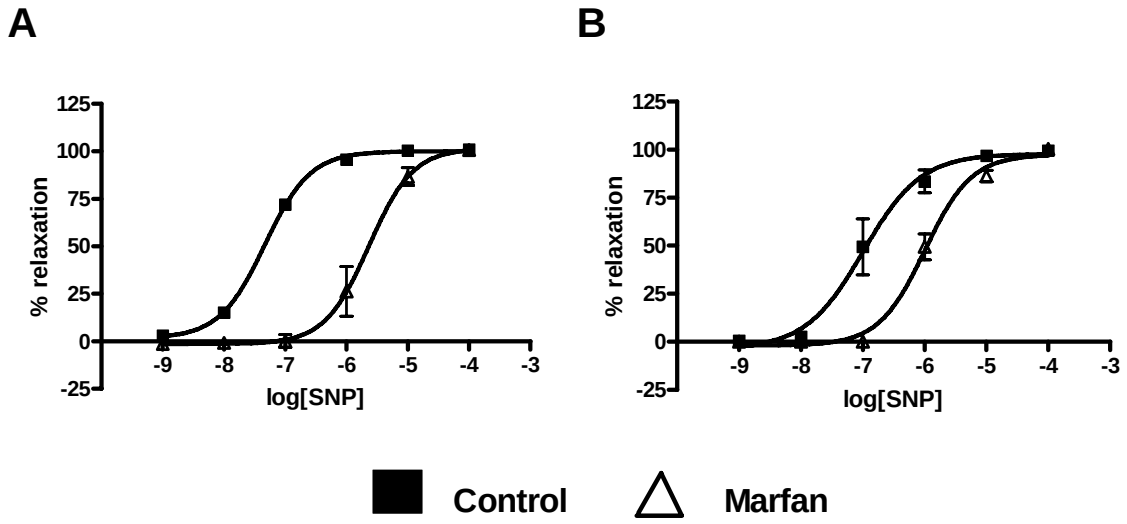

Figure 4.7 Endothelium-independent relaxation in mesenteric arteries from control and marfan mice. Concentration-response curve of sodium nitroprusside (SNP)-induced relaxation in phenylephrine (3 μM)-precontracted mesenteric arteries from control and marfan mice at **(A)** 6 and **(B)** 10 months of age (* - $P < 0.05$ vs. control, n = 8-12).

We then assessed the ACh response in the presence of L-NAME (200 μM), an inhibitor of nitric oxide synthase. Because impairment of ACh-induced vasorelaxation was most evident in the Marfan mice at 10 months of age, we focused our experiments on this age group. L-NAME preincubation inhibited maximal relaxation in the control vessels to 57.1 ± 4.6% of control values and but did not change potency (pEC_{50}: 5.88 ± 0.16). However, L-NAME neither significantly affect maximal relaxation (E_{max}: 38.7 ± 3.0%) to ACh nor potency (pEC_{50}: 5.95 ± 0.20) in Marfan vessels. To determine the contribution of the cyclooxygenase (COX) pathway, vessels were preincubated with indomethacin (10 μM), a non-specific COX inhibitor. In control vessels, indomethacin significantly increased maximal relaxation (E_{max}: 99.4 ± 2.2%) and potency (pEC_{50}: 6.58 ± 0.16), while in vessels from Marfan mice, maximal relaxation (E_{max}: 36.0 ± 3.3%) and potency (pEC_{50}: 5.56 ± 0.17) was decreased (Fig. 4.8A,B).

Neither maximal contraction (E_{max}; absence of indomethacin: 4.20 ± 0.70 mN; presence of indomethacin: 3.92 ± 0.41 mN) nor potency to PE (pEC_{50}; absence of indomethacin: 5.95 ± 0.23; presence of indomethacin: 6.12 ± 0.20) was significantly different in the presence of indomethacin in control mice. However, maximal contraction was significantly increased in the Marfan mice (E_{max}; absence of indomethacin: 2.60 ± 0.31 mN; presence of indomethacin: 4.62 ± 0.35 mN) but did not significantly change potency (pEC_{50}; absence of indomethacin: 5.66 ± 0.42; presence of indomethacin: 5.78 ± 0.31) (data not shown).

4.3.5 Nature of EDHF

The contribution of H_2O_2 in the EDHF-mediated relaxation was examined by the inhibitory effect of catalase (1000 $U \cdot mL^{-1}$), an enzyme that dismutates H_2O_2 to form water and oxygen. In the presence of indomethacin (10 μM) and L-NAME (200 μM), the addition of catalase to control vessels markedly reduced maximal relaxation (E_{max}) to 40.3 ± 7.8% of control, but did not significantly affect potency (pEC_{50}: 6.13 ± 0.32). Similarly, the addition of catalase to Marfan vessels markedly reduced E_{max} to 14.3% ± 2.3% of control values and decreased the potency (pEC_{50}: 5.27 ± 0.31) (Fig. 4.8C,D). To determine the role of gap junctions in the EDHF-mediated relaxation response, we used carbenoxolone (100 μM), a derivative of glycyrrhetinic acid and uncoupler of gap junctions (Tare *et al.,* 2002). In both control and Marfan mice, carbenoxolone had no inhibitory effect on the EDHF-mediated relaxation (Fig. 4.8C,D).

In the presence of L-NAME alone, catalase reduced E_{max} to 42.3 ± 3.2% in control vessels but did not change potency (pEC_{50}: 5.82 ± 0.23). In Marfan vessels, catalase and L-NAME reduced E_{max} to 18.6 ± 1.7% but did not affect potency (pEC_{50}: 6.38 ± 0.24). Catalase alone did not change potency (pEC_{50}: 5.99 ± 0.20) or maximal relaxation (E_{max}: 81.5 ± 5.6%) in control

mice**,** though in Marfan mice, catalase decreased potency to ACh (pEC_{50}: 5.80 ± 0.14), and decreased maximal relaxation (E_{max}: 30.2 ± 3.3%) (Table 1).

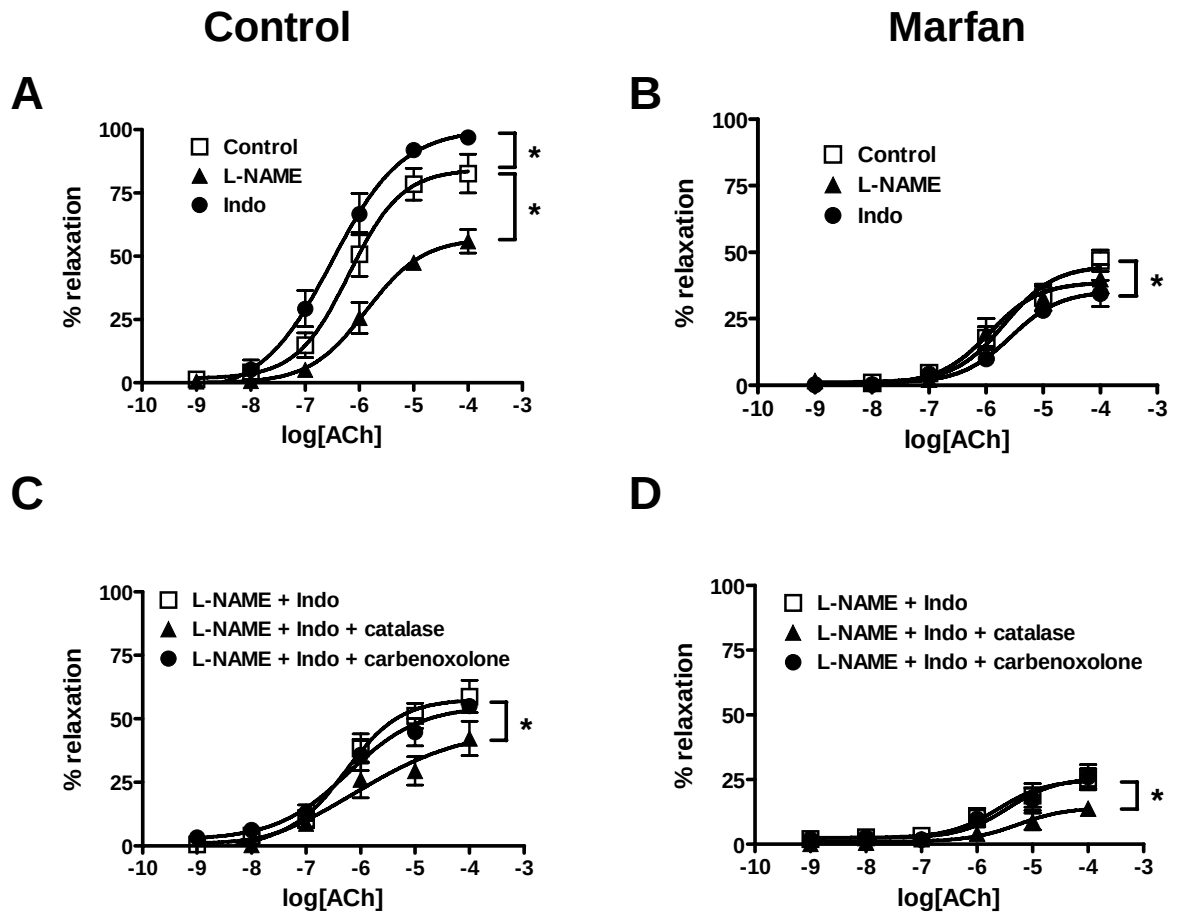

Figure 4.8 Effects of N_{ω}-Nitro-L-arginine methyl ester (L-NAME), indomethacin (Indo), and catalase on acetylcholine (ACh)-induced relaxation in control and marfan mice. The concentration-response curves of ACh are shown. **(A)** Control and **(B)** Marfan vessels were preincubated with L-NAME (200 μM) or indomethacin (10 μM) for 30 min and then contracted with phenylephrine (3 μM). **(C)** Control and **(D)** Marfan vessels were preincubated with catalase (1000 $U \cdot mL^{-1}$) or carbenoxolone (100 μM) in the presence of L-NAME (200 μM) and indomethacin (10 μM) for 30 min and then contracted with phenylephrine (3 μM). (* - $P < 0.05$, n = 8-12).

Table 1 Effects of different treatments on potency (pEC_{50}) and maximal (% of maximal response, E_{max}) acetylcholine (Ach)-induced relaxation in control and Marfan mice at 10 months of age

Strain	Control	Marfan
E_{max}		
No treatment	84.4 ± 4.8	44.9 ± 3.2
L-NAME	57.1 ± 4.6 *	38.7 ± 3.0
L-NAME + INDO	57.8 ± 4.3	25.3 ± 4.1 *
L-NAME + INDO + catalase	40.3 ± 7.8 #	14.3 ± 2.3 #
L-NAME + INDO + carbenoxolone	55.1 ± 5.2	24.3 ± 2.8
L-NAME + catalase	42.3 ± 3.2 *	18.6 ± 1.7
Catalase	81.5 ± 5.6 *	30.2 ± 2.4 *
INDO	99.4 ± 2.2 *	36.0 ± 3.3 *
pEC_{50}		
No treatment	6.03 ± 0.30	6.23 ± 0.16
L-NAME	5.88 ± 0.16	5.95 ± 0.20
L-NAME + INDO	5.73 ± 0.18	5.50 ± 0.12 *
L-NAME + INDO + catalase	6.13 ± 0.32	5.27 ± 0.31 #
L-NAME + INDO + carbenoxolone	6.23 ± 0.24	5.58 ± 0.17
L-NAME + catalase	5.82 ± 0.23	6.38 ± 0.24
Catalase	5.99 ± 0.20	5.80 ± 0.14 *
INDO	6.58 ± 0.16*	5.56 ± 0.17 *

Abbreviations: L-NAME, *N*ω-Nitro-L-arginine methyl ester, INDO, indomethacin
* - $P < 0.05$ without inhibitors in respective groups, # - $P < 0.05$ with L-NAME + INDO in respective groups.

4.3.6 Role of superoxide

To determine the role of reactive oxygen species, vessels were preincubated with superoxide dismutase (150 $U \cdot mL^{-1}$), an enzyme that converts superoxide to H_2O_2. In the control mice, superoxide dismutase had no significant effect on either the maximal contraction or potency in PE (3 μM)-induced contractions. Moreover, ACh-induced relaxation was also not affected. In contrast, superoxide dismutase potentiated the PE (3 μM)-induced contraction in the Marfan vessels and increased maximal contraction to control levels (E_{max}: 4.71 ± 0.61 mN).

Maximal relaxation to ACh was also improved (E_{max}: 74.5 ± 3.8%) and potency was also increased (pEC_{50}; 6.71 ± 0.13) (Fig. 4.9).

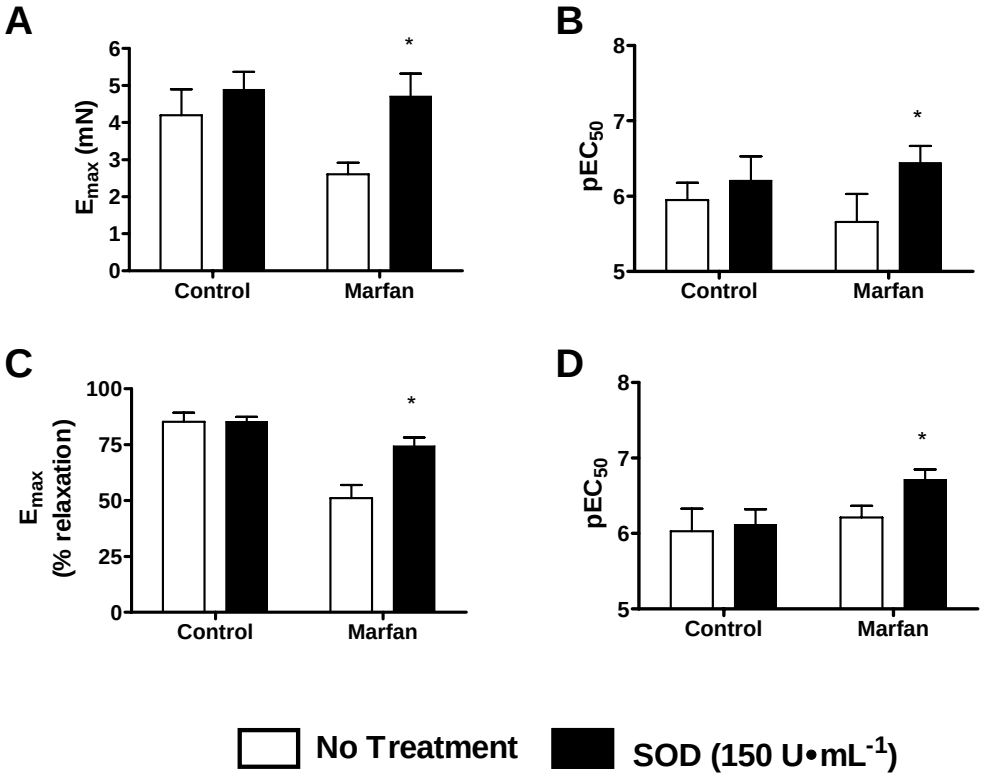

Figure 4.9 Effect of superoxide dismutase on phenylephrine (3 μM)-stimulated contraction and acetylcholine-mediated relaxation in mesenteric arteries from control and marfan mice. Bar graphs show **(A)** E_{max} and **(B)** pEC_{50} in response to phenylephrine (PE, 3 μM) in the presence and absence of superoxide dismutase (SOD, 150 U·ml^{-1}) at 10 months of age, while **(C)** E_{max} and **(D)** pEC_{50} show responses to acetylcholine (ACh, 10 μM-mediated relaxation. (* - $P < 0.05$ vs. control, n = 5-8, SOD, superoxide dismutase).

4.3.7 H_2O_2 production of endothelial cells

H_2O_2 production by endothelial cells was detected in the experiments using a laser confocal microscope with DCF, a peroxide-sensitive fluorescence dye. ACh (10 μM) application caused a significant increase in the DCF fluorescence intensity in endothelial cells, which was

unaffected by pretreatment with indomethacin (10 μM) and L-NAME (200 μM). When the vessel was pre-treated with catalase (1000 $U \cdot mL^{-1}$) in the presence of both indomethacin and L-NAME, the ACh-induced increase in the fluorescence intensity was abolished (Fig. 4.10).

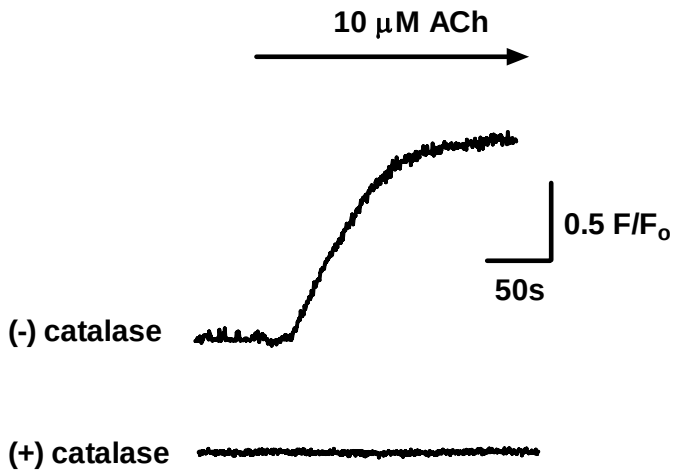

Figure 4.10 Production of endothelial hydrogen peroxide. Acetylcholine (ACh, 10 μM)-induced production of hydrogen peroxide (H_2O_2) by the endothelium detected as an increase in fluorescence intensity in dichlorodihydrofluorescein diacetate (DCF)-loaded endothelial cells in small mesenteric arteries of mice. The ACh-induced increase in fluorescence intensity was abolished when the artery was preincubated with catalase (1000 $U \cdot mL^{-1}$). All experiments were performed in the presence of N_ω-Nitro-L-arginine methyl ester (L-NAME, 200 μM) and indomethacin (10 μM). Representative traces shown are typical of the responses obtained in 23 cells from 4 mice.

4.4 Discussion

Using a genetically defined and validated mouse model of Marfan syndrome, we demonstrated increased vessel stiffness, reduced smooth muscle contractile function associated with decreased frequency of Ca^{2+} waves, decreased resistance to mechanical stress, and impaired endothelium-dependent and endothelium-independent relaxation in the small mesenteric arteries. We used appropriate control littermates to distinguish between observations owing to the

pathogenesis of Marfan syndrome from those owing to the physiological process of aging. We concluded that Marfan syndrome is a genetic disorder which affects not only the aorta and other large blood vessels, but also the resistance vasculature.

Degeneration of elastic fibers during the progression of Marfan syndrome is expected to decrease blood vessel elasticity. Indeed, vessel elasticity was decreased in Marfan vessels compared to the age-matched controls, although this was not apparent until 6 months of age (Fig. 4.2). This delayed effect may be due to the relative paucity of elastic fibers in the resistance vessels, as decreased vessel elasticity can always be seen in aorta from the same mouse model of Marfan syndrome starting at 3 months of age (Chung *et al.,* 2007a). Secondly, vessel wall weakening was also indicated by irreversible changes in vessel wall elasticity (Fig. 4.3) and reduced contractility after exposure to stretching (Fig. 4.4). Reduced contraction and irreversible changes in elasticity after stretching may be indicative of the 'breakage' of the physical linkage between smooth muscle cells and elastic fibers, which results in the changing of the phenotype in smooth muscle cells (Bunton *et al.,* 2001). It should be noted that aging is also associated with decreased vessel elasticity (Laurant *et al.,* 2004). Indeed, the elasticity of control vessels progressively decreased during aging, although the differences in elasticity between Marfan and control vessels persisted. This suggested that the increased vessel wall stiffness was due to the progression of Marfan syndrome.

The present study is the first to report aberrant contraction of smooth muscle cells in resistance vessels in Marfan syndrome. We showed that contraction in response to membrane depolarization and agonist-stimulation is suppressed. The decrease in the $\Delta L/L_o$ range in which active force is generated suggests that at high distention, the association between smooth muscle cells and extracellular matrix might be disrupted (Fig. 4.4, 4.5), while reduced active force may

be due to low intrinsic force generation of the contractile filaments or modifications in the coupling between the contractile elements and the cytoskeleton in smooth muscle cells (Rembold and Murphy, 1990). Additionally, decreased association between smooth muscle cells and elastic fibers would reduce the strain on the smooth muscle cells and blunt their response to agonist stimulation (Bunton *et al.,* 2001). Furthermore, upregulation of matrixmetalloproteinase-2 and matrixmetalloproteinase-9 in Marfan syndrome may inhibit Ca^{2+} entry from the extracellular space and reduce vessel contraction (Chew *et al.,* 2004; Chung *et al.,* 2007a; Chung *et al.,* 2008), although further investigation is required to elucidate possible involvement of calcium signaling and myofilament contractile mechanisms. Finally, the rate of vascular smooth muscle cell apoptosis is increased in Marfan syndrome, which may lead to vessel wall weakness and decreased contractile force (Nataatmadja *et al.,* 2003).

We also show in Appendix B that PE-induced Ca^{2+} waves are associated with tonic contraction in both control and Marfan mice. This is similar to that reported in other vessel preparations, where the asynchronous nature of the Ca^{2+} waves explains how summation of individual-cell Ca^{2+} waves can lead to tonic contraction, as the summation of Ca^{2+} signals in all the cells averages out to be a steady state Ca^{2+} increase in whole vessels (Ruehlmann *et al.,* 2000; Mauban *et al.,* 2001). A strong relationship between frequency of agonist-induced Ca^{2+} waves and tonic contraction, as well as the relationship between the number of cells displaying Ca^{2+} waves and generation of force, has been documented in other vascular preparations (Lee *et al.,* 2001; Dai *et al.,* 2007). A higher frequency of Ca^{2+} waves can enhance the myofilament activation by increasing average $[Ca^{2+}]_i$ over time. Furthermore, the activation of certain frequency-sensitive enzymes can potentially affect the level of contraction, such as Ca^{2+}-calmodulin kinase II, which has been found to be sensitive to the frequency of Ca^{2+} spikes *in*

vitro (De Koninck and Schulman, 1998). In mice at 6 and 10 months of age, the significant reduction in tonic contraction in the Marfan group is correlated with significantly decreased Ca^{2+} wave frequency and number of cells displaying Ca^{2+} waves. This implies that the decreased occurrence and/or frequency of Ca^{2+} waves are associated with decreased tonic contraction.

The reduction in frequency of PE-stimulated Ca^{2+} waves in Marfan mesenteric vessels may suggest inhibition of SR refilling. This is because a mechanism by which Ca^{2+} wave frequency could be decreased is by a reduced rate of refilling of the SR Ca^{2+} store. Since SR luminal Ca^{2+} can regulate inositol-1,4,5-triphosphate receptor channel opening probability, a reduced rate of SR Ca^{2+} refilling can lead to decreased frequency of SR Ca^{2+} release at the wave initiation site (Meldolesi and Pozzan, 1998). In resistance vessels, extracellular Ca^{2+} influx through L-type Ca^{2+} channels is central in the control of vascular tone and plays a significant role in maintaining Ca^{2+} homeostasis and contraction (Mulvany and Aalkjaer, 1990; Nelson *et al.,* 1990; Hughes, 1995). The upregulation of matrixmetalloproteinase-2 and matrixmetalloproteinase-9 enzymes in the same mouse model of Marfan syndrome used in these studies (Chung *et al.,* 2007a; Chung *et al.,* 2008), and the suggestion that both enzymes may inhibit Ca^{2+} influx through L-type Ca^{2+} channels (Chew *et al.,* 2004). This inhibition may occur through their interactions with specific cell proteins such as intercellular adhesion molecule-1 or stimulate proteinase-activated receptors and activate signaling pathways, all of which could lead to blockade of Ca^{2+} channels (Macfarlane *et al.,* 2001; Fiore *et al.*, 2002; Marutsuka *et al.*, 2002).

It should also be noted that there is a significant reduction in PE-induced Ca^{2+} wave frequency and cell recruitment in control mice from 6 to 9 months of age, although maximal tonic contraction is not similarly affected. Since advancing age has generally not been associated with decreased contraction in response to PE stimulation in resistance arteries (Hüsken *et al.,*

1994; Moreau *et al.,* 1998; Gros *et al.,* 2002), and in mice at 30 months of age, neither maximal peak height of Ca^{2+} release in response to PE nor L-type Ca^{2+} current are affected (del Corsso *et al.,* 2006), this may suggest that although Ca^{2+} wave signaling is affected during aging, tonic contraction is maintained by way of a compensatory mechanism. For example, no oscillatory Ca^{2+} signaling has been observed in humans, although PE-induced tonic contraction is supported by Rho-kinase (Crowley *et al.,* 2002). How then, can the reduced frequency of Ca^{2+} waves during in the control animals be explained? It has been suggested that the close association between the superficial SR and the plasma membrane is essential for SR refilling (Lee *et al.,* 2002; Fameli *et al.,* 2007), and separation of this association has been shown to decrease frequency of Ca^{2+} waves presumably through reduced Ca^{2+} refilling (Lee *et al.,* 2005). However, this hypothesis cannot be further investigated in this model without the use of electron microscopy. Nonetheless, the frequency of PE-induced Ca^{2+} waves is significantly reduced in the Marfan animals compared to their aged-matched controls at both 6 and 10 months of age, suggesting that the effects of Marfan syndrome play a greater role than the process of aging in this study.

The endothelium releases a variety of vasoactive mediators, including prostaglandins, NO, and EDHF to regulate smooth muscle contractility and thus vascular smooth muscle tone (Ramsey *et al.,* 1995; Boutouyrie *et al.,* 1997; Wilkinson *et al.,* 2002; Vanhoutte, 2004). The present study demonstrated that in Marfan mesenteric vessels, endothelium-dependent relaxation stimulated by ACh was significantly impaired at 6 and 10 months (Fig. 4.6), suggesting an impairment of NO release. In Marfan syndrome, the endothelium is a likely target as Fbn-1 rich microfibrils are present in the connective tissue immediately subjacent to arterial endothelial cells (Davis, 1994; Kielty *et al.,* 1996). Marfan syndrome is also associated with elevated plasma

levels of homocysteine, which attenuate endothelial function and limits NO bioavailability (Giusti *et al.,* 2003; Jiang *et al.,* 2005). Endothelial Akt/eNOS phosphorylation and mechano-signaling can be compromised through increased vessel wall stiffness, further reducing endothelium-dependent vasorelaxation (Peng *et al.,* 2003). However, there is conflicting data with regard to agonist-induced vasodilator responses in Marfan syndrome; Nakamura and colleagues (2000) showed inhibition of ACh-induced relaxation in the brachial artery of Marfan syndrome patients, while Wilson and colleagues (1999) showed that vasodilator responses to ACh and bradykinin were unaffected in the same artery. In addition, both groups found no impairment of the response to exogenous nitrovasodilators, while our studies demonstrated an approximately 100-fold reduction of sensitivity of smooth muscle cells of Marfan mice to NO at 6 months of age and a 10-fold reduction at 10 months of age (Fig. 4.7). This reduced sensitivity may be attributed to a number of factors. First of all, bioavailability of NO is decreased due to excessive amounts of reactive oxygen species in the pathogenesis of cardiovascular diseases (Cai and Harrison, 2000; Faraci and Didion, 2004). NO bioavailability is also decreased during ageing, which may explain the difference in SNP sensitivity between control and Marfan vessels at 6 and 10 months of age (Newaz *et al.,* 2006; Donato *et al.,* 2007). Finally, the predisposition of the medial layer to degeneration and fibrosis in Marfan syndrome may also physically inhibit the ability of the vessel to dilate (Dietz *et al.,* 1991; Pyeritz, 2000).

The findings from this study may have potentially important clinical implications, but should be viewed in the context of the existing *in vivo* data from human subjects. The apparent discrepancies highlighted above between human subjects and our studies may be explained by the following reasons: 1) relatively small groups of Marfan syndrome and non-Marfan syndrome patients were recruited for these studies (usually 20 or less), 2) a wide range of ages of Marfan

patients were recruited (from 11 to 61 years old), and 3) the vessels studied were not true resistance (<500 μm) vessels. As indicated by the data from the present study and others, pathogenesis of Marfan syndrome in the vasculature with respect to the functional properties varied during aging (Chung *et al.,* 2007a). Therefore, combining both pediatric and adult patients in the same study may perturb the results and data interpretation.

Furthermore, the conflicting results should also be viewed in the context of our mouse model. There are over 600 genetic mutations that have been identified to cause Marfan syndrome (Williams *et al.,* 2008). While missense mutations account for slightly over 60% of the mutations, 78% of the point mutations locate in the cbEGF modules and affect Ca^{2+} binding. A further 12% of these mutations are recurrent and affect a mutation hotspot, CpG, for a cysteine residue, representing the most common mutation in classic Marfan syndrome and providing the basis of the mouse model used in our studies (Boileau *et al.,* 2005; Gray and Davies, 1996). Therefore, although our model is useful to investigate the general pathogenesis of the most common type of Marfan syndrome, it may not be representative of all cases.

Although advancing age is associated with derangement of endothelial cells leading to a decrease in NO production (Gerhard *et al.,* 1996), the differences in ACh-induced relaxation between control and Marfan vessels persisted despite increasing age. It is unlikely that the effect of aging played a significant role in this study, as changes in ACh-mediated relaxation in control mice are not apparent until around 15 months of age (Bulckaen *et al.,* 2008). The same ACh-relaxation response in the control arteries between 3 and 10 month age-groups could be related to upregulation of alternative mechanisms to compensate for the decreasing NO bioavailability. EDHF has been shown to play a greater role in the face of reduced NO bioavailability during aging (McCullough *et al.*, 1997; Nishikawa *et al.*, 2000; Gaubert *et al.*, 2007).

ACh-mediated vasorelaxation is primarily dependent on NO in the secondary branch of mouse mesenteric artery (McGuire *et al.,* 2002; Ceroni *et al.,* 2007). Preincubation with the nitric oxide synthase inhibitor L-NAME significantly reduced ACh-mediated vasorelaxation in control vessels, but interestingly did not have any effect on ACh-mediated vasorelaxation in the Marfan vessels, suggesting that the endothelial NO pathway is significantly compromised in Marfan syndrome. COX-derived prostanoids are also involved in the regulation of vasomotor function and prostacyclin (PGI_2), produced from arachidonic acid through the COX-2 enzyme, is the most important of these (Smith *et al.,* 2000). Upregulation of COX-2 expression may also be induced through the loss of vessel elasticity (Vitarelli *et al.*, 2006), which leads to increased production of PGI_2 (Chung *et al.*, 2007c). In our study, blockade of the COX pathway with indomethacin inhibited ACh-mediated vasorelaxation in Marfan vessels. The upregulation of prostanoid-mediated relaxation may thus represent a compensatory mechanism of the Marfan endothelial cells in the apparent absence of NO-mediated vasorelaxation.

In addition to agonist-induced endothelium-dependent vasorelaxation, EDHF plays an important role in modulating vasomotor tone in the resistance vasculature through its hyperpolarization of smooth muscle cells (Shimokawa, 1999). However, its nature is still controversial; K^+, gap junctions, epoxyeicosatrienoic acids, and H_2O_2 are all thought to be potential candidates and the contribution of each appears to vary depending on the species tested and vessels used (Vanhoutte, 2004). In mouse mesenteric arteries, there are conflicting reports about the role of H_2O_2 as an EDHF (Matoba *et al.,* 2000; Ellis *et al.,* 2003). However, in our preparation the addition of catalase, an enzyme which dismutates H_2O_2 to form water and oxygen and thus lowers H_2O_2 concentration, in the presence of L-NAME and indomethacin reduced ACh-mediated vasorelaxation in the Marfan vessels to a greater degree than in control

vessels. This greater inhibition may be due to the upregulation of EDHF as a compensatory or back-up mechanism, which occurs when endothelial production of NO is impaired (Kilpatrick and Cocks, 1994; Corriu *et al.*, 1998). Although myoepithelial gap junctions have been suggested to provide the pathway for EDHF in mouse mesenteric artery (Dora *et al.,* 2003), we did not observe significant inhibition of ACh-mediated relaxation with carbenoxolone, an uncoupler of gap junctions, in either control or Marfan vessels. Therefore, it is unlikely that gap junctions mediate the EDHF response in our preparation.

It is well established that oxidative stress has a profound influence on vascular function, though the effect of oxidative stress on vasomotor response in the progression of Marfan syndrome has never been investigated. Oxidative stress has been reported to be involved in the pathogenesis of various cardiovascular diseases (Cai and Harrison, 2000; Faraci and Didion, 2004). Superoxide dismutase treatment was shown to reverse the hypersensitivity of the arteries in diabetic and hypertensive animal models and normalize the agonist-induced contraction to that of the control animals (Kanie and Kamata, 2000; Alvarez *et al.,* 2008). Although the mechanism of action of reactive oxygen species on smooth muscle cell contractility is still unclear (Lyle and Griendling, 2006), reactive oxygen species have been proposed to have multiple effects on calcium signaling in both vascular endothelial and smooth muscle cells (Elmoselhi *et al.,* 1996; Lounsbury *et al.,* 2000; Walia *et al.,* 2000). The impairment of the Ca^{2+} signaling pathway caused by oxidative stress may consequently lead to the alteration of vascular reactivity (Sener *et al.,* 2004). Thus, the removal of superoxide with superoxide dismutase may restore calcium signaling and thereby the contractile responses. Furthermore, oxidative stress may cause endothelial dysfunction through several direct and indirect pathways, the most well-known of which is the scavenging of NO by superoxide. Superoxide radicals bind to NO at a rate three

times faster than they bind to superoxide dismutase; therefore, excess superoxide production would increase the rate of NO degradation (Cai and Harrison, 2000; Schulz *et al.,* 2004). The improvement of endothelial function in the Marfan vessels by superoxide dismutase suggests that oxidative stress may be another contributor to endothelial dysfunction in Marfan syndrome.

In conclusion, our study indicates that in Marfan syndrome, endothelium-dependent and endothelium-independent vasodilation is impaired in resistance vessels. Furthermore, we have demonstrated that smooth muscle contractility is compromised and vessel stiffness is increased. Together, these vasomotor abnormalities in the resistance vessel may have a negative and detrimental impact on the overall cardiovascular function in Marfan syndrome.

4.5 References

Alvarez Y, Briones AM, Hernanz R, Perez-Giron JV, Alonso MJ, Salaices M (2008). Role of NADPH oxidase and iNOS in vasoconstrictor responses of vessels from hypertensive and normotensive rats. *Br J Pharmacol* **153**: 926–935.

Boileau C, Jondeau G, Mizuguchi T, Matsumoto N (2005). Molecular genetics of Marfan syndrome. *Curr Opin Cardiol* **20**: 194–200.

Boutouyrie P, Bézie Y, Lacolley P, Challande P, Chamiot-Clerc P, Benetos A *et al.* (1997). In vivo/in vitro comparison of rat abdominal aorta wall viscosity. Influence of endothelial function. *Arterioscler Thromb Vasc Biol* **17**: 1346–1355.

Briones AM, González JM, Somoza B, Giraldo J, Daly CJ, Vila E *et al.* (2003). Role of elastin in spontaneously hypertensive rat small mesenteric artery remodelling. *J Physiol* **552**: 185–195.

Bunton TE, Biery NJ, Myers L, Gayraud B, Ramirez F, Dietz HC (2001). Phenotypic alteration of vascular smooth muscle cells precedes elastolysis in a mouse model of Marfan syndrome. *Circ Res* **88**: 37-43.

Bulckaen H, Prévost G, Boulanger E, Robitaille G, Roquet V, Gaxatte C *et al.* (2008). Low-dose aspirin prevents age-related endothelial dysfunction in a mouse model of physiological aging. *Am J Physiol Heart Circ Physiol* **294**: H1562–70.

Cai H, Harrison DG (2000). Endothelial dysfunction in cardiovascular diseases: the role of oxidant stress. *Circ Res* **87**: 840–844.

Ceroni L, Ellis A, Wiehler WB, Jiang YF, Ding H, Triggle CR (2007). Calcium-activated potassium channel and connexin expression in small mesenteric arteries from eNOS-deficient (eNOS-/-) and eNOSexpressing (eNOS+/+) mice. *Eur J Pharmacol* **560**: 193–200.

Chew DK, Conte MS, Khalil RA (2004). Matrix metalloproteinase-specific inhibition of Ca2+ entry mechanisms of vascular contraction. *J Vasc Surg* **40**: 1001-10.

Chung AW, Au Yeung K, Sandor GG, Judge DP, Dietz HC, van Breemen C (2007a). Loss of elastic fiber integrity and reduction of vascular smooth muscle contraction resulting from the upregulated activities of matrix metalloproteinase-2 and -9 in the thoracic aortic aneurysm in Marfan syndrome. *Circ Res* **101**: 512-22.

Chung AW, Au Yeung K, Cortes SF, Sandor GG, Judge DP, Dietz HC *et al*. (2007b). Endothelial dysfunction and compromised eNOS/Akt signaling in the thoracic aorta during the progression of Marfan syndrome. *Br J Pharmacol* **150**:1075-83.

Chung AW, Yang HH, van Breemen C (2007c). Imbalanced synthesis of cyclooxygenase-derived thromboxane A2 and prostacyclin compromises vasomotor function of the thoracic aorta in Marfan syndrome. *Br J Pharmacol* **152**: 305–312.

Chung AW, Yang HH, Radomski MW, van Breemen C (2008). Long-term doxycycline is more effective than atenolol to prevent thoracic aortic aneurysm in marfan syndrome through the inhibition of matrix metalloproteinase-2 and -9. *Circ Res* **102**: e73-85.

Corriu C, Félétou M, Puybasset L, Bea ML, Berdeaux A, Vanhoutte PM (1998). Endothelium-dependent hyperpolarization in isolated arteries taken from animals treated with NO-synthase inhibitors. *J Cardiovasc Pharmacol* **32**: 944–950.

Crowley CM, Lee CH, Gin SA, Keep AM, Cook RC, Van Breemen C (2002). The mechanism of excitation-contraction coupling in phenylephrine-stimulated human saphenous vein. *Am J Physiol Heart Circ Physiol* **283:** H1271-81.

Dai J, Lee CH, Poburko D, Szado T, Kuo KH, van Breemen C (2007). Endothelin-1-mediated wave-like [Ca2+]i oscillations in intact rabbit inferior vena cava. *J Vasc Res* **44:** 495-503.

Davis EC (1994). Immunolocalization of microfibril and microfibrilassociated proteins in the subendothelial matrix of the developing mouse aorta. *J Cell Sci* **107**: 727–736.

De Koninck P, Schulman H (1998). Sensitivity of Ca2+/calmodulin-dependent protein kinase II to the frequency of Ca2+ oscillations. *Science* **279**: 227-230.

del Corsso C, Ostrovskaya O, McAllister CE, Murray K, Hatton WJ, Gurney AM, *et al.* (2006). Effects of aging on Ca2+ signaling in murine mesenteric arterial smooth muscle cells. *Mech Ageing Dev* **127:** 315-23.

Dietz HC, Cutting GR, Pyeritz RE, Maslen CL, Sakai LY, Corson GM *et al.* (1991). Marfan syndrome caused by a recurrent de novo missense mutation in the fibrillin gene. *Nature* **352**: 337-9.

Dobrin PB (1978). Mechanical properties of arteries. *Physiol Rev* **58**: 397–460.

Donato AJ, Eskurza I, Silver AE, Levy AS, Pierce GL, Gates PE *et al.* (2007). Direct evidence of endothelial oxidative stress with aging in humans: Relation to impaired endothelium-dependent dilation and upregulation of nuclear factor-kappaB. *Circ Res* **100**: 1659–1666.

Dora KA, Sandow SL, Gallagher NT, Takano H, Rummery NM, Hill CE *et al.* (2003). Myoendothelial gap junctions may provide the pathway for EDHF in mouse mesenteric artery. *J Vasc Res* **40**: 480–490.

Ellis A, Pannirselvam M, Anderson TJ, Triggle CR (2003). Catalase has negligible inhibitory effects on endothelium-dependent relaxations in mouse isolated aorta and small mesenteric artery. *Br J Pharmacol* **140**: 1193–1200.

Elmoselhi AB, Samson SE, Grover AK (1996). SR Ca2**+** pump heterogeneity in coronary artery: Free radicals and IP3-sensitive and -insensitive pools. *Am J Physiol* **271**: C1652–C1659.

Fameli N, van Breemen C, Kuo KH (2007). A quantitative model for linking Na+/Ca2+ exchanger to SERCA during refilling of the sarcoplasmic reticulum to sustain [Ca2+] oscillations in vascular smooth muscle. *Cell Calcium* **42:** 565-575.

Faraci FM, Didion SP (2004). Vascular protection: superoxide dismutase isoforms in the vessel wall. *Arterioscler Thromb Vasc Biol* **24**: 1367–1373.

Fiore E, Fusco C, Romero P, Stamenkovic I (2002). Matrix metalloproteinase 9 (MMP-9/gelatinase B) proteolytically cleaves ICAM-1 and participates in tumor cell resistance to natural killer cell–mediated cytotoxicity. *Oncogene* **21**: 5213–5223.

Gaubert ML, Sigaudo-Roussel D, Tartas M, Berrut G, Saumet JL, Fromy B (2007). Endothelium-derived hyperpolarizing factor as an in vivo back-up mechanism in the cutaneous microcirculation in old mice. *J Physiol* **585**: 617–626.

Gerhard M, Roddy MA, Creager SJ, Creager MA (1996). Aging progressively impairs endothelium-dependent vasodilation in forearm resistance vessels of humans. *Hypertension* **27**: 849–853.

Giusti B, Porciani MC, Brunelli T, Evangelisti L, Fedi S, Gensini GF *et al.* (2003). Phenotypic variability of cardiovascular manifestations in Marfan syndrome. Possible role of hyperhomocysteinemia and C677T MTHFR gene polymorphism. *Eur Heart J* **24**: 2038–2045.

Goffi L, Chan R, Boccoli G, Ghiselli R, Saba V (2000). Aneurysm of a jejunal branch of the superior mesenteric artery in a patient with Marfan's syndrome. *J Cardiovasc Surg* **41**: 321–323.

González JM, Briones AM, Starcher B, Conde MV, Somoza B, Daly C *et al.* (2005). Influence of elastin on rat small artery mechanical properties. *Exp Physiol* **90**: 463–468.

Gray JR, Davies SJ (1996). Marfan syndrome. *J Med Genet* **33**: 403–408.

Gros R, Van Wert R, You X, Thorin E, Husain M (2002). Effects of age, gender, and blood pressure on myogenic responses of mesenteric arteries from C57BL/6 mice. *Am J Physiol Heart Circ Physiol* **282**: H380-388.

Habashi JP, Judge DP, Holm TM, Cohn RD, Loeys BL, Cooper TK, Myers L *et al.* (2006). Losartan, an AT1 antagonist, prevents aortic aneurysm in a mouse model of Marfan syndrome. *Science* **312**: 117-21.

Hatrick AG, Malcolm PN, Burnand KG, Irvine AT (1998). A superficial femoral artery aneurysm in a patient with Marfan's syndrome. *Eur J Vasc Endovasc Surg* **15**: 459–460.

Hughes AD (1995). Calcium channels in vascular smooth muscle cells. *J Vasc Res* **32**: 353–370.

Hüsken BC, Hendriks MG, Pfaffendorf M, Van Zwieten PA (1994). Effects of aging and hypertension on the reactivity of isolated conduit and resistance vessels. *Microvasc Res* **48** :303-15.

Jiang X, Yang F, Tan H, Liao D, Bryan RM Jr, Randhawa JK *et al.* (2005). Hyperhomocystinemia impairs endothelial function and eNOS activity via PKC activation. *Arterioscler Thromb Vasc Biol* **25**: 2515– 2521.

Jondeau G, Boutouyrie P, Lacolley P, Laloux B, Dubourg O, Bourdarias JP *et al.* (1999). Central pulse pressure is a major determinant of ascending aorta dilation in Marfan syndrome. *Circulation* **99**: 2677–2681.

Judge DP, Biery NJ, Keene DR, Geubtner J, Myers L, Huso DL *et al.* (2004). Evidence for a critical contribution of haploinsufficiency in the complex pathogenesis of Marfan syndrome. *J Clin Invest* **114**: 172–181.

Judge DP, Dietz HC (2005). Marfan's syndrome. *Lancet* **366**: 1965-76.

Kanie N, Kamata K (2000). Contractile responses in spontaneously diabetic mice. I. involvement of superoxide anion in enhanced contractile response of aorta to norepinephrine in C57BL/KsJ(db/ db) mice. *Gen Pharmacol* **35**: 311–318.

Kielty CM,Wilson DG, Stuart G, Musumeci F, Cones CJ, Davies S *et al.* (1996). Fibrillin expression and deposition by vascular endothelial cells: implications for the Marfan syndrome. *Circulation* **94**: I-350.

Kilpatrick EV, Cocks TM (1994). Evidence for differential roles of nitric oxide (NO) and hyperpolarization in endothelium-dependent relaxation of pig isolated coronary artery. *Br J Pharmacol* **112**: 557– 565.

Laurant P, Adrian M, Berthelot A (2004). Effect of age on mechanical properties of rat mesenteric small arteries. *Can J Physiol Pharmacol* **82**: 269–275.

Lay CS, Yu CJ, Tyan YS (2006). Abdominal aortic dissection with acute mesenteric ischemia in a patient with Marfan syndrome. *J Chin Med Assoc* **69**: 326–329.

Lee CH, Poburko D, Kuo KH, Seow CY, van Breemen C (2002). Ca(2+) oscillations, gradients, and homeostasis in vascular smooth muscle. *Am J Physiol Heart Circ Physiol* **282:** H1571-83.

Lee CH, Poburko D, Sahota P, Sandhu J, Ruehlmann DO, van Breemen C (2001). The mechanism of phenylephrine-mediated [Ca(2+)](i) oscillations underlying tonic contraction in the rabbit inferior vena cava. *J Physiol* **534:** 641-650.

Lee CH, Kuo KH, Dai J, Leo JM, Seow CY, Breemen C (2005). Calyculin-A disrupts subplasmalemmal junction and recurring Ca2+ waves in vascular smooth muscle. Cell Calcium. **37:** 9-16.

Lounsbury KM, Hu Q, Ziegelstein RC (2000). Calcium signaling and oxidant stress in the vasculature. *Free Radic Biol Med* **28**: 1362–1369.

Lyle AN, Griendling KK (2006). Modulation of vascular smooth muscle signaling by reactive oxygen species. *Physiology (Bethesda)* **21**: 269–280.

Matoba T, Shimokawa H, Nakashima M, Hirakawa Y, Mukai Y, Hirano K *et al.* (2000). Hydrogen peroxide is an endothelium-derived hyperpolarizing factor in mice. *J Clin Invest* **106**: 1521–1530.

McCulloch AI, Bottrill FE, Randall MD, Hiley CR (1997). Characterization and modulation of EDHF-mediated relaxations in the rat isolated superior mesenteric arterial bed. *Br J Pharmacol* **120**: 1431–1438.

McGuire JJ, Hollenberg MD, Andrade-Gordon P, Triggle CR (2002). Multiple mechanisms of vascular smooth muscle relaxation by the activation of proteinase-activated receptor 2 in mouse mesenteric arterioles. *Br J Pharmacol* **135**: 155–169.

Macfarlane SR, Seatter MJ, Kanke T, Hunter GD, Plevin R (2001). Proteinase-activated receptors. *Pharmacol Rev* **53:** 245–282.

Marutsuka K, Hatakeyama K, Sato Y, Yamashita A, Sumiyoshi A, Asada Y (2002). Protease-activated receptor 2 (PAR2) mediates vascular smooth muscle cell migration induced by tissue factor/factor VIIa complex. *Thromb Res* **107**: 271–276.

Mauban JR, Lamont C, Balke CW, Wier WG. (2001). Adrenergic stimulation of rat resistance arteries affects Ca(2+) sparks, Ca(2+) waves, and Ca(2+) oscillations. *Am J Physiol Heart Circ Physiol* **280:** H2399-405.

Meldolesi J, Pozzan T (1998). The endoplasmic reticulum Ca2+ store: a view from the lumen. *Trends Biochem Sci* **23:** 10-4.

Milnor WR (1989). Properties of the vascular wall. In: Collins N (ed.).*Hemodynamics*. Williams & Wilkins: Baltimore, pp. 84–90.

Moreau P, d'Uscio LV, Lüscher TF (1998). Structure and reactivity of small arteries in aging. *Cardiovasc Res* **37:** 247-53.

Mulvany MJ, Aalkjaer C (1990). Structure and function of small arteries. *Physiol Rev* **70**: 921-61.

Murdoch JL, Walker BA, Halpern BL, Kuzma JW, McKusick VA (1972). Life expectancy and causes of death in the Marfan syndrome. *N Engl J Med* **286**: 804-8.

Nakamura M, Itoh S, Makita S, Ohira A, Arakawa N, Hiramori K (2000). Peripheral resistance vessel dysfunction in Marfan syndrome. *Am Heart J* **139**: 661–666.

Nataatmadja M, West M, West J, Summers K, Walker P, Nagata M, Watanabe T (2003). Abnormal extracellular matrix protein transport associated with increased apoptosis of vascular smooth muscle cells in marfan syndrome and bicuspid aortic valve thoracic aortic aneurysm. *Circulation* **108 Suppl 1**:II329-34.

Nelson MT, Patlak JB, Worley JF, Standen NB (1990). Calcium channels, potassium channels, and voltage dependence of arterial smooth muscle tone. *Am J Physiol* **259:** C3-18.

Newaz MA, Yousefipour Z, Oyekan A (2006). Oxidative stressassociated vascular aging is xanthine oxidase-dependent but not NAD(P)H oxidase-dependent. *J Cardiovasc Pharmacol* **48**: 88–94.

Ng CM, Cheng A, Myers LA, Martinez-Murillo F, Jie C, Bedja D *et al.* (2004). TGF-beta-dependent pathogenesis of mitral valve prolapse in a mouse model of Marfan syndrome. *J Clin Invest* **114**: 1586–1592.

Nishikawa Y, Stepp DW, Chilian WM (2000). Nitric oxide exerts feedback inhibition on EDHF-induced coronary arteriolar dilation in vivo. *Am J Physiol Heart Circ Physiol* **279**: H459–H465.

Ohba M, Shibanuma M, Kuroki T, Nose K (1994). Production of hydrogen peroxide by transforming growth factor-beta1 and its involvement in induction of egr-1 in mouse osteoblastic cells. *J Cell Biol* **126**: 1079–1088.

Peng X, Haldar S, Deshpande S, Irani K, Kass DA (2003). Wall stiffness suppresses Akt/eNOS and cytoprotection in pulse-perfused endothelium. *Hypertension* **41**: 378–381.

Pyeritz RE (2000). The Marfan syndrome. *Annu Rev Med* **51**:481-510.

Ramsey MW, Goodfellow J, Jones CJ, Luddington LA, Lewis MJ, Henderson AH (1995). Endothelial control of arterial distensibility is impaired in chronic heart failure. *Circulation* **92**: 3212–3219.

Reinhardt DP, Chalberg SC, Sakai LY (1995). The structure and function of fibrillin. *Ciba Found Symp* **192**: 128–143.

Rembold CM, Murphy RA (1990). Muscle length, shortening, myoplasmic [Ca2**+**], and activation of arterial smooth muscle. *Circ Res* **66**: 1354–1361.

Rosenbloom J (1993). Extracellular matrix 4: the elastic fiber. *FASEB J* **7**: 1208–1218.

Ruehlmann DO, Lee CH, Poburko D, van Breemen C (2000). Asynchronous Ca(2+) waves in intact venous smooth muscle. *Circ Res* **86:** E72-9.

Safar ME, London GM (1994). The arterial system in human hypertension. In: Swales JD (ed.). *Textbook of Hypertension*. London: Blackwell Scientific Publications, pp. 85–102.

Savolainen H, Savola J, Savolainen A (1993). Aneurysm of the iliac artery in Marfan's syndrome. *Ann Chir Gynaecol*. **82**: 203–205.

Schulz E, Anter E, Keaney JF Jr (2004). Oxidative stress, antioxidants, and endothelial function. *Curr Med Chem* **11**: 1093–1104.

Sener G, Paskaloglu K, Toklu H, Kapucu C, Ayanoglu-Dulger G, Kacmaz A *et al.* (2004). Melatonin ameliorates chronic renal failureinduced oxidative organ damage in rats. *J Pineal Res* **36**: 232–241.

Sheremet'eva GF, Ivanova AG, IuV B, Gens AP, Kocharian EZ (2004). A comparative study of the aortic wall in patients with Marfan's syndrome and Erdheim's disease. *Angiol Sosud Khir* **10**: 22–29.

Shimokawa H (1999). Primary endothelial dysfunction: atherosclerosis. *J Mol Cell Cardiol* **31**: 23–37.

Smith WL, DeWitt DL, Garavito RM (2000). Cyclooxygenases: structural, cellular, and molecular biology. *Annu Rev Biochem* **69**: 145–182.

Tare M, Coleman HA, Parkington HC (2002). Glycyrrhetinic derivatives inhibit hyperpolarization in endothelial cells of guinea pig and rat arteries. *Am J Physiol Heart Circ Physiol* **282**: H335–H341.

Vanhoutte PM (2004). Endothelium-dependent hyperpolarizations: the history. *Pharmacol Res* **49**: 503–508.

Vitarelli A, Conde Y, Cimino E, D'Angeli I, D'Orazio S, Stellato S *et al.* (2006). Aortic wall mechanics in the Marfan syndrome assessed by transesophageal tissue Doppler echocardiography. *Am J Cardiol* **97**: 571–577.

Walia M, Sormaz L, Samson SE, Lee RM, Grover AK (2000). Effects of hydrogen peroxide on pig coronary artery endothelium. *Eur J Pharmacol* **400**: 249–253.

Wilkinson IB, Qasem A, McEniery CM,Webb DJ, Avolio AP, Cockcroft JR (2002). Nitric oxide regulates local arterial distensibility in vivo. *Circulation* **105**: 213–217.

Williams A, Davies S, Stuart AG,Wilson DG, Fraser AG (2008). Medical treatment of marfan syndrome: a time for change. *Heart* **94**: 414–421.

Wilson DG, Bellamy MF, Ramsey MW, Goodfellow J, Brownlee M, Davies S *et al.* (1999). Endothelial function in Marfan syndrome: selective impairment of flow-mediated vasodilation. *Circulation* **99**: 909–915.

CHAPTER 5: CONCLUSIONS AND RECOMMENDATIONS FOR FUTURE WORK

5.1 Overall summary and conclusions

Vascular smooth muscle is essential to the regulation of blood pressure and dynamic regional blood flow, responding rapidly to the moment-to-moment metabolic demands of specific tissues and maintaining global vascular tone. This requires constant and minute control of cytosolic [Ca^{2+}], which is achieved through spatial and temporal partitioning of Ca^{2+} signals such that Ca^{2+} can simultaneously modulate contraction and processes such as gene transcription and oxidative metabolism. The subcellular architecture and arrangement of the SR, mitochondria, and PM in the form of Nanodomains all contribute to this partitioning of cytosolic Ca^{2+} gradients and signals, which may take the form of waves, sparks, puffs, and others (Macrez and Mironneau, 2004). The deterioration of this intricate ultrastructure may have pathological consequences (Lee *et al.,* 2005; Petersen *et al.,* 2006).

The studies presented in this thesis first examined the nature of agonist-induced mitochondrial Ca^{2+} elevations as indicators of localized cytosolic Ca^{2+} elevations due to reverse-mode NCX, providing important insights into the functional linkage between reverse-mode NCX and ROCs in vascular smooth muscle. This laid the foundation for examination of asynchronous wave-like Ca^{2+} oscillations in the basilar artery, in which reverse-mode NCX was found to be a crucial mediator of SR Ca^{2+} refilling to maintain ongoing Ca^{2+} oscillations. Finally, having established the importance of Ca^{2+} oscillations in maintaining tonic contraction in resistance-sized vessels, we extended this knowledge to a mouse model of vascular disease in Marfan syndrome, where it was discovered that aberrant Ca^{2+} wave signaling is associated with reduced smooth muscle contractile function, thus giving clues to the importance of Ca^{2+} wave signaling in vascular health.

5.1.1 Overview of NCX reversal in smooth muscle cells

It has become clear that reverse (Ca^{2+}-influx)-mode NCX plays an important role in maintaining Ca^{2+} homeostasis in vascular smooth muscle cells (Lee *et al.,* 2001; Fameli *et al.,* 2007). This is made possible through functional and physical coupling of NCX with ROCs, particularly at the nanodomain where the SR comes into close association with the PM (Lee *et al.,* 2002; Rosker *et al.,* 2004). In vascular smooth muscle, TRPC6 proteins form an important component of these channels (Inoue *et al.,* 2001; Lemos *et al.,* 2007). I investigated the process of TRPC and NCX coupling in vascular smooth muscle cells, using aequorin targeted to the mitochondria as a way to indirectly measure agonist-induced NCX reversal. I show that agonist-stimulated production of DAG is important to the increased Na^+ entry through the TRPC6 channels, which facilitates the reversal of NCX, and also show that Na^+ entry can be inhibited by PKC activation. However, this latter effect is not sufficiently prominent during purinergic stimulation to abolish the stimulatory effect of DAG. These observations are consistent with known properties of TRPC6 channels. Overall, we add to the growing body of work to show that ROCs are functionally coupled to reverse-mode NCX.

5.1.2 Overview of UTP-induced Ca^{2+} oscillations in rat basilar artery

Although Ca^{2+} waves have been observed to underlie tonic contraction in vascular smooth muscle preparations, little is known about this mechanism in the cerebral vasculature. A detailed mechanistic study of agonist-induced Ca^{2+} waves has never been done in the cerebral arteries. Using fluorescent Ca^{2+} indicators in conjunction with confocal microscopy, I showed that the underlying mechanism of UTP-induced Ca^{2+} waves in basilar artery is similar to what has been described in the large conductance vessels such as the IVC (Lee *et al.,* 2002). Importantly, I also

demonstrated a role for reverse-mode NCX. Multiple Ca^{2+} translocating proteins are involved as the Ca^{2+} waves appear to be produced by repetitive cycles of SR Ca^{2+} release which are mediated by IP_3Rs, followed by SERCA-mediated SR Ca^{2+} re-uptake of Ca^{2+} entry involving L-type voltage-gated Ca^{2+} channels, ROCs, and reverse-mode NCX. As the inhibition of IP_3Rs completely abolishes the Ca^{2+} waves while inhibition of RyRs has no effect, this suggests that the Ca^{2+} waves are induced from IP_3Rs and propagate by sequential release from one cluster of IP_3Rs to the next throughout the SR store. From studies conducted in *Xenopus* oocytes and from modeling simulations, IP_3Rs are thought to be arranged in clusters of around 25-35 receptors, which are 300-800nm in diameter and are several micrometers apart from each other (Swillens *et al.,* 1999; Shuai *et al.,* 2006), although these measurements need to be verified in the intact smooth muscle. The rising phase of the Ca^{2+} wave is thought to consist of a localized "initiation" component derived from the release of Ca^{2+} from one IP_3R in the cluster (a so-called Ca^{2+} puff), which is followed by an amplification component during which this release is augmented by Ca^{2+}-induced Ca^{2+} release by positive feedback at other IP_3Rs within the cluster. The Ca^{2+} which is released from the cluster then diffuses to the next cluster and initiates Ca^{2+} release, thus propagating Ca^{2+} release as a wave (McCarron *et al.,* 2004). The wave declines as IP_3Rs become inhibited due to the high localized Ca^{2+} concentration, as IP_3Rs are activated at a narrow range of Ca^{2+} concentration (~300nM), while higher concentrations inhibit the receptor (McCarron *et al.,* 2007; Fig 5.2). Alternatively, IP_3Rs may also become desensitized due to depletion of local Ca^{2+} stores.

Reverse (Ca^{2+} influx)-mode NCX is activated by the production of DAG, which then activates TRPC6 channels, initiating Na^+ influx, which ultimately serves to refill the SR store via reverse-mode NCX. Functionally, the UTP-induced asynchronous Ca^{2+} waves appear to underlie

EC coupling, as their abolishment through inhibition of SR Ca^{2+} re-uptake dramatically decreased tonic contraction, although average Ca^{2+} remained unchanged. We also show that the frequency of the Ca^{2+} waves is an important regulator of force generated. In general, the mechanisms of the Ca^{2+} waves in the basilar artery are similar to those in the large conduit vessels, indicating a common Ca^{2+} signaling mechanism in the vasculature.

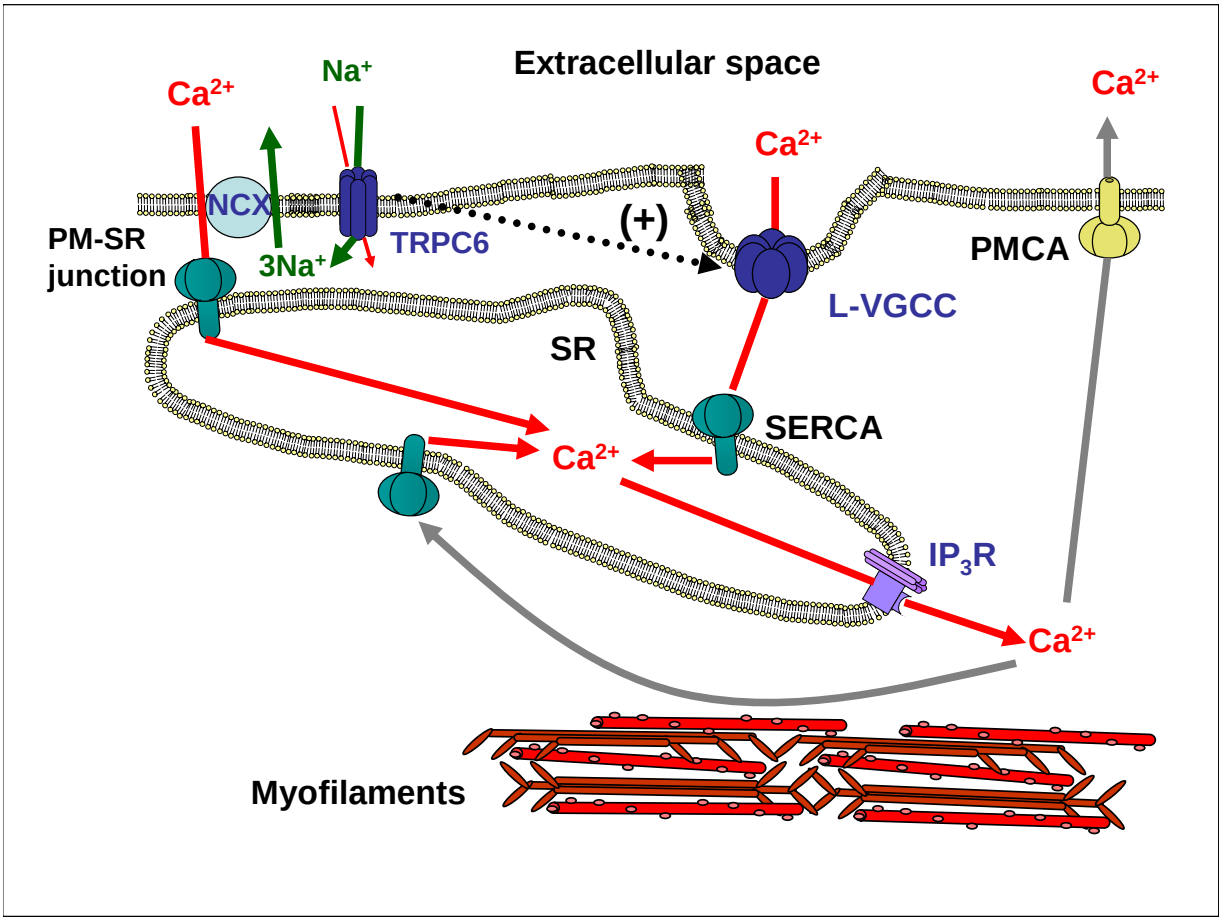

Figure 5.1: Model for UTP-induced Ca^{2+} waves in smooth muscle cells of rat basilar artery. (SR, sarcoplasmic reticulum; L-VGCC, L-type voltage-gated Ca^{2+} channel; NCX, Na^{+}/Ca^{2+} exchanger; TRPC, canonical transient receptor potential; IP_3R, IP_3 receptor; RyR, ryanodine receptor; SERCA, sarco-endoplasmic reticulum Ca^{2+}-ATPase; PMCA, plasma membrane Ca^{2+} ATPase).

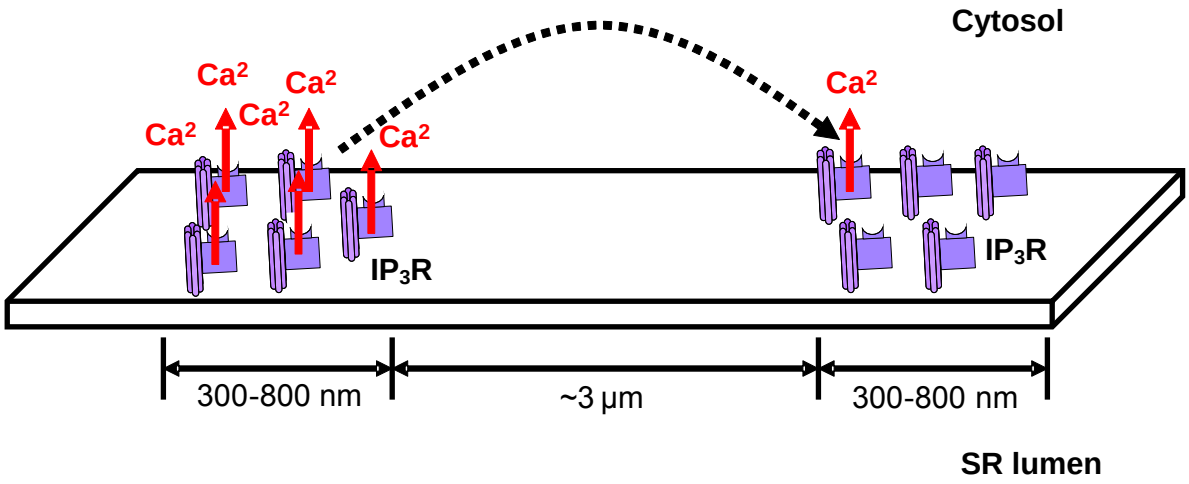

Figure 5.2: Model of Ca^{2+} wave propagation from *Xenopus* oocytes. Inositol 1,4,5-trisphosphate-medated Ca^{2+} signals propagate by sequential release from one cluster of inositol 1,4,5-trisphosphate receptors (IP_3Rs) to the next throughout the SR store. [Ca^{2+}] release from one IP_3R induces positive feedback Ca^{2+}-induced Ca^{2+} release from within the same cluster. The increasing [Ca^{2+}] then diffuses to an adjacent cluster (~3µm apart) and stimulates Ca^{2+}-induced Ca^{2+} release, resulting in the propagation of the wave (SR, sarcoplasmic reticulum). Figure adapted from McCarron *et al.,* 2007.

5.1.3 Overview of dysfunction of endothelium and smooth muscle cells in small arteries of a mouse model of marfan syndrome

Marfan syndrome is associated with endothelial dysfunction and reduction of smooth muscle contractility in the vasculature, particularly in the aorta (Chung *et al.,* 2007a,b), but little is known about how this disease affects the peripheral resistance vessels. Using a mouse model of Marfan syndrome, I determined that mesenteric artery smooth muscle cell contraction in response to phenylephrine and high potassium stimulation was reduced in Marfan mice compared to control, and more importantly, that reduced smooth muscle contractility in response to phenylephrine stimulation was associated with reduced recruitment of cells expressing

decreased frequency of Ca^{2+} waves. This observation is an important first step in drawing a possible link between vascular health and Ca^{2+} wave signaling. Although the specific mechanism explaining why there is reduced Ca^{2+} wave signaling needs to be examined, possible options include inhibition of Ca^{2+} entry through L-type Ca^{2+} channels from the extracellular space, which may be attributed to upregulation of matrixmetalloproteases (Chew *et al.,* 2004; Chung *et al.,* 2007a), as well as the disappearance of PM-SR junctions. Furthermore, I also showed that elasticity in mesenteric resistance vessels is decreased and endothelium-dependent and endothelium-independent relaxation is impaired.

5.2 Significance of work and future directions

The importance of Ca^{2+} as a signaling ion in vascular smooth muscle is apparent from how it regulates a plethora of different processes, from contraction to apoptosis. The ultrastructure of the vascular smooth muscle cell, particularly at the nanodomains formed by the close spatial association of the PM, SR and mitochondria allow diffusional barriers to Ca^{2+} and to other ions, allowing them to interact with a variety of transporters and exchangers. Such nanodomains were responsible for the indirect measurement of NCX reversal through mitochondria-mediated Ca^{2+} uptake and also for UTP-induced Ca^{2+} wave signaling, described Chapter II and III, respectively. Furthermore, the breakdown of these nanodomains may be responsible for decreased frequency of Ca^{2+} waves in vascular smooth muscle of mice with Marfan syndrome, as found in Chapter IV. My work from this thesis suggests there are many future experiments to be attempted and several relevant future studies are outlined below.

First of all, the study of NCX reversal mediated by Na^{+} influx from ROCs, presumably those composed of TRPC6, adds further evidence to the growing body of work supporting the

importance of the NCX as a Ca^{2+} entry mechanism. Indeed, Na^{+} influx following agonist stimulation has been directly visualized in cultured rat aortic smooth muscle cells (Poburko *et al.,* 2007). However, cultured cells have many disadvantages over intact tissue, including the alteration of expression of ion channels, transporters, receptors, and contractile proteins (Berra-Romani *et al.,* 2008). Therefore, a logical next step would be attempting to directly image Na^{+} influx following agonist stimulation in the intact tissue, and to determine if these Na^{+} transients are inhibited after inhibition of TRPC channels expression. Electrophysiological experiments in enzymatically dissociated cells using patch-clamp techniques to determine NCX currents at rest and following agonist stimulation would also provide direct and more accurate measurement of NCX reversal.

Secondly, the finding that Ca^{2+} waves underlie tonic contraction in the rat basilar artery, in addition to what is already known about the mechanism of Ca^{2+} waves in conduit vessels, may indicate that Ca^{2+} waves represent a common signaling mechanism in the vasculature. However, the question of why smooth muscle cells appear to have adopted Ca^{2+} waves as a way to activate contractile filaments is unknown, although there are a number of important considerations. First, Ca^{2+} as an intracellular signaling molecule is capable of activating a large number of effector molecules and processes. Ca^{2+} waves may be a mechanism to achieve high localized Ca^{2+} to allow effective activation of specific effector functions without a generalized activation of other Ca^{2+} sensitive pathways which may arise from a sustained local increase in Ca^{2+}. Second, the peak Ca^{2+} level of the Ca^{2+} wave may be sufficient to signal for contractile activation because the rate of Ca^{2+} dissociation from the calmodulin is much slower than the the rate of Ca^{2+} binding (Johnson *et al.,* 1996; Wilson *et al.,* 2002). In this case, the average Ca^{2+} achieved during agonist stimulation is lower than when a sustained rise in Ca^{2+} is used to stimulate contration; this has

been noted in the studies from the rat basilar artery presented in this thesis (Fig 5.3). Finally, certain frequency-dependent enzymes may be activated to a greater extent by Ca^{2+} waves, such as calmodulin kinase II and the transcription factor NF-AT (de Koninck and Schulman, 1998; Dupont and Goldbeter, 1998; Hu *et al.,* 1999). As Ca^{2+} waves represent a signaling mechanism which is widely utilized by a variety of smooth muscle cells to stimulate tonic contraction (Ruehlmann *et al.,* 2000; Lee *et al.,* 2002; Perez and Sanderson, 2005), it is unlikely that nature would adopt and preserve such a complex form of Ca^{2+} signaling without an underlying advantage. The role of Ca^{2+} waves in activating contraction may only be conclusively determined with direct observation of myosin light-chain kinase, as has been done with carbachol-induced elevation of Ca^{2+} in mouse bladder smooth muscle cells (Isotani *et al.,* 2004).

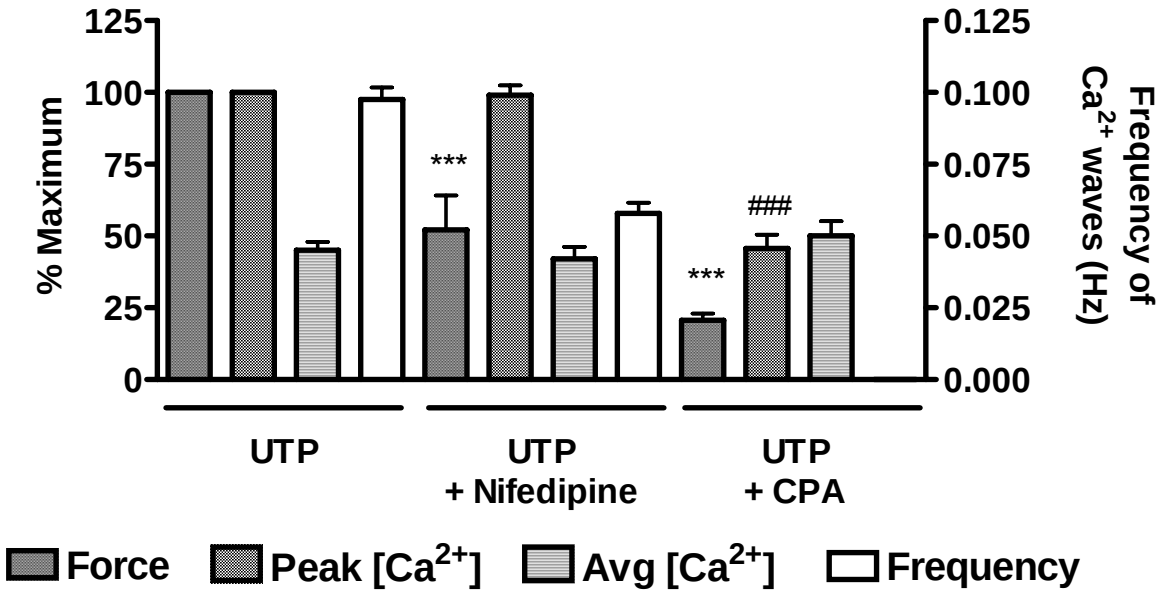

Figure 5.3: Ca^{2+} waves provide a more efficient stimulus for tonic contraction compared to steady elevation in average Ca^{2+}. The stimulation of rat basilar artery with UTP (100 μM) generates tonic contraction. The addition of nifedipine to UTP-induced Ca^{2+} waves significantly slows frequency and tonic contraction, but neither changes the Ca^{2+} peak of the oscillations nor average Ca^{2+}. However, the application of CPA to ongoing UTP-induced Ca^{2+} waves results in a significantly decreased tonic contraction, which is associated with significantly decreased peak Ca^{2+}, but elevated average Ca^{2+}. *** - $P < 0.001$ vs. UTP-induced tonic contraction, ### - $P < 0.001$ vs. UTP-induced peak $[Ca^{2+}]$.

Additionally, it was revealed that there is an important role for reverse (Ca^{2+}-entry)-mode NCX in the maintenance of Ca^{2+} waves, presumably through refilling of the SR at the PM-SR junctions. The driving force (the difference between membrane potential, V_m, and NCX reversal potential, E_{NCX}) determines the direction of net Ca^{2+} movement, and varies during agonist stimulation. NCX reversal (Ca^{2+} entry) occurs when $E_{NCX} < V_m$. In the arterial smooth muscle, agonist stimulation depolarizes the myocytes through the opening of ROCs, which results in Na^+ entry that builds up in the PM-SR junction. As $[Na^+]$ increases and V_m is depolarized, the thermodynamic driving force on the NCX begins to favour Ca^{2+} entry mode. Assuming for an activated cell, where V_m = -20mV, $[Na^+]_o$ = 140 mM, $[Ca^{2+}]_i$ = 10 μm, $[Ca^{2+}]_o$ = 2 mM, around 30mM Na^+ in the subplasmalemmal space is required before NCX reversal occurs, which is feasible given that such contentrations have been observed and mathematically predicted (Poburko *et al.,* 2006; Fameli *et al.,* 2007, Fameli *et al.,* 2009). Then, as the Ca^{2+} is taken up by the SR and the leading edge of the wave begins to decline, the membrane begins to repolarize and the driving force V_m-E_{NCX} again becomes negative and favours Ca^{2+} extrusion.

However, information on the time-dependent changes of V_m during Ca^{2+} oscillations has never been obtained. The use of V_m-sensitive fluorescent dye such as $DiBAC_4(3)$ would allow visualization of the changes in V_m during Ca^{2+} oscillations, as the dye fluctuates in intensity in response to changes in V_m (Rottenberg 1979; Freedman and Novak, 1989; Rottenberg 1989; Sguilla *et al.,* 2003). Another approach would require the enzymatic isolation of cells from the basilar artery and recording of E_m with the patch clamp technique before and during application of UTP. This would assume that the enzymatically dissociated cells also display the same Ca^{2+} oscillations as in the intact tissue. In these same cells, E_m could also be recorded by measuring

emitted fluorescence from $DiBAC_4(3)$, such that there will be two independent measurements and the means for calibration of the fluorescent measurements.

Thirdly, the finding that decreased smooth muscle contraction in Marfan syndrome was associated with decreased Ca^{2+} wave frequency and cell displaying Ca^{2+} waves is one of the first to reveal how Ca^{2+} wave signaling can be affected by vascular disease. Although not examined directly in this thesis, these Ca^{2+} waves (as in other vascular smooth muscles) are likely supported by the underlying PM-SR junctional cellular ultrastructure, which are important for SR Ca^{2+} refilling (Lee *et al.,* 2005; Fameli *et al.,* 2007). More evidence to support this theory comes from the observation that phenylephrine elicited tonic contractions in both mouse and human mesenteric arteries, but asynchronous Ca^{2+} waves were only seen in the mouse mesenteric artery smooth muscle cells (which had abundant superficial SR and many PM-SR junctions), while the human mesenteric artery smooth muscle cells (which had far less peripheral SR and was almost devoid of PM-SR junctions) displayed only single transient Ca^{2+} signal (Dai *et al.,* 2010). Finally, diabetes is also associated with separation of the superficial SR from the PM in the coronary artery (Witczak and Sturek, 2004). Therefore, the deterioration of PM-SR junctional complexes (and subsequent disappearance of oscillatory Ca^{2+} signaling) may be an important contributing factor in the etiology of vascular disease. Future studies which could directly test this hypothesis would involve a comparative study of the extent of PM-SR junctions between age-matched control and Marfan mice. Because the frequency of Ca^{2+} waves decreases as Marfan syndrome progresses, we speculate that there would be fewer PM-SR junctions in the diseased vessels compared to control.

If, however, the deterioration of PM-SR junctions causes the disappearance of Ca^{2+} waves, it should logically follow that their restoration would enable Ca^{2+} wave signaling to return. This

raises the question whether it is possible to restore Ca^{2+} wave signaling and/or PM-SR junctions following treatment, pharmacological or otherwise, of vascular diseases. Interestingly, exercise restores the diabetes-induced impaired structure between the superficial SR and the PM in the coronary artery (Witczak and Sturek, 2004). Additionally, the treatment of Marfan syndrome using doxycyline was found to normalize vasomotor function (Chung *et al.,* 2008). Does the restoration of PM-SR junctions following exercise induce Ca^{2+} waves, in the case of coronary artery? And does it follow that normalization of vasomotor function through doxycycline treatment is secondary to the restoration of PM-SR junctions? An interesting follow-up study to answer the latter question would be to compare control, doxycycline-treated, and untreated Marfan mice to determine if Ca^{2+} wave signaling is also normalized following treatment with doxycycline, with parallel electron microscopy studies to examine the cellular ultrastructure. A final unresolved mystery is the identity of the structural protein that is responsible for the regular spacing of the smooth muscle PM-SR junctions? Although the presence of connecting structures between the PM and SR have been known for many years (Somlyo, 1985), their composition remains unknown. The identification of these structures would be an important step in the possible development of therapeutic agents which would preserve their structure, Ca^{2+} wave signaling, and presumably vascular health.

5.3 Concluding remarks

The goal of the studies contained in this thesis was to gain a more comprehensive understanding of Ca^{2+} signaling in smooth muscle of blood vessels. The contributions made in this thesis enhance our understanding of Ca^{2+} signaling in healthy and diseased animal cells and the intact blood vessels. In particular, this work provides in some detail the mechanism and

function of agonist-induced Ca^{2+} waves and their relation to tonic contraction, as well as their underlying mechanisms. Ca^{2+} waves are clearly an important part of the regulation of vascular smooth muscle contraction and their disappearance may be linked to declining vascular health. Going forward, a better understanding of the relationship between Ca^{2+} waves, cellular ultrastructure, and vascular health may constitute an important step toward the development of therapeutic agents to preserve vascular health.

5.4 References

Berra-Romani R, Mazzocco-Spezzia A, Pulina MV, Golovina VA (2008). Ca2+ handling is altered when arterial myocytes progress from a contractile to a proliferative phenotype in culture. *Am J Physiol Cell Physiol* **295:** C779-90.

Chew DK, Conte MS, Khalil RA (2004). Matrix metalloproteinase-specific inhibition of Ca2+ entry mechanisms of vascular contraction. *J Vasc Surg* **40**: 1001-10.

Chung AW, Au Yeung K, Sandor GG, Judge DP, Dietz HC, van Breemen C (2007a). Loss of elastic fiber integrity and reduction of vascular smooth muscle contraction resulting from the upregulated activities of matrix metalloproteinase-2 and -9 in the thoracic aortic aneurysm in Marfan syndrome. *Circ Res* **101**: 512-22.

Chung AW, Au Yeung K, Cortes SF, Sandor GG, Judge DP, Dietz HC *et al*. (2007b). Endothelial dysfunction and compromised eNOS/Akt signaling in the thoracic aorta during the progression of Marfan syndrome. *Br J Pharmacol* **150**:1075-83.

Chung AW, Yang HH, Radomski MW, van Breemen C (2008). Long-term doxycycline is more effective than atenolol to prevent thoracic aortic aneurysm in marfan syndrome through the inhibition of matrix metalloproteinase-2 and -9. *Circ Res* **102:** e73-85.

Dai JM, Syyong H, Navarro-Dorado J, Redondo S, Alonso M, van Breemen C, Tejerina T (2010). A comparative study of α-adrenergic receptor mediated Ca2+ signals and contraction in intact human and mouse vascular smooth muscle. *Eur J Pharmacol* **In press**

De Koninck P, Schulman H (1998). Sensitivity of Ca2+/calmodulin-dependent protein kinase II to the frequency of Ca2+ oscillations. *Science* **279**: 227-230.

Dietz HC, Cutting GR, Pyeritz RE, Maslen CL, Sakai LY, Corson GM *et al.* (1991). Marfan syndrome caused by a recurrent de novo missense mutation in the fibrillin gene. *Nature* **352**: 337-9.

Dupont G, Goldbeter A (1998). CaM kinase II as frequency decoder of Ca2+ oscillations. *Bioessays* **20:** 607-10.

Fameli N, Kuo KH, van Breemen C (2009). A model for the generation of localized transient [Na+] elevations in vascular smooth muscle. *Biochem Biophys Res Commun* **389:** 461-5.

Fameli N, van Breemen C, Kuo KH (2007). A quantitative model for linking Na+/Ca2+ exchanger to SERCA during refilling of the sarcoplasmic reticulum to sustain [Ca2+] oscillations in vascular smooth muscle. *Cell Calcium* **42:** 565-575.

Freedman, J.C. and Novak, T.S. 1989. Optimal measurement of membrane potential in cells, organelles, and vesicles. Methods Enzymol. **172:** 102-122.

Hu Q, Deshpande S, Irani K, Ziegelstein RC (1999). [Ca(2+)](i) oscillation frequency regulates agonist-stimulated NF-kappaB transcriptional activity. *J Biol Chem* **274:** 33995-8.

Inoue R, Okada T, Onoue H, Hara Y, Shimizu S, Naitoh S, *et al.* (2001). The transient receptor potential protein homologue TRP6 is the essential component of vascular alpha(1)-adrenoceptor-activated Ca(2+)-permeable cation channel. *Circ Res* **88:** 325-32.

Isotani E, Zhi G, Lau KS, Huang J, Mizuno Y, Persechini A *et al.* (2004). Real-time evaluation of myosin light chain kinase activation in smooth muscle tissues from a transgenic calmodulin-biosensor mouse. *Proc Natl Acad Sci U S A* **101:** 6279-84.

Johnson JD, Snyder C, Walsh M, and Flynn M (1996). Effects of Myosin Light Chain Kinase and Peptides on Ca2+ exchange with the N and C terminal Ca2+ binding sites of calmodulin. *J Biol Chem* **271:** 761-767.

Lee CH, Poburko D, Kuo KH, Seow CY, van Breemen C (2002). Ca(2+) oscillations, gradients, and homeostasis in vascular smooth muscle. *Am J Physiol Heart Circ Physiol* **282:** H1571-83.

Lee CH, Poburko D, Sahota P, Sandhu J, Ruehlmann DO, van Breemen C (2001). The mechanism of phenylephrine-mediated [Ca(2+)](i) oscillations underlying tonic contraction in the rabbit inferior vena cava. *J Physiol* **534:** 641-650.

Lee CH, Kuo KH, Dai J, Leo JM, Seow CY, Breemen C (2005). Calyculin-A disrupts subplasmalemmal junction and recurring Ca2+ waves in vascular smooth muscle. *Cell Calcium* **37:** 9-16.

Lemos VS, Poburko D, Liao CH, Cole WC, van Breemen C (2007). Na+ entry via TRPC6 causes Ca2+ entry via NCX reversal in ATP stimulated smooth muscle cells. *Biochem Biophys Res Commun* **352:** 130-4.

Macrez N, Mironneau J (2004). Local Ca2+ signals in cellular signalling. *Curr Mol Med* **4:** 263-75.

McCarron JG, MacMillan D, Bradley KN, Chalmers S, Muir TC (2004). Origin and mechanisms of Ca2+ waves in smooth muscle as revealed by localized photolysis of caged inositol 1,4,5-trisphosphate. *J Biol Chem* **279:** 8417-27.

McCarron JG, Olson ML, Rainbow RD, MacMillan D, Chalmers S (2007). Ins(1,4,5)P3 receptor regulation during 'quantal' Ca2+ release in smooth muscle. *Trends Pharmacol Sci* **28:** 271-9.

Perez JF, Sanderson MJ (2005). The contraction of smooth muscle cells of intrapulmonary arterioles is determined by the frequency of Ca2+ oscillations induced by 5-HT and KCl. *J Gen Physiol* **125:** 555-67.

Petersen OH, Sutton R, Criddle DN (2006). Failure of calcium microdomain generation and pathological consequences. *Cell Calcium* **40:** 593-600.

Poburko D, Potter K, van Breemen E, Fameli N, Liao CH, Basset O, *et al.* (2006). Mitochondria buffer NCX-mediated Ca2+-entry and limit its diffusion into vascular smooth muscle cells. *Cell Calcium* **40:** 359-71.

Poburko D, Liao CH, Lemos VS, Lin E, Maruyama Y, Cole WC, van Breemen C (2007). Transient receptor potential channel 6-mediated, localized cytosolic [Na+] transients drive Na+/Ca2+ exchanger-mediated Ca2+ entry in purinergically stimulated aorta smooth muscle cells. *Circ Res* **101:** 1030-8.

Rosker C, Graziani A, Lukas M, Eder P, Zhu MX, Romanin C, *et al.* (2004). Ca(2+) signaling by TRPC3 involves Na(+) entry and local coupling to the Na(+)/Ca(2+) exchanger. *J Biol Chem* **279:** 13696-704.

Rottenberg, H. 1979. The measurement of membrane potential and deltapH in cells, organelles, and vesicles. *Methods Enzymol* **55:** 547-569.

Rottenberg, H. 1989. Proton electrochemical potential gradient in vesicles, organelles, and prokaryotic cells. *Methods Enzymol* **172:** 63-84.

Ruehlmann DO, Lee CH, Poburko D, van Breemen C (2000). Asynchronous Ca(2+) waves in intact venous smooth muscle. *Circ Res* **86:** E72-9.

Sguilla, F.S., Tedesco, A.C., and Bendhack, L.M. 2003. A membrane potential-sensitive dye for vascular smooth muscle cells assays. *Biochem Biophys Res Commun* **301:** 113-118.

Shuai J, Rose HJ, Parker I (2006). The number and spatial distribution of IP_3 receptors underlying calcium puffs in Xenopus oocytes. *Biophys J* **91:** 4033–4044.

Somlyo AP (1985). Excitation-contraction coupling and the ultrastructure of smooth muscle. *Circ Res* **57:** 497-507.

Swillens S, Dupont G, Combettes L, Champeil P (1999). From calcium blips to calcium puffs: theoretical analysis of the requirements for interchannel communication. *Proc Natl Acad Sci U S A* **96:** 13750-5.

Wilson DP, Sutherland C, Walsh MP (2002). Ca2+ activation of smooth muscle contraction: evidence for the involvement of calmodulin that is bound to the triton insoluble fraction even in the absence of Ca2+. *J Biol Chem* **277:** 2186-2192.

Witczak CA, Sturek M (2004). Exercise prevents diabetes-induced impairment in superficial buffer barrier in porcine coronary smooth muscle. *J Appl Physiol* **96:** 1069-79.

APPENDIX A

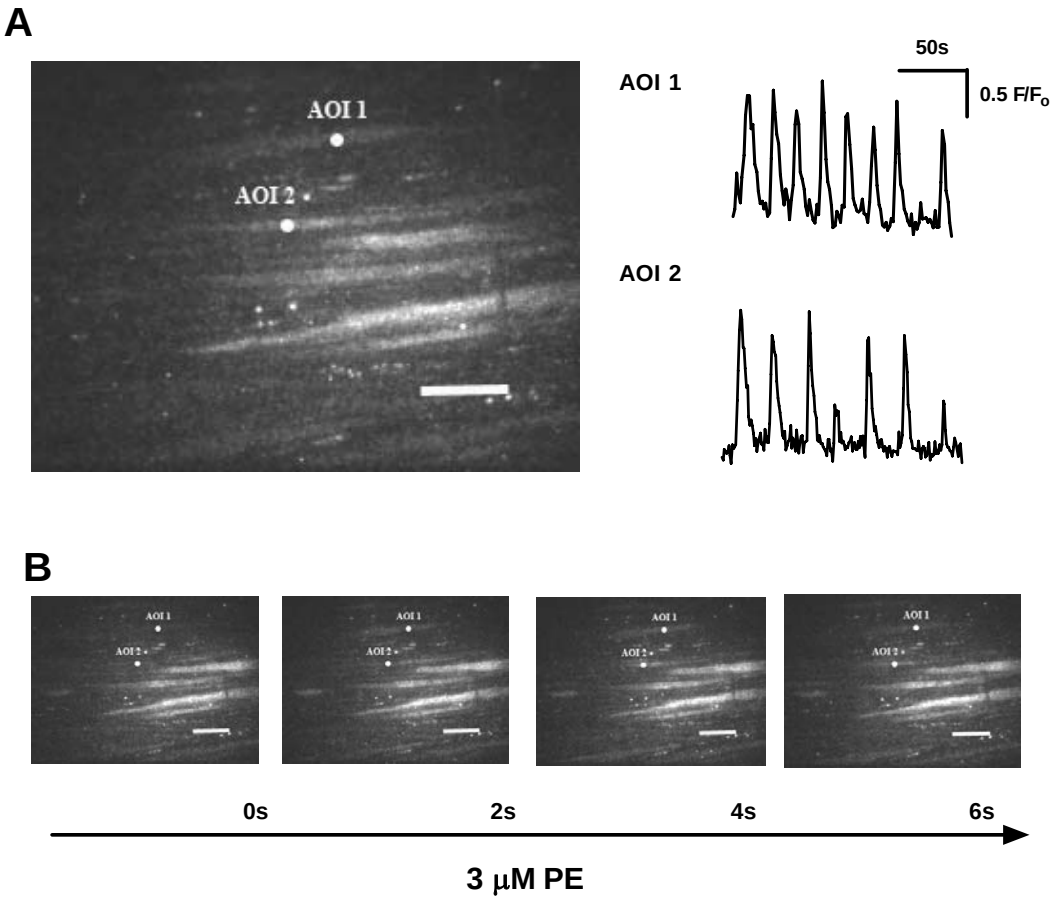

Phenylephrine (PE, 3 μM)-induced Ca^{2+} waves in mouse mesenteric artery. (A) $[Ca^{2+}]_i$ changes in 2 intracellular regions from 2 different smooth muscle cells upon PE stimulation are depicted in the Ca^{2+} traces taken from the steady state of PE-induced Ca^{2+} waves. It should be noted that the Ca^{2+} waves occurred at different frequencies. Experimental Ca^{2+} traces are representative of results from 58 cells in 6 animals. **(B)** Intact vascular smooth muscle cells challenged with PE (3 μM) displayed Ca^{2+} waves which originated from distinct intracellular foci and propagated along the longitudinal axis of the smooth muscle cells, as indicated by area of interest (AOI) AOI1 and AOI2. The AOI is 3x3 pixels (1.69 μm^2). Scale bar = 10 μm.

APPENDIX B

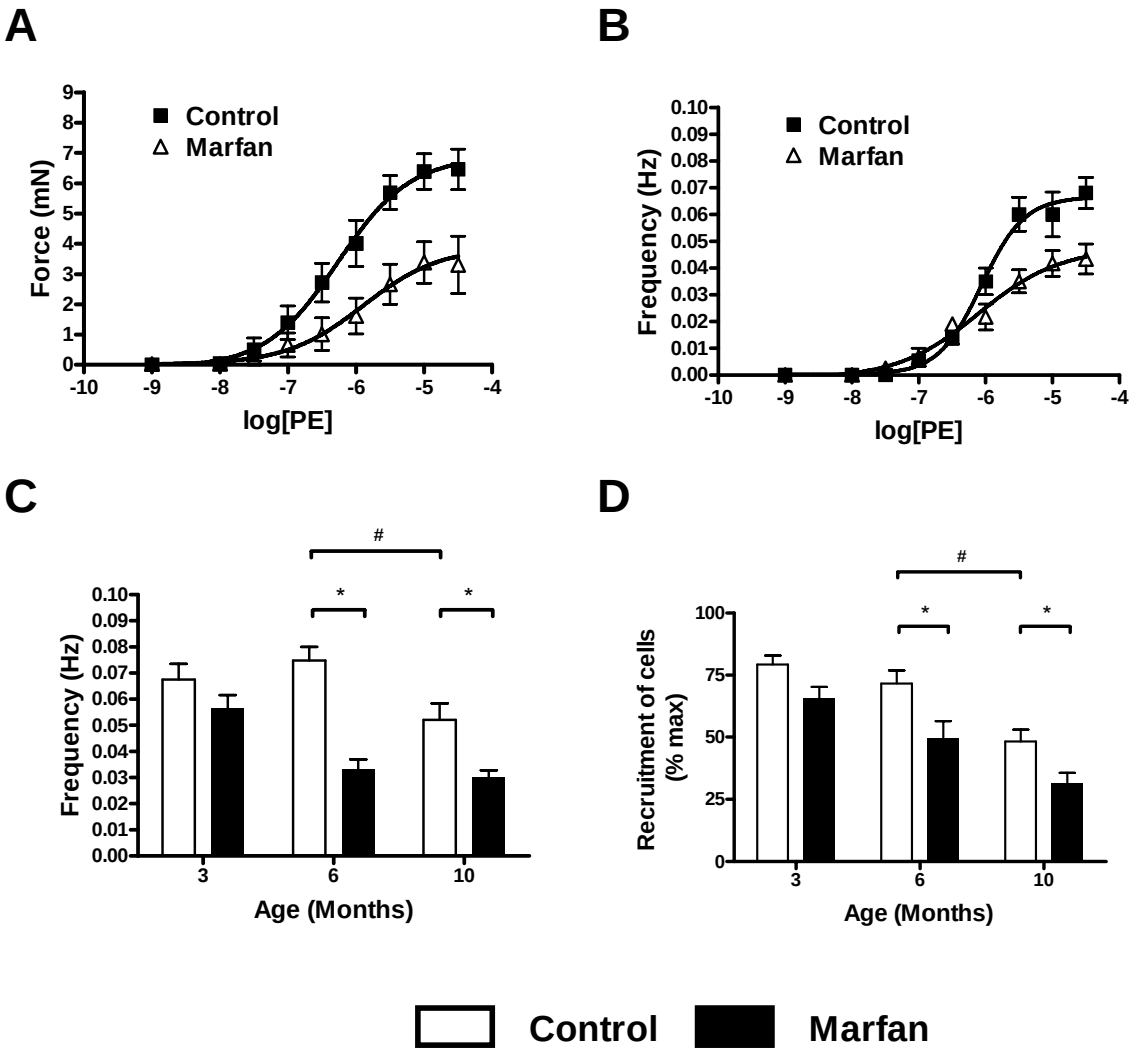

Properties of phenylephrine (PE, 3 μM)-induced Ca^{2+} waves underlying tonic contraction in mouse mesenteric artery. Concentration-response curves for PE-induced **(A)** tonic contraction and **(B)** Ca^{2+} wave frequency in control and Marfan mice at 6 months of age. **(C)** Reduced frequency of PE (3 μM)-stimulated Ca^{2+} waves in Marfan vessels compared to control vessels. **(D)** A decreased percentage of vascular smooth muscle cells in Marfan vessels displayed at least one Ca^{2+} wave compared to control vessels when stimulated with PE (3 μM) (n = 90 cells from 10 animals). The number of cells firing is expressed as a percentage of cells responding to maximal concentration. *, # - $P<0.05$

APPENDIX C

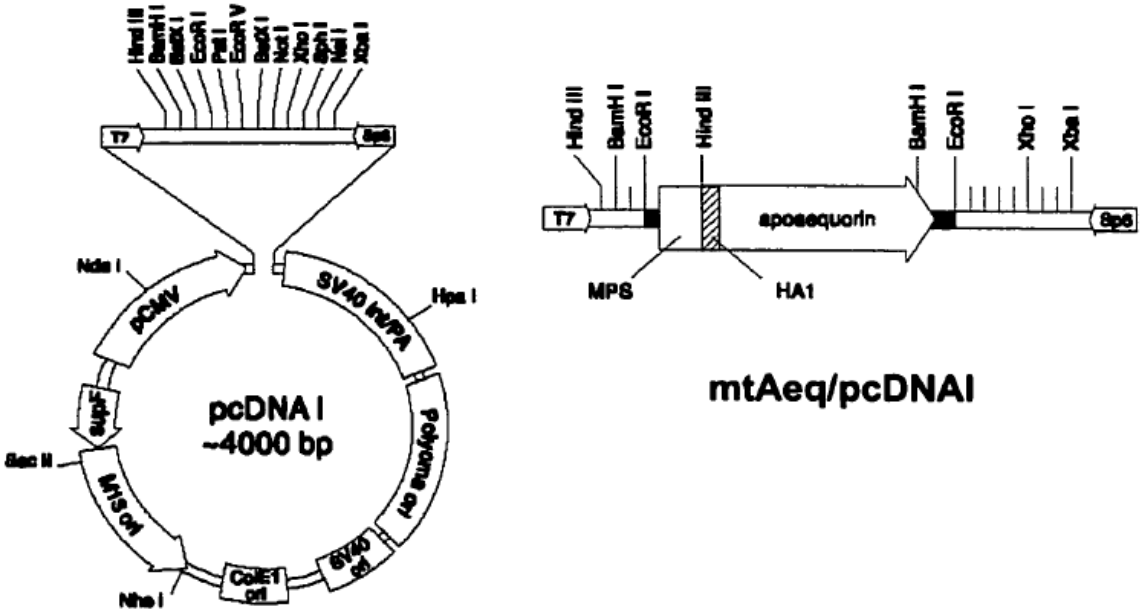

Plasmid map of pcDNA1-based aequorin expression vector. mtAeq/pcDNA1 shows the ~770bp DNA insert (ECOR1 fragment) with mitochondrial targeting presequence (MPS) of human cytochrome c oxidase subunit VIII, HA1 epitope and apoaequorin coding segments (From Challet thesis, 2001). The mtAeq/pcDNAI contains sequences encoding the mitochondrial targeting peptide from subunit VIII of human cytochrome c oxidase fused to an HA1 antigen and to apoaequorin. To amplify this pcDNAI-based plasmid, which carries the supF suppressor tRNA gene, a special host bacterium, MC1061/P3 E. Coli (Invitrogen, Groningen, NL), had to be used. The P3 plasmid in this host carries a wild-type kanamycin resistance gene, plus amber-mutant versions of both ampicillin and tetracyclin-resistance genes. Transformation of MC1061/P3 by a plasmid bearing a supf confers ampicillin and tetracyclin resistance by translational suppression of the defective genes. The amplification protocol was, in brief, the following. Competent bacteria were heat shocked in the presence of l00ng mtAeq/pcDNAI. They were grown in LB medium for 30min at 37°C and were seeded on LB-Agar plate containing 50ug/ml ampicillin. After an overnight incubation at 37°C, colonies of bacteria were isolated and were further grown overnight in 200ml LB medium with 50u.g/ml ampicillin. After bacterial suspension was centrifuged, plasmid was purified using the kit Nucleobond" AX500 (Machcry-Nagcl, Oensingen, CH). The identification of the purified plasmid was checked by enzyme digestion. ECORI restriction enzyme could be used alone or in combination with Hindlll (Pharmacia Biotech, Dubcndorf, CH).

APPENDIX D

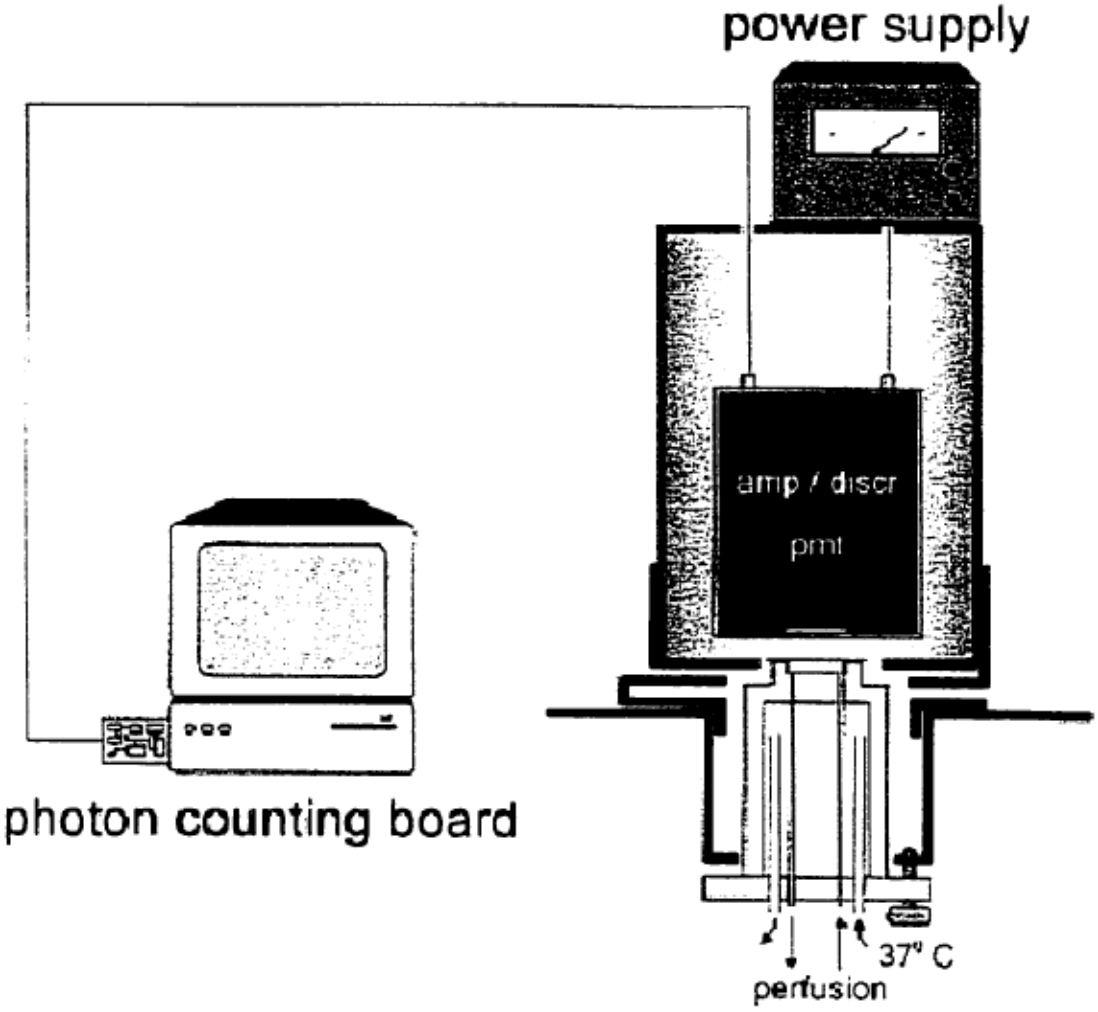

Luminometry setup. The cell chamber is constantly thermostated at 37 degrees with a water bath and perfused via a peristaltic pump at a rate of 1 mL/min. The smooth muscle cells, on Thermanox coverslips, are placed into the specifically designed chamber. Photons emitted by the cells are detected with a low noise photomultiplier tube (pmt, Thorn-EMI 9789A) connected to a high voltage power supply (Thorn-EMI, PM28B). Acquired data are recorded every second using an amplifier discriminator (amp/disc, Thorn-EMI, C640A) and a computer photon counting board (Thorn-EMI C660). Reproduced from Chiesa *et al.,* 2001.

APPENDIX E

List of Publications and Abstracts

The chapters in this thesis contain work that has been previously published in peer-reviewed journals. Material from this dissertation has been published in:

- **Syyong HT**, Chung AWY, Yang HHC, van Breemen C (2009). Dysfunction of endothelial and smooth muscle cells in small arteries of a mouse model of Marfan syndrome. *Br J Pharmacol* **158:** 1597-1608.
- **Syyong HT**, Yang HH, Trinh G, Cheung C, Kuo KH, van Breemen C (2009). Mechanism of asynchronous Ca(2+) waves underlying agonist-induced contraction in the rat basilar artery. *Br J Pharmacol* **156:** 587-600.
- **Syyong HT**, Poburko D, Fameli N, van Breemen C (2007). ATP promotes NCX-reversal in aortic smooth muscle cells by DAG-activated Na+ entry. *Biochem Biophys Res Commun* **357:** 1177-82.

Material from this dissertation has been presented in poster format at the following international meetings:

- **Syyong HT**, Lemos VS, Poburko DT, Liao CH, Pillai R, Fameli N, Kuo KH, van Breemen C. ATP-induced reversal of sodium-calcium exchanger and the role of the canonical transient receptor potential (TRPC) subfamily. Canadian Cardiovascular Congress - Vancouver, BC October 21-25, 2006. Canadian Journal of Cardiology, 22(Suppl D):211D

- **Syyong, HT**, Kuo, KH, and van Breemen, C. Mechanism of uridine 5'-triphosphate (UTP)-induced calcium waves in rat basilar artery. Experimental Biology, Washington, DC, USA, April 28-May 2, 2007. FASEB J. 2007 21:873.7

- **Syyong, HT**, Yang, C., Kuo, K.H., and van Breemen, C. Uridine 5'-triphosphate (UTP)-induced Ca^{2+} oscillations underlie tonic contraction in rat basilar artery. Canadian Cardiovascular Congress - Quebec City, QC Oct 20-24, 2007. Canadian Journal of Cardiology, 23(Suppl C):217C.

- **Syyong, H**, Yang, C, Trinh, G, Kuo, K.H., and van Breemen, C. Ultrastructural basis of asynchronous uridine 5'-triphosphate (UTP)-induced Ca(2+) waves in rat basilar artery. Experimental Biology - San Diego, CA, USA Apr 5-9, 2008. FASEB J. 2008 22:913.1.

Material from this dissertation has also been presented orally for the Graduate Student Seminar Series in the Department of Anesthesiology, Pharmacology and Therapeutics at UBC

APPENDIX F

Copies of the UBC animal care committee approval letters are included.

THE UNIVERSITY OF BRITISH COLUMBIA

ANIMAL CARE CERTIFICATE

Application Number: A07-0255

Investigator or Course Director: Cornelis Van Breemen

Department: Medicine, Faculty of

Animals:

Rats Sprague-Dawley 220

Start Date: **July 1, 2007**

Approval Date: **July 11, 2007**

Funding Sources:

Funding Agency: Canadian Institutes of Health Research (CIHR)

Funding Title: Calcium oscillations in vascular smooth muscle

Unfunded title: N/A

The Animal Care Committee has examined and approved the use of animals for the above experimental project.

This certificate is valid for one year from the above start or approval date (whichever is later) provided there is no change in the experimental procedures. Annual review is required by the CCAC and some granting agencies.

A copy of this certificate must be displayed in your animal facility.

Office of Research Services and Administration
102, 6190 Agronomy Road, Vancouver, BC V6T 1Z3
Phone: 604-827-5111 Fax: 604-822-5093

THE UNIVERSITY OF BRITISH COLUMBIA

ANIMAL CARE CERTIFICATE

Application Number: A06-1459

Investigator or Course Director: Cornelis Van Breemen

Department: Medicine, Faculty of

Animals:

Mice fibrilin 1 cys +/- mice, C1039G mutation; Fbn1 is on the Bl6 180

Start Date: **November 1, 2006** **Approval Date:** **November 10, 2006**

Funding Sources:

Funding Agency: Heart and Stroke Foundation of B.C. & Yukon

Funding Title: Cellular mechanisms of aortic pathogenesis in Marfan syndrome

Unfunded title: N/A

The Animal Care Committee has examined and approved the use of animals for the above experimental project.

This certificate is valid for one year from the above start or approval date (whichever is later) provided there is no change in the experimental procedures. Annual review is required by the CCAC and some granting agencies.

A copy of this certificate must be displayed in your animal facility.

Office of Research Services and Administration
102, 6190 Agronomy Road, Vancouver, BC V6T 1Z3
Phone: 604-827-5111 Fax: 604-822-5093

The University of British Columbia

ANIMAL CARE CERTIFICATE
BREEDING PROGRAMS

Application Number: A05-1480

Investigator or Course Director: Casey Van Breemen

Department: Pharmacology & Therapeutics

Animals: fibrilin 1 cys +/- mice, C1039G mutation; Fbn1 is on the Bl6 180

Approval Date: **December 8, 2005**

Funding Sources:

Funding Agency:	Canadian Marfan Association
Funding Title:	In-vitro assessment of endothelial and arterial smooth muscle function in a Marfan mouse model
Unfunded title:	N/A

The Animal Care Committee has examined and approved the use of animals for the above breeding program.

This certificate is valid for one year from the above approval date provided there is no change in the experimental procedures. Annual review is required by the CCAC and some granting agencies.

A copy of this certificate must be displayed in your animal facility.

Office of Research Services and Administration
102, 6190 Agronomy Road, Vancouver, V6T 1Z3
Phone: 604-827-5111 Fax: 604-822-5093